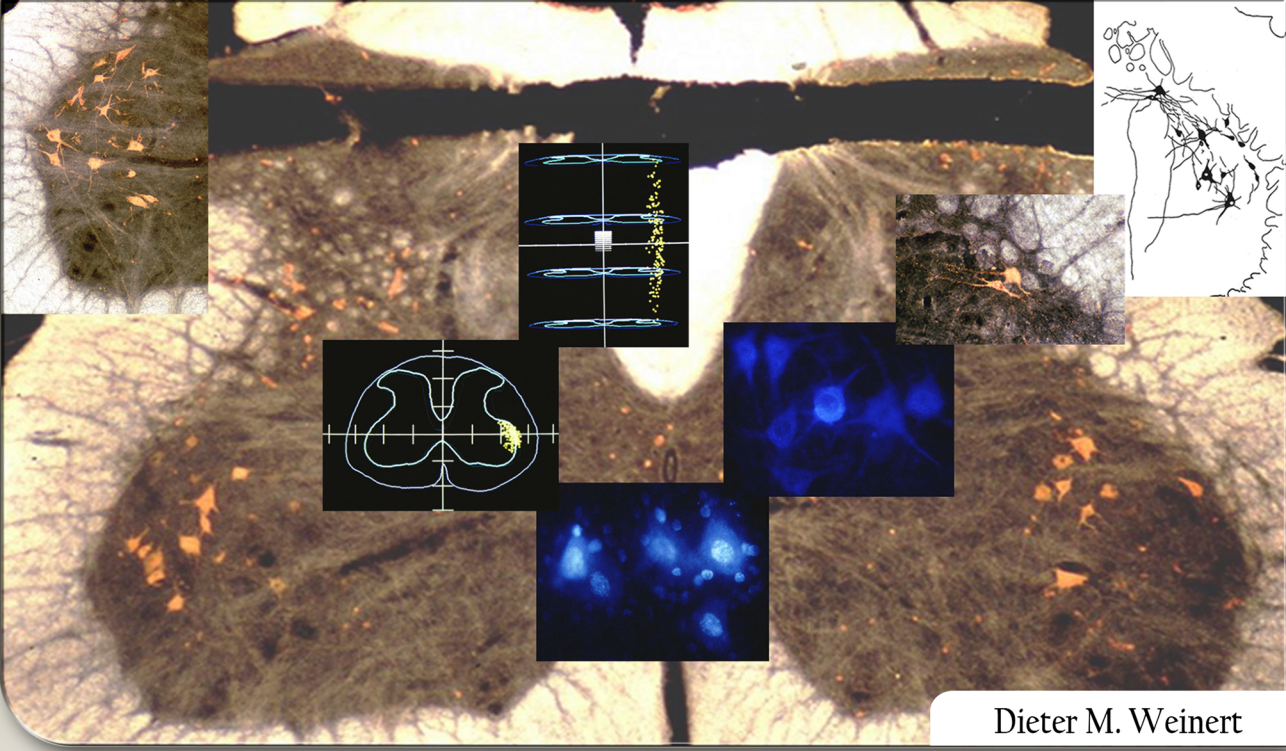

Dieter M. Weinert

Reorganization of a Spinal Motoneuron Nucleus following Autologous Nerve Graft in the Rat

Dieter M. Weinert

Reorganization of a Spinal Motoneuron Nucleus following Autologous Nerve Graft in the Rat

Reorganization of a Spinal Motoneuron Nucleus following Autologous Nerve Graft in the Rat

Dieter M. Weinert

First Edition
German First Edition, 2014

Manufactured and published by: BoD – Books on Demand, Norderstedt
Printed in Germany

Bibliographic information of the German National Library:
The German National Library lists this publication in the German National Bibliography; detailed bibliographic information is available at www.dnb.de.

ISBN 978-3-8391-6777-9

Contents

Preface ____ *XI*

Acknowledgments ____ *XIII*

Abbreviations ____ *XIV*

1. Introduction ____ *17*

1.1. The problems of peripheral neurosurgery ____ **17**

1.2. Neurobiological basics of peripheral neurosurgery ____ **21**

1.3. Objectives of the work ____ **26**

2. Materials and Methods ____ *27*

2.1. Tests using horseradish peroxidase (HRP) ____ **27**

2.1.1. Experiments in test series HRP1 ____ 27

2.1.1.1. Dissection, injection of HRP and integration in the HRP1P preliminary tests ____ 27

2.1.1.2. Radial nerve–common peroneal nerve autograft (HRP1G) ____ 30

2.1.2. Experiments in test series HRP2 ____ 30

2.1.2.1. Methodical changes in the HRP2P1 preliminary trials ____ 31

2.1.2.2. The diffusion of HRP into neighboring muscles (HRP2P2) ____ 32

2.1.2.3. External control tests (HRP2C) ____ 32

2.1.2.4. HRP2G graft series ____ 32

2.1.3. Experiments in test series HRP4 ____ 33

2.1.4. Experiments in test series HRP3 and HRP5 ____ 33
2.1.4.1. Retrograde labeling of the cell column of the sciatic nerve following transection and HRP nerve bath (HRP3P) ____ 34
2.1.4.2. The nucleus columns of the muscles innervated by the common peroneal nerve following transection and HRP nerve bath of the muscle nerve branches (HRP5C) ____ 35
2.1.4.2.1. Preparation of the muscle nerve branches of the tibialis anterior muscle (Figures 2.1 and 3.16) ____ 35
2.1.4.2.2. Preparation of the muscle nerve branches of the extensor digitorum longus muscle, the extensor hallucis proprius muscle, the extensor digitorum brevis muscle and the peroneus longus muscle (Figure 3.15) ____ 36

2.2. Experiments using the fluorescent markers Diamidino Yellow Dihydrochloride (DY) and Fast Blue (FB) ____ 36

2.2.1. Retrograde labeling of motor nucleus columns with fluorescent dyes ____ 37
2.2.1.1. Production and storage of the fluorescent dyes ____ 37
2.2.1.2. Handling and application of the fluorescent dyes ____ 37
2.2.1.3. Perfusion fixation ____ 37
2.2.1.4. Sections ____ 38
2.2.1.5. Histological counterstaining ____ 38
2.2.1.6. Microscopic evaluation ____ 38
2.2.2. The fluorescent dyes Diamidino Yellow (DY) and Fast Blue (FB) in the long-term test ____ 38

2.3. The combination of HRP with the fluorescent dye Diamidino Yellow ____ 39

2.4. Evaluation ____ 39

2.4.1. Macroscopic anatomy of the site and the spinal cord ____ 39
2.4.1.1. Morphometry of the spinal cord segments ____ 39
2.4.1.2. Intraspinal plexus ____ 40
2.4.1.3. The motor innervation area of the peroneal nerve ____ 40
2.4.1.4. Topographical anatomy of the innervation of the tibialis anterior muscle ____ 40
2.4.1.5. Anatomy of the graft site ____ 40

2.4.2. Microscopic evaluation and computer-aided reconstruction of the HRP tests 40
2.4.2.1. Depicting the section images (Figure 2.2) 40
2.4.2.2. The spinal cord section in the coordinates system 40
2.4.2.2.1. Positioning the coordinate axis 40
2.4.2.2.2. Classification of section quality 41
2.4.2.3. Localization and classification of the neurons in lamina IX 42
2.4.2.3.1. Numbering and localization 42
2.4.2.3.2. Exclusion of double labeled motoneurons 42
2.4.2.3.3. Classification of labeled neurons 42
2.4.2.3.4. Diameter and area calculation of the motoneurons 43
2.4.2.4. Morphology and measurements parameters of the motoneuron column of the tibialis anterior muscle 43
2.4.2.4.1. Morphology and segmental localization of the motoneurons 43
2.4.2.4.2. Cell count 43
2.4.2.4.3. Cell density 43
2.4.2.4.4. Diameter distribution 43
2.4.2.4.5. Type distribution 44
2.4.2.4.6. Reconstruction of the cell column of the tibialis anterior muscle 44
2.4.3. Microscopic evaluation of the fluorescence tests 44
2.4.3.1. Evaluation parameters 44
2.4.3.2. Long-term fluorescence trial: Reconstruction of the cell column of the tibialis anterior muscle 44
2.4.4. Microscopic evaluation for the application of HRP in combination with fluorescent markers 45
2.4.5. Protocol 45
2.4.6. Statistics 45

3. Results 46

3.1. Test animals 46
3.1.1. Overview of the number of test animals used 46
3.1.2. Perioperative neurological status of the test animals 46

3.2. Quality control of the spinal cord sections 48

3.3. Anatomy of the lumbar spinal cord, the intraspinal plexus and the innervation area of the peroneal nerve ____ 49

3.3.1. Morphometry of the spinal column and the lumbar spinal cord ____ 49

3.3.1.1. Height of vertebral bodies T11 to L6 ____ 49

3.3.1.2. Length of lumbar segments L1 to L6 ____ 50

3.3.1.3. Cross-sectional diameter of the lumbar segments ____ 51

3.3.1.4. The lumbar spinal cord cross-section ____ 51

3.3.1.5. The spinal cord segments in projection onto the spinal column (Figure 3.9) ____ 53

3.3.2. The intersegmental lumbar plexus in the Sprague-Dawley rat ____ 55

3.3.2.1. Length of anterior roots L1 to L6 ____ 55

3.3.2.2. Lumbar intersegmental anastomoses ____ 56

3.3.3. The innervation area of the common peroneal nerve ____ 58

3.3.3.1. Topography and distances of the nerve sections of the common peroneal nerve ____ 58

3.3.3.2. Variability of the muscle nerve branches supplying the tibialis anterior muscle and extensor digitorum longus muscle ____ 60

3.4. Parameters and reconstruction of the cell column of the tibialis anterior muscle following cell marking using HRP and fluorescent dyes ____ 62

3.4.1. The appearance of the labeled anterior horn cells ____ 62

3.4.2. The localization of motor nucleus columns on the spinal cord section ____ 65

3.4.2.1. Position and orientation of the motoneurons in lamina IX ____ 65

3.4.2.2. The diffusion of HRP into neighboring muscle compartments ____ 66

3.4.3. Control tests ____ 67

3.4.3.1. Control tests with HRP ____ 67

3.4.3.2. Control tests using fluorescent dyes ____ 72

3.4.3.3. The combined use of HRP and the fluorescent dye Diamidino Yellow ____ 75

3.4.4. Parameters of the cell column of the tibialis anterior muscle ____ 77

3.4.4.1. Segmental and vertebral localization of the nucleus column ____ 77

3.4.4.2. Morphology and localization of the tibialis anterior cell column ____ 80

3.4.4.3. Cell count of the motor tibialis anterior cell column (Figure 3.25) ____ 84

3.4.4.4. Cell density ____ 85

3.4.4.5. Diameter and area of the motoneurons of the tibialis anterior muscle ____ 87

3.4.4.6. Cell types in the cell column ____ 89
3.4.4.6.1. Classification according to the stain model of the HRP labeled motoneurons ____ 89
3.4.4.6.2. Classification of motoneurons by diameter ____ 91
3.4.4.7. Distribution of alpha and gamma motoneurons in the tibialis anterior nucleus column ____ 95
3.4.4.8. 2D and 3D reconstructions of the tibialis anterior nucleus column ____ 97

3.5. Parameters and reconstruction of the spinal cell column of the tibialis anterior muscle following a radial nerve-peroneal nerve autograft on the right ____ 98

3.5.1. Macroscopic evaluation of the graft throughout regeneration ____ 98
3.5.2. Segmental localization of the cell columns following a graft over time ____ 99
3.5.3. Morphology, orientation and localization of the tibialis anterior cell column following a graft ____ 101
3.5.3.1. 3D reconstructions of the tibialis anterior nucleus column following autograft ____ 107
3.5.4. Cell count of the motor tibialis anterior cell column ____ 109
3.5.5. Cell density ____ 110
3.5.6. Area and diameter of the cells of the tibialis anterior nucleus column ____ 112
3.5.7. Cell types in the cell column ____ 113
3.5.7.1. Postoperative classification of motoneurons by staining pattern ____ 113
3.5.7.2. Postoperative classification of motoneurons by diameter ____ 114
3.5.8. Postoperative distribution of cell types along the tibialis anterior nucleus column ____ 117
3.5.9. 2D reconstructions of motor nucleus columns following autograft over time ____ 118

4. Discussion ____ 122

4.1. Topographical-anatomical requirements for the use of retrograde labeling techniques ____ 122

4.1.1. Anatomy of the peroneal nerve innervation area ____ 122
4.1.2. Morphometry of the lumbar spinal cord ____ 123

4.2. Reliability of the application of retrograde tracers ____ 125

4.2.1. Horseradish peroxidase 125
4.2.2. Fluorescent dyes Diamidino Yellow and Fast Blue 128

4.3. Topography and organization of spinal motoneuron nuclei 130

4.4. Topography of the tibialis anterior nucleus column 133

4.5. Cell count of the tibialis anterior nucleus column in control experiments and following autograft 134

4.6. Cell diameter and cell types of the tibialis anterior nucleus column on the control and graft side 136

4.7. Functional consequences 139

5. Conclusion 143

Appendix 148

References 156

List of Tables 173

List of Figures 175

Index 180

Preface

When peripheral nerves are shortened following direct damage (severed due to injury) or indirect damage (pressure, tension, burns) as a result of a loss of substance, and a primary or secondary end-to-end suture is not possible, the gap will need to be bridged via an interposed nerve graft. In standard practice, a suitable cutaneous nerve is taken from the same patient during an additional operation performed at the same time. The motor and sensory scales employed in clinical practice to document the severity of the damage, the distribution pattern, and the progress evaluation are modifications of the schemata of Highet and Holmes (Highet and Holmes, 1943; Zachary and Holmes, 1946) and the British Medical Research Council (1954) (Nicholson and Seddon, 1957) and due to their limitation to a few neurological categories only, in no way cover the full extent of the neural damage.

The tasks performed by fine motor skills, the organization of complex movements against gravity and resistance, depth sensibility (kinesthesia, stereognosis) and the integrative function of tactile gnosis, which is so important for daily life, are not taken into account. This is also the case for paresthesias and hyperesthesias, vegetative sudomotor and vasomotor disorders and for vegetative-trophic skin disorders. It is often the case that these disorders can only be partially resolved, become chronic and impair the sensitivity and physical capabilities of the patient to a significant extent.

The goal of this research is to perform an experimental investigation into the possible causes of clinical failure further to peripheral nerve lesions. It is assumed from the outset that central effects following a peripheral nerve lesion and its repair have a major effect on the reinnervation process and the functional outcome. In the spine, faults appear in the innervation pattern of the end organs as changes in the structure and organization of motor cell nuclei and afferent projection fields. The tibialis anterior muscle, with its cell column in the spinal cord of the rat following autograft of a segment of the radial nerve in the partially excised common peroneal nerve, was used as the trial system, with limitation to the reinnervation of efferent nerve pathways.

This lesion and reconstruction model, together with the neural loss of substance and the interposition of a graft, is one of the most serious types of damage for which in clinical terms, a return of function is extremely unlikely. However, as this is an area in

which the consequences of damage are the most pronounced, changes in the structure and organization of a motoneuron nucleus will most probably be observed. To be able to track the regeneration of the motor units at the morphological-topographical changes of the spinal motoneuron pool over time, the retrograde transported marker substances horseradish peroxidase (HRP) and the fluorescent dyes Fast Blue (FB) and Diamidino Yellow (DY) were used in the lesion and control tests.

Acknowledgments

My heartfelt thanks to Dr. H. Jaksche, M.D., former Chief Physician of the Neurosurgery Department of the BG Unfallklinik Murnau, and at the time of these experiments, Chief Resident of the Neurosurgical University Hospital, Homburg/Saar, for performing the nerve grafts of test series HRP2G and for an excellent cooperation.

Thank you to Mr. H. Ludt, academic contributor in the neurosurgical research lab, for programming the Fortran program executed during CPM2 for the 3D reconstruction of motor cell columns, and for his kind allowance of my change requests. This program was indispensable during the initial phase and was replaced at a later stage by commercially available software.

For participation in the preliminary trials using the retrograde fluorescent dyes Diamidino Yellow and Fast Blue, I extend my heartfelt thanks to Dr. E. Eidelberg, M.D. at the Dept. of Surgery, Div. of Neurosurgery at the University of Texas Health Science Center, San Antonio, USA.

Finally, I am extremely grateful to Dr. A. Nacimiento for providing a place to work and for the variety of discussions on the topic.

Abbreviations

CPN	Common peroneal nerve
DMSO	Dimethyl sulfoxide
DY	Diamidino Yellow
EDL	Extensor digitorum longus muscle
EDB	Extensor digitorum brevis II and III muscles
EHL	Extensor hallucis longus muscle
EHP	Extensor hallucis proprius muscle
FB	Fast Blue
FG	Fast Green
HRP	Horseradish peroxidase
ip	Intraperitoneal
LG	Lateral gastrocnemius muscle
MN	Motoneuron
NEDB	Muscle nerve branches of the extensor digitorum brevis muscle II and III
NEDL	Muscle nerve branches of the extensor digitorum longus muscle
NEHP	Muscle nerve branches of the extensor hallucis proprius muscle
NPL	Nerve muscle branches of the peroneus longus muscle
NTA	Nerve muscle branches of the tibialis anterior muscle
RN	Radial nerve
PN	Peroneal nerve
PL	Peroneus longus muscle
PB	Peroneus brevis muscle
P IV	Peroneus IV muscle
P V	Peroneus V muscle

S	Spinal segment
SN	Sciatic nerve
TA	Tibialis anterior muscle
TN	Tibial nerve
VB	Vertebral body

1. Introduction

1.1. The problems of peripheral neurosurgery

The clinical results following the surgical treatment of peripheral nerve damage are often unsatisfactory (Dellon, 1981; Millesi, 1984; Mackinnon and Dellon, 1988; Kline, 1990; Michon et al., 1990). In a summary of the literature, Mackinnon and Dellon (Mackinnon and Dellon, 1988) note normal sensitivity in less than 1% of cases and a complete restoration of motor function in 5% of cases, further to the distal suture of the median nerve in the wrist. Lesions with a more proximal location, in the upper arm or forearm, have significantly worse outcomes. On average, autologous grafts, on the other hand, result in a return of sensitivity in 2% of cases, and in 20% of cases, enable motor function to be restored.

However, this data should not lead us to draw the conclusion of the overall superiority of grafts. Nerve gaps of considerable length below the neural sutures are also mentioned (Kirklin et al., 1949; Nicholson and Seddon, 1957; Sakellarides, 1962), which, given current knowledge and advances, would have been bridged with an autologous graft with a much more promising outcome (Millesi et al., 1972; Geldmacher, 1975; Millesi et al., 1976; Samii, 1981). This change to the therapeutic approach is based on a modified evaluation of the tension at the suture point (Millesi et al., 1972; Samii and Wallenborn, 1972) and in the benefits offered by microsurgical techniques (Ito and Ishikawa, 1964; Michon and Masse, 1964; Smith, 1964; however also see Braun, 1966; Millesi, 1967).

Stookey (Stookey, 1922) has already pointed out the damaging effects of tension after refreshing the nerve stumps and performing an end-to-end suture. The standard practice of closing larger nerve gaps after mobilization or transposition of the nerve by use of an epineurial suture, with the neighboring joints in a, to some extent, extreme flexion position, did however continue (Seddon et al., 1942; Seddon, 1947; Brooks, 1955; Nicholson and Seddon, 1957). His observation that intraneural bleeding occurs with the development of scar formation during the postoperative extension of the joint as far as the normal position, constituting a barrier for the growing axon sprouts, was initially given little attention (Cairns and Young, 1940; Highet and Holmes, 1943; Highet and Sanders, 1943).

Of the alternative strategies employed to bridge large nerve gaps (Davis and Cleveland, 1934; Sanders, 1942) the use of nerve grafts became discredited since the

disappointing results achieved by Platt (Platt, 1919) and the Medical Research Council (Council, 1920), despite several clinically successful trials (Foerster, 1916; Bunnell, 1927; Ballance and Duel, 1932; Duel, 1934). The reason for this was the frequent use of heterologous grafts, which as foreign bodies, were transformed by connective tissue and which, from both an experimental (however also see Gluck, 1880; Sanders and Young, 1942) and a clinical perspective (Sanders, 1942; Seddon, 1947, 1963), were classified as being of no benefit in functional terms. Homologous transplants have been performed in human patients since Albert (Albert, 1885) with varying outcomes (Duel, 1934; Seddon and Holmes, 1944; Spurling et al., 1945; Barnes et al., 1946). The use of short, thinly calibrated, predegenerated and blood group compatible grafts was made responsible for functional improvements (Sanders and Young, 1942; Seddon and Holmes, 1944) further to short facial lesions according to Duel (Duel, 1934). However, Seddon and Holmes (Seddon and Holmes, 1944) reported the complete failure of longer homologous grafts in four cases.

Sanders and Young (Sanders and Young, 1942) and Medawar (Medawar, 1944) were the first to highlight the significance of immunological factors for the rejection of homologous grafts. Nevertheless, opinions differ as to the localization of the fundamental antigenic components of a peripheral nerve. According to Levinthal et al. (Levinthal et al., 1978b), these are in the epineurium and the surrounding tissue. For myelin, antigenity has been proven by the induction of experimental allergic neuritis (Das Gupta, 1967; Ballin and Thomas, 1969). However, even in the absence of myelin, an antigen reaction is triggered (Aguayo et al., 1979). Further to phagocytosis of the myelin debris of degenerating class I and II neurites, allogenic Schwann cells express molecules of the main histocompatibility complex (MHC) and initiate the immune response as antigen-presenting cells. However, they survive for a short time only as they themselves are recognized as target cells of the rejection reaction (Wekerle et al., 1986; Ansselin and Pollard, 1990). At an ultrastructural level, an invasion of lymphocytes, plasma cells and activated macrophages takes place, with the subsequent destruction of the nerve architecture. The endoneurial sheath, essentially the guide rail for the subsequent growth of the axons, is fragmented and collapsed (Pollard and Fitzpatrick, 1973b). Collagen is deposited in excess around the nerve fiber groups, preventing not only regeneration, but also leading to the new formation and reorganization of fascicles, with disturbed vascularization (Schröder and Seiffert, 1970).

The fact that tissue dosage affects the intensity of the immune response offers a possible explanation for the lowered antigenity of transplanted homologous fascicles compared with the nerve trunk in the rat (Medawar, 1944; Levinthal et al., 1978b). Nevertheless, according to Singh (Singh, 1976) adequate rejection takes place even at a low volume of antigen tissue.

Inhibiting a graft rejection through physical (radiotherapy, freezing, lyophilization, preservation in various media), immunobiological (induction, developing a tolerance by a neonatal transfer of antigen, anti-lymphocyte and anti-thymocyte serum), pharmacological (azathioprine, cyclosporine A, hydrocortisone) and surgical measures (thymectomy, predenervation) was judged controversially (Sanders and Young, 1942; Marmor, 1963, 1972; Pollard and Fitzpatrick, 1973a; Zalewski and Silvers, 1980; Guttmann, 1981; Mackinnon et al., 1984; Zalewski and Gulati, 1984; Mackinnon et al., 1987a; Osawa et al., 1990). The objective is to modify the immune status of the recipient, or to

manipulate the protein specificity of the transplant. The cellular carriers of the graft antigens, endothelial cells and Schwann cells have been eliminated by repeated freezing and thawing (Ide, 1983; Gulati, 1998). The remaining basal lamina of the Schwann cells promotes the growth of the axons during regeneration. This model of acellular transplant serves not only to lower the immunogenicity of the nerve graft, it also makes it possible to assess the significance of individual morphological components of the nerve for regeneration (Ide et al., 1990).

Whilst animal experiments seem to show functional, beneficial reinnervation as a genuine possibility (Sanders and Young, 1942; Ikeda, 1966; Lewis and McLaurin, 1966; Ducker and Hayes, 1970; Mackinnon et al., 1984; Gulati and Cole, 1990), which is nevertheless disputed by a few authors (Weiss and Tayler, 1943; Seiffert et al., 1972; Singh, 1976), only a few reports of successful clinical outcomes in human patients have actually been published (Böhler, 1962; Marmor, 1963; Jacoby et al., 1970; Jacoby, 1972; however compare with Marmor, 1972). The most favorable outcomes from Jacoby (Jacoby et al., 1970; Jacoby, 1972) following the use of lyophilized homografts and their sheathing with homologous, lyophilized dura, did not stand up to a critical review (Kuhlendahl et al., 1972). In experiments on the rabbit, Samii and Scheinpflug (Samii and Scheinpflug, 1974) were able to demonstrate a sufficient level of neurotization on 5 millimeter long homologous and preserved interpositioned grafts, however the clinical, electromyographical and quantitative histological results were significantly poorer compared with autologous grafts.

Differences in neural vascularization and in the variability of the main histocompatibility complex (MHC) were named as the reasons for the discrepancies in the success of regeneration between primates and non-primates. Thus, the vascular network of the sciatic nerve in the rat is thought to be less dense than in humans and macaques (Ide et al., 1990; Osawa et al., 1990) and the MHC structurally similar but less complex (Levinthal et al., 1978b, a).

On the other hand, autologous grafts were not subject to a rejection reaction. Their functional capacity as bridging material was proven by Philipeaux and Vulpian (Philipeaux and Vulpian, 1870) in electrophysiological experiments in dogs, following the interpositioning of a 2 centimeter long lingual nerve segment in the hypoglossal nerve. Bielschowsky and Unger (Bielschowsky and Unger, 1917) proved the superiority of autografts compared to allografts histologically, and recommended non-essential cutaneous nerves to close any defects in human patients, a technique already employed by Foerster (Foerster, 1916). However, due to a lack of acceptance, clinical practice of this method was initially limited to individual cases only (Bunnell, 1927; Ballance and Duel, 1932; Duel, 1933; Seddon et al., 1942).

The reasons behind this development, in addition to technical-methodical inadequacies, were theoretically based misgivings with regard to the method (Brooks, 1955; Seddon, 1963):

- In many instances, a graft was not performed until the muscle tissue of the end organ was already irreversibly damaged, or advanced muscle atrophy made the specific reinnervation of the original end plates impossible (Gutmann and Young, 1944);

- Neuromas were incompletely resected, impeding the focused growth of the axon sprouts;

- Caliber variations between the nerve endings and the graft prevented the regeneration of a quantitatively sufficient number of axons across the proximal suture site. Thus, individual cutaneous nerves were used to bridge nerve trunks that were already used as defect material, but which necrotized centrally due to the lack of a nutrient supply (Bielschowsky and Unger, 1917; Holmes, 1947);

- It was believed that, due to their smaller diameter, sensory cutaneous nerves would not offer enough space for motor axons to grow, and that regeneration of motor axons would only be partially successful (Gutmann and Sanders, 1942). In contrast, Simpson and Young (Simpson and Young, 1945) demonstrated the fiber diameter's partial dependence on the growing axons;

- Long grafts would have less chance of regeneration due to the widely held conviction that they would be vascularized by the proximal end. According to the experimental findings by Hiller (Hiller, 1951), however, nerves are primarily revascularized by the surrounding tissue and less by the proximal nerve stump. A scarred nerve bed impairs or prevents the connection to the local tissue network;

- Connective tissues would grow out of the surrounding area into the distal suture site, making it necessary to perform a resection at a later point, once the regenerating axons have grown through the graft (Davis and Cleveland, 1934). This development is favored by retraction of the nerve stumps and shrinking of the interposed nerve tissue. It has not been possible to confirm this experimentally (Sanders and Young, 1942) or clinically (Seddon et al., 1942) following autotransplantation and coaptation of the nerve endings using plasma-fibrin glue, a method pioneered by Young and Medawar (Young and Medawar, 1940). In contrast, Millesi (Millesi, 1969a) had to perform a resection of the distal suture of 2.5 centimeters in all cases following an epineurial suture for autologous grafts. With the introduction of the interfascicular graft, this high quota has been lowered;

- To prevent the formation of a scar barrier, the suture sites were processed using the most varied types of material. However, as the proliferation of connective tissue fundamentally begins in the epineurium, lining on the scar formation has no effect and in any case, impairs blood supply. To prevent dehiscence of the sutures, the graft should be 10-15% longer than the defective gap (Seddon, 1947; Millesi, 1969a; Millesi et al., 1972).

It was only after these reservations had been eliminated, and the technical, staffing and clinical requirements for a favorable prognosis identified, that the autologous graft method finally began to spread more widely (Seddon, 1947; Brooks, 1955; Millesi, 1984). Its proponents were supported by experimental trials carried out by Gutmann and Sanders (Gutmann and Sanders, 1942) on the peroneal nerve in the rabbit. A comparison between end-to-end coaptation and the bridging of a 2 centimeter long nerve gap with the tibialis nerve on the opposite side did not lead to a different outcome in functional terms. In this case, the nerve endings were stabilized using a plasma-fibrin glue.

Even after a tension-free epineurial suture, histological evaluation of the connective tissue proliferation confirmed the equal value of both methods under favorable conditions (Millesi et al., 1972). The superiority of grafts, observed experimentally by Samii and Scheinpflug (Samii and Scheinpflug, 1974) and clinically by Usbeck (Usbeck, 1976), was not confirmed by Bratton (Bratton et al., 1979), Kline (Kline, 1990) and Michon (Michon et al., 1990).

1.2. Neurobiological basics of peripheral neurosurgery

Following severance of the peripheral nerve, the distal, degenerated nerve stump offers an ideal environment for sprouting axons (Brown and Everett, 1990; Wang et al., 1992). Although the histological picture of this Wallerian degeneration has been well known since its original description by Waller (Waller, 1850) and the spatial-temporal sequence has already been investigated several times on a morphological (Cajal, 1928; Lubinska, 1977) and electrophysiological basis (Causey and Stratmann, 1953) in various ways, the underlying mechanisms remained unknown for many years. Given the axonal degeneration, it was assumed that this was autolytically preceded by a calcium-dependent activation of proteases from the injury site (Schlaepfer, 1974). The intact vascular supply distal to the lesion guarantees the recruitment of myelomonocytic cells in the degenerating area and the removal of breakdown products. The interleukin-I secreted by the macrophages stimulates the proliferation of Schwann cells, which are induced to synthesize nerve growth factor (NGF) and which then form bands of Büngner (Heumann et al., 1987; Lindholm et al., 1987; Perry et al., 1987; Brown et al., 1991). There is disagreement as to whether only the migrated macrophages are necessary to break down the myelin debris (Beuche and Friede, 1984), or if Schwann cells are also needed for this process. A model was proposed for sensory and sympathetic nerve fibers which explains the cellular interactions and the significance of NGF as a tropic factor during regeneration and embryonal development (Johnson et al., 1988).

The hypothesis that, following axotomy, Schwann cells express NGF receptors, by means of which they present the nerve growth factor to the sprouting axons, could not

be confirmed by more recent research (Raivich et al., 1991). As motor axons are independent of NGF in their growth behavior, other as yet unknown trophic molecules were postulated (Smith and Appel, 1983; Oppenheim et al., 1988). Out of all these, ciliary neurotrophic factor is one possible candidate which is already present at high concentrations under physiological conditions in the sciatic nerve of the rat, and which promotes the survival of neonatal motoneurons whose axons have been severed (Stockli et al., 1989; Sendtner et al., 1990).

The existence of neurotropic factors in the denervated peripheral nerve stump was postulated by Forssman (Forssman, 1898), and later by Cajal (Cajal, 1928). The source of these factors was viewed as local, neurolemmal cells which are meant to determine the direction of growing axon sprouts by means of neurotropism or chemotaxis. The selective reinnervation of distal sensory or motor endoneurial sheaths by homogenous axons was assigned to the end organs themselves (Cajal, 1928). This hypothesis was put forward by Weiss and Taylor (Weiss and Tayler, 1944). In a series of multiple choice experiments using an homologous, aortoiliac bifurcation as a Y-prosthesis, they established that after severance, the axons would grow without direction, guided only by local, physical factors.

This concept of 'contact guidance' had a major influence on the reconstruction of peripheral nerve lesions, as now the outcomes were ascribed solely to mechanical causes in the suture area (Lundborg et al., 1986). However, the fascicle suture recommended for anatomical reasons by Langley and Hashimoto (Langley and Hashimoto, 1917) and by Sunderland (Sunderland, 1953) was not actually possible until the introduction of microsurgical techniques (Millesi, 1968, 1969b). Its objective was to restore the intraneural, topographical model and to prevent aberration of nerve fibers into the surrounding epineurium, a common consequence of the traditional epineurial suture according to Edshage (Edshage, 1964).

Nevertheless, despite the theoretical advantage of the fascicle suture, clinical outcomes remained disappointing. In comparison with the epineurial suture, the perineurial, fascicular suture proved to be in part superior both experimentally and clinically (Bora, 1967; Grabb et al., 1970; Ito et al., 1976; Brushart et al., 1983), however in some cases, no difference could be demonstrated (Bratton et al., 1979; Hudson et al., 1979; Young et al., 1981). To prevent a coaptation of sensory with motor fascicles in the case of a mixed nerve, an intraoperative distinction was made using electrical stimulation and recording of a muscle response (Hakstian, 1968), or via histochemical staining of cholinesterase and carbonic anhydrase activities (Gruber, 1976; Riley et al., 1988). In clinical practice, these procedures did not take off due to their difficult methodology, but also as a result of the concept of the plexiform structure of the peripheral nerves established by Sunderland (Sunderland, 1978). The numerous interfascicular connections are meant to lead to an almost constant new distribution of nerve fibers, and to make a precise coaptation of the corresponding fascicles impossible, in particular if substance has been lost. This concept has been abandoned in favor of a more somatotopic organization of the nerve fibers (Jabaley et al., 1980; Hallin, 1990; Brushart, 1991).

The fact that predenervated nerves used as the graft material can lead to faster growth of regenerating axon sprouts has already been described by Cajal (Cajal, 1928). Duel (Duel, 1934) reviewed this concept on the facial nerve in primates and was able to

demonstrate accelerated growth of up to 50%. The clinical results were even more favorable and as a result, this type of procedure was recommended, despite the need for two-stage surgical intervention. Experimentally, however, only a slight and not significant acceleration in the regeneration rate was measured in the peroneal nerve of the rabbit (Young and Holmes, 1940), or even no difference at all (Sanders and Young, 1942). For this reason, Seddon (Seddon, 1947) believed this approach to be unjustified. On the other hand, more recent experimental work by Kerns (Kerns and Lucchinetti, 1992) reports on a minor acceleration in growth when predenervated nerves are used.

Tests on C57BL/Ola mice (Lunn et al., 1990; Brown et al., 1991) revealed the different claims made by motor and sensory axons on their immediate environment during the regeneration process. With this particular trunk, following axotomy, distal degeneration was significantly retarded due to the almost complete absence of macrophages and Schwann cell mitosis. While the growth of sensory axons was significantly delayed, the regeneration speed of motor efferents remained unaffected. However, the motor axons broke through the original endoneurial sheath and regenerated on the Remak cells of unmyelinated nerve fibers. In these tests at least, the chemotactic stimulus of the breakdown products does not appear to be relevant, or, however, the corresponding trophic and tropic molecules are also present when distal degeneration does not take place. The Remak cells have a major significance in this context, as they express cell adhesion molecules, such as N–CAM and L1 glycoproteins (Mirsky et al., 1986).

In addition to myelin, neurotrophic factors (Richardson and Ebendal, 1982) and cell adhesion molecules (Daniloff et al., 1986; Martini et al., 1990) the glial cells of the peripheral nerve synthesize the components of the extracellular matrix (Bunge et al., 1983). For the individual components of the basal lamina, such as type 4 collagen, nidogen, entactin, laminin, fibronectin and heparan sulfate proteoglycan, various effects on cell adhesion, elongation and branching capability of the axons were assumed (Hantaz-Ambroise et al., 1987; Neuberger and Cornbrooks, 1989; Ide et al., 1990; Wang et al., 1992). The polar construction of the basal lamina is expressed by the varying distribution of laminin and fibronectin. While laminin is located on the interior of the basal lamina and the growing axons lead into the lumen of the endoneurial sheath, fibronectin is located on the exterior and inside the stroma and facilitates the adhesion of recruited macrophages (Wang et al., 1992). This renders the observation made by Holmes and Young (Holmes and Young, 1942) comprehensible, who had observed the typically regenerating axons between the Schwann cells and the basal lamina.

Doubts were now raised as to whether the Schwann cells were absolutely necessary for effective regeneration (Schröder and Seiffert, 1970; Ide, 1983; Sketelj et al., 1989). However, the most widely accepted concept assumes that, given their necessity, the sole presence of a basal lamina should not be sufficient for successful reinnervation (Keynes, 1987; Fawcett and Keynes, 1990).

This has decisive consequences for the use of alternative strategies to bridge larger nerve gaps. Trials using acellular grafts, in which the cellular components were damaged irreversibly by repeated freezing and thawing, were only successful up to a length of 20 millimeters (Zalewski and Gulati, 1982; Gulati, 1988; Gulati and Cole, 1990). Growth of the axons over distances of up to 7 centimeters was also described in non-human primates (Ide et al., 1990). The Schwann cells of the proximal nerve stump proliferate in parallel with axonal regeneration and migrate into the graft. There are indications that

their potential for migration is limited, and that this restricts the elongation of regenerating axons. Anderson (Anderson et al., 1991) was able to prevent growth of the axons following an acellular nerve graft using the multiple ligation of the proximal nerve stump. The maximum distance to which Schwann cells migrated into the graft without axonal contact was 8.5 millimeters where distal coaptation did not occur.

There appear to be differences in the temporal-spatial sequence of the regeneration processes between acellular grafts and synthetic tube materials. Whereas in the case of acellular grafts, the Schwann cells grow out behind the axonal regeneration front (Ide, 1983), the reverse sequence is true when Silastic or silicone tubing is used as bridging material (Politis et al., 1982; Williams et al., 1983). In the animal model, a critical distance of 10 millimeters between nerve endings was identified (Lundborg et al., 1982c). This distance can be enlarged by predenervation of the distal stump to 15 millimeters (Dahlin et al., 1988), and by changing the biochemical milieu of the chamber, to 20 millimeters (Madison et al., 1985; Müller et al., 1987).

The concept of using non-neural tissue or synthetic materials as a guide rail for regenerating axons in the case of extensive neural injuries is nothing new (Weiss and Tayler, 1944). In clinical terms, the advantages with respect to grafts lie in the fact that the need to anesthetize the donator nerve in the innervation area and the possible development of a painful neuroma are avoided. In addition, closure of a defect is possible when the length of the autologous nerve material is not sufficient due to the expansion of the lesion.

However, it was only the use of modern procedures of biochemical and electrophysiological analysis which led to knowledge of the cellular and molecular interplay which takes place during the regeneration process. Advances in manufacturing techniques have made it possible to integrate specific molecules, for example laminin, in the wall of synthetic chambers (Madison et al., 1985) and via their pore size, to determine the permeability for cells and substances (Jenq and Coggeshall, 1987; Aebischer et al., 1988; Aebischer et al., 1989). Using the fiber count, Jenq and Coggeshall (Jenq and Coggeshall, 1987) were able to demonstrate a stimulating effect of the external matrix on the growth behavior of the axon sprouts. It was also possible to investigate the trophic influence of the distal nerve stump on the growing nerve fibers and their morphology (Lundborg et al., 1986). The fluid conditioned during regeneration in the chamber has a stimulating effect on adhesion, migration and proliferation of Schwann cells in culture (Le-Beau et al., 1988) and has neurotrophic activity for sensory and sympathetic ganglia (Longo et al., 1983). Conversely, this regeneration model was viewed as a trial system for potentially neurotrophic factors (Horowitz, 1989; Hollowell et al., 1990; Müller, 1990).

In addition to synthetic materials such as silicone (Lundborg et al., 1982b; Williams et al., 1988; Evans et al., 1991), acrylic (Hurtado et al., 1987; Aebischer et al., 1988), collagen (Archibald et al., 1991), polyglycolic acid (Mackinnon and Dellon, 1990b) and Millipore (Bassett et al., 1959), numerous other resorbable synthetic polyesters were used. In order to clarify the neurobiological relationships and to influence the regeneration process, the chamber interior was divided into compartments by a nitrocellulose strip (Danielsen et al., 1988), or silicone tubing was vascularized by the subcutaneous arteries (Kosaka, 1990). As the presence of Schwann cells is a prerequisite for axon elongation following the formation of exudate and a fibrin matrix (Williams et

al., 1988), tests were performed by Guénard (Guenard et al., 1992) in which syngeneic glial cells were added to the chambers. It revealed that at a higher concentration of Schwann cells, the number of myelinated fibers in the regeneration chamber rose; however, the fiber count for the autologous grafts was not achieved.

Alternatively, veins and muscle grafts were used both experimentally and in clinical practice as bridging material for short defect gaps (Norris et al., 1988; Gattuso et al., 1989; Walton et al., 1989; Glasby et al., 1990). Due to their structure, they favor the longitudinal orientation of the sprouting axons. For muscle extracts, the growth-stimulating effects on neurites and the neurotrophic impact on fetal and embryonal motoneurons of various species has been proven in cell cultures (Smith and Appel, 1983). In rats and rabbits, the basal lamina of the muscle tissue has also proven to be of equal value to the autologous grafts in functional, electrophysiological and histological terms (Fawcett and Keynes, 1986). Compared with autografts, in sheep, Glasby (Glasby et al., 1990) counted a significantly higher number of myelinated fibers distally in 5 centimeter long autologous muscle grafts. The clinical results with autologous veins (Walton et al., 1989), autologous muscle grafts (Norris et al., 1988) and regeneration chambers of polyglycolic acid (Mackinnon and Dellon, 1990a) for the reconstruction of short, digital neural defects in human patients are at the very least comparable with the classic nerve graft.

In order to specify the indication for the use of these alternative methods, Evans (Evans et al., 1991) performed an epineurial end-to-end suture, or closed the defect using silicon tubing for a gap between the nerve endings measuring 5 millimeters, after severing the sciatic nerve, in the rat. Using functional, electrophysiological and histomorphometric measurement parameters, the results were compared with and without rotating the proximal nerve stump by 180°. This manipulation was performed to provoke fascicular misinnervation. It transpired that there was no functional difference between the reconstruction using a nerve chamber and the suture of the homonymous fascicle; however, for the suture of the heteronymous fascicle, the nerve chamber was significantly superior. This led to the conclusion that, in the case of unclear fascicular topography, repair using a regeneration chamber would be the preferred method.

The significance of neurobiological factors that influence regeneration quality independently of the level of technical perfection was already pointed out by Hubbard (Hubbard, 1972). According to Mackinnon and Dellon (Mackinnon and Dellon, 1988), better clinical outcomes from advances in microsurgical techniques cannot be expected. The greater possibilities of intraneural manipulation can even increase the risk of damage, and the precise fascicle suture can prevent neurotropic factors from taking effect (Mackinnon et al., 1987b).

In this paradigm, the choice of distance between the nerve endings is crucial if neurotropic and neurotrophic factors are to control the growth of the regenerating axons. This has been proven by Brushart and Seiler (Brushart and Seiler, 1987) on the femoral nerve in the rat. In experiments using Y-prostheses made of inert, non-permeable silicone material, the motor axons of the nerve trunk had the same chance of growing in the sensory or the motor branch. Using HRP as the retrograde transported marker, they were able to demonstrate evidence of selective reinnervation of the distal motor nerve trunk by motor axons for a gap of 5 millimeters but not, however, for a gap measuring 2 millimeters. The explanation for this preference was understood by the authors to be

less a result of neurotropic mechanisms and much more due to neurotrophic mechanisms, which led to a decline in misoriented axons. This time-dependent process of the re-specification of axonal connections, which is also known as pruning, was demonstrated in a slightly modified model, even without end organ contact (Brushart, 1988, 1989).

Also, the concept proposed by Millesi (Millesi et al., 1972), that regeneration using an interfascicular nerve graft without tension is better than an end-to-end suture with moderate tension, was not confirmed (Bratton et al., 1979). Restoration of the fascicular topography at the suture site was not observed histologically (Hudson et al., 1979). The underlying reason lies in the retrograde degeneration of the proximal nerve stump, which leads to a restructuring with the formation of 'mini fascicles' (Morris et al., 1972; Mackinnon et al., 1985), which was referred to as 'neuromatous neurotization' (Schröder and Seiffert, 1970).

1.3. Objectives of the work

When peripheral nerves are damaged following direct severance due to an injury, or indirectly as a result of pressure, tension or a burn, the nerve gap which arises as a result can be bridged by a nerve graft if a primary or secondary end-to-end suture does not produce an acceptable level of tension at the suture site. For this purpose, a suitable cutaneous nerve can be removed from the same patient during an additional operation, performed at the same time as the main intervention.

To experimentally investigate the possible reasons for clinical failure following peripheral neural lesions, it is assumed that the central effects after a lesion and the repair of a peripheral nerve have a major influence on the reinnervation process and the functional outcome. Faults in the innervation pattern of the end organs manifest as changes in the structure and organization of motor cell nuclei and afferent projection fields.

The tibialis anterior muscle and its cell column in the spinal cord of the rat, further to autograft of a radial nerve segment in the partially excised common peroneal nerve, was used as the test system in this series of experiments. This lesion and reconstruction model, together with the neural loss of substance and the interposition of a graft, is one of the most serious types of damage for which in clinical terms, a return of function is extremely unlikely. Over time, the consequences of damage appear as changes to the structure and organization of a motoneuron nucleus. Horseradish peroxidase (HRP) and fluorescent dyes Fast Blue (FB) and Diamidino Yellow (DY), which are also retrograde transported dyes, were used in the lesion and control tests in order to track the regeneration process using the morphological-topographical changes to the spinal motoneuron pool.

2. Materials and Methods

The results of this study are based on tests performed on 45 male Sprague-Dawley rats. In the overwhelming majority of the experiments, retrograde labeling of the cell column of the tibialis anterior muscle was performed via injection of the enzyme horseradish peroxidase (HRP) into the muscle. Changes to the injection plan and application method, the use of fluorescent dyes Diamidino Yellow (DY) and Fast Blue (FB) as marker substances and the selection of other muscles or nerve branches as the test system became necessary as the intramuscular injection of HRP would often lead to the mismarking of motoneurons in neighboring muscles (Burke et al., 1977; Richmond et al., 1978; Janjua and Leong, 1981; McHanwell and Biscoe, 1981a; Haase, 1990). Alternatively, the nerve muscle branches of the corresponding muscle were dissected and, following transection, immersed in a marker substance solution. Table 2.1 provides an overview of the experiments performed.

2.1. Tests using horseradish peroxidase (HRP)

2.1.1. Experiments in test series HRP1

The objective of this part of the trial was the adaptation of the protocols described in the literature for enzyme histochemistry with HRP to the specific requirements of this test series (HRP1P) and the development of a graft concept which would be suitable for the respective issue (HRP1G).

2.1.1.1. Dissection, injection of HRP and integration in the HRP1P preliminary tests

To mark the cell column of the tibialis anterior muscle, two Sprague–Dawley rats (R327: 280g and R743: 350g) were anesthetized using pentobarbital (Nembutal®, Sanofi; 6.5 mg/100g body weight) via intraperitoneal injection. After shaving and disinfecting the lower extremities, the right and left muscles were exposed under clean but not aseptic conditions. Anatomically, the V-shaped tibialis anterior muscle is immediately lateral to the tibia. It is 3.5 cm long, measured from its origin at the lateral epicondyle to its insertion in the medial cuneiform bone. The muscle tapers distally and runs into its tendon around 1 cm above the ankle joint.

Table 2.1 Summary of all tests showing retrograde tracer and application methods employed.

Test		Rat	Application of the tracer	Transport time (hours/days)	Lesion type
1. Enzyme histochemistry (HRP)					
HRP1	HRP1P	R327	TA right/left: 0.45 ml HRP 5%	48	
		R743	TA right/left: 0.45 ml HRP 5%	53	
	HRP1G	R731	TA right/left: 0.45 ml HRP 5%	50	RN–CPN graft on the right
		R732	TA right/left: 0.45 ml HRP 5%	52	RN–CPN graft on the right
		R733	TA right/left: 0.45 ml HRP 5%	49	RN–CPN graft on the right
HRP2	HRP2P1	R764	TA right/left: 20 µl HRP 20%; TA left: FG 0.1%	50	
		R765	TA right/left: 10 µl HRP 40%; TA left: FG 0.1%	46	
		R766	TA right/left: 5 µl HRP 40%; TA left: FG 0.1%	49	
		R817	TA right/left: 5 µl HRP 40%; TA left: FG 0.1%	53	
		R807	TA right/left: 5 µl HRP 40%; TA left: FG 0.1%	51	
	HRP2P2	R948	TA right/left: 4 µl HRP 40%	46	CPN transection on the right side
		R963	TA right/left: 4 µl HRP 40%	45	CPN transection on the right side
	HRP2C	R1074	TA right/left: 4 µl HRP 40%	52	
		R1075	TA right/left: 4 µl HRP 40%	53	
		R1078	TA right/left: 4 µl HRP 40%	48	
		R1079	TA right/left: 4 µl HRP 40%	49	
	HRP2G	R823	TA right/left: 5 µl HRP 40%	46	RN–CPN graft on the right
		R834	TA right/left: 4 µl HRP 40%	56	RN–CPN graft on the right
		R835	TA right/left: 4 µl HRP 40%	53	RN–CPN graft on the right
		R809	TA right/left: 4 µl HRP 40%	50	RN–CPN graft on the right
		R827	TA right/left: 4 µl HRP 40%	52	RN–CPN graft on the right
		R832	TA right/left: 4 µl HRP 40%	61	RN–CPN graft on the right
		R831	TA right/left: 4 µl HRP 40%	50	RN–CPN graft on the right
		R824	TA right/left: 4 µl HRP 40%	48	RN–CPN graft on the right
		R822	TA right/left: 4 µl HRP 40%	50	RN–CPN graft on the right
HRP3	HRP3P	R818	SN right/left: HRP 40%	65	
HRP4	HRP4P	R1080	TA right/left: 4 µl HRP 40%	50	SN glue on the right side
HRP5	HRP5C	R1081	Preparation SN/PN		
		R1103	Preparation SN/PN		
		R1104	Preparation PN		
		R1105	Preparation PN		
		R1146	Preparation PN		
		R1095	NTA, right: HRP 40%	61	
		R1106	NTA right/left: HRP 40%	53	
		R1107	NEDB right/NEHP left: HRP 40%	71	
		R1115	NEDL right/NPL left: HRP 40%	62	
		R1149	NTA left: HRP 40%	71	
2. Fluorescence (DY/FB)					
F1	F1P1	R552	TA, right: 5 µl DY 2%; LG, left: 5 µl FB 2%	6 days	
		R575	TA, right: 5 µl FB 2%; TA, left: 5 µl DY 2%	4 days	
		R644	TA, right: 5 µl FB 2%; TA, left: 5 µl DY 2%	6 days	
		R645	TA, right: 5 µl FB 2%; TA, left: 5 µl DY 2%	6 days	
		R711	TA right/left: 5 µl FB 2%; LG right/left: 5 µl DY 2%	9 days	
	F1P2	R808	TA, right: 5 µl FB 2%; TA, left: 5 µl DY 2%	56 days	
3. HRP-Fluorescence (DY)					
HRPF1	HRPF1P	R1113	[1] NTA right/left: DY 2%; CPN right/left: HRP 40%	9 days/72 hours	
HRPF2	HRPF2P	R1156	[1] TA right/left: 5 µl DY 2%; CPN right/left: HRP 40%	9 days/68 hours	

Abbreviations:
P: Preliminary trial; G: Graft trial; C: Control test.
TA: Tibialis anterior muscle; LG: Lateral gastrocnemius muscle; NTA: Nerve muscle branches of the TA; NEHP: Nerve muscle branch of the extensor hallucis proprius muscle; NEDB: Nerve muscle branches of the extensor digitorum brevis muscle; NEDL: Nerve muscle branches of the extensor digitorum longus muscle; NPL: Nerve muscle branch of the peroneus longus muscle.
SN: Sciatic nerve; PN: Peroneal nerve; CPN: Common peroneal nerve; RN: Radial nerve.
HRP: Horseradish peroxidase; DY: Diamidino Yellow; FB: Fast Blue; FG: Fast Green.
[1] There are 6 days respectively between the application of Diamidino Yellow and HRP.

At its widest point, the tibialis anterior muscle measures 0.7 cm and its depth at this point is 0.5 cm (measurements from R575, 280 g). The cutaneous incision was performed 3 millimeters lateral to the sharp-edged anterior border of the tibia along a connecting line from the proximal to the distal tibial epiphysis. Care was taken to keep the muscle fascia intact. For the injection, 0.45 milliliters of a 5% HRP solution in sodium chloride (type VI, Sigma) was drawn into an insulin injection with an angled needle (G26). At the end of the injection, which was performed slowly, the muscle appeared to have a brown coloring for a few minutes. The cannula was left in the injection site for 2 minutes respectively, to prevent the solution from running out. The injection sites were sealed off using cyanoacrylate adhesive, the muscle flushed with a sterile saline solution and the skin closed (not too tightly) with single head sutures (Mersilene® 3–0, Ethicon).

After a survival time of 48 or 53 hours, the animals were perfused transcardially to induce deep narcosis with pentobarbital (Nembutal®, Sanofi; 8.0 mg/100g body weight). The abdomen was opened up to the axillary line via rib incision to the costal arch on the right and left. The axillary thoracotomy was performed by making an incision along the axillary line up to the axilla. The diaphragm was subsequently cut through on the anterior thoracic wall, and the thoracic wall folded up. After exposing the aortic root, the left ventricle tip was incised, the perfusion hose inserted as far as the ascending aorta and fixed in place with a bulldog clamp. Venous drainage of the perfusion fluid was guaranteed by an incision in the right atrium.

The test animals first received a 300 ml perfusion of a washing solution (0.8% saccharose, 0.8% NaCl, 0.4% glucose, 1% sodium nitrite in a 0.06 M phosphate buffer pH 7.4), then 500 ml of a fixing solution (2% formaldehyde, 1.25% glutaraldehyde in a 0.12 M phosphate buffer, pH 7.4) at a constant perfusion pressure of 120 mm Hg.

To remove the spinal cord, while in the prone positon and after fixing, a dorsal incision was made in the skin across the entire length of the spinal column on the median. After exposing the back muscles and dissecting the ribs, the lower thoracic intercostal nerves and the sciatic nerve mediocaudal to the head of the hip were exposed. The spinal column was laminectomized from T11 to S4 using a Luer cutter and pliers, and the spinal cord severed cleanly at the 12th rib, between thoracic vertebrae 11 and 12. The spinal cord was secured using the glass hook, and the anterior and posterior roots exposed. The roots of T13 to L6 of R347 were marked in segments using colored silk thread and trimmed distally to the marking knot. The mobilized spinal cord was placed in buffered 10% glucose solution (0.1 M phosphate buffer pH 7.4) for the purpose of marking and measuring the segments. The solution, cooled to 4 to 10° C, was replaced when warm. The spinal cord roots were ordered under microscopic control, the remaining dura removed and the segment borders thereby labeled in such a way that minutien pins with a diameter of 100–150 micrometers were made to penetrate the posterior horns of the spinal cord using Dumont tweezers. The insertion site was selected between the entry zones of the root fibers for the respective posterior roots on the right side (Figure 3.11). Segment length and spinal cord diameter at the segment borders were tapped using a pair of dividers, transferred onto protocol paper and measured. The spinal cord was then severed between L1/L2 and between L6/S1 using a razor blade, the right root L5 marked with a colored thread and all anterior and posterior roots trimmed short.

Following a storage period of up to 3 days in a glucose interim solution (Mesulam et al., 1980), the spinal cord block was frozen at –70°C in n–hexane, blocked and cut at

–18°C to –22°C in a Bright cryostat. The transversal sections measuring 40 micrometers thick were removed from the cryostat blade using preheated chromalaun gelatin coated slides (Pappas, 1971) and air-dried until enzyme histochemical staining took place.

For HRP histochemistry, the protocol proposed by Mesulam (Mesulam, 1978; Mesulam et al., 1980) was used in a modified form, without prior flushing with distilled water, without a stabilization bath of sodium nitroprusside and omitting histological counterstaining. After a 20 minute preincubation period in a 0.1% sodium nitroferricyanide solution (Sigma®, S–0501), adjusted to a pH of 3.3 in a 0.2 M acetate buffer, the reaction was started using tetramethylbenzidine (Sigma®, T–2885) as a dye with 0.3% hydrogen peroxide. The sections were air-dried, covered with DePeX (Serva®) and a cover slip, and evaluated.

2.1.1.2. Radial nerve–common peroneal nerve autograft (HRP1G)

The radial nerve from the distal upper arm was chosen as the graft due to its similarity in diameter to the common peroneal nerve. Under pentobarbital narcosis (Nembutal®, Sanofi; 6.5 mg/100g body weight), longitudinal incisions were made in three of the Sprague–Dawley rats (R731, R732, R733; body weight 200–250 g) in the skin of the dorsal lower third of the upper arm, and the radial nerve exposed between the long and lateral heads of the triceps brachii muscle. A nerve segment measuring 1 cm long was excised before the radial nerve was divided into its superficial and deep branch and preserved in physiological saline solution until the reimplantation was performed. A cutaneous incision was then made on the same side, at the level of the fibula head, parallel to the direction of the fibers of the biceps femoris muscle and the common peroneal nerve shown between the biceps femoris anterior and posterior muscles. The common peroneal nerve was severed at its crossover point with the superior muscular artery (Greene, 1955) and the radial nerve segment coapted, using microsurgical techniques, with a perineurial end-to-end suture respectively (Zeiss surgical microscope OpMi–9; Ethilon® 6–0, Ethicon). The superior muscular artery is the strongest branch of the popliteal artery and runs between the biceps femoris and the lateral gastrocnemius muscle in the caudal direction. The skin was closed at the upper and lower extremities using a continuous suture (Mersilene® 3–0, Ethicon).

2.1.2. Experiments in test series HRP2

3D reconstructions of the spinal nucleus columns from HRP1 revealed a partially considerable mislocalization of the motoneurons outside the expected area of the cell column of the tibialis anterior muscle (Figure 3.18). For this reason, the method was modified in the HRP2 preliminary trials in order to reduce the number of mismarked neurons (HRP2P1). Their number and localization were quantified by injection of an HRP solution into the tibialis anterior muscle after severing the common peroneal nerve on the same side (HRP2P2). The HRP2C test series represented the external control for the HRP2G graft series. Changes to the HRP2G graft series related to access to the common peroneal nerve and the choice of suture material.

2.1.2.1. Methodical changes in the HRP2P1 preliminary trials

In order to avoid the respiratory depression and low therapeutic index of pentobarbital which led to failures, particularly in the case of longer operation times with the need for subsequent injections to continue the narcosis, a mix of Vetranquil® (Albrecht), Rompun® (Parke Davis) and Ketanest® (Bayer) was injected intramuscularly in the 2:9:10 ratio into the gluteus maximus muscle in the R764 and R765 trials (0.12 milliliters/100 g body weight). Due to the side effects observed (stiff posture, noise sensitivity, anxiety, enduring aftereffects) the subsequent trials switched back to pentobarbital (Narkoren®, Merieux; 6.5 mg/100g body weight). The depth of the narcosis was evaluated in all trials using the reaction to sounds, flight reflex upon pain stimuli on the toes, corneal reflex, respiratory rate and the effect of trigeminal irritants.

In all tests, the HRP solution on the left side contains 0.1% Fast Green (Fast Green. FCF, Color Index No. 42053) (Conn, 1969). This dye facilitates a visual check of the distribution of HRP in the muscle (Hardman and Brown, 1985, 1987). Table 2.2 shows the methodological parameters:

Table 2.2 Test series HRP2P1 with the addition of Fast Green on the left.

Rat	R764	R765	R766	R817	R807
HRP concentration	20%	40%	40%	40%	40%
Volume (µl)	20	10	5	5	5
Injection plan[1] (X µl)	5 X 4	5 X 2	1 X 2 2 X 1 2 X 0.5	1 X 2 2 X 1 2 X 0.5	1 X 2 2 X 1 2 X 0.5
Quantity (mg)	4	4	2	2	2
Fast Green 0.1%	Left	Left	Left	Left	Left
Marking of the needle tip (mm)	5	4	3	3	3
Application	Manual	Telescopic arm	Telescopic arm	Telescopic arm	Telescopic arm
Injection time (min)	1	2	2	2	2
Waiting time (min)	5	5	5	5	5
Orientation angle	30°-45°	20°-30°	20°-30°	20°-30°	20°-30°
[1] Lowest injection quantity at the muscle ends.					

To inject the HRP solution, a Hamilton syringe was used and its needle tip marked in order to prevent a deep injection or puncture of the muscle. The injection plan of trials R766 to R807 was modified so that, in the part of the muscle with the greatest diameter, the largest volume would be applied in the middle and a low volume would be applied in a shifted z-pattern in the tapering ends. Due to the long dwell time of the cannula in the muscle, it was not necessary to seal the injection site and the muscle surface was flushed further with sterile saline solution.

From R766, the perfusion was supplemented by the prior injection of 1 ml, and then later of 0.5 ml, of a 2% sodium nitrite solution, with 200 units of heparin sodium per 100g body weight. For this purpose, a 1 cm long incision was made in the midclavicular line over the left clavicle and the jugular vein punctured at an angle of 10° through the pectoralis major muscle (Waynforth, 1980).

The subsequent perfusion was carried out according to a plan by Mesulam (Mesulam, 1982), but in a modified form (Table A.1, Appendix). To prevent artefacts,

the sodium nitroprusside quantity was reduced to 180 mg for the enzyme histochemical development (Table A.2, Appendix). According to Mesulam's protocol (Mesulam, 1982), half the sections were histologically counterstained with neutral red, or according to Adams (Adams, 1980), with thionine and then all sections covered with DePeX and evaluated (Tables A.3 and A.4, Appendix).

2.1.2.2. The diffusion of HRP into neighboring muscles (HRP2P2)

Two trials would be performed in order to establish whether labeling of the motoneurons in the lumbar spinal cord would occur following transection of the common peroneal nerve and the subsequent injection of an HRP solution into the tibialis anterior muscle. Under pentobarbital narcosis (Narkoren®, Merieux; 6.5 mg/100g body weight), after a cutaneous incision parallel to the right femur at the level of the fibula head, the common peroneal nerve was accessed between the biceps anterior and biceps posterior muscles. The nerve was severed at the crossover point with the superior muscular artery, and the proximal and distal nerve stumps were inhibited. The proximal end was drawn through a 4 mm long PVC hose and the ends sealed using polyether rubber impression material (Impregnum F®, ESPE). The skin was reclosed using continuous sutures (Mersilene® 3–0). For application of the 40% HRP solution, the tibialis anterior muscle was exposed as described in 2.1.1.1, and 4 µl of the solution injected into 6 portions of the muscle (into the midsections of the muscle, 4 X 0.85 µl, into the muscle ends, 2 X 0.3 µl). The injection time was 1 minute respectively and the cannula was left in place in the muscle for 5 minutes. Perfusion and enzyme histochemistry were carried according to the plan indicated above (2.1.2.1), without histological counterstaining.

2.1.2.3. External control tests (HRP2C)

The four experiments in this test series were used as an external control for the HRP2G graft series. The question of the extent to which a topographical and numerical right-left symmetry exists for the motor cell columns of the tibialis anterior muscle was also up for clarification. The injection and perfusion plan, including enzyme histochemistry, has been adopted from HRP2P2.

2.1.2.4. HRP2G graft series

The eight tests in the HRP2G graft series – one test did not meet the section quality criteria for the three-dimensional reconstruction and evaluation – are the key focus of this work. In order to investigate the time-dependent changes to the organization of a motor cell column following a lesion and repair of a peripheral nerve, the radial nerve - peroneal nerve autograft model already discussed in HRP1G was used. Modifications to the method related to improvements to surgical access and the strength of the suture material.

As described in test series HRP1G, in Sprague-Dawley rats (body weight 200-250 g) under pentobarbital narcosis, a 1 cm long radial nerve segment was excised on the right side and preserved in a saline solution until its retransplantation in the right common peroneal nerve. After performing a cutaneous incision in the center of the lateral side of the right lower extremity, the common peroneal nerve was exposed between the

biceps anterior and posterior muscles at the crossover point with the superior muscular artery. Using the surgical microscope, the nerve was severed and the radial nerve segment coapted with one epiperineurial end-to-end Ethilon® 10–0 thread. After the continuous sutures were completed, the animals were returned to their cages and had free access to food and water from the first postoperative day onwards. To assess the clinical-neurological deficits over time, the animals were examined once a week to test their pain perception on the arch of the foot, paralysis, toe-spreading reflex (Gutmann and Sanders, 1942) and postural control.

After 2, 4, 8 and 10 weeks, the animals were again anesthetized and injections were performed as per the injection plan for HRP2P2 of 4µl of a 40% HRP solution into the tibialis anterior muscle on both sides. In both animals (R823 and R809), 5µl HRP solution was injected (4 X 1 µl, 0.5 µl respectively into the distal and proximal muscle ends). The perfusion and enzyme histochemistry methods were taken from HRP2P2.

2.1.3. Experiments in test series HRP4

In the HRP4P trial, the sciatic nerve on the right side was severed and then coapted using nerve glue. By injecting an HRP solution into the tibialis anterior muscle on both sides and the retrograde labeling of the spinal motoneuron nucleus, the control side was used as an external reference. The nerve fibrin glue was selected as an alternative to the neural graft in the HRP1G and HRP2G series.

For this purpose, one Sprague-Dawley rat (R1080; body weight 245 g) was anesthetized with pentobarbital and an incision of 2 cm made in the skin between the vastus lateralis muscle and the biceps anterior muscle on the right side. The sciatic nerve was mobilized, underlaid with Parafilm and severed cleanly 5 mm before its division into the tibial nerve and the common peroneal nerve (Figure 3.13). The nerve endings were flushed using physiological saline solution and coaptation guaranteed using fibrin glue (TISSUCOL® Duo S, Immuno).

The time span between transection and gluing of the nerves was kept short, so that contact of the fibrin glue with the nerve cross-section as a result of retraction of the nerve stumps could be avoided. After the fibrin glue had hardened, the skin was closed using single button sutures. 24 days later, under pentobarbital narcosis, 4 µl of a 40% HRP solution was injected into both tibialis anterior muscles respectively. The injection plan as well as the perfusion performed 50 hours later, with the subsequent enzyme histochemistry, corresponded to the HRP2P2 trial.

2.1.4. Experiments in test series HRP3 and HRP5

After intramuscular injection of an HRP solution, motor cell columns of the tibialis anterior muscle were revealed in test series HRP1, HRP2 and HRP4, and contained a numerically highly varied population of motoneurons, even outside of a compact nucleus area. The partially diffuse topographical arrangement of the cells in 2D and 3D reconstructions led to suspicions of mismarking.

Thus the objective of test series HRP5 was the labeling of the motor nucleus column of the tibialis anterior muscle using an alternative method, without the drawback of the diffusion of HRP into neighboring muscle compartments, as was the case for

muscle injection. To achieve this objective, the peripheral nerve was severed and the proximal nerve ending bathed in an HRP solution (De Vito et al., 1974; Takahashi et al., 1980; Leong and Tan, 1987).

These control and reference tests were used to exclude mismarked motoneurons and to thus correct the relative frequency of morphologically classified neurons, cell count, cell density, diameter distribution and the topographical anatomy of the spinal cell column.

2.1.4.1. Retrograde labeling of the cell column of the sciatic nerve following transection and HRP nerve bath (HRP3P)

The method of application of the HRP tracer on the proximal nerve stump was initially carried out on a nerve with a larger diameter. Under pentobarbital narcosis, access on the left side was selected through a cutaneous incision between the vastus lateralis and biceps anterior muscles, as previously done in test HRP4P. After mobilization, the sciatic nerve was cleanly severed with a razor blade 5 mm above the cutaneous nerves going out towards the lateral side of the extremity (Figure 3.13). Care was taken to achieve a smooth, perpendicular intersection. The nerve was subsequently underlaid with Parafilm and a thin slit compress, and the proximal nerve stump inserted into a 7 millimeter long PVC hose with an internal diameter of 2 millimeters. The distal end of the tubes was sealed with bone wax.

The filling of the container with 2% DMSO (Sigma) in physiological saline solution was replaced after a contact time of 15 minutes with a 40% HRP solution. After 30 minutes, the HRP solution was taken out, the tubes washed repeatedly with physiological saline solution and then removed. Following a continuous cutaneous suture, a similar procedure was performed on the other side without using a DMSO solution. The perfusion 65 hours later and the enzyme histochemistry were performed according to the plan in HRP2P2.

2.1.4.2. The nucleus columns of the muscles innervated by the common peroneal nerve following transection and HRP nerve bath of the muscle nerve branches (HRP5C)

The focus of this test series was on labeling the spinal nucleus columns of the tibialis anterior muscle. In preparation, the sciatic nerves and the innervation areas of the common peroneal nerves of five rats were systematically prepared and the distances of the individual nerve segments were measured up to the branch points and muscle hili. These tests concerned animals which died intraoperatively of respiratory arrest during the waiting period between surgery and perfusion in laboratory pilot projects, or which were prepared after a scheduled perfusion (Figures 3.13-3.15). Five animals in total were assigned for labeling of the tibialis anterior cell nucleus (R1095, R1106 and R1149), the cell columns of the extensor digitorum longus on the right and the peroneus longus muscle on the left (R1115), the extensor digitorum brevis muscle on the right and the extensor hallucis proprius on the left (1107). The perfusion after an HRP transport time of 55 to 74 hours and the associated enzyme histochemistry followed the schema from HRP2P2.

2.1.4.2.1. Preparation of the muscle nerve branches of the tibialis anterior muscle (Figures 2.1 and 3.16)

The cutaneous incision between the head of fibula and the anterior border of the proximal tibia was distally extended up to the crossover into the tendon of the muscle. The broad insertion tendon of the biceps anterior, posterior and accessorius muscles, streaming into the regional fascia of the musculature of the lower leg and the tibia crest, were obliquely severed. Further preparation took place from the tendon of the tibialis anterior

Figure 2.1 Dissection and application of HRP to severed muscle nerve branches. ***a***, Labeling the nerve branches, ***b***, Immersion of the branches in a DMSO solution, ***c***, Application of HRP, ***d***, Closing the catheter.

muscle, out proximally into the space between the tibialis anterior muscle and the extensor digitorum longus muscle. After inserting the wound retractor, the deep peroneal nerve and the proximally outbound muscle nerve branches were prepared under the surgical microscope, while sparing the vessels. The point of departure of the strongest nerve branch supplying the tibialis anterior muscle between the peroneus longus and brevis muscles, as well as the nerve branches after access into the TA muscle compartment, were exposed.

Depending on the number of muscle nerve branches and their topography, one or (seldom) two catheters were used for the HRP nerve bath (Figure 3.16). The catheters were cut from a PVC perfusion hose with a 2 mm outer diameter to a length of 3 mm. After looping the muscle nerve branches (Ethilon ® 9-0, Ethicon) onto the hilus, they were distally severed and led through the prepared PVC tubes. The proximal hose opening was sealed with polyether rubber impression material (Impregnum F®, ESPE) and the partially open tubes filled with a 2% DMSO solution. After 10-15 minutes, the liquid was exchanged for a 40% HRP solution in 2% DMSO. The contact time for the HRP solution ranged from 45 minutes (R1095) to 2 hours (R1149). The HRP solution was then removed, catheters and surrounding area flushed several times with Ringer's solution, the distal end closed off with the above impression material and continuous sutures made in the skin.

2.1.4.2.2. Preparation of the muscle nerve branches of the extensor digitorum longus muscle, the extensor hallucis proprius muscle, the extensor digitorum brevis muscle and the peroneus longus muscle (Figure 3.15)

The nerve branches to the extensor digitorum longus, extensor hallucis proprius and extensor digitorum brevis muscles were prepared via the established access route. To mark the cell column of the extensor digitorum longus muscle (R1115), a single catheter was inserted, despite two separate outgoing nerve branches. The thin caliber of the short nerve branches to the extensor digitorum brevis muscle and the extensor hallucis proprius muscle called for a 2 mm long catheter.

In order to plot the motor nucleus columns of the extensor digitorum brevis muscle, the deep peroneal nerve was distally severed immediately after exiting the nerve branch of the extensor hallucis proprius muscle. The usually single nerve branch to the peroneus longus muscle was prepared following a longitudinal incision at the level of the head of the fibula, after detaching the biceps anterior muscle and locating the common peroneal nerve. Catheters were inserted and HRP applied according to the principles drawn up for the tibialis anterior muscle.

2.2. Experiments using the fluorescent markers Diamidino Yellow Dihydrochloride (DY) and Fast Blue (FB)

In addition to the HRP enzyme, fluorescent dyes are also suitable for the retrograde labeling of cells in the central and peripheral nervous system (Kristensson, 1970; LaVail and LaVail, 1972; Kuypers and Huisman, 1984). These experiments used the fluorescent

dyes Diamidino Yellow and Fast Blue. In different species, both substances are effectively transported over longer distances and due to similar transport times, can be used in trials for double labeling (Bentivoglio et al., 1980; Keizer et al., 1983). Due to the marking of different cell structures and the various colors, they are generally easily distinguishable. In addition to the advantage that they diffuse less as suspensions into neighboring structures and consequently the mismarking of spinal cells is less likely (however, see Illert et al., 1982), in comparison with the HRP method they offer the advantage of easier histological processing, without costly and extensive histochemical procedures. As well as proving the collateral connections in the central nervous system (Keizer and Kuypers, 1989; Reinoso and Castro, 1989; Verburgh et al., 1990), the topographical identification of spinal motor cell columns is also possible following the peripheral application of various fluorescent dyes to the nerve or muscle (Fritz et al., 1986b; Swett et al., 1986; Hoover and Durkovic, 1991).

2.2.1. Retrograde labeling of motor nucleus columns with fluorescent dyes

2.2.1.1. Production and storage of the fluorescent dyes

For this test series and long-term trial R808, a 2% suspension of Diamidino Yellow (Sigma®) and Fast Blue (Sigma®) in 2% DMSO (Sigma®) was produced (Keizer et al., 1983). Both dyes were portioned into 50 µl units, frozen for later use and stored in the dark at –20° C (Skagerberg et al., 1985). Due to the poor solubility behavior, the dyes were agitated for 5 minutes prior to freezing and use (Conde, 1987) and, in the trials from R575 on, also given ultrasound pulses at 50° C for 15 minutes (Branson Sonifier Cell Disrupter B15).

2.2.1.2. Handling and application of the fluorescent dyes

In 5 Sprague-Dawley rats (R552, R575, R644, R645 and R711; weight 180-280 g), the surgical access route to the tibialis anterior muscle was selected according to trial series HRP1P using pentobarbital anesthesia (Narkoren®, Merieux; 6.5 mg/100g body weight). In 4 test animals, after exposure of the muscle, 5 X 1µl FB was injected slowly on the right and 5 X 1µl DY injected slowly on the left at various points using a Hamilton syringe. In rat R711, 5 X 1µl FB was also injected into the extensor digitorum longus on the right and 5 X 1µl DY on the left.

2.2.1.3. Perfusion fixation

After 4–6 days, the rats were transcardially perfused into a deep narcosis using pentobarbital (Narkoren®, Merieux; 8.0 mg/100g body weight), first with a washing solution (300 ml 1.5% saline solution, 0.4% sodium nitrite in a 0.1 M phosphate buffer at a pH of 7.2, 500 units of heparin), then with a fixing solution (200 ml 4% paraformaldehyde solution in a 0.1 M phosphate buffer at a pH of 7.2). Dissection of the spinal cord was performed as per trial series HRP1P, in which segments L2 to L6 were refixed for 12 hours at 8°C in the fixing solution, then measured and stored for a further 12 hours in a sugar solution (30% raw sugar solution in 0.1 M phosphate buffer, pH 7.2).

2.2.1.4. Sections

After freezing and blocking, the spinal cord block was cut transversally with a section thickness of 40 µm. The sections were removed from the chromalaun gelatin (Merck®) coated slides (Pappas, 1971; Conde, 1987) and covered with Entellan (Merck®).

2.2.1.5. Histological counterstaining

For some of the sections, an H&E stain or Nissl stain with Cresyl violet was performed (Romeis, 1968), in order to test compatibility with the fluorescent marking and the possibility of a morphometric evaluation. The dye concentrations and the incubation parameters have been systematically modified for this purpose (Tables A.5 to A.9, Appendix).

2.2.1.6. Microscopic evaluation

To evaluate the sections, the Leitz® microscope MPV2 was used with an incident light filter block for fluorescence excitation at 340-380 nm (Leitz® Ploemopak A). A 100 W Hg d.c. gas discharge lamp served as the light source. On the basis of an emission maximum at 460 nm and transportation characteristics, Fast Blue can be verified in the cytoplasm as a blue substance. Diamidino Yellow is deposited in the cell nuclei of the motoneurons and satellite cells and is identified as a yellow dye.

2.2.2. The fluorescent dyes Diamidino Yellow (DY) and Fast Blue (FB) in the long-term test

To be able to perform experiments with a double labeling of the fluorescent dyes alone or in combination with HRP, it had to be verified whether the substances are still traceable in the neuron after a longer dwell time, and whether a quantitative morphometric evaluation is possible.

To answer this question, 5µl of Fast Blue were injected into the right tibialis anterior muscle and 5µl of Diamidino Yellow into the left tibialis anterior muscle, according to the above injection plan (see 2.1.2.1) and test animal R808 perfused after a survival time of 56 days. In contrast to the methodology described above, a 10% paraformaldehyde solution was used for perfusion and refixing (Kuypers and Huisman, 1984).

2.3. The combination of HRP with the fluorescent dye Diamidino Yellow

The simultaneous use of HRP and fluorescent dyes for double labeling was tested in 2 trials. The fluorescent dye was injected into either the tibialis anterior muscle or the nerve muscle branches immersed in a DY suspension prior to application of the HRP.

For the DY nerve bath (R1113), the muscles and their nerve branches were first exposed on both sides according to HRP5C, and after a 15-30 minute pretreatment, the distal nerve endings immersed in a 2% DMSO solution in a 2% DY suspension for 60 minutes. After emptying the catheter, the site was flushed several times with a physiological saline solution, the open ends of the catheters sealed using Impregnum impression material (Impregnum F®, ESPE) and the skin closed by continuous suture.

Access for injection into the muscle was chosen according to HRP1P and 5µl of the DY suspension injected into 5 points along the tibialis anterior muscle. After 9 days, further to cutaneous incision of around 1.5 cm long, the vascular nerve bundle of the common peroneal nerve was exposed by means of access between the biceps anterior and posterior muscles in both rats. Prior to entry into the muscle compartment, the nerve was looped, severed and placed into a catheter measuring approximately 4 mm long, according to HRP5C. After pretreatment with 2% DMSO, it was exchanged for a 40% HRP solution that had been left in the catheter for 45-60 minutes. The HRP solution was then drawn off and the catheter and site flushed several times with a physiological saline solution.

After 68 and 72 hours, respectively, the animals perfused under pentobarbital narcosis according to HRP1P, with the difference being that a 4% paraformaldehyde solution was used for fixing.

2.4. Evaluation

2.4.1. Macroscopic anatomy of the site and the spinal cord

2.4.1.1. Morphometry of the spinal cord segments

Following perfusion and dissection of the spinal cord, the border of the entry zones of neighboring posterior roots were marked with minutien pins in order to measure the lumbar segments (Figure 3.11). The distances of the segment length on both sides, which were taken with a pair of dividers, and the cross-sectional diameter of the spinal cord at the level of the minutien pins were recorded. To make it possible to assign the segment length and the motor nucleus columns to the vertebral bodies, their length was measured from upper edge to upper edge, and the proximal end of the spinal cord segment measured in relation to the vertebral body height.

2.4.1.2. Intraspinal plexus

In some animals, the length of the lumbar anterior roots was measured from the root entry zone in the spinal cord to the union with the posterior roots. An intraspinal fiber exchange between the nerve roots was observed (Figures 3.10 and 3.11).

2.4.1.3. The motor innervation area of the peroneal nerve

In 3 rats (R1079, R1081, and R1103), the sciatic nerve and peroneal nerve were prepared with the branches of their muscle nerve branches, and the distances between the nerve sections measured (Figures 3.13 and 3.14).

2.4.1.4. Topographical anatomy of the innervation of the tibialis anterior muscle

The topography of the nerve muscle branches leading to the tibialis anterior muscle were depicted and copied in 15 cases (Figure 3.16).

2.4.1.5. Anatomy of the graft site

In all rats with grafts, following perfusion of the animals the radial nerve autograft was exposed, a semi-quantitative evaluation of the adhesion performed, the length of the grafted segment and the distance from the distal suture to the entry point of the common peroneal nerve into the peroneal compartment measured (Figure 3.39).

2.4.2. Microscopic evaluation and computer-aided reconstruction of the HRP tests

2.4.2.1. Depicting the section images (Figure 2.2)

After an initial orienting examination, the spinal cord sections were copied in the length and segmental expansion of the cell column and the number of labeled cells were determined, and then copied via drawing tube (Olympus® BH2-DA) with an total magnification of 46x in the dark field with 4-fold objective magnification (Olympus® BHS). The outlines of the white and gray matter, the central canal, the exit point of the anterior and posterior roots and the HRP marked neurons in lamina IX were copied according to Rexed (Rexed, 1952, 1964), the dendrites and axons provided that they were also stained.

2.4.2.2. The spinal cord section in the coordinates system

2.4.2.2.1. Positioning the coordinate axis

For the purpose of quantitative evaluation, a clear film with a coordinates system drawn onto it and a grid was overlaid onto the section images in such a way that the origin of the coordinates system corresponds with the center of the central canal, and the distances between the respective points on the medial boundary of the posterior horns are identical

Figure 2.2 ***a***, Spinal cord section with HRP labeled cells. ***b***, Outline drawing with applied coordinates system for localization of the motoneurons.

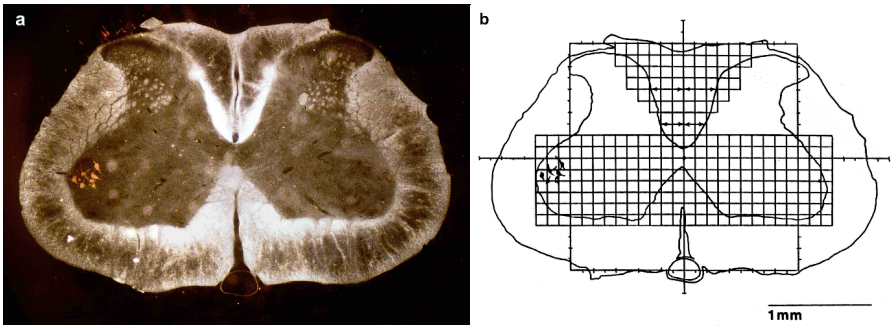

to the ordinate. In sections without a central canal due to tears or distortions, the subsequent section was used as a reference and the position of the central canal transferred (Figure 2.2).

2.4.2.2.2. Classification of section quality

The quality of the sections was evaluated. Regarding the assignment to subtypes A or B, the distances from the origins of the coordinates system to a tangent onto the gray and white matter were measured parallel to the ordinate or abscissa, the quotient determined and the distribution depicted by a value of 100. For measured values outside of 100 ± 10 on the horizontal, the section was evaluated as subtype B. The limit value was selected in the range of three times the mean cell diameter.

Table 2.3 Evaluation of section quality.

Type 1:	No tears or minor tears limited to the white substance
Type 2:	Tears in the gray substance or in the gray and white substance, but not in lamina IX
Type 3:	Tears in the gray substance or in the gray and white substance in lamina IX
Subtype A:	No, or only minimal compressions, elongations or distortions
Subtype B:	Rough compressions, elongations or distortions; Sectional plane not perpendicular to the longitudinal axis of the spinal cord

As the section quality is a fundamental determining factor for the quantitative evaluation of the material, tests using a type 3B share of over 3% in the motoneuron nucleus area were excluded from a quantitative analysis.

2.4.2.3. Localization and classification of the neurons in lamina IX

2.4.2.3.1. Numbering and localization

The identification of labeled motoneurons was carried out by assignment to the numbered grid fields of the transparent film and by the addition of x, y and z coordinates.

The assignment to a field number in the grid is used for an initial position assessment and to determine the cell density. The grid consists of quadrants with an edge length of 5 mm. The customary sign assignment applies to the count in the four quadrants of the oriented coordinate axis. Cells located on the edges are assigned to the field with the lower field count (Figure 2.2).

After field assignment in the grid, the position of the cells in the spinal cord cross-section was measured in absolute millimeters and calculated as a relative percentage value, based on the limitation of the gray substance. The value on the z axis in the craniocaudal numbering method was defined by the section number at a section thickness of 40 micrometers. The x, y and z coordinates were also used to number the identified neurons. Mismarked motoneurons outside a definable cell column were excluded from further evaluation. For this purpose, the coordinates for the cell columns for which HRP had been applied directly to the nerve were used as a comparison. Motoneurons outside the maximum relative coordinates of these nucleus columns were viewed as potentially mismarked cells and excluded.

2.4.2.3.2. Exclusion of double labeled motoneurons

To avoid counting cell fragments in the neighboring sections twice and thereby producing a false high cell count, the section drawings were first projected over each other and the localization and morphology of potential fragments compared. In individual cases, detailed records of the cells were produced at higher magnification for the purpose of clarification.

2.4.2.3.3. Classification of labeled neurons

The neurons were classified based on the intensity of the HRP labeling. The distinctions were as follows:

Table 2.4 Classification of HRP labeled motoneurons.

I.	**Cells**	
	IA	All features discernible: Soma, nucleus as cutout shape and cell protuberances
	IB	Soma and protuberances labeled, cell nucleus hidden due to intensive staining
	IC	Soma labeled, nucleus visible, protuberances not discernible (ring shape)
	ID	Soma labeled, nucleus and protuberances not discernible (full moon shape)
	IE	Soma incompletely labeled or dye spread diffusely at a low intensity in the cytoplasm, cell nucleus and cell protuberances not discernible
II.	**Artifacts**	

2.4.2.3.4. Diameter and area calculation of the motoneurons

Using a graphics tablet (Summagraphics®, SummaSketch III) and proprietary software, the cell contours were read into the computer at 20 times objective enlargement and the mean diameter of the neurons calculated based on the area.

2.4.2.4. Morphology and measurements parameters of the motoneuron column of the tibialis anterior muscle

2.4.2.4.1. Morphology and segmental localization of the motoneurons

On the basis of the marking of the segment borders by minutien pins, the segmental position of the motor nucleus column of the tibialis anterior muscle was determined and correlated to the height of the vertebral bodies. The length, diameter and shape of the nucleus column were shown using three-dimensional reconstructions of the cell columns. The middle section of the spinal cord cross-section marked by minutien pins was used as the segment border (Figures 3.11 and 3.17a).

2.4.2.4.2. Cell count

The cell count of the motor nucleus columns was provided in neighboring sections after correction for double-counted cells. For this purpose, the profiles and the absolute and relative coordinates of the motoneurons were compared in bordering section images, and the probability of double counting of cell fragments estimated. In test series using HRP labeling of the cell column of the tibialis anterior muscle, incorrectly located cells were identified following 3D reconstruction of the nucleus column and by comparison with the motoneuron coordinates further to application of HRP to severed nerve branches and excluded from the evaluation process (see 3.4.3.1).

2.4.2.4.3. Cell density

Cell density was calculated for the reconstructed 2D and 3D nucleus columns of the control tests (n = 16) and the graft experiments (n = 8) in a transversal, horizontal and sagittal section level, interpolated over 8 craniocaudal sections of the cell column (Figures 3.30, 3.31 and 3.48), or based on the already available cell totals for the grid fields (Figures 3.21-3.23 and Figures 3.44-3.46).

2.4.2.4.4. Diameter distribution

The distribution of the cell diameter along the craniocaudal axis of the cell columns was calculated and presented for the experiments performed in the reconstructed control tests (Figures 3.32-3.34 and Figure 3.49).

2.4.2.4.5. Type distribution

The diameter of the neuron types classified by HRP dye density (2.4.2.3.3) was compared between the control series HRP2 and HRP5 and graft series HRP2G (Figures 3.35 and 3.50).

Classification of the motoneurons into different size categories was carried out according to the diameter distributions. Alpha 1, alpha 2 and gamma motoneurons were distinguished based on their bi- or trimodal distribution in histograms, and their percentage share in the nucleus columns and, after subdivision into 4 craniocaudal segments, calculated for the control and graft series (Figures 3.37 and 3.52).

2.4.2.4.6. Reconstruction of the cell column of the tibialis anterior muscle

2D and 3D reconstructions of the motor cell columns were performed. The absolute x, y and z coordinates of the motoneurons and the lateral, ventral and dorsal limitation of the gray spinal cord matter had already been measured as part of the initial evaluation after marking the section images. It was therefore possible to produce a three-dimensional image of the cell column of a single experiment. To be able to show the cell columns of several tests together, the relative x and y position of a cell was assigned to the tangent on the gray matter parallel to the ordinate or abscissa of the applied coordinates system. The comparability in the z axis was achieved by a standardization of the segment length to 100%, whereby differences in the intermediary segment length L3 to L5 from every test were not considered (Figures 3.24, 3.38 and 3.53-3.55).

2.4.3. Microscopic evaluation of the fluorescence tests

2.4.3.1. Evaluation parameters

The spinal cord sections of the fluorescence tests were evaluated using UV incident light excitation (Leitz® MPV2 with Leitz® Ploemopak A, first Xenon 75 W, then mercury 100 W as the light source). Under these conditions, a distinction of the cells marked with Diamidino Yellow or Fast Blue was possible based on the color and marking of different cell structures. The cell count was corrected by the double counted cell fragments in the neighboring sections. The cell columns of the tibialis anterior and gastrocnemius lateralis muscles were measured at their longitudinal expansion and a segmental localization was performed.

2.4.3.2. Long-term fluorescence trial: Reconstruction of the cell column of the tibialis anterior muscle

The sections for long-term test R808 were photographed under UV excitation at an enlargement of 50 times (Agfachrome® 1000RS) and the cutout photos stapled together after edge comparison. As explained in 3.4.2, after application and alignment of the coordinates system, the white and gray spinal cord matter was measured at its maximum extension, and the position of the motoneurons stipulated absolutely, and also relatively, in relation to the limitation of the gray substance. This enables the shared reconstruction

and representation of the cell columns further to fluorescence and HRP marking (Figures 3.24 and 3.38).

2.4.4. Microscopic evaluation for the application of HRP in combination with fluorescent markers

An evaluation of tests R1113 and R1156, in which HRP was combined with fluorescent markers Diamidino Yellow and Fast Blue, was carried out only for cell count and segmental localization of the nucleus column of the common peroneal nerve.

2.4.5. Protocol

Protocols were drawn up for both the fluorescence and the HRP tests, in order to document the trial sequence and the results:

Table 2.5 Protocol forms for documentation of the trial parts.

1.	Surgical protocol
2.	Clinical progress
3.	Handling protocol
4.	Initial evaluation
	• Evaluation protocol
	• Section quality
	• Area
	• Cell types
	• Cell density
	• Cell column parameters
5.	Topography of the cell columns in the spinal cord
6.	Test evaluation

2.4.6. Statistics

For correlations of morphometric parameters (vertebral body length, segmental length and weight), the product moment-correlation coefficient according to Pearson was employed. In a sufficient number of the experiments, tests were conducted for group differences in quantitative characteristics (length of anterior roots, segmental length and diameter, cell counts, cell diameter) by means of t-test, and in multiple groups for significant differences by means of variance analysis and posttest according to Tukey. Nonparametric tests were used if prerequisites were missing (Mann-Whitney test, H-test by Kruskal and Wallis with posttest according to Dunn). The cell types were tested by classification according to the intensity of the HRP marking, or with respect to the diameter, for distribution differences along the nucleus column using the $\chi 2$ test. The statistical tests were calculated using the software programs SigmaStat (SPSS Inc.®) and GraphPad (Graphpad Software®). All tests were two-tailed; $p<0.05$ was graded as having low significance, $p<0.01$ as significant and $p<0.001$ as highly significant (Motulsky, 1995).

3. Results

3.1. Test animals

3.1.1. Overview of the number of test animals used

The loss quota of the 50 animals originally used for the various sub-projects was 28%. Only 18% of the Sprague-Dawley rats were lost as a result of the anesthetic during surgical procedures. The loss rate in test series HRP5 was initially 55% due to the considerably longer operation times owing to the dissection of the muscle nerve branches and application of HRP to the nerve, with the need to repeat further injections of pentobarbital. Three animals (6%) were lost due to perfusion or subsequent processing.

For 37 test animals, the retrograde labeled motor cell columns of the lumbar spinal column were evaluated quantitatively, which comprised of 29 HRP tests, 6 tests after application of the fluorescent dyes Fast Blue and Diamidino Yellow and 2 tests in which HRP was combined with fluorescent markers. In 19% of the experiments using HRP, marking of the motoneurons was insufficient with a low cell count (also see Nicolopoulos-Stournaras and Iles, 1983). A majority of the lost animals were used for anatomical-topographical and morphometric measurements (Table 2.1).

3.1.2. Perioperative neurological status of the test animals

The test animals that were operated on were extensively examined, behaviorally and neurologically. During the postoperative process, possible weight bearing, restrictions of pain and movement and neurological deficits could thereby be reliably assessed. Experience shows that the effect of the general anesthetic on the day of surgery lasted for another few hours and the test animals had an increased need for sleep. After the sole injection of a retrograde transported tracer into the muscle, in individual cases, protection of the corresponding extremity appears immediately postoperatively and is no longer observed on the following day. Neurological deficits and signs of pain did not occur in the test animals at any point.

With the application of either HRP or fluorescent dyes to the severed muscle nerve branches, in acute trials, the functional loss of the tibialis anterior muscle is compensated for the least. Until perfusion on the following day, the trial animals show unusual dorsal flexion in the affected foot joint, with a marked pain-avoiding posture when standing and running and a tendency to bend the extremity at the knee joint, to avoid contact of

the foot with the ground. Hypesthesia or hyperpathy around the cutaneous suture was no longer clearly evident on the first postoperative day. The size of the catheter used for the nerve bath and the thusly induced local mass influences retention of the gait, although all test animals were able to stand independently on their rear extremities.

Following a radial nerve-peroneal nerve autograft on the right, motor deficits were most easily demonstrated by a test in which the rat, after raising up on its hind legs by holding up its tail, shows a dorsiflexion of the foot with spread toes in a typical fashion. This placement reaction was evident during the first 2 postoperative weeks. In the first postoperative week, there became apparent an insensitivity over the dorsum of the foot, and in the adjacent skin areas not innervated by the common peroneal nerve, an oversensitivity to tactile stimuli. Between the 3rd and 4th postoperative weeks, the ability to spread toes and dorsiflexion in the ankle were, in the rare comparison, even weaker, and after 8 weeks a restriction of movement was no longer definitely present. At this point it was no longer possible to prove any sensitivity disturbances.

Table 3.1 *a*. Quality assessment of the spinal cord sections using basic parameters (presence or lack of the central canal, number of missing sections, evaluation of section quality in qualitative terms and using quantitative measurements).

		R327	R766	R1074	R1095	R1149	R1107	R808	Total
Central canal									
Shown	n	58	83	67	73	57	12	36	**386**
	%	*82.9*	*98.8*	*100.0*	*93.6*	*100.0*	*100.0*	*100.0*	***96.5***
Not shown	n	12	1	0	5	0	0	0	**18**
	%	*17.1*	*1.2*	*0.0*	*6.4*	*0.0*	*0.0*	*0.0*	***3.5***
Section quality									
S1-A	n	0	44	25	22	57	10	34	**192**
	%	*0.0*	*52.4*	*37.3*	*28.2*	*100.0*	*83.3*	*94.4*	***56.5***
S1-B	n	0	0	2	0	0	0	2	**4**
	%	*0.0*	*0.0*	*3.0*	*0.0*	*0.0*	*0.0*	*5.6*	***1.2***
S2-A	n	40	18	22	55	0	1	0	**136**
	%	*57.1*	*21.4*	*32.8*	*70.5*	*0.0*	*8.3*	*0.0*	***27.2***
S2-B	n	16	0	1	0	0	0	0	**17.0**
	%	*22.9*	*0.0*	*1.5*	*0.0*	*0.0*	*0.0*	*0.0*	***3.5***
S3-A	n	14	22	17	1	0	1	0	**55**
	%	*20.0*	*26.2*	*25.4*	*1.3*	*0.0*	*8.3*	*0.0*	***11.6***
S3-B	n	0	0	0	0	0	0	0	**0**
	%	*0.0*	*0.0*	*0.0*	*0.0*	*0.0*	*0.0*	*0.0*	***0.0***
Missing sections									
n		1	2	1	0	1	0	0	***5***
%		*1.1*	*1.8*	*1.1*	*0.0*	*1.4*	*0.0*	*0.0*	***0.8***
Dimension									
White matter									
right/left	M	103.6	101.8	103.6	100.5	100.9	99.9	101.0	**101.6**
	s	*4.4*	*3.0*	*5.0*	*2.2*	*3.3*	*2.5*	*3.4*	***3.4***
d/v	M	103.2	102.7	111.6	107.9	100.2	98.8	99.0	**103.3**
	s	*4.7*	*6.9*	*12.1*	*6.6*	*2.7*	*2.1*	*8.0*	***6.2***
Gray matter									
right/left	M	106.3	101.9	100.7	101.1	100.2	105.2	100.0	**102.2**
	s	*6.8*	*2.3*	*5.2*	*2.1*	*4.6*	*7.1*	*4.8*	**4.7**
d/v	M	153.3	150.8	145.3	175.6	180.6	148.4	174.0	**161.1**
	s	*10.6*	*9.2*	*17.1*	*9.9*	*10.2*	*8.8*	*9.9*	**10.8**

Abbreviations:
For classification of the sections, see 2.4.2.2.2.
M: Mean, *s*: Standard deviation; d: dorsal, v: ventral.

During the preoperative and postoperative observation periods, no mutilations or a refusal to eat or drink occurred in any of the test animals. The surgical sites remained consistently unremarkable and wound healing took place within a few days.

3.2. Quality control of the spinal cord sections

Due to incomplete marking or a lack of specificity of the marking of the target nucleus column, 10 experiments in the HRP series were excluded from further evaluation, including a reconstruction of the cell columns.

The tests listed in Table 2.1 fulfilled the conditions stipulated in 2.4.2.4 as a prerequisite for reconstruction. The cell columns following the retrograde transport of fluorescent dyes could be reconstructed, except for long-term test R808 due to missing technical and instrument-related requirements.

Table 3.1 *b*. Quality assessment of the spinal cord sections in graft series HRPG2.

		R823	R834	R835	R809	R827	R831	R824	R822	Total	3.1 a+b
Central canal											
Shown	n	80	94	76	80	96	88	82	66	**662**	**1048**
	%	*94.1*	*95.9*	*100.0*	*93.0*	*95.0*	*100.0*	*100.0*	*98.5*	***97.1***	***96.4***
Not shown	n	5	4	0	6	5	0	0	1	**21**	**39**
	%	*5.4*	*4.1*	*0.0*	*7.0*	*5.0*	*0.0*	*0.0*	*1.5*	***2.9***	***3.6***
Section quality											
S1-A	n	18	0	1	12	73	88	81	64	**337**	**529**
	%	*21.2*	*0.0*	*1.3*	*14.0*	*72.3*	*100.0*	*98.8*	*95.5*	***50.4***	***48.7***
S1-B	n	0	0	0	0	0	0	1	1	**2**	**6**
	%	*0.0*	*0.0*	*0.0*	*0.0*	*0.0*	*0.0*	*1.2*	*1.5*	***0.3***	***0.6***
S2-A	n	22	45	32	43	23	0	0	1	**166**	**302**
	%	*25.9*	*45.9*	*42.1*	*50.0*	*22.8*	*0.0*	*0.0*	*1.5*	***23.5***	***27.8***
S2-B	n	0	5	3	0	1	0	0	0	**9**	**26**
	%	*0.0*	*5.1*	*3.9*	*0.0*	*1.0*	*0.0*	*0.0*	*0.0*	***1.3***	***2.4***
S3-A	n	44	47	39	30	4	0	0	1	**165**	**220**
	%	*51.8*	*48.0*	*51.3*	*34.9*	*4.0*	*0.0*	*0.0*	*1.5*	***23.9***	***20.2***
S3-B	n	1	1	1	1	0	0	0	0	**4**	**4**
	%	*1.2*	*1.0*	*1.3*	*1.2*	*0.0*	*0.0*	*0.0*	*0.0*	***0.6***	***0.4***
Missing sections											
n		1	1	4	6	1	0	3	0	***16***	***21***
%		*0.9*	*0.8*	*4.3*	*4.6*	*0.6*	*0.0*	*2.8*	*0.0*	***1.7***	***1.4***
Dimension											
White matter											
right/left	M	98.7	102.8	100.7	97.5	102.3	100.5	101.4	100.5	**100.6**	**101.0**
	s	*2.8*	*5.0*	*3.0*	*3.7*	*3.7*	*2.1*	*3.3*	*3.1*	***3.3***	***3.4***
d/v	M	124.5	110.4	112.5	113.0	111.5	106.1	105.7	102.0	**110.7**	**107.3**
	s	*5.7*	*10.2*	*8.4*	*7.8*	*8.6*	*5.3*	*8.6*	*4.9*	***7.4***	***6.8***
Gray matter											
right/left	M	99.7	101.0	103.4	100.4	101.3	98.7	101.5	101.7	**101.0**	**101.5**
	s	*3.0*	*5.6*	*3.4*	*4.0*	*2.8*	*2.2*	*3.2*	*3.0*	***3.4***	***4.0***
d/v	M	195.0	151.6	177.2	172.5	165.2	169.6	172.2	174.3	**172.2**	**167.0**
	s	*13.4*	*13.7*	*10.7*	*14.5*	*10.5*	*8.5*	*10.2*	*12.2*	***11.7***	***11.3***

Abbreviations:
For classification of the sections, see 2.4.2.2.2.
M: Mean, s: Standard deviation; d: dorsal, v: ventral.

The mean rate of missing sections in tests using reconstructed cell columns was 1.4%, and for all quantitatively evaluated tests, 1.9%. On average, the central canal was in 96.4% of the sections retained and the lowest value was 82.9% for R327. Here, however,

the central canal and thus the central point of the coordinates system could be transferred from the immediately neighboring section images. Overall, 3.3% of the sections were classified as subtype B based on the established criteria. The highest value of the reconstructed series was calculated for R327 with 22.9%, thus almost one quarter of the sections contain a cell coordinates error of at least 100 µm.

Referring to the white or gray matter, the spinal cord half quotients with values of 101.0 and 101.5 are almost symmetrical, and the error far below the cell diameter. The dorsoventral quotient of gray matter was 107.3, for white matter 167.0 and has thus shifted in favor of the dorsal spinal cord sections. The proportion of approximately 50% of type S3-A sections is high in the R823, R834 and R835 tests, without this having led to a fundamental change to the spinal cord symmetry due to compression or elongation.

3.3. Anatomy of the lumbar spinal cord, the intraspinal plexus and the innervation area of the peroneal nerve

3.3.1. Morphometry of the spinal column and the lumbar spinal cord

3.3.1.1. Height of vertebral bodies T11 to L6

The weight of the morphometrically evaluated male Sprague-Dawley rats lies between 220 g and 553 g. The length of the lumbar spinal column L1-L6 measures 45.8 mm on average, with a span of 39.1 mm to 51.2 mm. The vertebral bodies increase in height from L1 upwards and reach a maximum at L4 and L5 (Table A.10, Appendix). The variation coefficients for the measured results lie between 2.9% and 16.5%. A statistically significant correlation exists between the weight of the rats and vertebral body length L1-L6 (product-moment correlation according to Pearson, $r = 0.933$, $P < 0.001$).

Figure 3.1 Length of the vertebral bodies (mean values in mm).

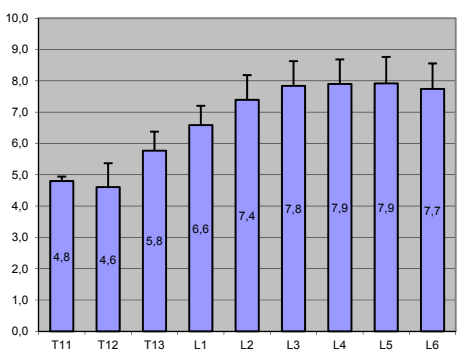

Figure 3.2 Dependency of the vertebral body length on weight.

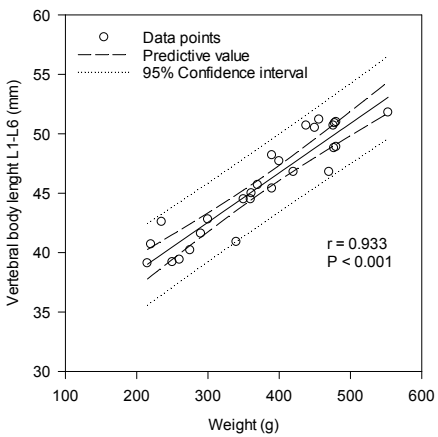

3.3.1.2. Length of lumbar segments L1 to L6

The rat's rounded thoracic spinal cord transitions into the 6 horizontal oval lumbar segments, and proceeds again towards the sacrum in a rounded spinal cord section. The total length of the lumbar spinal cord amounts in external measurement to 17.3 ± 1.6 mm. The segment lengths decrease continuously from L1 to L6 up to approximately 2/3 of the initial length, with the exception of the first two lumbar segments which have a similar linear expansion. Contingent upon the various methods of measurement, segment length differentiates between external and internal measurement (Tables A.11 and A.12, Appendix).

Figure 3.3 Segment length with external (***a***) and internal (***b***) measurement (mean values in mm). *Right* diagram side: Segment length with measurement on the right spinal cord side, *left* diagram side: Measurements on the left.

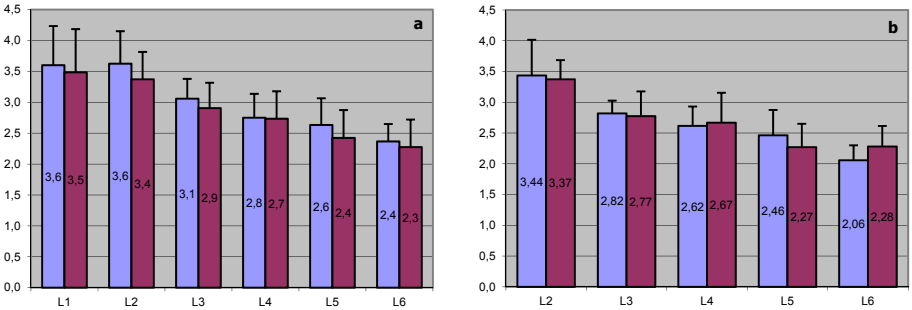

Figure 3.4 Dependency of the length of the lumbar spinal cord on weight for external (***a***) and internal (***b***) measurement.

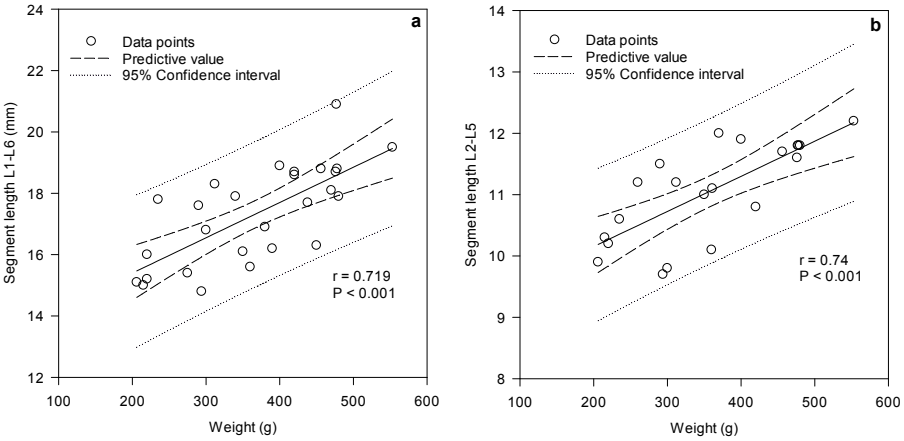

When measuring the parameters after freezing and cutting the tissue and the subsequent enzyme histochemistry, slightly lower values are measured in all segments. Although the absolute difference of segments L2-L6 seems low at 0.3 mm (external measurement: 13.8 ± 1.1, internal: 13.5 ± 1.0), the differences are statistically significant after the formation of associated measured values (Wilcoxen test, P = 0.004).

Despite noticeably different side measurements in a few segments (Figure 3.3), the differences for lumbar segments L2-L6 are not statistically significant for the external or internal measurements (Mann-Whitney U test, P = 0.345 resp. = 0.622). Between the weight of the rats and the length of the lumbar spinal cord, compared with vertebral body length, there exists a less distinct but still significant correlation (external measurement: r = 0.719, P<0.001; internal measurement: r = 0.738, P<0.001).

3.3.1.3. Cross-sectional diameter of the lumbar segments

The cross-sectional diameter of the spinal cord was measured externally from T12 to L6. It measures 3.0 mm on average and increases in width from the lower thoracic segments onwards, reaching a maximum at L3, and then falls again. The smallest lumbar cross-section diameter at the level of L6 is 2.2 mm. The mean segment length L1-L6 is 2.9 mm. The ratio of segment length to segment width falls from L1 (1.11:1) to a minimum at L3 and L4 (both 0.83) and regains a value of 1.01:1 at L6 (Tables A.13 and A.15, Appendix).

Figure 3.5 Cross-sectional diameter of the segments (mean values in mm).

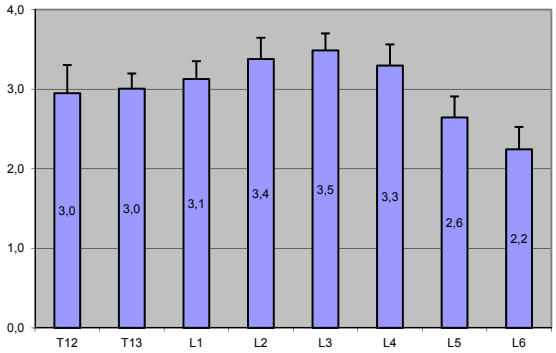

3.3.1.4. The lumbar spinal cord cross-section

In the lumbar segments, the central canal has an extremely oval shape and lies ventrally to the spinal cord center (Table A.16, Appendix). The dorsoventral ratio of the spinal cord halves, based on the central canal as the central point, is 1.07:1 for the white matter and 1.67:1 for the gray matter. The ratio of the cross-sectional diameter to the longitudinal diameter of the white matter decreases in segments L3 (1.47:1) over L4 (1.42:1)

towards L5 (1.36:1) relevant for the motor nucleus column of the tibialis anterior muscle. The gray matter quotients fall accordingly (L3 1.54:1; L4 1.52:1; L5 1.46:1). The white matter decreases in cross-sectional diameter from L3 to L5, less in the longitudinal diameter, while the gray matter holds the largest expansion in segment L4 (Table A.15, Appendix). The ratio of gray to white matter increases from L3 to L5 in the cross-sectional diameter (L3 0.75:1; L4 0.79:1; L5 0.79:1) and longitudinal diameter (L3 0.72:1; L4 0.73:1; L5 0.74:1).

Figure 3.6 Cross-sectional diameter of the spinal cord segments L3-L5 (internal measurement in mm).

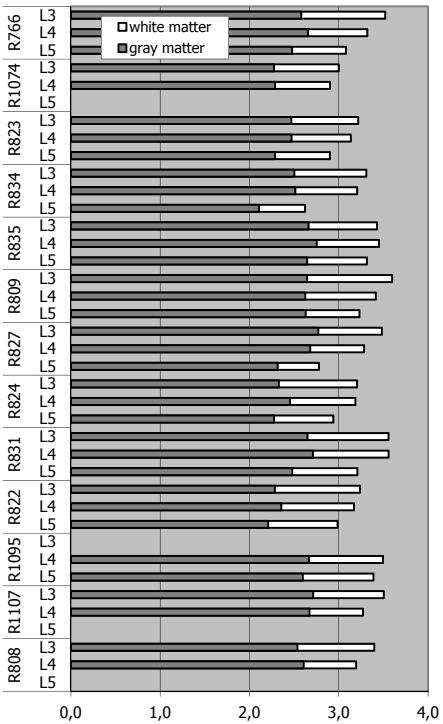

Figure 3.7 Longitudinal diameter of the spinal cord segments L3-L5 (internal measurement in mm).

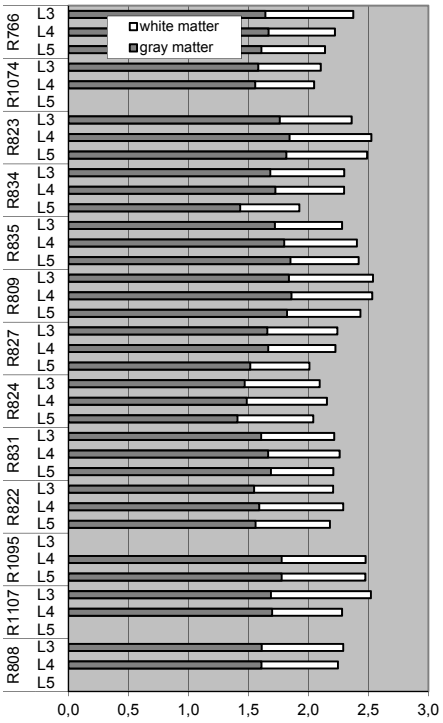

3.3.1.5. The spinal cord segments in projection onto the spinal column (Figure 3.9)

The projection of spinal cord segments L1-L6 onto the spinal column is subject to a variability of 1 to 1.5 segments (Figure 3.8). An awareness of this variability is key when planning the surgical access route further to labeling tests or spinal surgical intervention.

Figure 3.8 Difference in height localization between the spinal cord and spinal column.

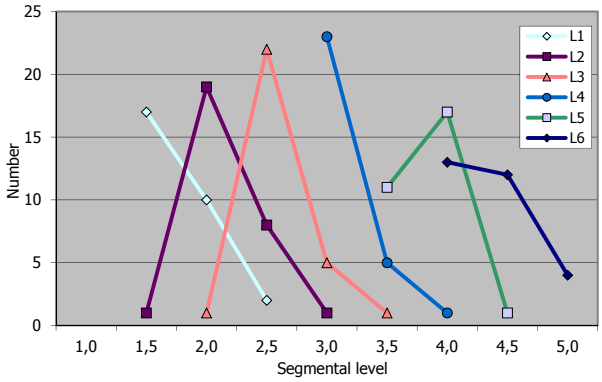

The difference between the spinal cord segment and the position of the corresponding vertebral body in the caudal direction increases almost regularly from 1.5 to 4 segments. Of a total number of 29 test animals, most of the spinal segment for L1 lies 1.5 segments above the vertebral body segment with the same name, i.e. at level of T12/13. On the other hand, in the majority of cases, spinal segment L6 projects onto vertebral body L2. Based on segments L3, L4 and L5, which are relevant for the nucleus column of the tibialis anterior muscle, the L3 segment can be found at the level of the vertebral bodies T12/13 to L1, and segment L4 at the level of vertebral bodies T13 to L1. Segment L5 is located at the level of the crossover area from T13/L1 to L1/L2.

It must be taken into account that the elongation of the proximal spinal cord segments cannot be used, as the severance point was made at the intervertebral disc level and the corresponding segment of the spinal cord is generally only partially present.

Figure 3.9 Segments L1 to L6 projected onto the spinal column for external measurement. VB: Vertebral body, S: Spinal segment.

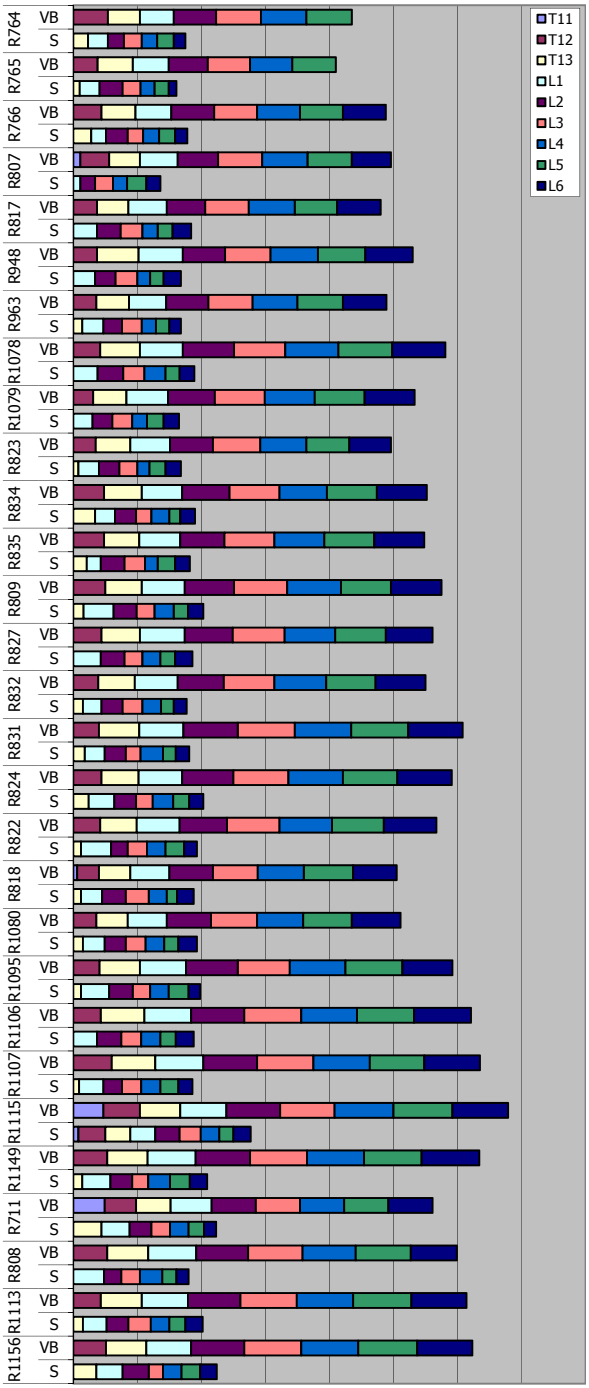

3.3.2. The intersegmental lumbar plexus in the Sprague-Dawley rat

3.3.2.1. Length of anterior roots L1 to L6

In a few test animals, the lengths of the anterior and posterior roots from the union point around the spinal ganglion to the entry point in the spinal cord were measured on the right and left sides (Figure 3.10).

With the measurement method used, there were no verifiable differences between the length of the anterior and posterior roots. The numerous neural cross connections between neighboring nerve roots, which lead to lengthening of the distances, were not taken into account when measuring the length of the anterior roots. The side differences for the lengths are statistically not significant for all nerve roots (t test, $\alpha = 0.05$).

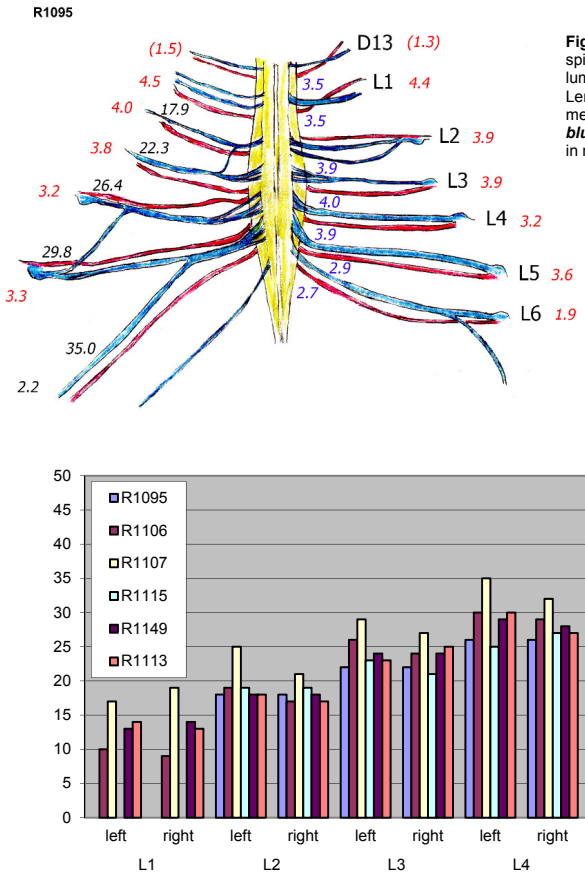

Figure 3.10 Morphometry of the lumbar spinal cord. *Above:* Preparation of the lumbar spinal cord with nerve roots. Length of the anterior roots: ***black***, segment length: ***red***, segment diameter: ***blue***. *Below:* Length of the anterior roots in mm (ordinate axis).

The length of the anterior roots increases from an average 13.6 mm for L1 to 39.3 mm for L6, which corresponds to a tripling of the initial length (Table A.14, Appendix). Nerve roots L3 to L5, which innervate the tibialis anterior muscle, have clearly different root lengths ranging from 24.2 mm (L3), 28.6 mm (L4) and 33.8 mm (L5).

The different lengths of the nerve roots, which constitute an average of 5.1 ± 0.6 mm between neighboring roots, partially contribute to the distinct distance between the end organ and the neural processing structures of the spinal cord and can be observed in the choice of survival time in retrograde labeling tests, and thereby in the transport time of the matter.

3.3.2.2. Lumbar intersegmental anastomoses

The macroscopically visible connections between neighboring nerve roots was evaluated in 8 test animals without producing histological section images for the precise fiber orientation. For all animals, anastomoses of varying sizes were found between the posterior roots (Tables 3.2 and 3.3, Figure 3.11). However, there was no evidence of fiber connections between the anterior and posterior roots. Nerve root L5 is the nerve root with the widest diameter, and can be used as an initial orientation aid during dissection. Measured at the normal diameter of the respective posterior root, the anastomoses are predominantly thinly-calibered and, to some extent, difficult to maintain during preparation. The direction of the exchanged fiber connections primarily runs from the proximally located nerve root to the directly caudally located nerve root. In 28% of the total 25 anastomoses, the fiber exchange runs from the caudal to the proximal posterior root. Due to a lack of histological research on the junctions, however, an aberrant fiber orientation against the macroscopic direction cannot be excluded.

Table 3.2 Intersegmental lumbar plexus.

Rat	Test	Dorsal anastomoses		Observations
		Left	Right	
R1080	HRP4P	L5/6	L3/4;L4/3;L4/5;L6/5;L5/6	
R1115	HRP5	L6/S1	L3/4;L4/5;L5/6	
R1106	HRP5	L4/5		
R1107	HRP5		L2/3;L3/4	
R1149	HRP5	L2/3;L6/S1	L4/3;L5/4;S1/L6	L4/5 left/right running together at the exit
R1095	HRP5	L2/3;L3/4		L5/6 left running together at the exit
R1113	HRPF1P	L5/6;L6/S1	L5/6	
R1156	HRPF2P	L5/4	L4/5	
The first number indicates the proximal origin of the anastomosis.				

Noticeably, a fiber exchange between nerve roots L1 and L2 cannot be proven. Most anastomoses are found between L3/4, L4/5 and L5/6. Furthermore, there is no fiber exchange predilection point, i.e. anastomoses occur with identical frequency both close to and far from the spinal cord. Also, the exit type of the anastomosis from the main root, whether the angle is more acute or obtuse, is not dependent on the localization. In two cases, the anastomosis connected the proximal nerve root directly to the spinal ganglion.

Short, shared pathways of two nerve roots which only separate distally, are less common. In one case, a dorsal double root was shown in the examined test specimen.

Table 3.3 Frequency of intersegmental dorsal anastomoses.

Root	Animals with anastomoses	Number of anastomoses		Total	
		Left	Right		
L1/2	0	0	0	0	
L2/3	3	2	1	3	
L3/4	5	1	5	6	
L4/5	5	2	4	6	
L5/6	3	2	4	6	1 X PR-DRG
L6/S1	3	3	1	4	1 X PR-DRG
PR: Posterior root, DRG: Spinal ganglion.					

Figure 3.11 Difficulty of a determination using the intersegmental plexus.

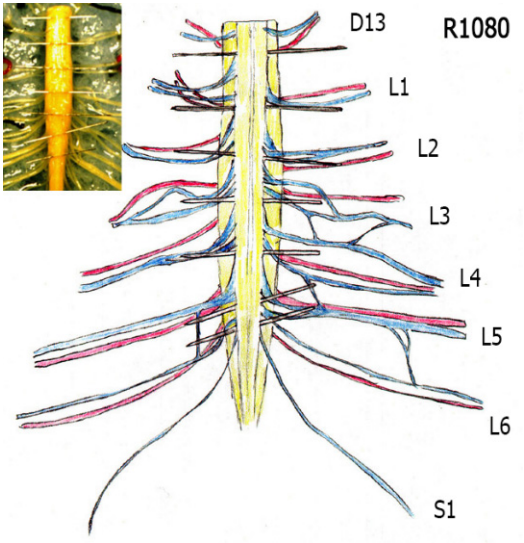

3.3.3. The innervation area of the common peroneal nerve

3.3.3.1. Topography and distances of the nerve sections of the common peroneal nerve

In 12 rats (15 sides), the peripheral innervation area of the common peroneal nerve was dissected and its terminal branches measured. The nerve section of the common peroneal nerve received special consideration after leaving the sciatic nerve, on which the radial nerve autograft in the graft series was made.

Figure 3.12 Anatomy of the peroneal nerve innervation area (R1104).

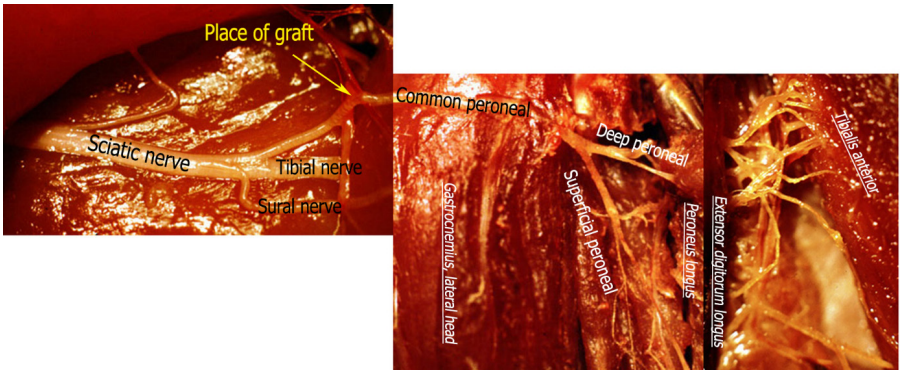

The mean total length of the pathway from the hilus of the tibialis anterior muscle to the entry of the innervated nerve roots into the spinal cord is 123.7 mm for L3, 120.2 mm for L4 and 117.4 mm for L5. After branching off from the sciatic nerve, the common peroneal nerve crosses under the superior muscular artery which runs directly along the gastrocnemius compartment (Greene, 1955), a branch from the popliteal artery. The autologous radial nerve segment is inserted at this intersection point. The distance to the entry of the muscle nerve branches in the tibialis anterior muscle lies between 21.1 mm (R1081) and 21.4 mm (R1079).

Before the common peroneal nerve enters into the peroneal compartment between the peroneus quintus and peroneus longus muscles, the nerve is fixed with short connective tissue to the fascia of the lateral gastrocnemius muscle. After entry of the nerve into the compartment, it splits between the peroneus longus and brevis muscles, limited laterally by the peroneus quintus muscle, into the superficial and deep peroneal nerves. The peroneus longus muscle is innervated as the first muscle of a nerve branch that proceeds from bifurcation, or more often after bifurcation from the deep peroneal nerve. The superficial peroneal nerve distally approaches the peroneus brevis muscle in a medial direction, and reaches the dorsum of the foot after going under the cruciate ligament. The number and exit point of the muscle nerve branches to the peroneus brevis, peroneus quartus and peroneus quintus muscles vary. As a rule, the peroneus longus and peroneus quartus muscles are supplied by one muscle nerve branch each, and the peroneus brevis

and quintus muscles by one to two muscle nerve branches. In one example (R1103), an accessory peroneal nerve branches off out of the superficial peroneal nerve, runs lateral to the main branch between the peroneus IV and V muscles and in its course to the proximal dorsum of the foot, provides nerve branches to the peroneus brevis and peroneus IV and V muscles which innervate the distal portion of the muscle.

Figure 3.13 The innervation area of the common peroneal nerve: Schematic drawings with longitudinal measurement of the nerve segments (distances in millimeters).

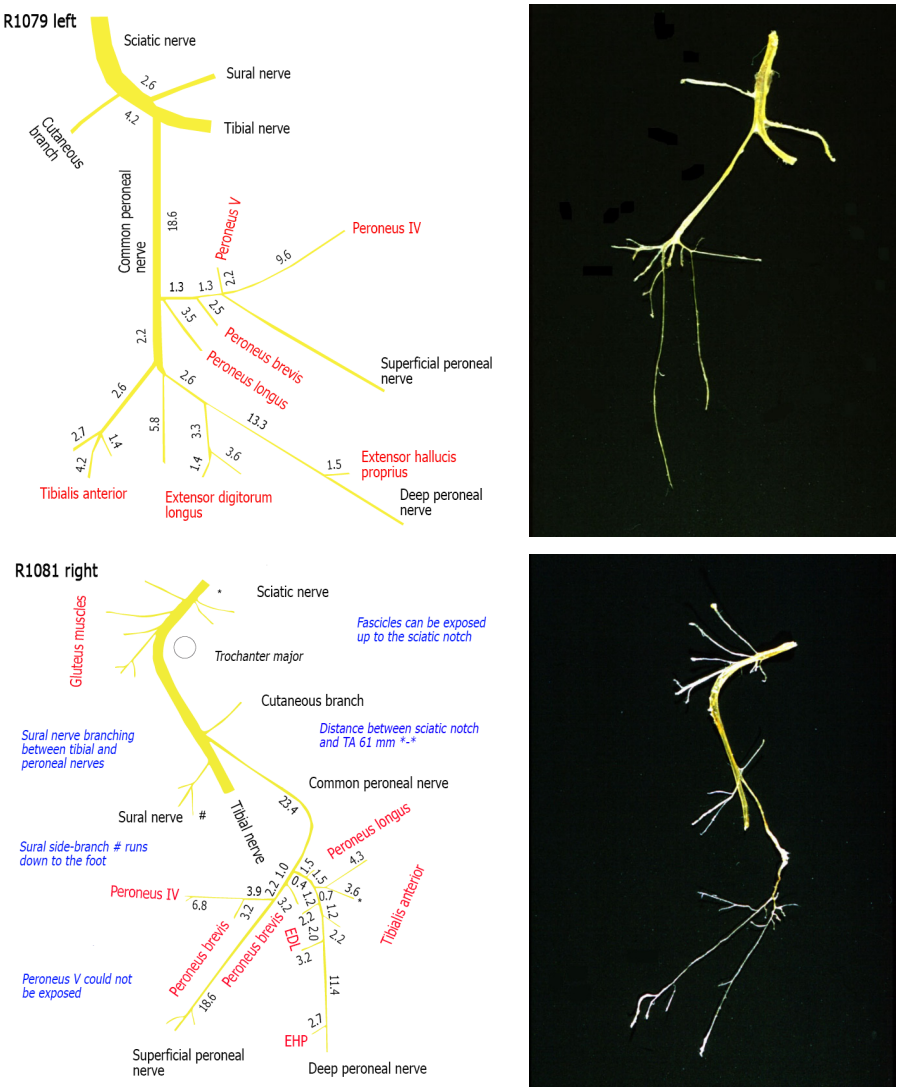

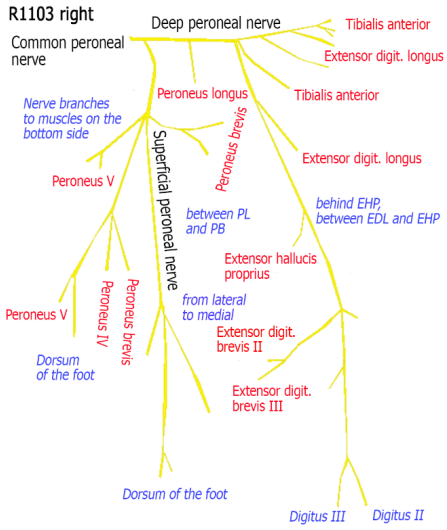

Figure 3.14 Branches of the common peroneal nerve (R1103).

After it exits the muscle nerve branch feeding the peroneus longus muscle, the deep peroneal nerve crosses below the extensor digitorum longus muscle. Here it provides, in varying numbers, nerve branches to the tibialis anterior and extensor digitorum longus muscle, and runs between both muscles to the extensor hallucis proprius muscle, which it feeds with a thin nerve branch halfway to the dorsum of the foot. In the area of the cruciate ligament which it crosses under, a nerve branch branches off which then splits to innervate the extensor digitorum brevis II and III muscles. The final branch runs between digits II and III. As the largest muscle, the tibialis anterior muscle is innervated by 1-3 muscle nerve branches, the extensor digitorum longus muscle by 2 and the extensor hallucis proprius muscle and extensor digitorum II and III muscles each by 1 muscle nerve branch, respectively.

3.3.3.2. Variability of the muscle nerve branches supplying the tibialis anterior muscle and extensor digitorum longus muscle

The quantity and exit of muscle nerve branches to the innervated muscles are significant for retrograde l tests, if the application of the substances directly onto the nerves after being severed before entering the muscle is to follow, as in the HRP5 and HRPF1 test series. The distribution pattern of the nerve branches and the spatial dimensions in the application area have decisive influence on whether the chosen method is viable. Based on the above mentioned test series, this signifies whether the use of slender containers filled with the marking material is possible. As the nucleus column of the tibialis anterior

Figure 3.15 The innervation area of the deep peroneal nerve.

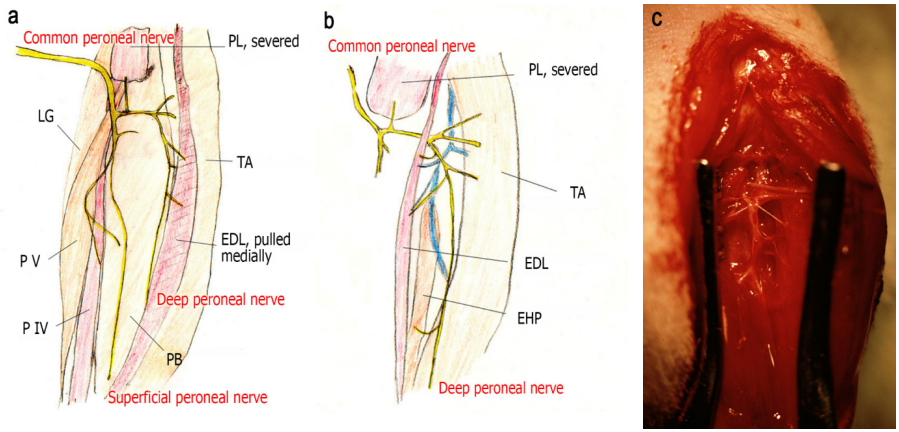

muscles and its motor units represents the test system in the HRP2 graft series, and knowledge of the topography of the cell column followed in part of the test on the direct application of the tracer to the severed muscle nerve branches, the branching pattern of these branches was investigated more closely.

The tibialis anterior muscle is innervated by 1-3 muscle nerve branches. A major nerve trunk that has a similar diameter or a larger caliber than the distally moving deep peroneal nerve will regularly isolate itself, and the tibialis anterior artery crosses over and moves into the proximal third of the muscle. In 47% of cases investigated, a smaller branch branches off from the main trunk and then reenters the muscle proximally. In Figure 3.13, this branch has not been recorded as an independent nerve branch. In 87%, the tibialis anterior muscle is innervated by at least one other muscle nerve branch that is distinctly thinner and, in the majority of cases, leaves the deep peroneal nerve after exiting the nerve branches to the extensor digitorum longus muscle. However, the second nerve branch can also branch off together with the main branch (R1103, Figures 3.14 and 3.16) or with another side branch (R1149, Figure 3.16) of the deep peroneal nerve. A third side branch generally leaves the deep peroneal nerve as an independent muscle nerve branch.

During application of HRP or the fluorescent markers onto severed muscle nerve branches, one filled container was usually adequate for the main branch and its diverting side branch. In the case of two muscle nerve branches, two containers were used - or three, if the distance between the nerve branches was too great.

Figure 3.16 Branching model of the muscle nerve branches supplying the tibialis anterior muscle (1-3) and the extensor digitorum longus muscle.

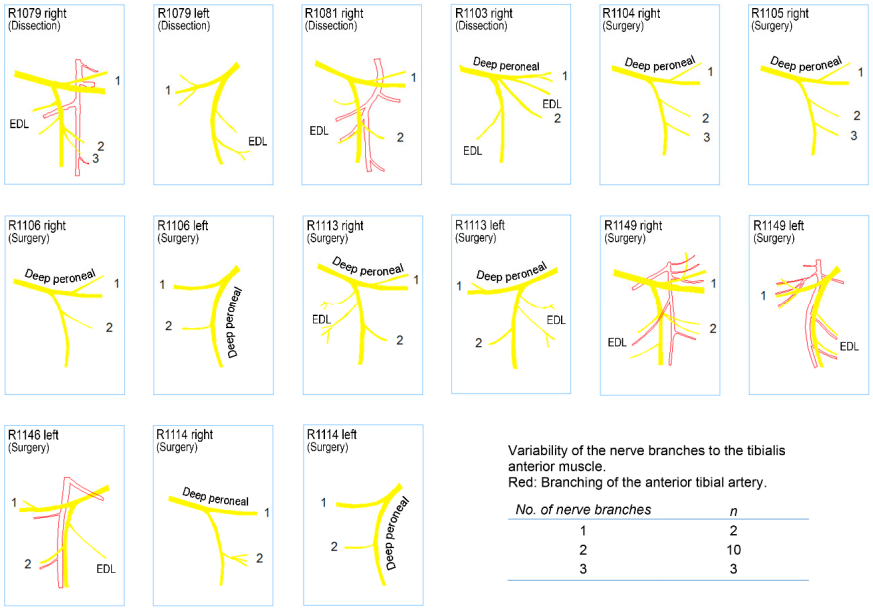

Variability of the nerve branches to the tibialis anterior muscle.
Red: Branching of the anterior tibial artery.

No. of nerve branches	*n*
1	2
2	10
3	3

3.4. Parameters and reconstruction of the cell column of the tibialis anterior muscle following cell marking using HRP and fluorescent dyes

3.4.1. The appearance of the labeled anterior horn cells

The HRP enzyme is a glycoprotein (40 kDa) which, in the presence of hydrogen peroxide, catalyzes the oxidation of benzidine, leading to a dye product which can be verified under a light microscope. After injection of HRP into the target muscle, or immersion of the muscle nerve branches in a HRP solution, retrograde transportation of peroxidase to the motoneuron takes place. Intracellular imaging of the dye product is possible by selection of a suitable time span between application and enzyme histochemistry. Using tetramethylbenzidine as a dye, the reaction product appears as a golden color in the dark field and as a dark blue to brown-black color in the light field, depending on the density of the dye in the cytoplasm (Figure 3.17, b-h). The reaction product is generally distributed in a granular fashion, with an elevated concentration around the nucleus, which remains free from the dye. The cell components are marked with different densities; their appearance ranges from motoneurons, whose dendritic tree is completely filled with the dye product, to cells with a dull, yet still granular distribution of the dye so the cell border is not reliably definable (Figure 3.17, i-k).

Figure 3.17 Morphology of the motoneurons labeled with HRP (***a-h***) and the fluorescent dyes Fast Blue (***l-m***) and Diamidino Yellow (***n-o***). Motoneurons following immersion of the sciatic nerve in a HRP solution (**R818, *a, i-k***). Spinal cord cross-section with insertion channel transverse through the posterior horns using minutien pins for segment marking (**R818, *a***). Tibialis anterior motoneurons following application of HRP to the muscle nerve branches (**R1095, *b-d***) or injection into the muscle (**R766, *e-h***). Reconstruction of the anterior horn cells with their fiber orientation in 6 adjacent section images (with dendraxon, ***d***). Motoneurons of the cell column of the tibialis anterior muscle, 56 days after the injection of FB into the muscle (**R808, *p-s***). Combination of HRP and DY. Injection of DY into the tibialis anterior muscle 9 days prior to immersion of the peroneal nerve in a 40% HRP solution (**R1156, *t-v***).

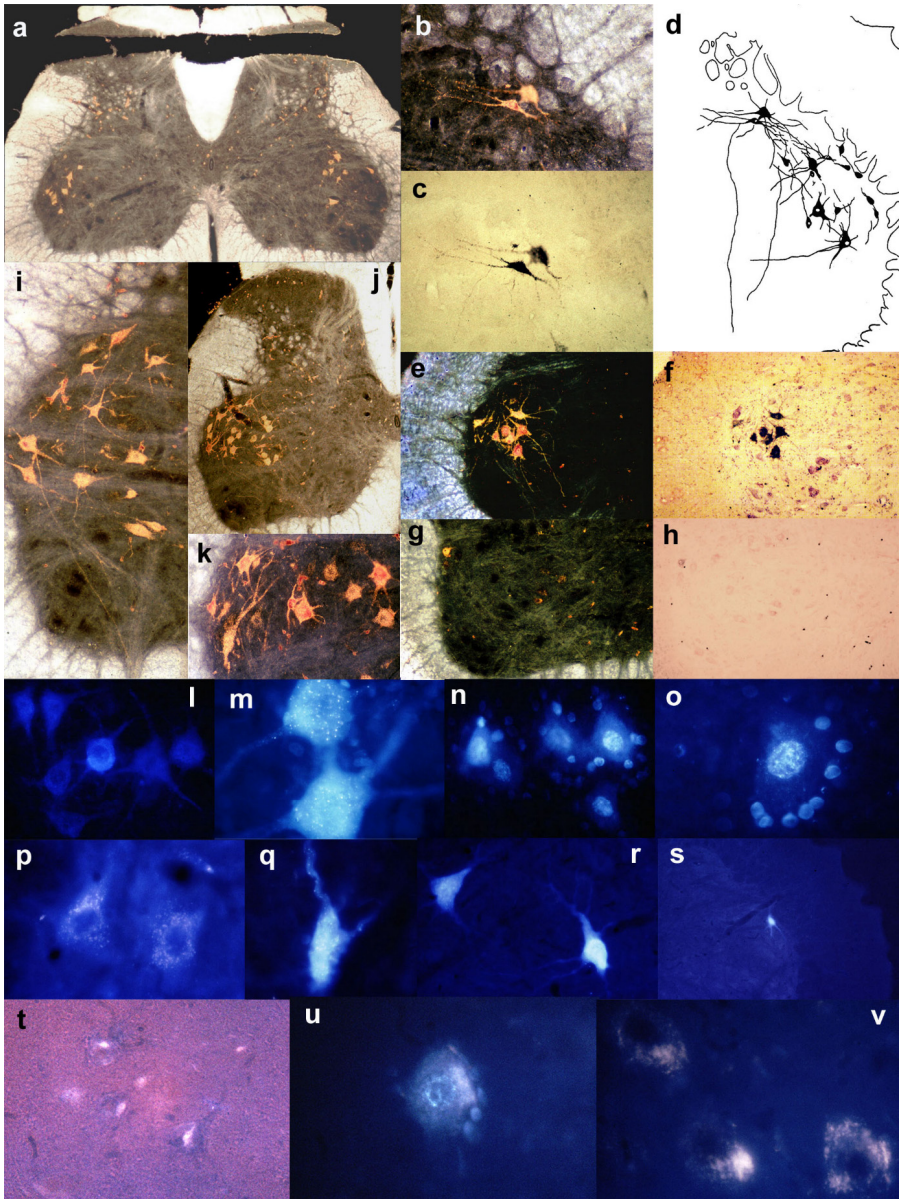

The nucleus is often not visible due to a concentration of the reaction products that is too low or too high in the cytoplasm. In the case of intensive staining, the axons should be tracked from the cell exit to the anterior root (Figure 3.17, i). Through reconstruction of multiple following section images, the dendrite and axon progression can be extensively illustrated and the outflow relationships of axons clarified (dendraxon in Figure 3.17, d: see Linda et al., 1985).

In comparison with neutral red, the Nissl counterstain with thionine as the dye (Adams, 1977, 1980) has the disadvantage in that weak HRP labeling of the cells is overlaid and not detectable. On the other hand the nucleoli, whose localization is a criterion in comparing cell fragments of a cell in adjacent sections, are consistently stained. Due to the risk of overstaining, only a few sections of one trial are counterstained (Figure 3.17, f and h).

The fluorescent dyes Fast Blue and Diamidino Yellow are simultaneously visible under UV stimulation of 340-380 nm in retrograde labeled cells (Figure 3.17, l to o). Compared with other fluorescent markers, they offer the advantage of a comparable transportation time in the peripheral nervous system. Thus they can be applied to the exit point at the same time. Compared with Diamidino Yellow, Fast Blue offers better water solubility, greatly simplifying application (Kuypers and Huisman, 1984).

Fast Blue (Figure 3.17, l and m) leads to a diffuse blue staining of the cytoplasm and dendrites, with a changing density of small, silver granules which can often be tracked as far as the cell protuberances. The nuclei of the glial cells neighboring these cells are almost consistently marked with a diffuse blue. In long-term experiments (R808, Figure 3.17, p-s), the cytoplasm often has a faintly blue coloration with yellow-orange granules (Figure 3.17, p). The dendrites regularly appear torqued, with no change in shape of the cell bodies and independent of the use of Fast Blue or Diamidino Yellow (Figure 3.17, q and r).

Diamidino Yellow (Figure 3.17, n and o) is characterized by a non-homogenous yellow-whitish staining of the cell nucleus and the satellite nuclei. The cytoplasm presents itself as pale yellowish and primarily homogenous, with fine whitish granules that are, comparatively, rarely present. In long-term experiments (R808), the cytoplasmatic silver-white granules of some cells become prominent. Overall, the section has a blue coloration when filter block A by Leitz is used.

The combination of fluorescent marker Diamidino Yellow with HRP (R1114 and R1156, Figure 3.17, t-v) and the use of a 4% paraformaldehyde solution for perfusion has negative effects on the quality and quantifiability of the labeling. (1) The HRP labeled motoneurons have weak staining only, the cell borders are less contoured and as a result, the cell count cannot be determined with certainty (Figure 3.17, t); (2) morphometric measurements of the cells and cell column are generally not possible; (3) Diamidino Yellow positive motoneurons in lamina IX according to Rexed (Rexed, 1964; Brichta and Grant, 1985) often show the familiar, finely granulated light yellow-white nucleus coloration and staining of the satellite cell nuclei. The cytoplasm is predominantly depicted as a diffuse, light yellow, though compact, dark yellow to ochre-colored areas are repeatedly in evidence (Figure 3.17, u). In addition, cells with a non-homogenous granular cytoplasm marking are present beyond the anticipated area of the nucleus column of the tibialis anterior muscle, whereby the cell nuclei are then hollowed and adjacent glial cells are not marked (Figure 3.17, v); (4) double marked cells cannot be

reliably identified, as the compact, yellow-stained portions are often difficult to project onto the cell nucleus of an HRP marked motoneuron (Figure 3.17, t); (5) based on the yellow-orange staining of the cytoplasm following use of Fast Blue in the long-term experiment, and on a likewise yellow ochre-colored staining of the cytoplasm following combined use of HRP and Diamidino Yellow, these fluorescent markers should not be implemented for double labeling in longer test durations due to poor discriminability (Kuypers and Huisman, 1984).

3.4.2. The localization of motor nucleus columns on the spinal cord section

3.4.2.1. Position and orientation of the motoneurons in lamina IX

The HRP-TMB labeled cell column of the tibialis anterior muscle particularly displays predominantly smaller, more oval than round-shaped, peripheral cells in the dorsolateral segment of the anterior horn, bordering on the white matter. The cells are oriented in their longitudinal axis parallel to the border of the gray matter, whereby primary dendrite exits come to view more frequently at the poles and less at the cell sites (Figure 3.17, d and i). The other medially located motoneurons have, depending on the intensity of the marking, an oftentimes round or polygonal shape with a radial dendritic tree pointing in all directions. The axons of the oval, peripheral cells branch off ventrally and run linearly or curve medially to the anterior root. In the other medially located cells, the axons can, rarely, also follow dorsally from their exit on the lateral side of the neuron. From the position of the cell in a mediolateral direction, the ventral progress of the axons cannot be predicted, and lateral motoneurons can send out axons to the medial as well as the lateral side of the anterior root (Figure 3.17, e and i). Following application of HRP to the severed sciatic nerve, two separate cell complexes are shown in lamina IX across the segmental length L3 to L6, with overlapping in the peripheral area (Figure 3.17, j). The lateral nucleus group corresponds to the cell column of the common peroneal nerve (also R1156, not shown), which extends segmentally from L3 to L5. The medial nucleus group with inclusion of segments L3 to L6 corresponds to the cell column of the tibial nerve (Swett et al., 1986).

3.4.2.2. The diffusion of HRP into neighboring muscle compartments

In preliminary trials (HRP1P) and the HRP1 graft series, labeled neurons were shown to be medially and dorsomedially outside of the cell column following injection of 450 µl of a 5% HRP solution into the tibialis anterior muscle, alongside a compact nucleus

Figure 3.18 *R327* (*HRP1P*), 3D reconstruction of the nucleus column of the tibialis anterior muscle following injection of a 5% HRP solution into the muscle. *Right side:* **yellow**, *left side:* **red**. Mismarked motoneurons outside the cell column of the tibialis anterior muscle are circled in red.

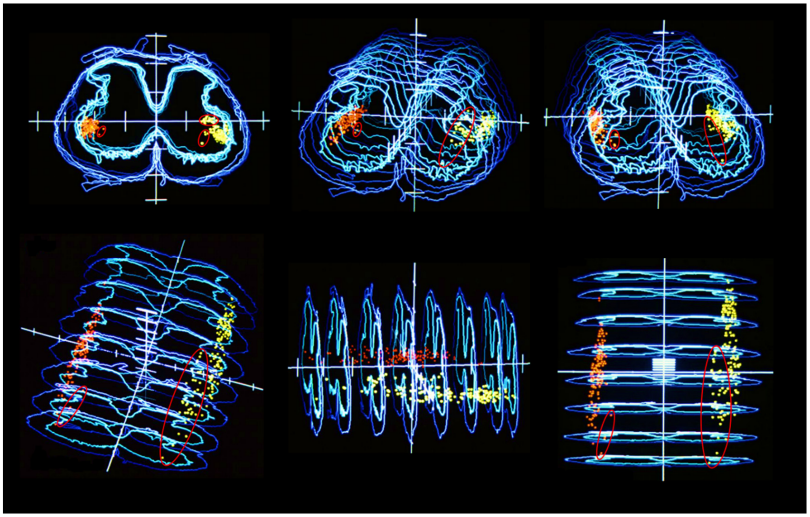

column in the lateral portion of lamina IX in varying numbers (Figure 3.18). 3D reconstructions of the motoneuron column proved to be superior to the two-dimensional sectional drawings in evaluating the affinity of neurons to the cell column. Based on these reconstructions, motoneurons that are partially apparent as a second cell column repeatedly isolated themselves from the center of the nucleus column of the tibialis anterior muscle (see Figure 3.19, encircled in red and Figure 3.20). It is thought that the medial cell group arises as a result of the diffusion of HRP into the dorsal muscle compartment innervated by the tibial nerve with subsequent retrograde transport of the tracer. The dorsomedial motoneurons are located in an area which contains axons from the medial plantar and lateral plantar nerves and the terminal branch of the deep peroneal nerve. A diffusion of HRP into the foot musculature of the rat is probable here (Romanes, 1951; McHanwell and Biscoe, 1981a; Nicolopoulos-Stournaras and Iles, 1983).

Local distinctions of the cell density are graphically recorded in the reconstructions, where inhomogeneities can be interpreted in the sense of the clustering in a cell column or of the superposition of two neighboring cell columns, but a differentiation is not ordinarily successful.

Under the paradigm that motor cell columns represent individual muscles or muscle groups and are organized as discreet and homogenous entities within a defined area in the spinal cord, the neurons outside of the cell column that can be defined in tests must be excluded as mismarked neurons from quantitative evaluation (Romanes, 1964; Burke and Rymer, 1976). For the cell groups shown in Figures 3.18-3.20 that are medial to the cell column of the tibialis anterior muscle, this exclusion is successful considering the 3D reconstructions. However, mismarked cells within the cell column can only be minimized by checking potential error sources and by adapting the HRP application regime.

3.4.3. Control tests

3.4.3.1. Control tests with HRP

In the four preliminary trials of the HRP1P series, volume and concentration of the HRP solution injected into the tibialis anterior muscle were varied and Fast Green was added in 0.1% concentration to the left side of the solution (Hardman and Brown, 1985, 1987). This has the advantage that the distribution in the muscle, which turns dark green, can be better tracked and contamination after removing the point of the needle can be detected sooner. Multiple injections were performed with the goal of achieving complete distribution in the muscle. In place of the free-handed injection of the tracer with a Hamilton syringe, a telescopic arm was used during application in order to prevent the puncture site from widening during the injection and subsequent waiting period with withdrawal of HRP from the muscle. The point of the injection cannula was equipped with a locking mechanism in order to ensure the injection into the tibialis anterior muscle. Severing all muscle nerve branches not touching on the target muscle proved not to be feasible in control tests for the peroneus nerve's innervation area, due to the small spatial dimensions in the rat. In addition, it came about that damage to the axons leading to the target muscle within the scope of the somewhat difficult preparation impedes the retrograde transport of HRP.

Despite optimized methods, it could not be avoided that motoneurons were distinctly marked in varying numbers outside the boundaries of the cell column (Figure 3.19) (McHanwell and Biscoe, 1981a). The percentage of these neurons were able to be reduced in comparison to R327 (HRP1P) from an average of 14.3% to 3.4% (HRP2P1 on the right). Although the low sample size does not allow for a statistical analysis, a dependence of the number of mismarked motoneurons on the injected quantity of HRP can be assumed. Its percentage was reduced by 52.3% (right) and 20.9% (left, HRP with Fast Green) by halving HRP from 4 mg to 2 mg.

After the addition of 0.1% Fast Green (Fast Green FCF, Color Index No. 42053) (Conn, 1969) to the HRP solution, the share of mislocated cells increased with statistical significance to 18.7% (t test, $P = 0.031$). This unexpected effect of Fast Green is not reported by other working groups with similar objectives and methods (Hardman and Brown, 1985, 1987).

Table 3.4 Mislabeled motoneurons following HRP application.

Test series	Rat	Trans-port time (h)	Side	HRP (%)	Vol. (µl)	HRP (mg)	FG	Injection plan (µl)	Inj. time (min.)	Waiting time (min.)	Applica-tion	Mis-labeled cells (%)	Cell-count[1]
HRP1P	R327	48	Right	5	450	22.5	-	1 (450)	1	-	Manual	36 (24.8)	109
			Left	5	450	22.5	-	1 (450)	1	-	Manual	5 (3.8)	127
HRP2P1	R764	50	Right	20	20	4	-	5 (4)	1	5	Manual	5 (5.6)	84
			Left	20	20	4	+	5 (4)	1	5	Manual	45 (20.5)	175
	R765	46	Right	40	10	4	-	5 (2)	2	5	Telescopic arm	5 (3.6)	132
			Left	40	10	4	+	5 (2)	2	5	Telescopic arm	75 (21.4)	275
	R766	49	Right	40	5	2	-	1 (2), 2 (1), 2 (0.5)	2	5	Telescopic arm	2 (1.9)	103
			Left	40	5	2	+	1 (2), 2 (1), 2 (0.5)	2	5	Telescopic arm	51 (19.8)	246
	R817	53	Right	40	5	2	-	1 (2), 2 (1), 2 (0.5)	2	5	Telescopic arm	2 (2.4)	80
			Left	40	5	2	+	1 (2), 2 (1), 2 (0.5)	2	5	Telescopic arm	20 (15.7)	107
HRP2P2	R948	46	Right	40	4	1.6	-	4 (0.85), 2 (0.3)	1	5	Telescopic arm	36 (100.0)	36
			Left	40	4	1.6	-	4 (0.85), 2 (0.3)	1	5	Telescopic arm	0 (0.0)	81
HRP2C	R1074	52	Right	40	4	1.6	-	4 (0.85), 2 (0.3)	1	5	Telescopic arm	7 (6.6)	101
			Left	40	4	1.6	-	4 (0.85), 2 (0.3)	1	5	Telescopic arm	22 (15.5)	110
	R1075	53	Right	40	4	1.6	-	4 (0.85), 2 (0.3)	1	5	Telescopic arm	2 (1.8)	109
			Left	40	4	1.6	-	4 (0.85), 2 (0.3)	1	5	Telescopic arm	0 (0.0)	130
	R1078	48	Right	40	4	1.6	-	4 (0.85), 2 (0.3)	1	5	Telescopic arm	22 (15.9)	116
			Left	40	4	1.6	-	4 (0.85), 2 (0.3)	1	5	Telescopic arm	18 (12.1)	131
	R1079	49	Right	40	4	1.6	-	4 (0.85), 2 (0.3)	1	5	Telescopic arm	0 (0.0)	112
			Left	40	4	1.6	-	4 (0.85), 2 (0.3)	1	5	Telescopic arm	0 (0.0)	112
HRP4P	R1080	50	Right	40	4	1.6	-	4 (0.85), 2 (0.3)	1	2	Telescopic arm	0 (0.0)	122
HRP2G	R823	46	Left	40	5	2	-	4 (1), 2 (0.5)	1	5	Telescopic arm	43 (27.7)	112
	R834	56	Left	40	4	1.6	-	4 (0.85), 2 (0.3)	1	5	Telescopic arm	8 (6.3)	118
	R835	53	Left	40	4	1.6	-	4 (0.85), 2 (0.3)	1	5	Telescopic arm	52 (32.9)	106
	R809	50	Left	40	4	1.6	-	4 (0.85), 2 (0.3)	1	5	Telescopic arm	5 (3.9)	122
	R827	52	Left	40	4	1.6	-	4 (0.85), 2 (0.3)	1	5	Telescopic arm	26 (20.0)	104
	R831	50	Left	40	4	1.6	-	4 (0.85), 2 (0.3)	1	5	Telescopic arm	12 (10.1)	107
	R824	48	Left	40	4	1.6	-	4 (0.85), 2 (0.3)	1	5	Telescopic arm	4 (4.1)	93
	R822	50	Left	40	4	1.6	-	4 (0.85), 2 (0.3)	1	5	Telescopic arm	2 (2.2)	87
HRP5C	R1095	61	Right	40	-	-	-	-	-	-	-	0 (0.0)	175
	R1149	71	Left	40	-	-	-	-	-	-	-	0 (0.0)	122

R948: Transection of the common peroneal nerve on the right prior to HRP injection in the tibialis anterior muscle.
HRP5C: Application of HRP to the severed muscle nerve branches supplying the tibialis anterior muscle.
Cell count[1] after correction by doubled and mismarked cells. FG = Fast Green (0.1%).

The disproportional increase in the total number of motoneurons (Figure 3.20) linked to an increased cell density (Figure 3.19) with use of HRP and Fast Green also implies labeled neurons within the cell column of the tibialis anterior muscle which possibly innervate other muscles or muscle groups, and cannot be separated by an analysis of the cell coordinates alone. What remains unresolved is whether the effects of Fast Green can be achieved through an improved intake of HRP at the nerve endings in the muscle and a facilitated diffusion into other muscle compartments.

Figure 3.19 *R766* (*HRP2P1*), three-dimensional reconstruction of the tibialis anterior muscle cell column. *Right side:* **yellow**, *left side:* **red**. Addition of 0.1% Fast Green on the left. Mislabeled motoneurons outside the cell column of the tibialis anterior muscle are circled in red.

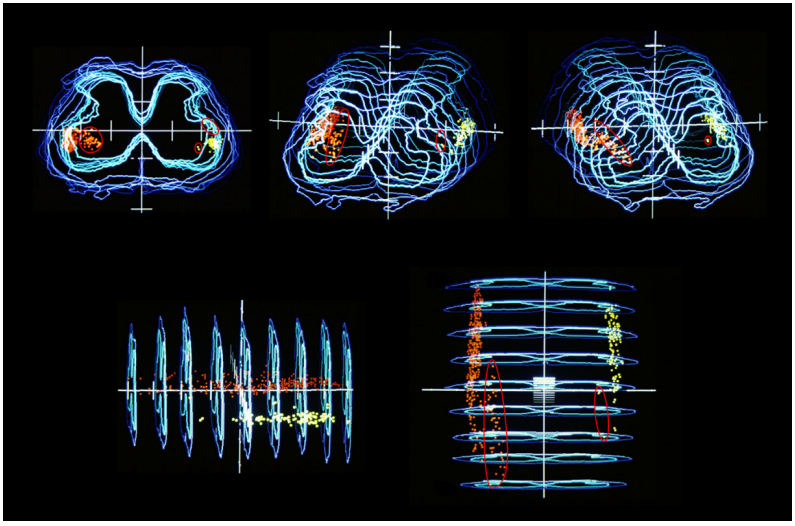

In addition to the diffusion of the tracer over greater distances (Janjua and Leong, 1981; Haase and Hrycyshyn, 1986; Haase, 1990), lymphogenous and vascular transport paths also come into consideration for artificial cell marking (Broadwell and Brightman, 1976; Fox and Powley, 1989). Severing the proximal nerve trunk, with inhibition and additional isolation of the nerve stump with sealed PVC pipe material prior to injection of

Figure 3.20 Cell count of the motoneuron column of the tibialis anterior muscle following correction of duplicated and mislabeled neurons.

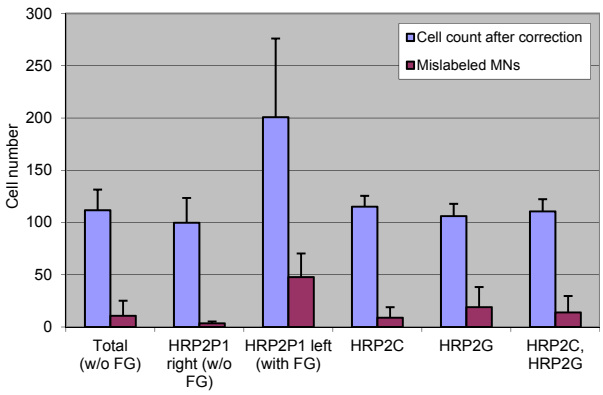

HRP into the tracked muscle, cannot completely prevent mismarking. In the HRP2P2 test series (Table 3.4, R948 on the right), the right common peroneal nerve was severed prior to bilateral HRP injection into the tibialis anterior muscle. Even though most of the medial, less ventrolaterally labeled motoneurons on the right side imply diffusion of HRP into the tibial nerve and the innervation area of the femoral nerve, and are definable as cell layers by the discreet cell column of the tibialis anterior muscle, occasional motoneurons of the peroneal nerve cell pool are marked. This can only be explained by a diffusion of the tracer from the injection site to the transection site and intake over axons that are intact or damaged by manipulation, or alternatively, by lymphogenous and vascular transport routes (Krishnan and Singer, 1973). The percentage of these mismarked neurons is negligible, however, at <1%, based on the normal cell count of the tibialis anterior muscle.

The nerval intake of the HRP enzyme takes place during the nerve bath method (Takahashi et al., 1980) under direct visual control. Here, an exposed nerve trunk or muscle nerve branch is severed and the proximal nerve stump immersed in a HRP solution for a defined period of time. While using appropriate materials and safety precautions (e.g. Parafilm support), leakage of the catheter with discharge of the HRP solution and possible mismarking of motoneurons of other cell columns can be avoided. The methodical limits are then reached with small test animals if keeping the small muscle nerve branches undamaged is not successful during preparation. In comparison to the methodically simple muscle injection, losses of test animals are greater. The reason, as a result of the longer preparation times, is because of a higher complication rate from the narcosis (HRP injection: 12%, HRP nerve bath: 42%) and a higher number of tests with insufficient retrograde transport of the enzyme (HRP injection: 13%, HRP nerve bath: 45%). Table 3.5 shows a compilation of the tests in which HRP was applied to severed nerves and a sufficient transport resulted. 3D reconstructions of the cell column of the tibialis anterior muscle (Figures 3.21 and 3.22) show a compact, fusiform nucleus column in lamina IX according to Rexed (Rexed, 1952), ventrolaterally on the border to the white spinal cord matter. Labeled motoneurons outside of this cell column cannot be delimited. In contrast to the reconstructions of the nucleus column following injection of HRP into the muscle (Figures 3.18 and 3.19), there is no indication of an apparent mismarking of other spinal neurons.

Table 3.5 Cell count following the application of HRP to various nerves and muscle nerve branches.

Test series	Rat	Marking	Side	HRP (%)	DMSO 2% contact time (min.)	HRP contact time (min.)	HRP transport time (hours)	Cell count[1]
HRP3	R818	Sciatic nerve	Right	40	15	30	65	1398
		Sciatic nerve	Left	40	15	30		1673
HRP5	R1095	Tibialis anterior muscle	Right	40	15	45	61	175
	R1149	Tibialis anterior muscle	Left	40	10	120	71	122
	R1107	Ext. digit. brevis muscle	Right	40	15	60	71	11
		Ext. hall. proprius muscle	Left	40	15	60	71	4
HRPF2	R1156	Common peroneal nerve	Right	40	15	60	68	382

Cell count[1] after correction by doubled and mislabeled cells.
For R818 and R1156, the number of doubled cells following HRP2G was calculated at 14%.

Allowing for the relative cell coordinates, the nucleus column of the tibialis anterior muscle in tests R1095 and R1149 stretches out over the framework's abscissa from x = +70.3 to +98.4%, and over the ordinate from y = –38.7 to +53.3%. The area defined by these cell coordinates is considered as the maximum area in which motoneurons of the tibialis anterior muscle cell column are located, under physiological conditions, in the transversal plane. The comparison with the cell positions following muscle injection serves, in first approximation, the identification and exclusion of mismarked motoneurons. The assessment includes the results of the HRP labeling of other cell columns

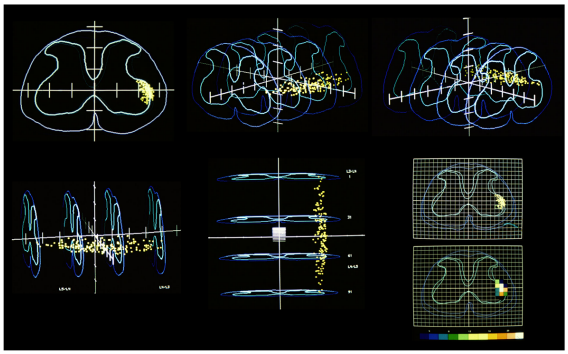

Figure 3.21 *R1095*, 3D reconstruction of the nucleus column of the tibialis anterior muscle. Application of HRP to the muscle nerve branches. Expansion of the cell column on the spinal cord section in relative coordinates:
x = +70.3 to +98.4%,
y = -36.7 to +53.3%.

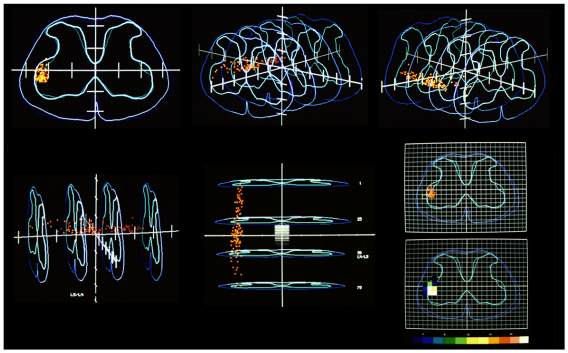

Figure 3.22 *R1149*, 3D reconstruction of the nucleus column of the tibialis anterior muscle. Application of HRP to the muscle nerve branches. Expansion of the cell column on the spinal cord section in relative coordinates:
x = -77.4 to -98.3 %,
y = -38.7 to +48.4 %.

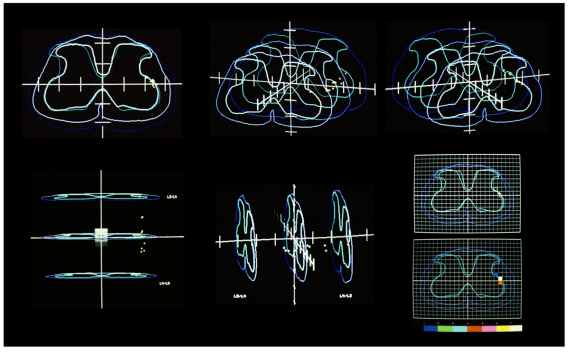

Figure 3.23 *R1107*, 3D reconstruction of the nucleus column of the extensor digitorum brevis II and III muscle. Application of HRP to the muscle nerve branches. Expansion of the cell column on the spinal cord section in relative coordinates:
x = +78.7 to +95.2 %,
y = -25.0 to +13.3 %.

(Table 3.5) and of the fluorescence tests regarding the localization of the nucleus column (see 3.4.3.2).

When the cell counts are corrected to the percentage of mismarked neurons on the basis of these criteria, an average cell count of 108.7 ± 15.3 (n = 24, see Figure 3.25) emerges for the nucleus column of the tibialis anterior muscle following HRP muscle injection. The percentage of mismarked neurons amounts to 9.6% (11.6 ± 14.7 cells). Despite reduction of the injected quantity of HRP to 1.6 mg, the portion of mismarked cells is extremely variable, and reaches 32.9% in a given case (HRP2G). The average number of motoneurons of all HRP tests in which the tibialis anterior muscle was labeled amounts to 111.7 ± 19.7 (n = 26), with a percentage of mismarked neurons at 7.8% (10.7 ± 14.5 cells). The four tests which added Fast Green to the HRP solution (HRP2P1 on the left) were not included as outliers in this evaluation.

The tibialis anterior muscle cell column has a percentage of 7.3% in the motoneuron pool of the sciatic nerve and 29.2% in the cell pool of the common peroneal nerve. Within the area that the motoneurons of the sciatic nerve occupy on the spinal cord cross-section in lamina IX, the cell column of the common peroneal nerve lays dorsolaterally complexed to the border to the white matter. Reconstructions of the small foot musculature (extensor digitorum brevis II and III muscle, Figure 3.23) innervated by the deep peroneal nerve show a cell column on the dorsolateral border of the spinal cord at the L4 level. This nucleus column is shown by combining multiple motoneurons from various test animals by means of the calculated relative cell coordinates amid the TA cell area (Figure 3.24).

3.4.3.2. Control tests using fluorescent dyes

Apart from the tests applying HRP to various nerves or muscle nerve branches, tests using fluorescent markers also served in terms of localization and cell count as the control. Following the data performed in Table 3.6 and after correcting the motoneuron count through double and mismarking, an average cell count of 98.9 ± 10.8 (n = 7) was calculated for the tibialis anterior muscle, and an average cell count of 68.0 (n = 2) was calculated for the lateral gastrocnemius muscle. A statistical analysis of the differences in average cell count of the tibialis anterior muscle cell column following injection of Fast Blue (97.2 ± 12.6; n = 5) or Diamidino Yellow (103.0; n = 2) cannot be performed due to a low sample size. Comparison with the cell count following HRP injection shows a low average cell count of the cell columns following injection of fluorescent dyes, without which statistically significant differences can here be verified (t test, P = 0.126).

Assessment of position and morphology of the cell columns took place after qualitative examination of the histological sections, without morphometric evaluation. 3D reconstructions could not be produced due to lacking technical-instrumental requirements, with the exception of R808. The cell layers of the tibialis anterior muscle are limited on spinal cord segments L3 to L4, and form a definable nucleus column on the lateral side of the anterior horn. As with the cell column of the long-term experiment R808, but different from the HRP application to the nerve (HRP5), the dorsolateral waist of the spinal cord is spared of marked motoneurons (Figure 3.24). The nucleus column of the lateral gastrocnemius muscle is located medially to the nucleus column of the tibialis anterior muscle, as well as reliably delimited and caudal in height to the spinal

cord segments L4 and L5. Both nucleus columns have a fusiform appearance, with an area of lowered cell density at the ends. Mislabeled neurons outside of the area of the cell columns can neither be uniquely determined following muscle injection of Fast Blue nor by Diamidino Yellow.

Table 3.6 Labeling of spinal cell columns using fluorescent dyes.

Test series	Rat	Labeling	Side	Tracer	Concen-tration (%)	Vol. (µl)	Quan-tity (mg)	Transport -time (d)	Cell count	Cell count[1]
F1P1	R575	Tibialis anterior muscle	Right	FB	2	5	0.1	4	91	82
			Left	DY	2	5	0.1	4	-	-
	R644	Tibialis anterior muscle	Right	FB	2	5	0.1	6	131	113
			Left	DY	2	5	0.1	6	122	105
	R645	Tibialis anterior muscle	Right	FB	2	5	0.1	6	124	107
			Left	DY	2	5	0.1	6	118	101
	R711	Tibialis anterior muscle	Right	FB	2	5	0.1	9	109	94
			Left	FB	2	5	0.1	9	105	90
		Lat. gastrocnemius muscle	Right	DY	2	5	0.1	9	76	65
			Left	DY	2	5	0.1	9	83	71
F1P2	R808	Tibialis anterior muscle	Right	FB	2	5	0.1	56	33	30
			Left	DY	2	5	0.1	56	20	17

Cell count[1] after correction of duplicate and mislabeled cells.
Aside from R575 and R808, the number of doubled cells following HRP2G was calculated at 14%.
R575 left: insufficient labeling.
Abbreviations:
FB: Fast Blue, DY: Diamidino Yellow.

For the reconstructed long-term fluorescence experiment (Figure 3.24, R808), during consideration of the relative border coordinates of the tibialis anterior muscle from the HRP5 test series there arose suspicion of 2 mismarked motoneurons on the left side. Microscopic examination of selected muscle sections showed fluorescing material that was indigenous and concentrated at the injection site and in the muscle nerve branches. The muscle fascia was respected as a barrier from the fluorescent dyes, so a peripheral diffusion of the tracer into neighboring muscle compartments is unlikely as a reason for the mismarking. In addition to wash-out procedures in other neurons in the scope of reprocessing the specimens, a trans-neural transport which be benefited by the long dwell time of the fluorescent dye in the motoneuron is also possible as an explanation.

To facilitate a morphometric evaluation with quantitative analysis of parameters of the cell column, multiple test series were performed with the goal of checking the compatibility of histological cell staining with the fluorescent dyes. After preparing Nissl stains, outline drawings of the white and gray matter and the anterior horn cells should be made from the section specimens in the light field, and then the fluorescent marked motoneurons should be identified and labeled. Despite variation of the reagents used, concentrations, exposure time and other parameters (Tables A.5 to A.9 in the Appendix), a satisfactory result with retention of fluorescence and a sufficient contrasting of the motoneurons could not be achieved. One reason lies in the difficulty of constantly adjusting the color intensity of the Nissl stain in such a way that the fluorescence of the motoneurons are not masked. The reduction of the concentration and the alteration of the draining and differentiation times led, in some of the tests, to wash-out procedures with fuzzy cell boundaries and diffuse fluorescence even of distant neurons in the anterior horn. In addition, the auto-fluorescence of eosin and the distinctly intense light red

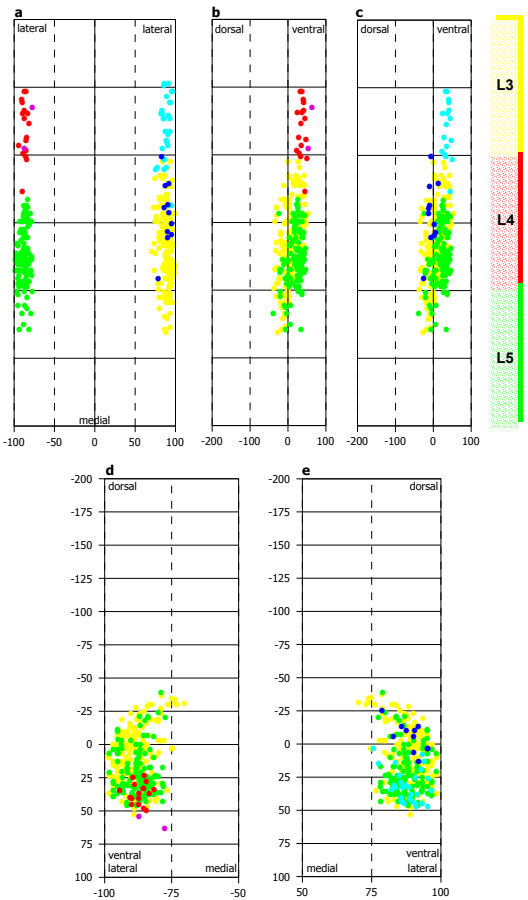

Figure 3.24 Combination of several motor nucleus columns.
a, relative cell position on the mediolateral, ***b***,***c*** on the dorsolateral axis and ***d***,***e*** on the spinal cord cross-section. *R1095* (yellow) 179 tibialis anterior motoneurons, R1149 (green) 124 motoneurons. In both experiments, the severed muscular nerves were immersed in plastic containers with a 40% HRP solution for 45 minutes and 120 minutes, respectively. *R1107* (dark blue), application of a 40% HRP solution to the deep peroneal nerve distal to the muscle nerve branch supplying the extensor hallucis proprius muscle, to mark the extensor digitorum brevis II and III muscle.
R808 (FB on the right: light blue, DY on the left: red), long-term fluorescence experiment (survival time 56 days) to check the preservability of the fluorescent dyes. Possible mismarking of two motoneurons on the left (***d***, violet). Injection of 5 µl of a 2% DY or FB suspension into the tibialis anterior muscle.
a, the right side of the spinal cord is shown on the right half of the image, ***b***, left side, ***c***, right side. After an HRP nerve bath, the TA cell columns were also transferred to the dorsoventral (***b*** and ***c***) and axial projections (***d*** and ***e***) on the opposite side.

(staining with Cresyl violet) or yellow-greenish (staining with hemalaun) background staining under UV excitation impeded recognition of the fluorescent-labeled motoneurons.

In order to be able to quantitatively evaluate morphological parameters of spinal nucleus columns prior to and after a lesion, and in the course of regeneration processes, using double and multiple markings with fluorochromes alone or in combination with HRP, first the preservability of Fast Blue and Diamidino Yellow was reviewed in a long-term experiment. In comparison to the average cell count of the nucleus column of the tibialis anterior muscle following a survival time of the animals from 4 to 9 days, the cell count after 56 days is 76.2% (23.5 MN; n = 2) lower (R808, Table 3.6 and Figure 3.25). In addition to the distinct reduction, a side difference of the cell count of 56.6% is also noticeable, which is not verifiable in the F1P1 test series. The side difference in cell counts amounts here to 0.3% (cell count on the right: 99.0 ± 13.8, on the left: 98.7 ± 7.8). 2D reconstructions of the cell column from the long-term experiment show that the fluorescence-marked motoneurons appear only in the ventral compartment of the area that the tibialis anterior muscle cell column generally occupies (Figure 3.24). Due to the low cell count and the incomplete labeling of the motoneuron pool, the applied fluorescent dyes are consequently not suited for a quantitative evaluation in longer survival times.

3.4.3.3. The combined use of HRP and the fluorescent dye Diamidino Yellow

To retain the regeneration process at different points in time following lesion and repair of a peripheral nerve, experiments were also begun in addition to the long-term fluorescent test which purported a compatibility test between the HRP enzyme histochemistry and the methods of fluorescent marking. The nucleus columns of the common peroneal nerve and tibialis anterior muscle served as the test system. The experimental protocol provided for bringing Diamidino Yellow into contact with the severed muscle nerve branches of the tibialis anterior muscle or injecting it into the muscle. After a transport time of 9 days, a 40% HRP solution was applied at the severed common peroneal nerve. The tests were performed identically on both sides and the application on the nerves took place according to the criteria of test series HRP5.

After immersion of the muscle nerve branches of the tibialis anterior muscle in a 2% suspension of Diamidino Yellow, no fluorescently marked spinal motoneurons could be detected after a contact time of 60 minutes. In contrast to the other fluorescent dyes (Illert et al., 1982; Katan et al., 1982), Diamidino Yellow is numbered among the substances which are absorbed by the severed nerve endings (Crockett et al., 1987; Puigdellivol-Sanchez et al., 1998; Puigdellivol-Sanchez et al., 2002) and should be compatible with the HRP enzyme histochemistry (Warton et al., 1988). Indeed, a wash-out effect was indicated by the TMB enzyme histochemistry (Conde, 1987) which can lead to a reduction of cell count.

A contributory cause from the manipulations as part of the methodical difficulties of filling the small-dimensioned catheter that is sealed on one side with the viscous fluorescent dye and bringing it into contact with the nerve endings should likewise not be excluded.

Figure 3.25 Cell counts of different muscles or nerves following retrograde transport of HRP or fluorescent dyes. The error indicators following the HRP nerve bath show the maximum values, and the standard deviation in other tests.

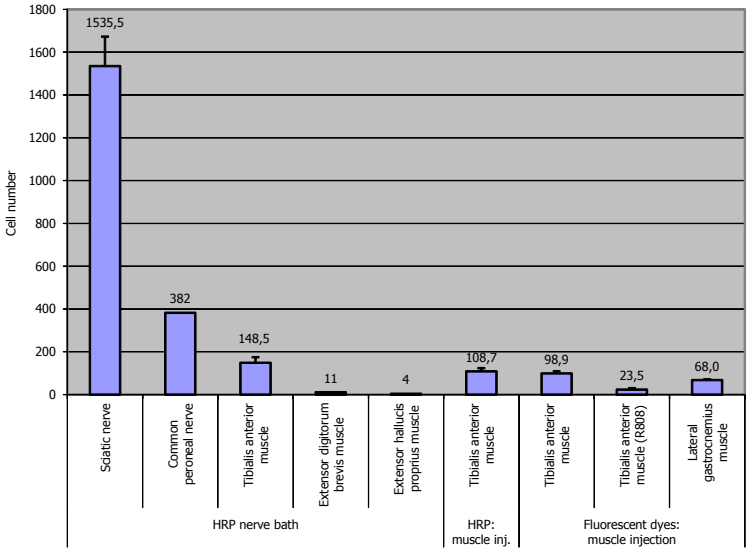

If Diamidino Yellow is injected into the tibialis anterior muscle prior to HRP application to the common peroneal nerve, the TMB enzyme histochemistry will lead, in addition to a distinctly reduced cell count, to a non-homogenous, partially atypical fluorescent marking also outside of the area generally occupied by the TA cell column (see 3.4.1, Figure 3.17, t-v). The intensity of HRP labeling is weakened in comparison to the tests with exclusive use of HRP, and the cell boundaries are often not clearly defined. The reason for this lies in the necessary conversion of the perfusion recommended by Mesulam (Mesulam, 1982) with glutaraldehyde and paraformaldehyde into a 4% paraformaldehyde solution alone, as glutaraldehyde is supposed to drastically reduce the intensity of fluorescent staining and change its characteristics (Kevetter and Willis, 1982; Kuypers and Huisman, 1984). On the other hand, there are reports according to which the increase in the concentration of paraformaldehyde leads to a stronger reduction of HRP enzyme activity than the increase in the concentration of glutaraldehyde (Rosene and Mesulam, 1978). A cell count of the common peroneal nerve cell column that is too low due to weakly stained, and thereby overlooked, motoneurons cannot be precluded (Figure 3.25). The quantitative analysis of cell parameters is only possible to a limited extent, based on the methodological difficulties performed.

3.4.4. Parameters of the cell column of the tibialis anterior muscle

3.4.4.1. Segmental and vertebral localization of the nucleus column

Following retrograde transport of HRP or the fluorescent dyes Diamidino Yellow and Fast Blue, the topographical positions in terms of the spinal cord segments from 51 spinal nucleus columns were recorded (Figures 3.27 and 3.28). Most of the data (n = 35) comes from the nucleus column of the tibialis anterior muscle (HRP muscle injection n = 22; HRP nerve bath n =5; FB muscle injection n = 2). The tests with Fast Green added to the HRP solution must be regarded as outliers (HRP2P1 on the left, n = 4), as a higher percentage of mismarked motoneurons is apparent, based on 3D reconstructions, and the long-term fluorescence experiment (F1P2, n = 2) shows only a partial labeling of the TA cell column. Other target structures were other muscles (HRP nerve bath: extensor digitorum brevis II and III muscle; DY muscle injection: lateral gastrocnemius muscle) or nerve trunks (HRP nerve bath: sciatic nerve, common peroneal nerve).

Figure 3.26 Segmental position of 31 cell columns of the tibialis anterior muscle. The relative positions of the cranial and caudal poles of the TA cell columns and of the average are indicated in percentage values following standardization of the segments to 100. The delineated histograms illustrate the segmental frequency distribution. The percentage data of the right ordinate applies to the length of the nucleus columns.

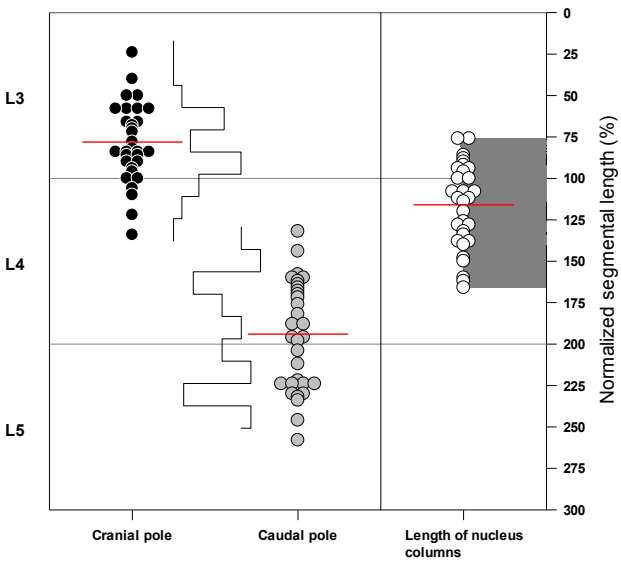

Figure 3.27 Segmental localization of the motoneuron columns.

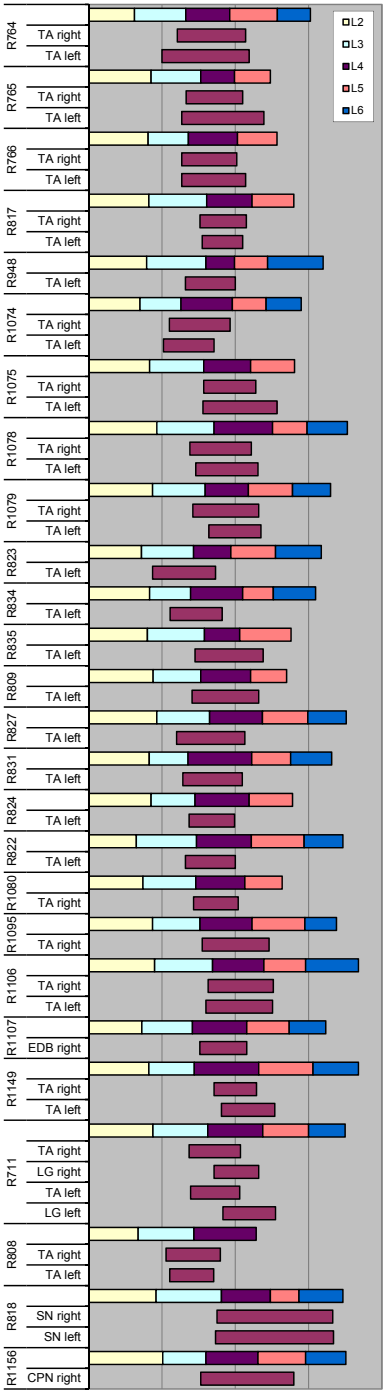

Figure 3.28 Segmental and vertebrogenic localization of the different motoneuron columns. VB: Vertebral body, S: Spinal segment.

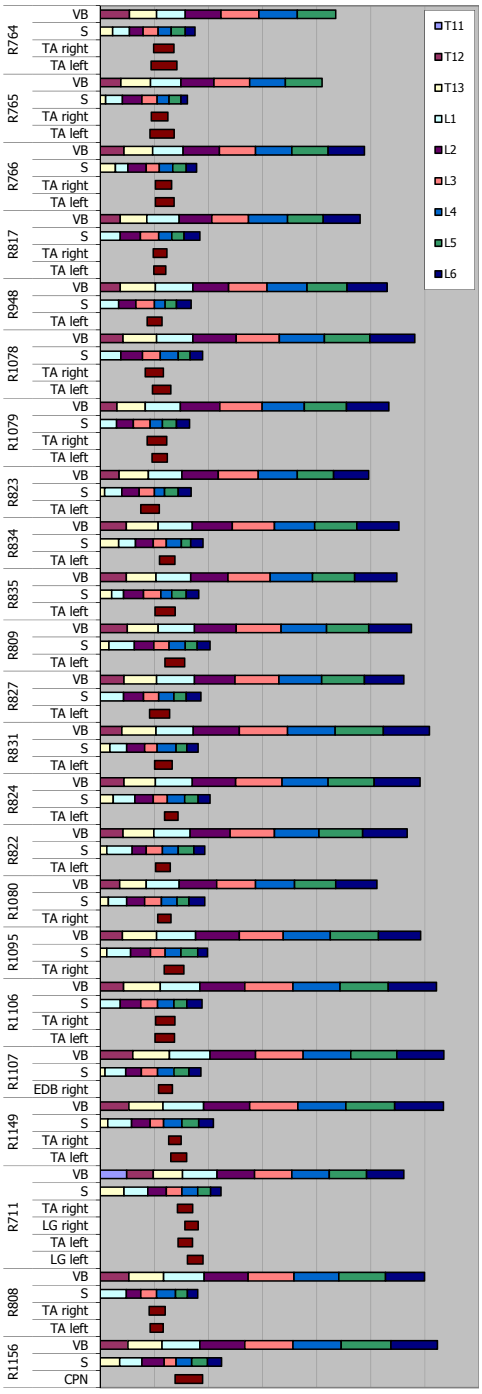

The segmental location of 10 cell columns of the tibialis anterior muscle after a radial nerve-common peroneal nerve autograft and other lesion tests is shown in Figure 3.40, and is discussed with the results of the graft series.

The nucleus column of the tibialis anterior muscle of the Sprague-Dawley rat is located in the spinal cord segments L3 to L5. In all 31 evaluated cell columns, motoneurons are present in segment L4 (n = 35, if HRP2P1 is considered after addition of FG). The L3 segment is included in 83.9% (n = 26) of the motoneuron columns, L5 in 41.9% (n = 13). The variability of the location of the rostral and caudal cell poles is 1 1/10 and 1 1/4 segments respectively (rostral: 110.8%, caudal 125.7%). The frequency distribution shows a bimodal distribution between the starting and ending points of the cell columns, with two local maxima above and below the averages. The distances between the maxima are not identical, and are larger for the distal end of the cell columns. The differences in length of the motoneuron columns are not statistically significant (t test, P = 0.998) for groups with a cranial (n = 6) or caudal (n = 6) location to the proximal column end. The differentiation of the cell columns into two groups (see Figures 3.27 and 3.28), depending on their craniocaudal position in the spinal cord, is the central correlate of the pre- and post-fixation of the lumbosacral efferents described by Sherrington (Sherrington, 1892; Romanes, 1951; Nicolopoulos-Stournaras and Iles, 1983).

In 67.7% (n = 21) of cases, the nucleus column of the tibialis anterior muscle stretches out over two segments, with preference for L3 and L4 (81.0%; L4, L5: 19.0%). The L3 to L5 segments are included in 29.0% (n = 9), while in 3.2% (n = 1) the cell column is nevertheless located in a lower cell count and a possibly insufficient marking of the motoneurons in one segment (R1149 on the right).

Analysis of the segmental affinity of the neurons from 30 TA cell columns (3765 motoneurons) after muscle injection of HRP or fluorescent markers, or after HRP nerve bath, resulted in a percentage of 27.6% in L3, 68.6% in L4 and 3.8% in L5.

The statistical analysis of the side differences for the start and end coordinates and the length of the TA nucleus columns showed no significant difference (t test, P > 0.7; n = 8). The addition of Fast Green to the HRP solution in test series HRP2P1 does not lead to a statically demonstrable change in position of the cell column, despite an increase in the number of mismarked motoneurons (t test, P > 0.441).

An allocation of 35 motoneuron columns to the spinal cord segments and also to the vertebral bodies could be established (Figure 3.28). The evaluation comprised the cell columns of the tibialis anterior muscle (n = 31), the lateral gastrocnemius muscle (n = 2), the extensor digitorum longus muscle (n = 1) and of the common peroneal nerve (n = 1). In terms of the localization to the spinal column, the cell column of the tibialis anterior muscle stretches from the lower third of the T13 to the middle of L1, but here can reach to the lower third. In 45.2% (n = 14), the cell column projects itself onto part of these two vertebral bodies. When a vertebral body is affected alone, it concerns almost exclusively L1 (n = 16); only the left TA cell column from the long-term fluorescent experiment can be found at the level of T13.

The cell column of the extensor digitorum longus II and II muscle is located at the level of segment L4, and thereby lies within the area which the nucleus column of the tibialis anterior muscle can occupy. The nucleus column projects itself onto the thoracic-lumbar transition area, in particular onto the caudal portion of the T13. In one test (R711), the cell columns of the tibialis anterior and lateral gastrocnemius muscles were

marked using a fluorescent double labeling. In comparison to the TA nucleus columns with an expansion from mid-L3 to mid-L4, the LG cell columns are shifted caudally by an approximate ½ segment length, and reach from the rostral portion of L4 to L5. The nucleus column can be well defined medial to the TA cell column on the spinal cord cross section. The LG nucleus column can be related to the proximal half of the vertebral body L1.

After application of an HRP solution to the severed sciatic nerve motoneurons that formed symmetrical nucleus columns, extending from the distal end of the L3 to the L6 segment, were labeled on both sides of the spinal cord. The motoneuron column of the common peroneal nerve has a cranial end at the level of the cranial sciatic nerve pole, but reaches only into the caudal L5 segment. The cell column lies at the level of vertebral body L1 and the cranial section of L2.

3.4.4.2. Morphology and localization of the tibialis anterior cell column

A morphometric evaluation was performed on 16 cell columns of the tibialis anterior muscle after an HRP nerve bath or injection of an HRP solution into the muscle. In Tables 3.7 and 3.8, doubled and mismarked motoneurons were considered and the values of the parameters corrected.

In 2D reconstructions of the TA cell columns (Figure 3.29, Figures 3.41 to 3.43 left), a fusiform nucleus column was shown in every test, which tapered off at the ends and is here characterized by the appearance of individual motoneurons. The caudal nucleus pole (R327 left, R766 right, R831 left, R822 left) is more frequently identified as the cranial pole (R327 right) by a loosening of the cell layers and by separately located motoneurons. In 68.8% (n =11), the reconstructions show a higher cell density in the upper third or the upper half of the nucleus column. R1095 differentiates herein from the other tests with a homogenous cell distribution in the proximodistal direction. Indeed, local density difference of the motoneurons appear along the longitude course of the border of the cell column. These ‘beads’ (Romanes, 1951; Burke et al., 1977) are prominent on the medial and dorsal sides of the nucleus column, but cannot always be clearly and regularly detected in tests following HRP muscle injection. It is rare (R327 right, R1075 right, n = 2, 12.5%) that there is a discontinuity in terms of a tandem cell column.

The nucleus column of the R835 left test shows a distinct cell reduction in the distal half next to a non-homogenous distribution of motoneurons, so an incomplete labeling of the cell pool can be presumed.

Table 3.7 Parameters of the cell column of the tibialis anterior and extensor digitorum brevis muscles (*R1107*).

Parameters	R327		R766		R1074		R1095	R1149	R1107
	Left	Right	Left	Right	Left	Right	Right	Left	Right
A1. Localization (mm)									
Mediolateral	-0.92/-1.24	0.88/ 1.28	-0.96/-1.3	0.96/ 1.37	-0.79/-1.15	0.81/ 1.15	0.96/ 1.35	-1.00/-1.28	1.03/ 1.26
Dorsoventral	0.06/-0.30	0.00/-0.41	0.19/-0.36	0.09/-0.36	-0.09/-0.41	-0.06/-0.41	0.24/-0.34	0.26/-0.28	0.17/-0.09
Localization (%)									
Mediolateral	-75.9/ -96.5	70.5/ 96.7	-70.8/-98.4	75.0/ 98.5	-70.9/-98.2	73.1/ 98.1	70.3/ 98.4	-77.4/-98.3	78.7/ 95.2
Dorsoventral	-8.8/ 45.2	0.00/ 53.3	-29.0/ 53.1	-12.1/ 53.3	14.3/ 53.3	9.4/ 53.3	-36.7/ 53.3	-38.7/ 48.4	-25.0/ 13.3
A2. Segment height	-	-	L3,L4,L5	L3,L4	L3,L4	L3,L4	L4,L5	L4,L5	L4
A3. Vertebral body height	-	-	L1 rostral/ L1 caudal	L1 rostral/ L1 center	-	-	L1 center	L1 rostral/ L1 center	D13 rostral/ L1 center
B1. Morphology									
Form	Spindle	Spindle	Spindle	Spindle	Spindle	Spindle	Spindle	Spindle	Spindle
Orientation									
a) Mediolateral	l-l	l-l	l-l	l-l	l-l	l-l	l-l	l-l	m-l-m
b) Dorsoventral	v-v	v-c	v-v	v-v	v-c	v-c	v-d	v-d	c-d
B2. Length (mm)	2.68	2.52	3.48	3.00	2.76	3.32	3.64	2.92	2.56
B3. Width (mm)									
Largest diameter									
a) Mediolateral	0.30	0.36	0.34	0.32	0.36	0.28	0.39	0.28	0.08
b) Dorsoventral	0.36	0.34	0.55	0.38	0.25	0.34	0.55	0.50	0.18
Largest expansion									
a) Mediolateral	0.32	0.41	0.34	0.41	0.36	0.34	0.39	0.28	0.23
b) Dorsoventral	0.36	0.41	0.56	0.45	0.32	0.34	0.58	0.54	0.26
Width (%)									
Largest diameter									
a) Mediolateral	19.4	23.0	27.6	21.9	27.3	19.6	28.1	20.9	5.0
b) Dorsoventral	54.0	44.2	80.7	56.3	36.2	44.0	87.8	73.1	25.8
Largest expansion									
a) Mediolateral	20.6	26.2	27.6	23.5	27.3	25.1	28.1	20.9	16.5
b) Dorsoventral	54.0	53.3	82.2	65.4	39.0	44.0	90.0	85.1	38.3
B4. Cell count[1]	127	109	246	103	110	101	175	122	11
B5. Area (µm²)									
Mean	-	-	-	-	957.0	952.3	662.2	785.8	507.6
SD	-	-	-	-	381.7	390.3	298.2	377.2	267.1
MIN	-	-	-	-	329.0	352.0	150.0	210.0	259.0
MAX	-	-	-	-	2049.0	1940.0	1582.0	1854.0	1189.0
B6. Diameter (µm)									
Mean	-	-	-	-	34.2	34.1	28.3	30.7	24.8
SD	-	-	-	-	6.8	7.2	6.3	7.5	6.0
MIN	-	-	-	-	20.5	21.2	13.8	16.4	18.2
MAX	-	-	-	-	51.1	49.7	44.9	48.6	38.9
B7. Cell types (%)									
IA	33.9	22.9	-	-	13.7	9.9	28.0	26.2	18.2
IB	7.9	6.4	-	-	44.2	37.4	48.6	13.9	0.0
IC	16.5	27.5	-	-	1.1	2.2	4.0	20.5	18.2
ID	3.9	1.8	-	-	3.2	2.2	4.0	13.9	27.3
IE	37.8	41.3	-	-	37.9	48.4	15.4	25.4	36.4
II	1.6	0.0	0.0	0.0	0.0	0.0	0.0	0.8	0.0

Cell count[1] after correction by doubled and mislabeled cells.
HRP muscle injection: R327, R766, R1074; HRP application to the muscle nerve branches: R1095, R1149.
Abbreviations:
lateral: l, medial: m, ventral: v, dorsal: d, central: c.

Transversal reconstructions (Figure 3.38), with the relative coordinates based on the position of the cells in the segment and on the lateral and ventral demarcation of the gray matter, show an expansion of the nucleus column following HRP nerve bath (R1095, R1149) to the dorsal edge of the anterior horn. With the exception of test R766 left, in which the addition of Fast Green to the HRP solution led to a distinct increase in the number of mismarked motoneurons, this area is not included after muscle injection of the tracer.

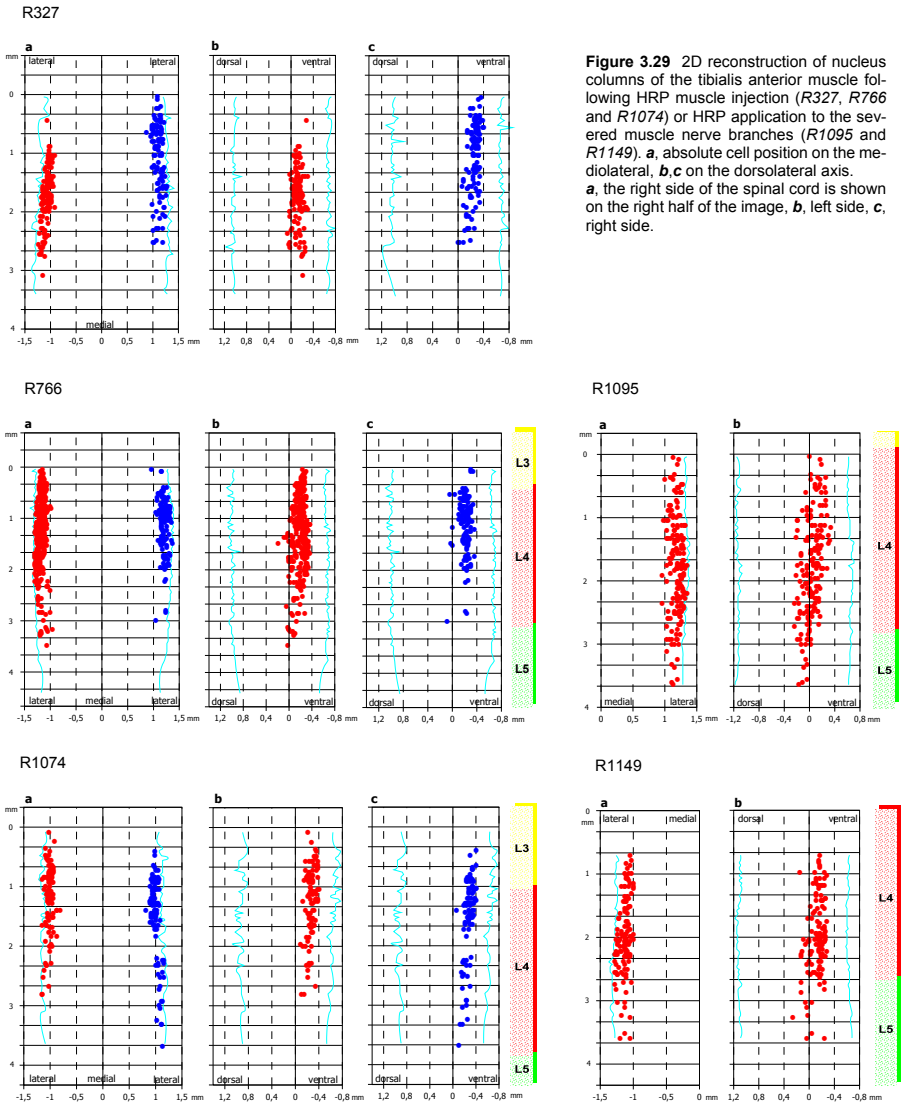

Figure 3.29 2D reconstruction of nucleus columns of the tibialis anterior muscle following HRP muscle injection (*R327*, *R766* and *R1074*) or HRP application to the severed muscle nerve branches (*R1095* and *R1149*). ***a***, absolute cell position on the mediolateral, ***b***,***c*** on the dorsolateral axis. ***a***, the right side of the spinal cord is shown on the right half of the image, ***b***, left side, ***c***, right side.

Table 3.8 Parameters of the cell column of the tibialis anterior muscle on the control side in graft series *HRP2G*.

Parameters	R823 Left	R834 Left	R835 Left	R809 Left	R827 Left	R831 Left	R824 Left	R822 Left
A1. Localization (mm)								
Mediolateral	-0.92/-1.22	-0.98/-1.24	-0.85/-1.35	-0.92/-1.30	-0.96/-1.41	-0.96/-1.39	-0.90/-1.26	-0.90/-1.15
Dorsoventral	0.02/-0.28	-0.06/-0.38	0.00/-0.36	0.13/-0.38	0.13/-0.34	-0.06/-0.30	-0.06/-0.30	-0.00/-0.30
Localization (%)								
Mediolateral	-70.5/-96.6	-74.2/-96.7	-70.7/-96.9	-70.3/-100.0	-70.3/-98.5	-70.3/-98.5	-71.2/-100.0	-78.2/-100.0
Dorsoventral	-3.4/ 46.4	9.7/ 51.5	0.0/ 53.5	-18.2/ 53.1	-20.7/ 53.3	10.0/ 50.0	12.0/ 52.2	00.0/ 52.0
A2. Segment height	L3,L4	L3,L4	L3,L4,L5	L3,L4,L5	L3,L4	L3,L4	L3,L4	L3,L4
A3. Vertebral body height	D13 caudal/ L1 rostral	L1 rostral/ L1 center	D13 caudal/ L1 center	L1 center/ L1 caudal	D13 caudal/ L1 rostral	D13 caudal/ L1 rostral	L1 center	L1 rostral/ L1 center
B1. Morphology								
Form	Spindle	Spindle	Spindle	Spindle	Spindle	Spindle	Spindle	Spindle
Orientation								
a) Mediolateral	l-m	l-l	l-l	l-m	l-m	l-m	l-l	l-l
b) Dorsoventral	v-v	v-v	v-v	c-v	v-v	v-c	v-v	v-c
B2. Length (mm)	3.44	2.84	3.72	3.64	3.72	3.24	2.48	2.72
B3. Width (mm)								
Largest diameter								
a) Mediolateral	0.30	0.26	0.41	0.38	0.43	0.39	0.36	0.23
b) Dorsoventral	0.30	0.30	0.34	0.51	0.47	0.24	0.24	0.28
Largest expansion								
a) Mediolateral	0.30	0.26	0.50	0.38	0.45	0.43	0.36	0.25
b) Dorsoventral	0.30	0.32	0.36	0.51	0.47	0.24	0.24	0.30
Width (%)								
Largest diameter								
a) Mediolateral	26.1	22.5	25.6	27.8	25.2	28.1	28.8	20.8
b) Dorsoventral	49.8	38.9	53.3	66.8	74.0	38.9	40.2	48.0
Largest expansion								
a) Mediolateral	26.1	22.5	26.2	29.7	28.2	28.2	28.8	21.8
b) Dorsoventral	49.8	41.8	53.3	71.3	74.0	40.0	40.2	52.0
B4. Cell count[1]	112	118	106	122	104	107	93	87
B5. Area (µm²)								
Mean	937.5	1094.3	959.6	957.2	1071.9	1118.7	782.6	853.4
SD	330.6	399.2	361.5	406	398	440.2	376.2	328.7
MIN	374	234	329	329	307	411	130	179
MAX	1874	2480	1850	1914	2476	2338	1843	1578
B6. Diameter (µm)								
Mean	34.0	36.7	34.3	34.1	36.3	37.0	30.6	32.3
SD	6.1	7.0	6.7	7.4	6.9	7.6	7.8	6.7
MIN	21.8	17.3	20.5	20.5	19.8	22.9	12.9	15.1
MAX	48.8	56.2	48.5	49.4	56.1	54.6	48.4	44.8
B7. Cell types (%)								
IA	33.9	59.8	28.6	39.8	53.4	48.6	14.7	50.7
IB	18.3	18.8	16.3	18.6	19.4	19.6	45.3	17.8
IC	10.1	5.1	14.3	12.7	1.9	6.5	9.3	4.1
ID	16.5	8.5	10.2	9.3	2.9	8.4	2.7	2.7
IE	21.1	7.7	30.6	19.5	22.3	16.8	28.0	24.7
II	5.5	1.7	3.1	1.7	1.9	4.7	0.0	2.7

Cell count[1] after correction by doubled and mislabeled cells.
Abbreviations:
lateral: l, medial: m, ventral: v, dorsal: d, central: c.

The orientation of the TA cell columns in horizontal reconstructions, and in the craniocaudal direction is 75% laterolateral, i.e. the cell columns run along the lateral border of the white matter. In the remaining 25%, the long axis of the nucleus column is lateromedially oriented. In sagittal reconstructions, 50% of the TA nucleus columns run ventroventrally in a longitudinal direction. In 7 of the 16 TA nucleus columns (43.8%), the orientation is ventrocentral, and ventrodorsal when crossing over the zero level defined by the central canal. This impression of a ventrodorsal orientation of the nucleus column of the tibialis anterior muscle is even further reinforced considering the relative cell coordinates and the combination of multiple cell columns in a figure made possible thereby (Figure 3.38).

In the mediolateral direction, the cell column of the tibialis anterior muscle stretches from 0.92 ± 0.06 mm to 1.28 ± 0.08 mm (relative coordinates: 72.5 ± 2.8% to 98.1 ± 1.2%), and from 0.05 ± 0.11 mm to -0.34 ± 0.05 mm in the dorsoventral direction (relative coordinates: -7.0 ± 17.4% to 51.6 ± 2.7%). The side differences in the coordinates are not significant (t test, $P > 0.181$).

The mean diameter of the TA nucleus column is 0.34 ± 0.06 mm (relative: 24.5 ± 3.3%) in horizontal reconstructions and 0.37 ± 0.11 mm (relative: 55.4 ± 16.3%) in sagittal reconstructions. In projection on the spinal cord cross-section, the TA nucleus column has a maximum expansion of 0.36 ± 0.07 mm (relative: 25.7 ± 2.9%) on the mediolateral axis and 0.39 ± 0.11 mm (relative: 58.5 ± 17.2%) on the dorsoventral axis. The average length of the TA nucleus column in the 16 reconstructed tests was calculated to be 3.13 ± 0.44 mm. Statistically significant differences do not appear between the values of the right and left nucleus columns for the diameter/expansion parameters (t test, $P > 0.229$) nor for length (t test, $P > 0.386$).

A distinct difference is apparent when comparing localization measures between the tests with an HRP nerve bath (R1095, R1149) and tracer application by muscle injection. While the values for diameter (HRP nerve bath 24.5 ± 5.1%; HRP muscle injection 24.6 ± 3.3%) and maximum expansion of the nucleus column correspond with each other (HRP nerve bath 24.5 ± 5.1%; HRP muscle injection 25.8 ± 2.8%), the values in sagittal reconstructions following application to the muscle nerve branches are larger (diameter: HRP nerve bath 80.5 ± 10.4%; HRP muscle injection 51.8 ± 13.7%; expansion: HRP nerve bath 87.6 ± 3.5%; HRP muscle injection 54.3 ± 13.9%). A statistical evaluation is not possible, based on the low sample size of the tests following HRP nerve bath.

Regarding the segmental and vertebrogenic height localization of the cell columns, see 3.4.4.1.

3.4.4.3. Cell count of the motor tibialis anterior cell column (Figure 3.25)

While using HRP as a retrograde transported cell marker, an average cell count of 111.7 ± 19.7 (n = 26) emerges for the nucleus column of the tibialis anterior muscle, with a percentage of mislabeled cells of 8.7%. The form of application of the tracer remained unconsidered here. Following HRP muscle injection, 108.7 ± 15.3 (n = 24) motoneurons are marked, the percentage of mislabeled cells totaling to 9.6%. Including the FG tests,

the cell count increases to 123.6 ± 43.2 (n = 30) with the percentage of mislabeled motoneurons at 11.2% (Table 3.4). When the muscle nerve branches supplying tibialis anterior muscles are prepared and immersed in an HRP solution, the average number of motoneurons is higher at 148.5 (n = 2; Table 3.5). The number of double marked cells was individually determined for the tests (Tables 3.7 and 3.8) in which a reconstruction of the cell columns was prepared, by means of the outlines of the cell fragments and their coordinates. The number of double labeled motoneurons of the tibialis anterior muscle cell column reached an average of 13.9 ± 4.7%, with a span between 5.0% and 22.9%.

The cell count of the TA nucleus column following injection of Diamidino Yellow or Fast Blue into the muscle is lower compared to the HRP tests at 98.9 ± 10.8 (n = 7). As a reconstruction of the cell columns was not possible due to lacking technical-mechanical requirements (with the exception of test R808), the double count of cell fragments was avoided solely by the assessment of cell morphology in neighboring sections.

3.4.4.4. Cell density

To calculate the cell density of the tibialis anterior muscle nucleus column, the reconstructed control tests and the control sides of the graft series HRP2G (Table 2.1) were divided into 8 sections. Beginning with the relative cell coordinates, a visualization of the interpolated distribution took place by means of 2D diagrams in the transversal, horizontal and sagittal sectional planes (Figures 3.30 and 3.31).

After a summation of the density values of all control tests (n = 16), it becomes apparent that the motoneurons within the cell column of the tibialis anterior muscle are uniformly distributed. The cell density is highest in the upper third of the cell column and gradually decreases caudally. The gradient is asymmetrical in the mediolateral direction, and is steeper medially than it is laterally. In terms of the cell column overall, the cell density only decreases laterally by 25% up the border on the gray matter.

Figure 3.30 Interpolated cell density figure from 16 TA cell columns on the control side in the ***a***,***b*** transversal, ***c***,***d*** horizontal and ***e***,***f*** sagittal sectional planes. The numerical data from the x and y axes correspond to relative coordinates, based on the boundary of the spinal cord. The z axis depicts the rostrocaudal expansion of the nucleus column which was divided into 8 sections. To represent all control tests, the relative cell coordinates were totalized in a grid with an edge length of 10% and 15% (***a***,***b***) or of 10% and 1/8 of the nucleus column in a craniocaudal direction (***c***-***f***).

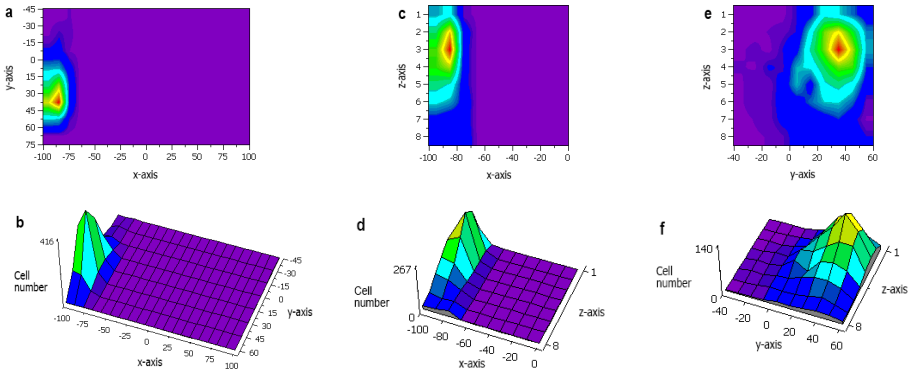

Figure 3.31 Cell density of the TA cell column on the ***a***, transversal, ***b***,***c*** horizontal and ***c***,***e*** sagittal sectional planes. The ordinates and abscissa in ***a*** denote the relative coordinates based on the boundary of the gray spinal cord matter. For the display in ***b***-***e***, the cell columns were divided into 8 sections and the interpolated cell density distribution was calculated. Figures ***b*** and ***d*** represent the left, and ***c*** and ***e*** the right sides of the spinal cord.

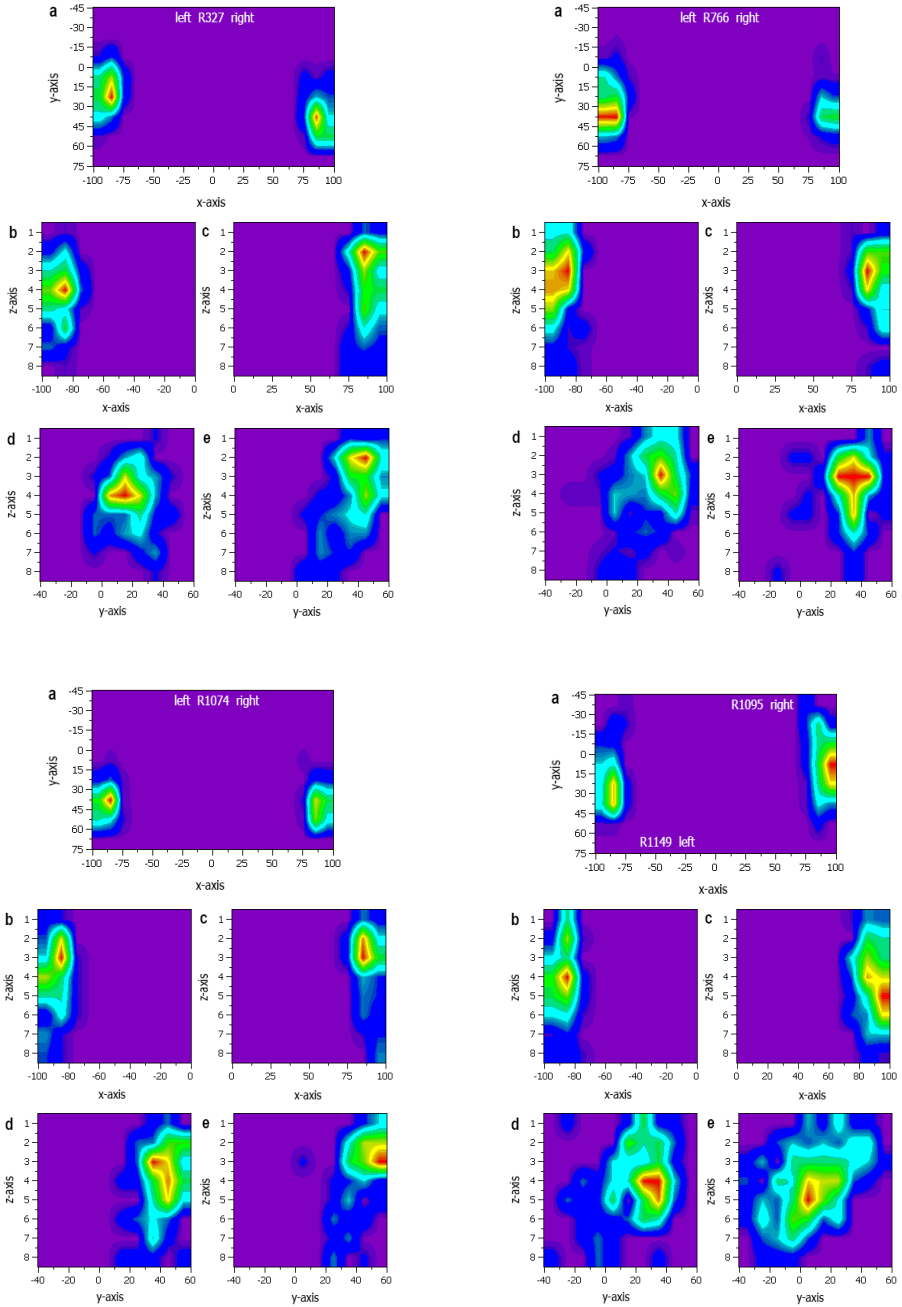

In relative coordinates, the area of the highest cell density is located on the spinal cord cross-section, between 80% and 90% in the mediolateral direction and between 30% and 45% in the dorsoventral direction. The center of the highest cell density lies clearly ventral to the central canal.

Following the results of the individual tests, the maximum cell density lies at the level of segment 3/8 in 50% of the reconstructed TA cell columns. The cell density is highest in the upper 3 segments in 68.8% of the cell columns, and in 25% in the middle area of the cell column. In one test (R824) the maximum is at 6/8, where the cell column is characterized by a plateau of approximately equal cell density from 3/8 to 6/8.

In 81.3% of the nucleus columns, the highest neuronal density is located on the horizontal plane between 80% and 90%, and between 90% and 100% in 18.7% of the nucleus columns. In a projection onto the sagittal sectional plan, the maximum density is at 30% and 45% in 68.8% of the nucleus columns, between 15% and 30% in 25% of the columns, and between 0% and 15% for 6.2% of the columns.

The tests following an HRP nerve bath (R1095 and R1149) are characterized by the location of the largest cell density in the nucleus column center, with a slight offset in the dorsal direction.

3.4.4.5. Diameter and area of the motoneurons of the tibialis anterior muscle

For the motoneurons on the control sides of the reconstructed TA nucleus columns (n = 12, Tables 3.7 and 3.8), an average area of 917.4 ± 399.1 µm^2 was measured with a span of values from 130.0 µm^2 to 2480.0 µm^2. The calculate diameter is 33.3 ± 7.5 µm (span

Figure 3.32 Histograms of area and diameter for the motoneurons of 12 HRP labeled cell columns of the tibialis anterior muscle.

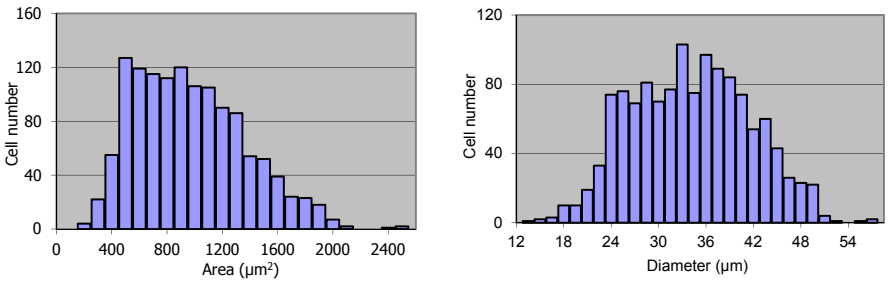

12.9 µm to 56.2 µm). Histograms of all 12 HRP tests show a unimodal distribution patter for area and diameter (Figure 3.32). However, no symmetrical, uniform distribution results from the histogram of diameter distribution, with an additional local maximum diameter at 25 µm. When comparing the HRP2 tests series (muscle injection) to HRP5 (nerve bath), a significantly lower average diameter of TA motoneurons is seen following an HRP nerve bath (Table 3.9, Mann-Whitney test, $P<0.0001$).

Aside from the average values, the minimum and maximum values from both test series also differentiate with a clear difference of 7.6 µm for the upper limiting diameter. The

Table 3.9 Diameter and area of the MN following HRP muscle injection and HRP nerve bath.

Test series	Number of CC	Diameter (µm)			Area (µm²)		
		M ± s	Min	Max	M ± s	Min	Max
HRP2	10	34.6 ± 7.2	12.9	56.2	979.0 ± 395.7	130.0	2480.0
HRP5	2	29.3 ± 6.9	13.8	48.6	713.0 ± 337.8	150.0	1854.0

Abbreviations:
CC: Cell columns, M: Mean, s: Standard deviation,
Min: Minimum value, Max: Maximum value.

cumulated figure of the diameter values (Figure 3.33) shows a left shift of the HRP5 curve which runs up to a 50% value steeper, and then flatter, than the HRP2 curve runs. Responsible for this is the higher percentage of neurons with a low diameter, and not the lower span of the HRP5 values.

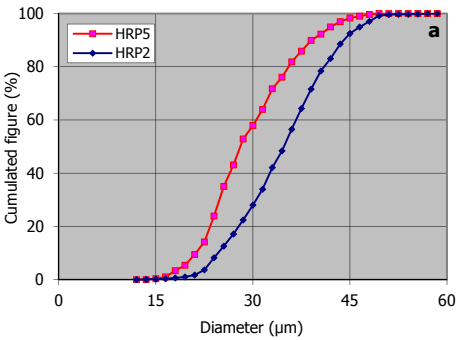

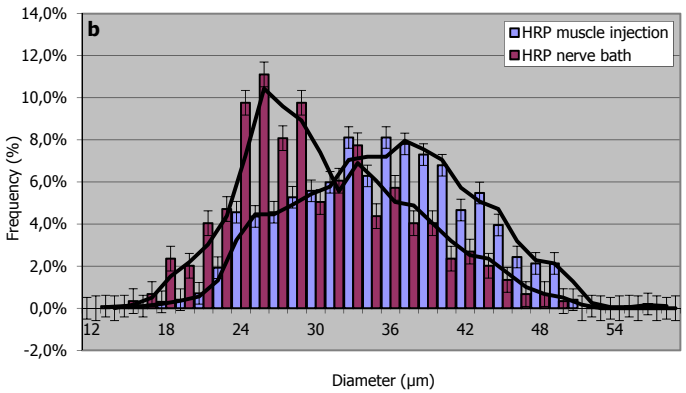

Figure 3.33 ***a***, Cumulated figure and ***b***, distribution of the cell diameter in test series HRP5 and HRP2.

Depictions of the three-dimensional distribution of cell diameter show no systematic clustering of specific size classes within the cell columns (Figure 3.34). In some cell columns (R823, R1074 left, R1095 and R1149), a diameter preference between 40–50 µm for the cranial half of the nucleus column is present. The largest motoneurons (diameter 50-60 µm) can be located in all sections of the nucleus column.

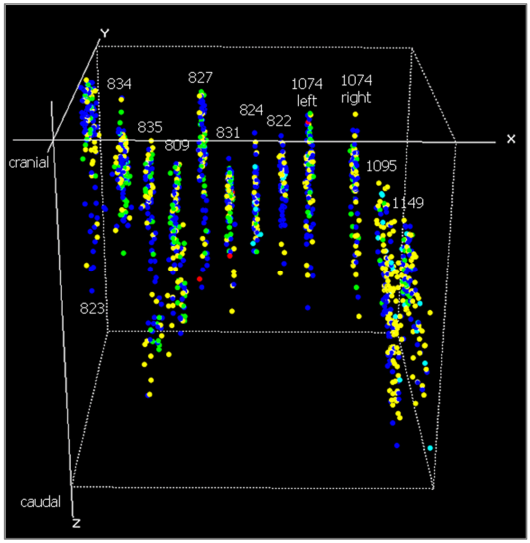

Figure 3.34 Diameter distribution of the motoneurons from 12 nucleus columns in the craniocaudal (z axis), mediolateral (x axis) and ventrodorsal (y axis) directions; light blue (10-20 µm), yellow (20-30 µm), blue (30-40 µm), green (40-50 µm) and red (50-60 µm).

3.4.4.6. Cell types in the cell column

3.4.4.6.1. Classification according to the stain model of the HRP labeled motoneurons

The motoneurons of the TA nucleus column that were marked with HRP and stained with the dye tetramethylbenzidine were divided into 6 classes based on the marked cell structures and the intensity of the marking (Materials and Methods 2.4.2.3.3; Figure 3.35). Types IA to IE denote motoneurons, and type II denotes artifacts and can include cell fragments that do not spatially relate to motoneurons in neighboring sections.

Figure 3.35 *Left:* Frequency of cell types based on the HRP marking pattern in the experiments from test series ***HRP2*** (n = 10) and ***HRP5*** (n = 2). *Right*: Depiction of the average diameters and their standard deviation for cell types from the 2 test series. The cell types are consolidated into groups IA+B, IC+D, IE and II.

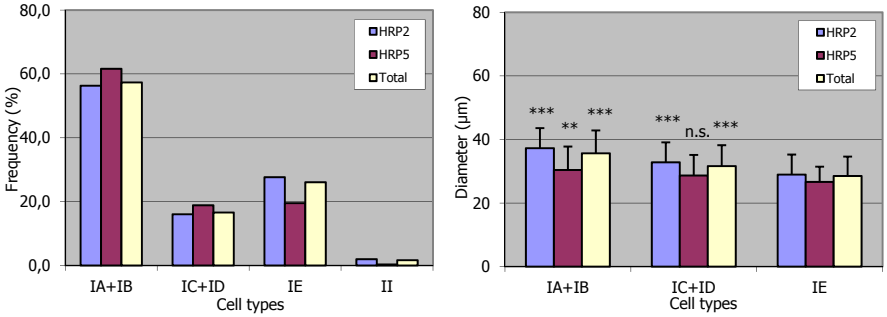

When the motoneurons of the morphometrically evaluated HRP tests are classified based on HRP labeling characteristics, 57.3% of the cells prove to be type IA (33.4%) and IB motoneurons (23.9%). Together with type IC (9.9%) and ID neurons (6.6%), with a total of 73.9% they represent a cell pool with clear cell boundaries and a marking intensity sufficient for morphometric evaluation. The percentage of the weakly or partially stained type IE motoneurons is 26.1%, the dye products classified as artifacts are 1.6%.

The frequencies of the individual types in test series HRP2 and HRP5 differentiate only slightly despite the different type of application. The percentage of the type IE motoneurons is higher after muscle injection (HRP2: 27.7%) than after an HRP nerve bath (HRP5: 19.5%). The type II percentage is low for both test series (HRP2: 2.0%, HRP5: 0.3%). The frequencies of cell types IA to IE are distributed statistically differently in test series HRP2 and HRP5 (χ^2 test, $P<0.001$).

To answer the question of whether the different cell types also correspond to motoneurons with different diameters, the average diameter was calculated for some cell types. The results for test series HRP2 and HRP5 are shown the histograms from Figure 3.35. Compatible cell types were consolidated into groups IA+B, IC+D and IE for this purpose. The cell classes differentiate significantly in diameter, both for the overall cell population and for the HRP2 series (H test by Kruskal and Wallis, post-test according to Dunn, $P<0.001$). By contrast, significant differences in diameter are only present for the test series HRP5 when compared to the cell types IA+B vs. IE ($P<0.01$).

The overall low average values of the cell diameters following HRP nerve bath (Table 3.9) are also reflected in the smaller cells of the individual cell types, where the difference from test series HRP2 is most evident for cell group IA+B. The test series HRP2 and HRP5 exhibit significant differences regarding the diameter of their cell types (Mann-Whitney test, IA+B and IC+D: $P<0.001$, IE: $P<0.019$).

According to Figure 3.35, a decline in cell diameter from IA+B to IE emerges for the overall motoneuron population as well as test series HRP2 and HRP5, depending on the classification (all MN: IA+B 35.6 µm, IC+D 31.6 µm, IE 28.5 µm). For the HRP2 series and considering all HRP marked motoneurons, this decline can also be substantiated for the cell types IA to IE that weren't grouped. Consequently it comes about that complete and more intensely labeled motoneurons exhibit a larger cell diameter than small motoneurons whose cell marking is less thick and, in part, is also incomplete. This carries weight in the context of the discovery by some authors that smaller cells correspond to gamma motoneurons and also exhibit a higher labeling intensity due to their tonic activity (Eccles et al., 1960; Bryan et al., 1973; Strick et al., 1976; Burke et al., 1977).

3.4.4.6.2. Classification of motoneurons by diameter

Unlike the summation histograms from the experimental series HRP2 and HRP5 (Figure 3.35), in which a homogenous distribution is shown in terms of areas and diameters, bi- or trimodal distributions can been detected in differently notable characteristics in the histograms of the individual tests. In the 12 reconstructed HRP tests in which the TA nucleus column was labeled, a distribution of diameter into 2 size classes is discernable in 75%. The remaining 25% show a bimodal distribution with a not as easily definable limiting diameter. A trimodal distribution of diameter is well shown in 50% of the histograms. However, in all tests of the control series, a classification of the diameters into 2 or 3 size classes is possible based on the histograms. Due to the partially undiscernible bi- or trimodality on the graft site of the HRP2G test series, the limiting diameter was defined at 28.5 µm to classify the alpha and gamma motoneurons, and at 37.5 µm to differentiate large and small alpha cells (Pellegrini et al., 1977; Brushart and Mesulam, 1980; Ha et al., 1980; Peyronnard and Charron, 1980; Johnson, 1986; Hashizume et al., 1988).

Table 3.10 Morphometric parameters of the gamma, alpha 1 and alpha 2 motoneurons following classification based on the histograms from test series ***HRP2*** (TA muscle injection) and ***HRP5*** (HRP nerve bath). Compare with **Figure 3.37**.

	Alpha MN		**Gamma MN**		**Gamma/ Alpha+Gamma**
	Cell count	Diameter (µm)	Cell count	Diameter (µm)	
HRP2	77.5 ± 16.0	37.3 ± 5.5	21.6 ± 4.2	24.8 ± 2.9	0.22 ± 0.06
HRP5	79.5 ± 17.7	34.4 ± 5.0	69.0 ± 19.8	23.4 ± 3.0	0.46 ± 0.02

	Alpha 1 MN			**Alpha 2 MN**		
	Cell count	Diameter (µm)	Alpha 1/ Alpha+Gamma	Cell count	Diameter (µm)	Alpha 2/ Alpha+Gamma
HRP2	38.3 ± 11.0	41.4 ± 4.1	0.39 ± 0.10	39.6 ± 13.3	33.3 ± 3.1	0.39 ± 0.11
HRP5	32.5 ± 3.5	39.4 ± 3.5	0.22 ± 0.03	47.0 ± 14.1	31.0 ± 2.3	0.31 ± 0.02

Anatomical and electrophysiological studies have verified neurons of various sizes in the area of the spinal anterior horn (Eccles et al., 1960; Nyberg-Hansen, 1965; Van Buren and Frank, 1965; Janzen et al., 1974). The larger cells represent alpha motoneurons, while the smaller cells depict a mix of gamma motoneurons, Renshaw cells and interneurons (Eccles et al., 1960; Johnson and Sears, 1988). Gamma motoneurons topographically neighbor the alpha motoneurons in the motoneuron nucleus, and are generally smaller than they are in terms of diameter (Eccles et al., 1960; Bryan et al., 1972; Ulfhake and Cullheim, 1981; Johnson, 1986; Moschovakis et al., 1991).

Figure 3.36 Histograms of areas and diameters in test series ***HRP5*** and ***HRP2***. The classification of diameter took place based on the distribution pattern in different size classes. With missing bi- or trimodal distribution of diameter, a limiting diameter of 28.5 µm was taken as a basis for differentiating alpha to gamma motoneurons, and a limiting diameter of 37.5 µm for differentiating type S and type FG motoneurons.

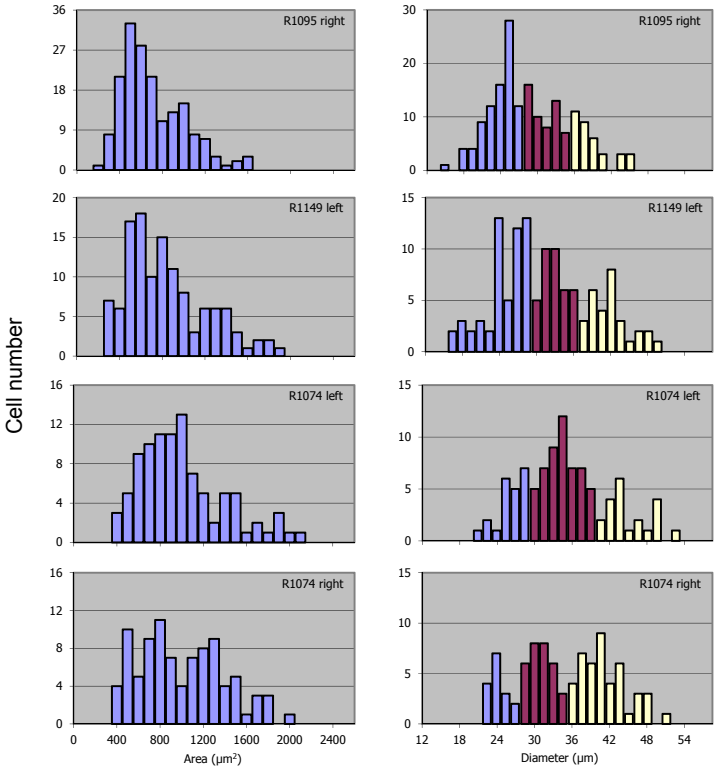

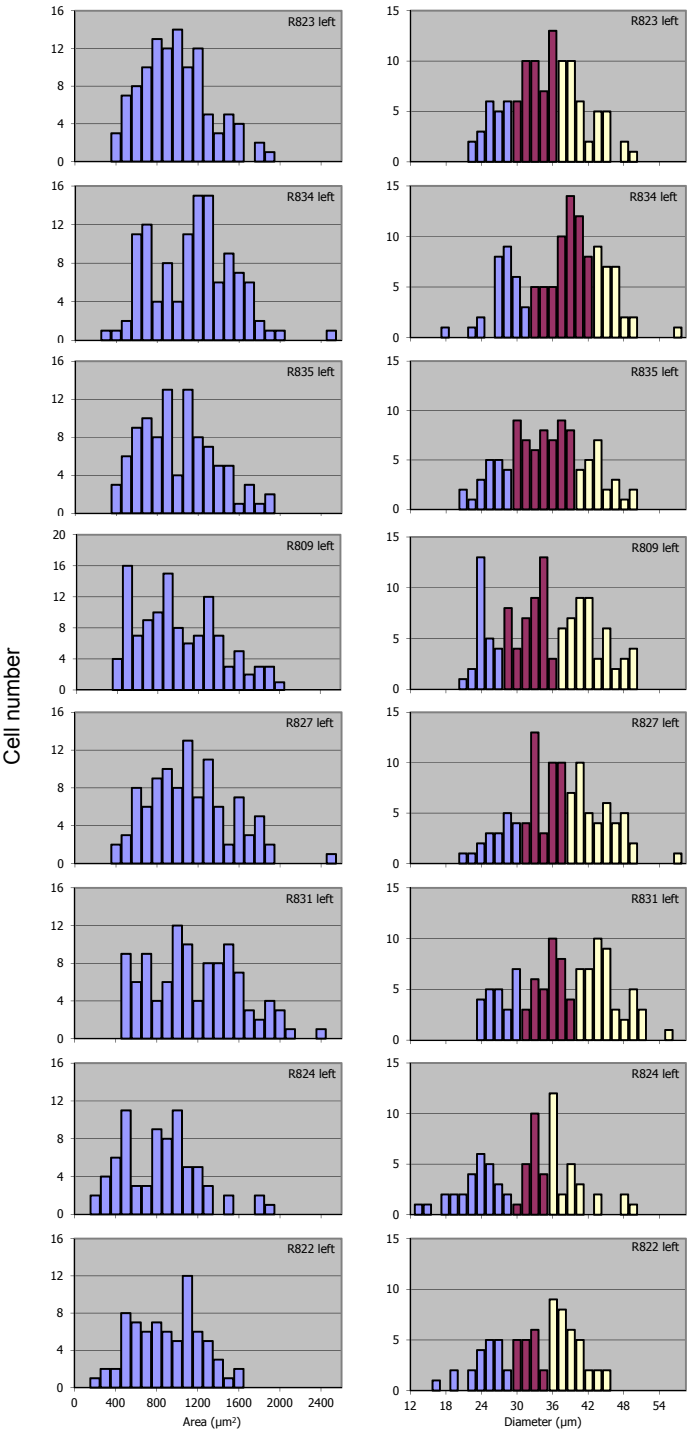
Cell number
R823 left
R834 left
R835 left
R809 left
R827 left
R831 left
R824 left
R822 left
Area (µm²)
Diameter (µm)

The measurement of nerve conduction velocity of beta motoneurons resulted in lower values compared to alpha motoneurons, so that a distinct size of the somata between the alpha and gamma neurons was indirectly deduced (Emonet-Denand et al., 1975; McHanwell and Biscoe, 1981b). As the portion of the beta system at the innervation of the tibialis anterior muscle of the rate is not known, this cell population was not considered for classification of the motoneurons.

Based on histochemical and physiological features, the alpha motoneurons and the muscular units innervated by them were differentiated into different populations of motor units, where smaller alpha motoneurons innervate slow type S (slow) muscle fibers and larger motoneurons innervate faster type FF (fatigue resistant) and type FR (fast-fatigable) muscle fibers (Henneman and Olson, 1965; Burke et al., 1973; Burke et al., 1974).

Corresponding to these experimental results, the three definable size classes from the histograms of Figure 3.36 were assigned to the gamma, alpha 1 and alpha 2 motoneurons (Pellegrini et al., 1977; Ha et al., 1980). The border area between these entities is ideally characterized by a depression in the diameter distributions and lies between 27.0 µm and 30.0 µm for the gamma/alpha 1 transition area, with a mean of 28.4 ± 1.2 µm. For the alpha 1/alpha 2 border area, there is a span of 34.5 µm to 40.5 µm with a mean of 36.6 ± 2.3 µm.

Under consideration of the different application of the HRP tracer in test series HRP2 and HRP5, slightly deviating average limiting diameters are calculated (HRP2, n = 10; gamma/alpha 1: 28.5 ± 1.2 µm, alpha 1/alpha 2: 36.3 ± 2.4 µm. HRP5, n = 2; gamma/alpha 1: 28.8 µm, alpha 1/alpha 2: 35.3 µm).

Following classification of the HRP labeled motoneurons into the different size classes, the respective diameter averages were calculated, separately for test series HRP2 and HRP5 (Table 3.10). Following muscle injection (HRP2), there is a diameter of 24.8 ± 4.2 µm for the cells classified as gamma motoneurons and a diameter of 37.3 ± 5.5 µm for the class of alpha motoneurons. The percentage of gamma motoneurons in the overall cell population is 22% in the HRP2 test series, and is thereby markedly lower than in the HRP5 series with 46%. Following an HRP nerve bath, the average diameters differentiate less in comparison to the HRP2 series for the gamma (23.4 ± 3.0 µm) than for the alpha cell pool (34.4 ± 5.0 µm).

Under the paradigm of a possible classification of the cells into gamma, alpha 1 and alpha 2 motoneurons, there is an average diameter of 41.4 ± 4.1 µm for the alpha 1 motoneurons after TA muscle injection (HRP2), and 33.3 ± 3.1 µm for the alpha 2 motoneurons. The percentage of the motoneuron pool is 39% each time. Although the cell count of the alpha motoneurons differs only marginally between the HRP2 and HRP5 series with a difference of 2 neurons, the percentage of alpha 1 and alpha 2 motoneurons in the cell pool following HRP nerve bath is markedly different. Above all it is decreased for the larger alpha 1 MN with 22%, while the percentage of the smaller alpha 2 MN is 31%. The average diameters are, by contrast, equally lower by approximately 2 µm for the alpha 1 and alpha 2 MN (alpha 1: 39.4 ± 3.5 µm, alpha 2: 31.0 ± 2.3 µm).

3.4.4.7. Distribution of alpha and gamma motoneurons in the tibialis anterior nucleus column

The distribution of the HRP labeled alpha 1, alpha 2 and gamma motoneurons is shown in Figure 3.36 for all 12 nucleus columns together and for the individual tests. To record the changes in frequency of the cell types in the craniocaudal axis of the cell column, the TA nucleus columns were divided into four equidistant sections and the percentage portions of the classified motoneurons were plotted (Figure 3.37, right half of the image).

Figure 3.37 Distribution of the alpha 1, alpha 2 and gamma motoneurons in the HRP control tests. The *left* half of the image depicts the distribution of motoneurons over the overall cell column, and the *right* side shows after allocation of the nucleus column into 4 segments from cranial to caudal.

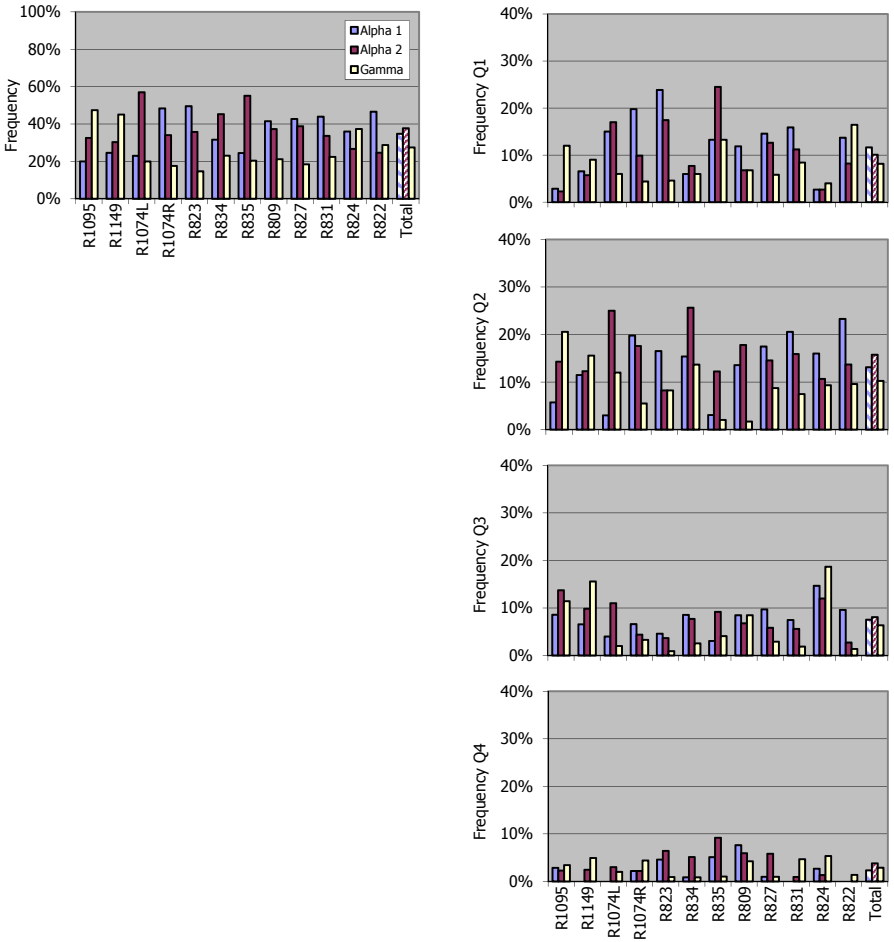

Considering all motoneurons of the 12 nucleus columns, there is an alpha-gamma quotient of 2.6 for the overall cell column. This quotient has a maximum at 2.8 in the second quarter of the nucleus column, decreases caudally and reaches a minimum at 2.1 in the fourth quarter. It can also be deduced from the frequency distribution in the four segments of the TA nucleus column that the cell count in the second quarter is the highest at 39.1%. The percentage of alpha motoneurons is also highest in this section. The percentage of alpha 2 motoneurons is highest in the overall cell population and in the three lowest sections of the cell column. The percentage of alpha 1 motoneurons is only higher in the cranial segment. The comparison of the cranial halves with the caudal halves of all of the nucleus columns shows a proportionally stronger reduction in cell count for the alpha 1 than for the alpha 2 and gamma motoneurons. Based on the cell count of the individual segments, the relative percentage of the alpha 1 motoneurons decreases continuously from cranial 39.0% to caudal 25.9%, while the percentage of gamma motoneurons increases continuously from 27.3% over the four sections to 31.9%. The relative percentage of the alpha 2 motoneurons is also higher in the caudal quarter at 42.2% than in the proximal quarter (33.8%).

A clear difference is evident when comparing the test series following HRP muscle injection and application of the tracer on the severed nerve branches. As already depicted in the cumulated distribution of diameter values (Figure 3.33), the portion of smaller motoneurons is markedly higher after HRP nerve bath than after muscle injection, where the average alpha-gamma quotient is 1.2. The gamma motoneurons are also the most frequently occurring cell type in the four sections (exception: R1095 third quarter). In contrast, in 80% of the HRP2 nucleus columns the percentage of gamma motoneurons is lowest, and in 60% alpha 1 motoneurons are the most frequent cell type. As in the HRP2 series, the alpha-gamma quotient is highest in the middle segments of the HRP5 nucleus columns.

The comparison of the cell columns amongst each other reveals a variability in terms of the percentage of classified motoneurons. Indeed, if the distribution pattern of cell types in the four sections of the nucleus column are compared with the overall cell column, an identical distribution pattern is verifiable in 60.4%. In 66.7% similar distributions of the alpha 1, alpha 2 and gamma motoneurons appear in two sections of the cell column, and in 41.7% they even appear in 3 sections.

3.4.4.8. 2D and 3D reconstructions of the tibialis anterior nucleus column

Following transformation of the absolute coordinates into relative ones, it's possible to simultaneously depict multiple cell columns in 2D and 3D reconstructions. Figure 3.38 shows the localization of 8 TA nucleus columns after HRP labeling, 2 TA nucleus columns after long-term fluorescence marking (R808) and the cell column of the extensor digitorum brevis II and III muscle after HRP nerve bath (R1107). For reasons of clarity, the 8 TA nucleus columns are not included on the control side of the HRP2G graft series; they're listed with the nucleus columns following autologous grafts under 3.5.9 (Figure 3.53). The reconstructions corresponding to Figure 3.38 in 3D space were already shown in Figure 3.18 (R327), Figure 3.19 (R766) and Figures 3.21-3.23 (R1095, R1149, and R1107). By way of comparison, Figure 3.29 shows 2D representations of the nucleus columns based on absolute coordinates.

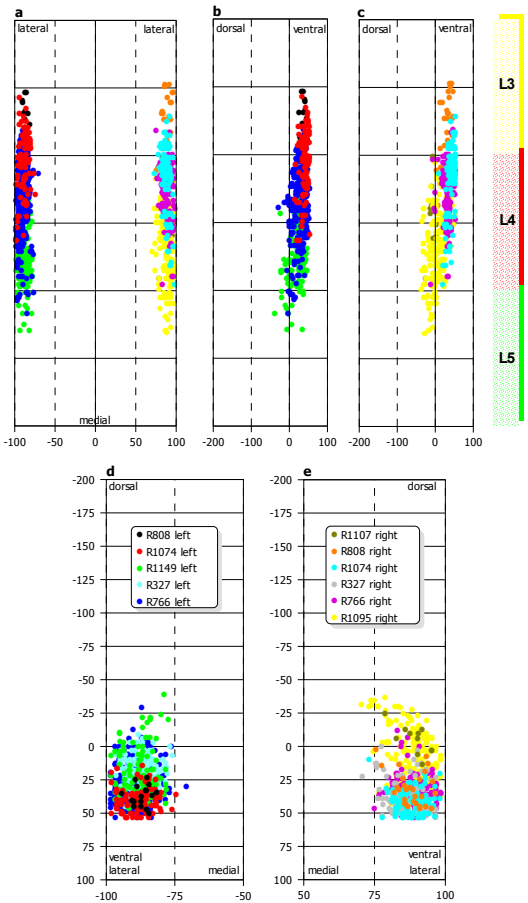

Figure 3.38 2D reconstructions of 10 cell columns of the tibialis anterior muscle following HRP muscle injection (*R327*, *R766*, *R1074*), HRP nerve bath (*R1095*, *R1149*) and following muscle injection of the fluorescent dyes DY and FB (*R808*). First, the nucleus column of the extensor digitorum brevis II and III muscles is shown on the right after HRP nerve bath. The nucleus columns of *R327* are only shown on the transversal reconstructions due to missing segmental attribution.
For the reconstructions of the nucleus columns, the relative cell coordinates in the segment and on the spinal cord cross section were calculated based on limiting lines of the gray matter. ***a***, relative cell position on the mediolateral, ***b***,***c*** on the dorsolateral axis and ***d***,***e*** on the spinal cord cross-section.

The segmental variability of 10 nucleus columns of the tibialis anterior muscle (center L3 to center L5) and the orientation of the cell columns parallel to the craniocaudal axis of the spinal cord in the horizontal plane, and from cranioventral to caudodorsal in the sagittal plane are vividly shown in Figure 3.38, a-c. An area ventral to the central canal (relative coordinates: x = ±75% to ±100%, y = 0% to approx. 53.3%) of the motoneurons of all 10 TA cell columns is occupied on spinal cord cross-sections (Figure 3.38, d-e). The dorsal extension in the border area to the gray matter, in contrast, consists only of motoneurons following HRP nerve bath (R1095, R1149) or addition of FG to the injected HRP solution (R766 on the left). The motoneurons of the extensor digitorum brevis II and III muscles (R1107) are also located in this area.

3.5. Parameters and reconstruction of the spinal cell column of the tibialis anterior muscle following a radial nerve-peroneal nerve autograft on the right

3.5.1. Macroscopic evaluation of the graft throughout regeneration

Following autograft and a regeneration time of 2, 4, 8 and 10 weeks, the site was exposed once again and the graft as well as the peripheral nerve were assessed in terms of continuity, scar formation, intraneural neuroma and the position of the suture material. In addition, the length of the graft and the distance from the distal suture site to the entrance of the nerve into the peroneal compartment were measured (Table 3.11, Figure 3.39).

Clear macroscopic abnormalities were observed on 4 of the 9 examined autografts. In three cases, a considerable scar formation and adhesion of the nerves with the muscle fascia of the biceps femoris muscle were present. Intraneural neuromas were clearly visible in 3 grafts, less clearly in R827 because a long, subtle distension was present. In one case (R835) there did not exist the expected continuity between graft and distal nerve stump. The graft had grown together with the muscle fascia, after it had apparently undone the suture and a dehiscence of the nerve endings had occurred. The proximity of the distal nerve stump, and possibly its direct contact with the graft center, could have led to an atypical sprouting of the axons at this site into the peripheral nerve.

Noticeable caliber differences proximal and distal to the graft were macroscopically discernible in the cases of R827 and R822. For R827, the diameter was distally lesser than the graft, for R822 it was proximally lesser.

The average length of the graft lay at 6.0 ± 1.6 mm, and the

Table 3.11 Evaluation and measurement of the graft site.

Rat	Length of the interposition graft	[1]Distance to the muscle	Scar formation
R823	8.0	5.0	+++
R834	4.0	7.0	+
R835	-	-	+++
R809	5.0	-	+++
R827	7.0	4.0	++
R832	7.0	6.0	+
R824	7.0	7.5	+
R831	-	-	+
R822	4.0	7.0	+

Length data in mm. The proximal and distal suture sites are shown as vertical lines in the diagram. [1]Up to entering the peroneal compartment.

distance from the distal suture site to the entrance of the nerves into the peroneal compartment was measured at 6.1 ± 1.4 mm.

The regeneration result, measured as the number of verifiable motor units in relation to the control side, is correlated in one time group to the percentage of scar formation or the presence of an intraneural neuroma. After 2 weeks, the highest regeneration quota is measured for R834, after 4 weeks the result for R827 is better than for R809 based on the minor scar formation. Compared with R831 and R824, the worst regeneration result appears for R822 after 8 and 10 weeks respectively, as here the graft indicates a neuroma in otherwise similar scar rations.

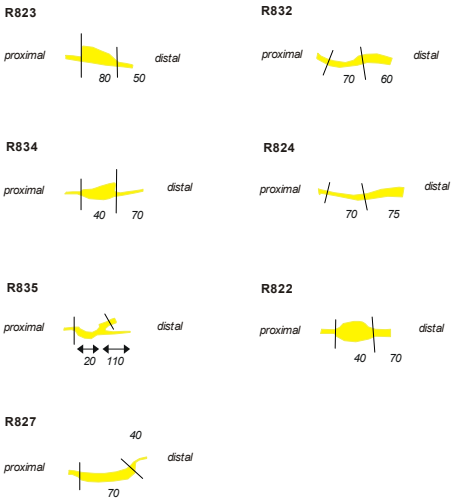

Figure 3.39 The preparation drawings on the graft site on the right are not to scale, and for reasons of clarity are shown exaggeratedly. The distances were measured between the still visible suture sites, and from the distal suture site to the entrance of the common peroneal nerve into the peroneal compartment. The percentage of scar formation in the area of the autologous radial nerve interposition graft was semi-quantitatively evaluated.

3.5.2. Segmental localization of the cell columns following a graft over time

Following radial nerve-common peroneal nerve autograft, the retrograde labeled TA motoneurons are primarily located in segments L4 (100%) and L5 (67.7%). In contrast to the control tests, the motoneurons of segment L3 are still involved in only 12.5% of the nucleus columns at innervation of the tibialis anterior muscle (control: 83.9%). Direct comparison with the opposite side as an internal control shows a caudal offset of all nucleus columns on the graft side (Figure 3.40). The gaps between the cranial nucleus pole on the graft and control sides are largest 2 weeks after transplantation, and decrease over time until they are smallest after 10 weeks. After 2 weeks the cell columns consist of single to a few motoneurons and form a cell layer with a, compared to the control side, low average expansion. After 8 to 10 weeks, the reinnervation of the muscle has

progressed far enough that cell columns have arisen from the cell layer which, in comparison to the control side, also have a larger longitudinal expansion. Proportionate to the control tests, the cell columns are as a rule distributed over 2 segments (control tests: 67.7%, graft side: 75.0%). Expansion over 3 segments is rare (control tests: 27.0%, graft side: 12.5%).

Figure 3.40 Segmental localization of the motoneuron columns following lesion or graft. PC#: Transection of the common peroneal nerve.

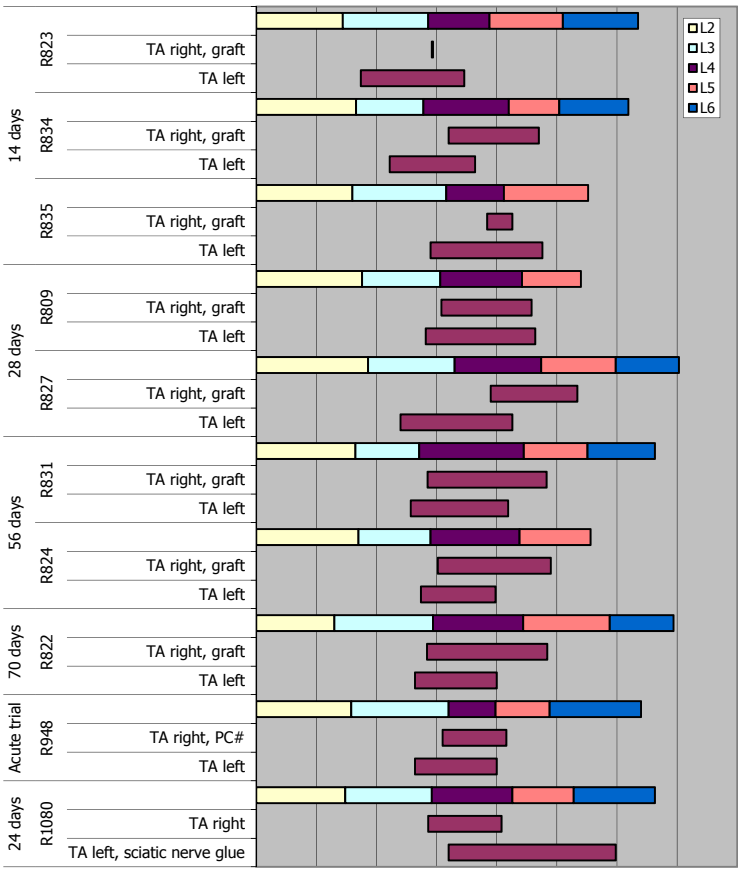

In terms of the segmental position of the motoneurons, there are clear differences after transplantation in the internal reference side as well as in the calculated percentages for all control experiments (see 3.4.4.1). On the internal control side, 36.5% of the motoneurons are located in L3, 60.5% in L4 and 3.0% in L5. After a regeneration period of 2 weeks, the percentage portions amount to 0.0% for L3, 73.3% for L4 and 26.7% for

L5. In the L5 segment, the percentage rose to 36.4% after 4 weeks (L3: 0.0%, L4: 63.6%). First, L5 involvement decreases after 8 weeks (L3: 0.0%, L4: 95.5%, L5: 4.5%), and after 10 weeks motoneurons are also located in segment L3 (L3: 8.8%, L4: 79.4%, L5: 11.8%).

In addition, in Figure 3.40 the nucleus columns are depicted following unilateral severance of the common peroneal nerve and bilateral HRP muscle injection into the tibialis anterior muscle. Counter-intuitively, following transection a cell column is shown in comparable segmental localization to on the control side. These nucleus columns can only have arisen from diffusion of the tracer into neighboring muscle compartments and possibly from absorption into existing nerve trunks with a mismarking of spinal motoneurons. Based on the segmental localization of the cell column alone, mismarking is not implied.

HRP muscle injection into the tibialis anterior muscle after sciatic nerve bonding leads expectedly to a clear expansion into caudal segments, as due to a misinnervation of peripheral effectors, axons of the tibial nerve have also erroneously connected to the tibialis anterior muscle. Comparison with Figure 3.27 shows a comparable segmental expansion of the marked TA cell columns with the nucleus column of the sciatic nerve under physiological conditions.

3.5.3. Morphology, orientation and localization of the tibialis anterior cell column following a graft

In Figures 3.41-3.43, the TA nucleus columns of the control and graft sides are reconstructed based on absolute coordinates after different regeneration periods. The depiction of the graft side comprises, in addition to the reinnervated nucleus column of the tibialis anterior muscle, motoneurons that lie outside of the area defined by the control tests and were classified as mismarked. Depending on the number of labeled motoneurons, in Tables 3.12 and 3.13 the morphology of the cell layers is described as either a point (1-2 MN), a line (3-10 MN) or a spindle (more than 10 MN). The fusiform appearance of the nucleus columns typical for control series is first reached on the graft side after a survival time of 4 weeks with R827.

The orientation of the TA nucleus columns runs in the craniocaudal direction in horizontal reconstructions, 50% in laterolateral and 37.5% in lateromedial. At late regeneration periods after 8-10 weeks, the nucleus columns only exhibit a laterolateral orientation, as it occurs in 75% of controls.

In contrast to the control side, on which the nucleus columns in the sagittal plane have a ventroventral direction and motoneurons only sporadically cross over the zero level defined by the central canal, all cell columns have a ventrodorsal orientation after 8-10 weeks (37.5%). The percentage of nucleus columns with a ventroventral oriented longitudinal axis is, as in the control series, 50%. After a regeneration period of 2 weeks, only individual motoneurons or a few cell clusters are present (Figure 3.41). The clusters are clearly spatially separated from each other (R834). In the mediolateral direction, the motoneurons of the TA nucleus column are located from 0.90 ± 0.12 mm to 1.01 ± 0.09 mm (relative coordinates: $73.1 \pm 2.8\%$ to $78.0 \pm 0.2\%$), in the dorsoventral direction from -0.15 ± 0.02 mm to -0.24 ± 0.04 mm (relative coordinates: $22.3 \pm 1.8\%$ to $41.7 \pm 11.8\%$).

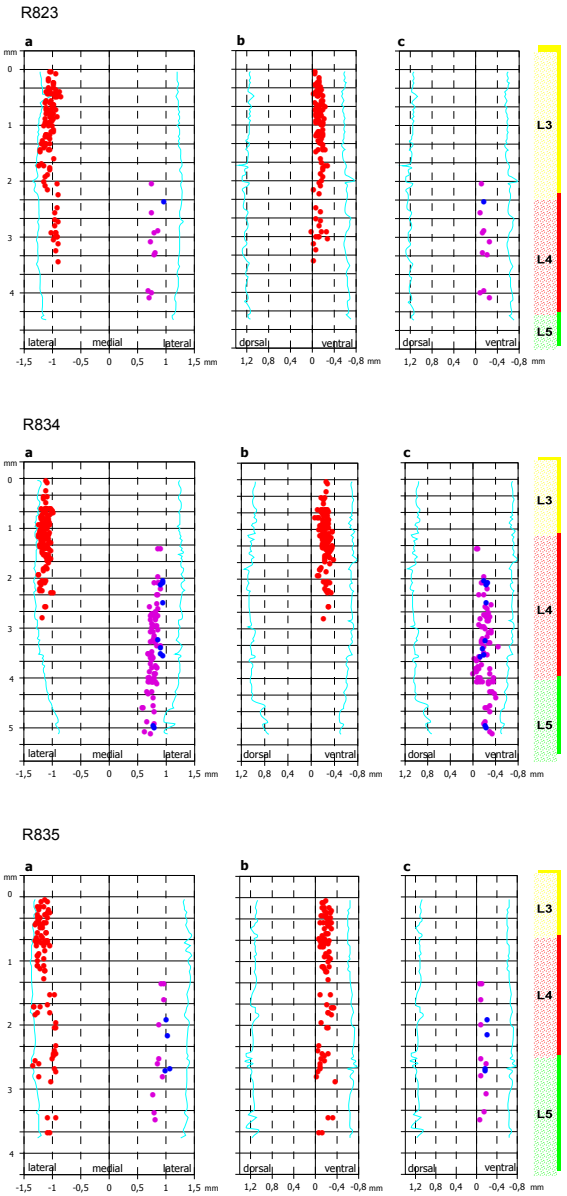

Figure 3.41 2D reconstructions of the tibialis anterior nucleus column 2 weeks after radial nerve-peroneal nerve autograft. *Left*: control side, *right*: graft side with reconstruction of the TA cell column (blue) and of motoneurons that were classified as mislabeled based on relative coordinates (violet).
a, absolute cell position on the mediolateral, ***b***,***c*** on the dorsolateral axis
a, the right side of the spinal cord is shown on the right half of the image, ***b***, left side, ***c***, right side.

In horizontal reconstructions, the nucleus columns have a mean diameter of 0.06 ± 0.03 mm (relative: 4.5 ± 2.2%) and a maximum expansion of 0.10 ± 0.07 mm (relative: 5.0 ± 2.6%) in the mediolateral direction. Along the dorsoventral axis in a sagittal sectional plane, the average diameter amounts to 0.05 ± 0.02 mm (relative: 6.5 ± 3.9%), the largest expansion 0.07 ± 0.05 mm (relative: 13.5 ± 14.2%). In this early phase of reinnervation, the craniocaudal area in which the HRP labeled TA motoneurons are discernible is markedly smaller than in control tests, with a length of 1.29 ± 1.53 mm.

After 4 weeks (Figure 3.42) the number of reinnervated motor units has more than doubled from an average of 5 (4.5%) to 11 (9.7%). The motoneurons are, in contrast to the tests after 2 weeks, also laterally located up to the border of the white matter.

Figure 3.42 2D reconstructions of the tibialis anterior nucleus column 4 weeks after radial nerve-peroneal nerve autograft. *Left*: control side, *right*: graft side with reconstruction of the TA cell column (blue), mislabeled motoneurons (violet).

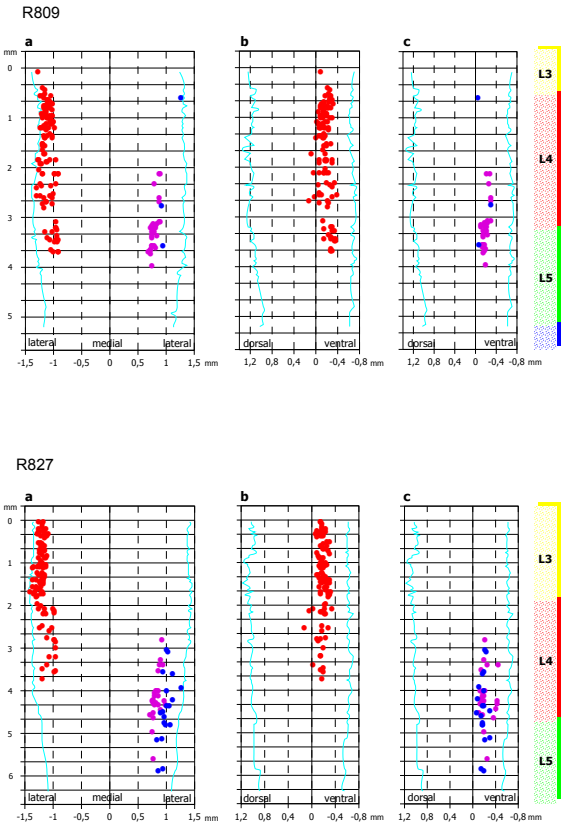

In the mediolateral direction, the mutual area of both cell columns reaches from 0.88 ± 0.06 mm to 1.26 mm (relative coordinates: 70.7 ± 0.3% to 96.0 ± 1.1%), dorsoventrally from –0.05 ± 0.01 mm to –0.30 mm (relative coordinates: 8.5 ± 3.1% to 45.0 ± 7.1%).

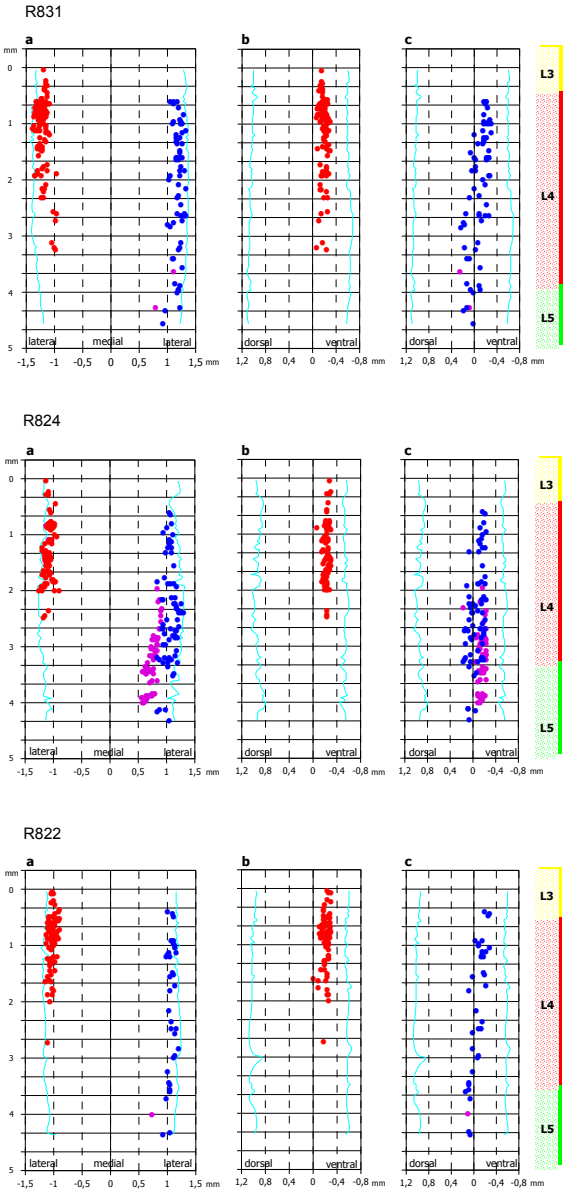

Figure 3.43 2D reconstructions of the tibialis anterior muscle nucleus column 8 weeks (*R831*, *R824*) and 10 weeks (*R822*) after radial nerve-peroneal nerve autograft. *Left*: control side, *right*: graft side with reconstruction of the TA cell column (blue), mislabeled motoneurons (violet).

Table 3.12 Parameters of the TA cell column following radial nerve-common peroneal nerve autograft on the right.

Parameters	R823 Right	R834 Right	R835 Right	R809 Right	R827 Right	R831 Right	R824 Right	R822 Right
A1. Localization (mm)								
Mediolateral	0.96/ 1.00	0.77/ 0.94	0.98/ 1.07	0.92/ 1.26	0.83/ 1.26	0.92/ 1.32	0.83/ 1.30	0.92/ 1.20
Dorsoventral	-0.15/-0.19	-0.13/-0.26	-0.17/-0.21	-0.04/-0.30	-0.06/-0.30	0.24/-0.30	0.17/-0.24	0.15/-0.28
Localization (%)								
Mediolateral	76.3/79.2	71.0/ 77.8	71.9/ 78.1	70.5/ 95.2	70.9/ 96.7	74.6/ 98.4	70.7/ 100.0	83.6/ 96.6
Dorsoventral	21.9/27.4	20.7/ 50.0	24.2/ 33.3	6.3/ 40.0	10.7/50.0	-34.3/ 50.0	-32.0/ 44.0	-25.9/ 50.0
A2. Segment height	L4	L4,L5	L4,L5	L4,L5	L4,L5	L4,L5	L4,L5	(L3),L4,L5
A3. Vertebral body height	L1 rostral	L1 center/ L1 caudal	L1 rostral	L1 center/ L1 caudal	L1 rostral/ L1 center	L1 rostral/ L1 center	L1 center/ L1 caudal	L1 rostral/ L1 caudal
B1. Morphology								
Form	Point	Line	Line	Line	Spindle	Spindle	Spindle	Spindle
Orientation								
a) Mediolateral		l-m	l-l	l-m	l-m	l-l	l-l	l-l
b) Dorsoventral		v-v	v-v	v-v	v-v	v-d	v-d	v-d
B2. Length (mm)	0.04	3.00	0.84	3.00	2.88	3.96	3.76	4.00
B3. Width (mm)								
Largest diameter								
a) Mediolateral	0.04	0.05	0.09	0.11	0.36	0.32	0.47	0.20
b) Dorsoventral	0.04	0.07	0.04	0.25	0.24	0.50	0.39	0.30
Largest expansion								
a) Mediolateral	0.04	0.17	0.09	0.34	0.43	0.40	0.47	0.28
b) Dorsoventral	0.04	0.13	0.04	0.26	0.24	0.54	0.41	0.43
Width (%)								
Largest diameter								
a) Mediolateral	2.9	5.4	6.2	8.3	24.3	23.8	26.4	11.1
b) Dorsoventral	5.5	8.3	9.1	33.3	37.6	73.1	68.5	53.7
Largest expansion								
a) Mediolateral	2.9	6.8	6.2	24.7	25.8	23.8	29.3	13.0
b) Dorsoventral	5.5	29.3	9.1	33.7	39.3	84.4	76.0	75.9
B4. Cell count[1]	1	10	4	3	19	64	68	34
B5. Area (µm²)								
Mean	1342.0	1241.3	1384.0	1042.3	1089.9	1109.9	1018.9	817.1
SD		450.7	301.2	209.5	321.2	408.9	473.8	357.3
MIN	1342.0	553.0	1050.0	913.0	331.0	420.0	148.0	352.0
MAX	1342.0	2210.0	1771.0	1284.0	1773.0	1976.0	2254.0	1874.0
B6. Diameter (µm)								
Mean	41.3	39.2	41.8	36.3	36.8	36.8	35.0	31.5
SD		7.1	4.5	3.6	5.9	7.2	8.6	6.9
MIN	41.3	26.5	36.6	34.1	20.5	23.1	13.7	21.2
MAX	41.3	53.0	47.5	40.4	47.5	50.2	53.6	48.8
B7. Cell types (%)								
IA	0.0	30.0	0.0	0.0	21.1	43.8	33.8	38.2
IB	0.0	50.0	0.0	0.0	31.6	14.1	26.5	26.5
IC	0.0	0.0	0.0	0.0	0.0	6.3	7.4	0.0
ID	100.0	20.0	25.0	33.3	15.8	12.5	2.9	5.9
IE	0.0	0.0	75.0	66.7	31.6	23.4	29.4	29.4
II	0.0	0.0	0.0	33.3	0.0	6.3	1.5	2.9

Cell count[1] after correction by doubled and mismarked cells.
Abbreviations:
lateral: l, medial: m, ventral: v, dorsal: d, central: c.

Table 3.13 Parameters of the TA/F cell column on the right following autograft.

Parameters	R823 Right	R834 Right	R835 Right	R809 Right	R827 Right	R831 Right	R824 Right	R822 Right
A1. Localization (mm)								
Mediolateral	0.68/ 0.85	0.58/ 0.90	0.77/ 0.96	0.68/ 0.90	0.71/ 0.98	0.79/ 1.11	0.56/ 0.92	0.73/ 0.77
Dorsoventral	-0.09/-0.26	0.00/-0.45	-0.06/-0.19	-0.11/-0.30	-0.11/-0.45	0.26/ 0.09	0.17/-0.24	0.11/ 0.15
Localization (%)								
Mediolateral	57.1/ 67.8	50.9/ 78.7	57.1/ 69.2	53.3/ 68.3	56.9/ 76.7	62.7/ 83.9	50.9/ 70.0	64.2/ 64.2
Dorsoventral	14.3/ 42.9	0.0/ 70.0	9.4/ 30.0	15.6/ 43.8	17.9/ 71.4	-40.0/-14.3	-27.6/ 45.8	-18.5/-18.5
A2. Segment height	L3,L4	L4,L5	L4,L5	L4,L5	L4,L5	L4,L5	L4,L5	L4
A3. Vertebral body height	L1 rostral	L1 rostral/ L1 caudal	L1 rostral/ L1 center	L1 center/ L1 caudal	L1 rostral/ L1 center	L1 center	L1 center/ L1 caudal	L1 rostral
B1. Morphology								
Form	Spindle	Spindle	Line	Spindle	Spindle	Point	Spindle	Point
Orientation								
a) Mediolateral	l-l	l-m	l-m	l-m	l-l	l-m	l-m	
b) Dorsoventral	v-v	c-v	v-v	v-c	v-v	d-c	c-c	
B2. Length (mm)	2.08	3.80	2.16	1.88	2.84	0.64	2.08	0.04
B3. Width (mm)								
Largest diameter								
a) Mediolateral	0.12	0.21	0.17	0.17	0.27	0.04	0.27	0.04
b) Dorsoventral	0.17	0.45	0.10	0.19	0.32	0.04	0.41	0.04
Largest expansion								
a) Mediolateral	0.17	0.32	0.19	0.22	0.27	0.32	0.36	0.04
b) Dorsoventral	0.17	0.45	0.13	0.19	0.34	0.17	0.41	0.04
Width (%)								
Largest diameter								
a) Mediolateral	10.2	27.8	11.7	13.0	19.8	3.0	14.2	3.8
b) Dorsoventral	22.7	70.0	16.7	25.6	53.5	6.1	71.6	7.3
Largest expansion								
a) Mediolateral	10.7	27.8	12.1	15.0	19.8	21.2	19.1	3.8
b) Dorsoventral	28.6	70.0	20.6	28.2	53.5	25.7	73.4	7.3
B4. Cell count[1]	10	76	10	30	25	2	56	1
B5. Area (µm²)								
Mean	660.8	1127.7	879.3	1104.0	1115.5	1256.0	975.1	1488.0
SD	182.3	391.1	442.9	408.1	327.7	401.6	413.5	
MIN	221.0	402.0	480.0	391.0	320.0	972.0	234.0	1488.0
MAX	844.0	1921.0	1936.0	1916.0	1733.0	1540.0	2069.0	1488.0
B6. Diameter (µm)								
Mean	28.7	37.3	32.7	36.8	37.2	39.7	34.4	43.5
SD	4.7	6.8	7.6	7.3	6.0	6.4	7.7	
MIN	16.8	22.6	24.7	22.3	20.2	35.2	17.3	43.5
MAX	32.8	49.5	49.6	49.4	47.0	44.3	51.3	43.5
B7. Cell types (%)								
IA	0.0	30.3	10.0	30.0	16.0	50.0	33.9	0.0
IB	0.0	28.9	10.0	33.3	36.0	50.0	19.6	0.0
IC	20.0	5.3	0.0	10.0	8.0	0.0	10.7	0.0
ID	10.0	17.1	0.0	16.7	12.0	0.0	7.1	100.0
IE	70.0	18.4	80.0	10.0	28.0	0.0	28.6	0.0
II	0.0	0.0	0.0	0.0	0.0	50.0	1.8	0.0

Cell count[1] after correction by doubled cells.
Abbreviations:
lateral: l, medial: m, ventral: v, dorsal: d, central: c.

When compared with the values after a regeneration period of 2 weeks, the diameter as well as the maximum expansion of the nucleus column have increased. In the horizontal sectional plane, the diameter of the cell column amounts to 0.24 ± 0.18 mm (relative: 16.3 ± 11.3%), the largest expansion 0.39 ± 0.06 mm (relative: 25.3 ± 0.8%). In the sagittal sectional plane, the diameter of the cell column was measured at 0.25 ± 0.01 mm (relative: 35.5 ± 3.0%), and the largest expansion at 0.25 ± 0.01 mm (relative: 36.5 ± 4.0%). The nucleus column increases in length to 2.94 ± 0.08 mm.

For the cell columns 8 and 10 weeks (Figure 3.43) after peripheral, autologous nerve graft, a mutual analysis of the morphometric parameters was performed. Between 4 and 8 or 10 weeks, respectively, the average cell count of TA motoneuron columns increased again to 55.3 (57.8%) cells. All motoneuron columns have a fusiform appearance with, in comparison to the control side, a scattered cell profile. The motoneurons of the tibialis anterior nucleus column are located from 0.89 ± 0.05 mm to 1.27 ± 0.06 mm in the mediolateral direction (relative coordinates: 76.3 ± 6.6% to 98.3 ± 1.7%), and from 0.19 ± 0.05 mm to -0.27 ± 0.03 mm in the dorsoventral direction (relative coordinates: -30.7 ± 4.3% to 48.0 ± 3.5%). The diameter of the nucleus column in horizontal reconstructions is 0.33 ± 0.14 mm in the mediolateral direction (relative: 20.4 ± 8.2%). The maximum expansion already reached the values of the control series 4 weeks after transplantation, and is almost unchanged in horizontal reconstructions after 8-10 weeks at 0.38 ± 0.10 mm (relative: 22.0 ± 8.3%). In sagittal reconstructions, the diameter as well as the maximum expansion of the cell column increase between 4 and 8 or 10 weeks respectively following transplantation, and reach the values of the HRP5 control tests. Dorsoventrally, the diameter of the cell column amounts to 0.40 ± 0.10 mm (relative: 65.1 ± 10.1%), and the maximum expansion 0.46 ± 0.07 mm (relative: 78.8 ± 4.9%). At 3.91 ± 0.13 mm, the length of the cell column has the largest craniocaudal expansion of all examined time periods following transplantation.

With a sufficient cell count in reconstructions, motoneurons denoted as mismarked form an autonomous nucleus column which then can be delimited by the nucleus column of the tibialis anterior muscle. In the case of individual neurons, the relative coordinates serve compartmentation in comparison to the cell coordinates of the TA motoneuron column. Mismarked cells are normally located medially to the TA nucleus column on horizontal reconstructions, and in the sagittal sectional plane they are mixed with the TA motoneurons.

3.5.3.1. 3D reconstructions of the tibialis anterior nucleus column following autograft

To visualize the central changes of a motoneuron nucleus following lesion of a peripheral nerve and its repair with an autologous nerve graft in the reinnervation procedure, three-dimensional reconstructions of the TA motoneuron pool were prepared. In Figures 3.44-3.46 the cell columns on the control and graft sides, including their cell density distributions on the transversal sections, are depicted after 4, 8 and 10 weeks. In comparison to the control side, the reconstructions on the graft side show fewer cell dense nucleus columns in a larger dorsolateral area, with singular motoneurons in the periphery. The gap between the cranial nucleus pole on the control and graft sides decreases

over the course of reinnervation of the tibialis anterior muscle. As measured by the increasing number of motor units, the regeneration quota in the cited examples is 18.3% after 4 weeks, 59.8% after 8 weeks and 39.1% after 10 weeks. The localization of all nucleus columns in a framework can be evaluated, beginning with the relative coordinates of the motoneurons in two-dimensional reconstructions (see Figures 3.53-3.55).

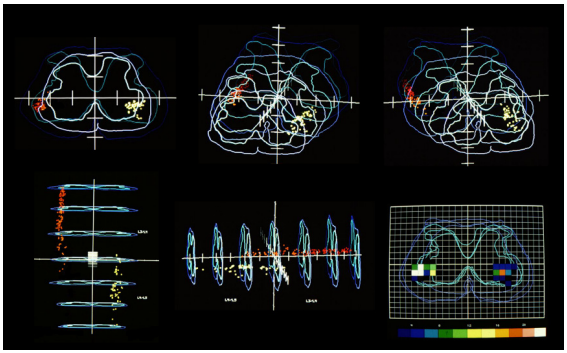

Figure 3.44 *R827*, 3D reconstruction of the TA nucleus column 4 weeks after a radial nerve-common peroneal nerve autograft *right* (yellow), control side *left* (red). The scaling of the color scale is identical in Figures 3.44-3.46. The cell count of the graft to control side is 18.3%.

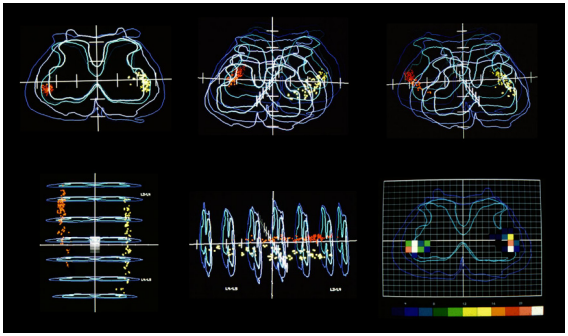

Figure 3.45 *R831*, 3D reconstruction of the TA nucleus column 8 weeks after a radial nerve-common peroneal nerve autograft *right* (yellow), control side *left* (red). The cell count of the graft to control side is 59.8%.

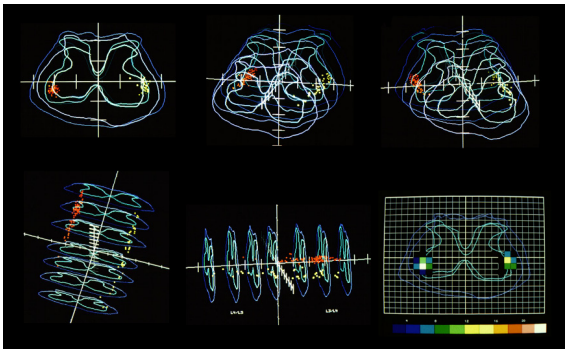

Figure 3.46 *R822*, 3D reconstruction of the TA nucleus column 10 weeks after a radial nerve-common peroneal nerve autograft *right* (yellow), control side *left* (red). The cell count of the graft to control side is 39.1%.

3.5.4. Cell count of the motor tibialis anterior cell column

The nucleus column of the tibialis anterior muscle after HRP muscle injection consists of 108.7 ± 15.3 (n = 24) cells, with a percentage of mismarked motoneurons of 9.6% (see 3.4.4.3). In the HRP2G graft series, 106.1 ± 11.8 (n = 8) motoneurons are labeled, and the percentage of neurons located outside of the TA nucleus area is 15.2% higher. In Figure 3.47, the average cell count (CC) is listed for the respective periods following autograft on the control side and the graft side. On the graft side, the labeled cell population is differentiated into mismarked motoneurons (CC/F) and the motoneuron pool of the tibialis anterior muscle (CC-CC/F). The cell counts are adjusted by the number of double marked neurons, through comparison of cell profiles in neighboring sections and their relative coordinates. The percentage of double labeled cells on the control side is 13.8 ± 0.9%, and 15.6 ± 5.4% on the graft side.

Figure 3.47 Cell count of the TA motoneurons on the control and graft sides following HRP muscle injection.

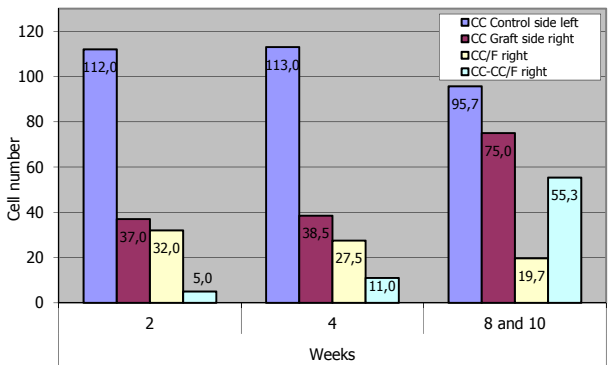

Based on the cell count of the corresponding control group, the percentage of motoneurons on the graft side increases from 33.0% (2 weeks) to 78.4% (8, 10 weeks). The difference is clearest between 4 and 8 weeks, with a doubling of the percentage values. Parallel thereto, the quota of mismarked motoneurons decreases from the initial 86.5% (2 weeks) to 26.2% (8, 10 weeks). As a consequence of these changes over time, the cell count of the TA motoneuron pool increases from 13.5% after 2 weeks and 28.6% after 8 weeks to 73.8% after 8 and 10 weeks. Taking account of the cell count of the opposite side as an internal control, there emerge regeneration quotas of 4.5% (2 weeks), 9.7% (4 weeks) and 57.8% (8, 10 weeks).

Comparison between the outcomes after 8 and 10 weeks shows differences in the number of mismarked motoneurons whose percentage after a regeneration period of 8 weeks is 30.5%, and 2.9% after 10 weeks. The regeneration quota amounts to 66.0% after 8 weeks and 39.1% after 10 weeks.

3.5.5. Cell density

The cell density distributions of all reconstructed nucleus columns of the tibialis anterior muscle following HRP application in control experiments (n = 16) are already shown in Figure 3.30. Figure 3.48 facilitates direct comparison of cell distributions between the TA cell columns on the control and graft sides of the HRP2G test series at the examined regeneration periods.

Compared with the overall TA motoneuron population, the density distributions on the control side of the HRP2G test series do not differ from each other. The nucleus columns consist of motoneurons in an expansion of x = 80% - 90% and y = 20% - 45%, and local density maximums at the levels of segments 2/8 to 3/8. The cell pool area reaches in the mediolateral direction to the border of the gray matter, with a less steep decrease in cell frequency in the lateral direction than in the medial.

After a regeneration period of 2 weeks, separate individual cell clusters with multiple local density maximums are shown, which are distributed over the entire cell column. After 4 weeks the area of the highest cell density lies in the center of the nucleus column, and after 8 and 10 weeks it is the rostral segments 1/8 to 2/8.

In the transversal sectional plane (Figure 3.48, a), the density maximums are at a similar position to that on the control side after 2 and 4 weeks. In relative coordinates, the motoneurons extend mediolaterally from 70% - 80% (4 weeks 70% - 90%) and dorsoventrally from 20% - 40%.

After 8 and 10 weeks, another expansion of the cell pool takes place with density maximums at 20% to 45% in the dorsal direction; in the mediolateral direction the nucleus column has a marginal position corresponding to the control tests, with the highest cell density at 80% to 100%. Comparison of individual experiments on the graft side after 8 and 10 weeks, however, still shows the presence of multiple local density maximums and no homogenous frequency distribution. On sagittal reconstructions, the cell columns in the dorsoventral direction have an expansion similar to the nucleus columns of the HRP5 series.

Figure 3.48 Cell density distribution of the TA cell column on the control side (***a***, left half of image, ***b*** and ***d***) and the graft side (***a***, right half of image, ***c*** and ***e***). The tests with identical postoperative survival times are consolidated. Representation on the ***a***, transversal, ***b***,***c*** horizontal and ***c***,***e*** sagittal sectional planes. The ordinates and abscissa in ***a*** denote the relative coordinates based on the boundary of the gray spinal cord matter. For the display in ***b***-***e***, the cell columns were divided into 8 sections and the interpolated cell density distribution was calculated.

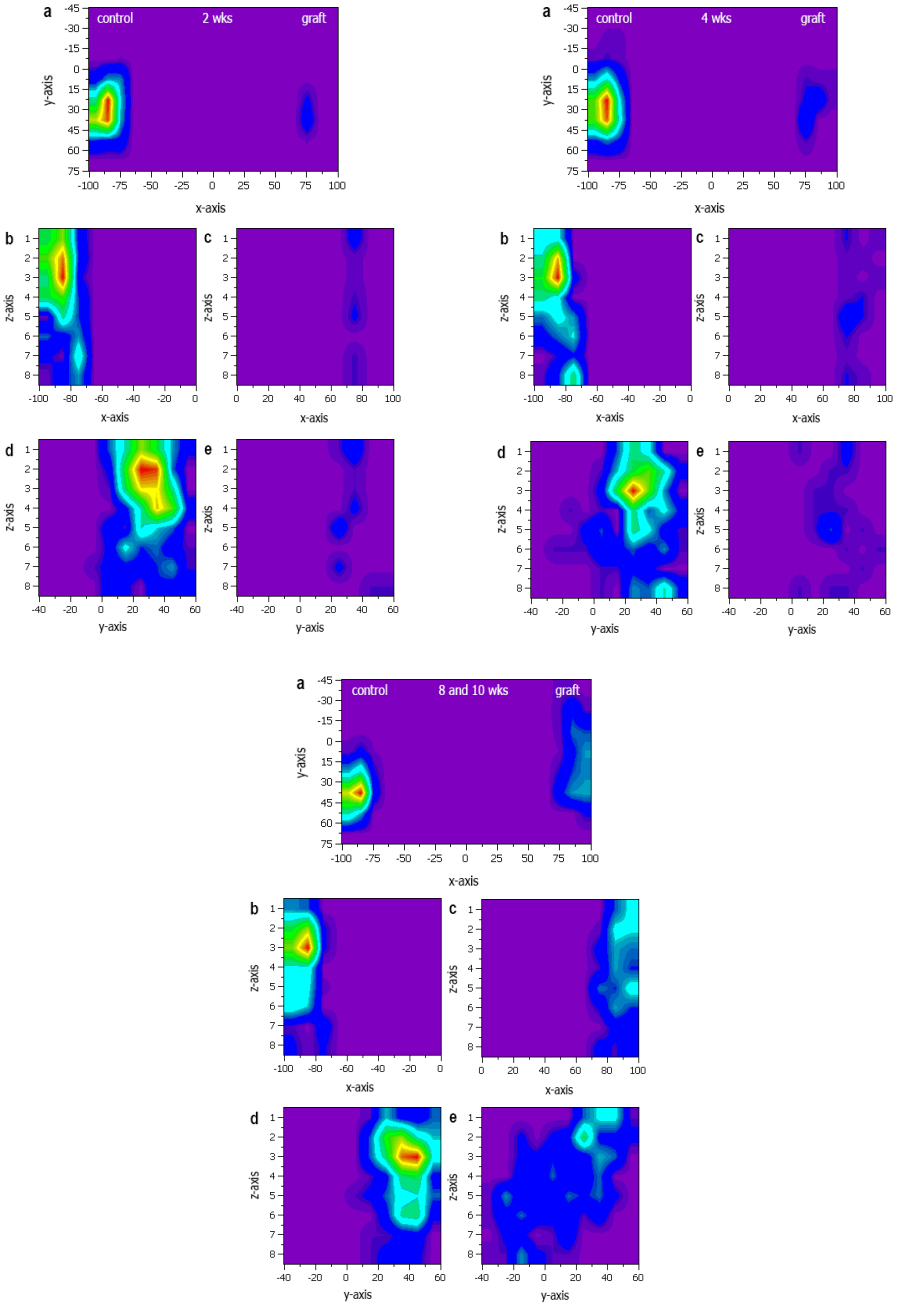

3.5.6. Area and diameter of the cells of the tibialis anterior nucleus column

In addition to the diameter and area values following HRP muscle injection mentioned in Table 3.9 (diameter: 34.6 ± 7.2 µm, span 12.9 µm to 56.2 µm), the control values of the opposite side serve as an internal reference for the comparison of values on the graft side.

Table 3.14 Diameter and area of the TA motoneuron columns following autograft.

Test series	Time post-op. (weeks)	Number of CC	Diameter (µm)			Area (µm²)		
			M ± s	Min	Max	M ± s	Min	Max
HRP2G	2	3	40.0 ± 6.2	26.5	53.0	1286.1 ± 426.9	553.0	2210.0
	4	2	36.7 ± 5.5	20.5	47.5	1283.4 ± 436.7	331.0	1773.0
	8	2	35.8 ± 8.0	13.7	53.6	1058.3 ± 443.8	148.0	2254.0
	10	1	31.5 ± 6.9	21.2	48.8	817.1 ± 357.3	352.0	1874.0

Abbreviations:
CC: Cell column, M: Mean, s: Standard deviation,
Min: Minimum value, Max: Maximum value.

If the diameters of the HRP2G control side are divided into the time classes 2, 4 and 8-10 weeks, no significant differences emerge between the groups (ANOVA, P>0.05). On the graft side, a significant difference is only calculated when comparing the mean diameters between 2 and 8 or 10 weeks (ANOVA, P = 0.0369, posttest according to Turkey).

Figure 3.49 Cumulative representation of diameters on the control side and graft side following different postoperative periods.

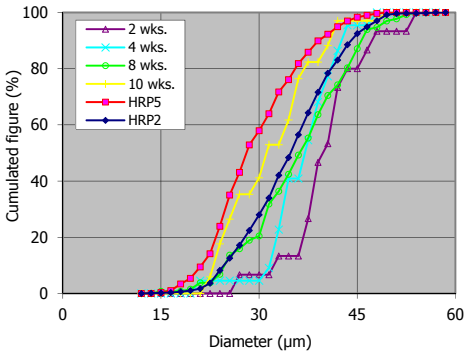

According to Table 3.14, the mean diameter 2 weeks after transplantation is markedly increased in comparison to the reference values, and decreases continuously over time to standard values after 10 weeks. Direct comparison between control and graft side of each individual test shows that the diameters on the graft side exhibit increased values,

with the exception of R822 (Tables 3.8 and 3.12). Taking into account the overall motoneuron population on the graft side, the span of the diameter values is at 13.7 µm to 53.6 µm and does not differentiate from the control tests. However, if the individual time groups are compared separately, the span of diameter values is consistently smaller than on the corresponding control side. The difference of the initial 12.4 µm after 2 weeks continuously drops to 1.8 µm after 8 and 10 weeks respectively. The reasons for this are the higher minimum values as opposed to the control values as well as the lower maximum values of diameters.

The cumulated representation in Figure 3.49 shows the distribution of diameter values following different regeneration periods in relation to two control groups. The significantly lower mean diameter of the motoneurons following HRP nerve bath (HRP5) in comparison to HRP muscle injection (HRP2) was already pointed out in 3.4.4.5.

The cumulated curves differentiate from the remaining sigmoid curve shape after 2 and 4 weeks by an initial shoulder area with a flat slope, which transitions into a steep curve area. After 2 weeks, this transition area is located at 37.5 µm, and at 30.0 µm after 4 weeks. Corresponding to this process, with a marked shift to the right in the lower curve section, a deficit of smaller motoneurons in the first 4 weeks can be deduced. The progress of the curve approached the control curve after 8 weeks, and there is a slight shift of the curve to the right in the middle section. After a regeneration period of 10 weeks, the cumulated diameters lie between the curves of the HRP5 and HRP2 control series and correspond to a restored distribution pattern.

3.5.7. Cell types in the cell column

3.5.7.1. Postoperative classification of motoneurons by staining pattern

The frequencies of cell types according to the HRP marking pattern on the graft side differentiate only negligibly from the control series (compare Figure 3.35 with Figure 3.50). The percentage of type IA and IB cells is 58.1% for the TA nucleus column, 14.3% for types IC and ID and 27.6% for IE. The motoneurons classified as mismarked outside of the TA area are composed of type IA and IB neurons with a percentage of 52.9%. Type IC and ID neurons have a percentage of 21.0%, type IE neurons 26.2%. The percentage of fragments and unclassified dye products is low (HRP2: 3.4%, HRP2/F: 1.0%). Statistical testing of frequency distribution between the control series and the two groups on the graft side (HRP2 and HRP2/F) verifies a homogenous population ($\chi 2$ test, $P = 0.304$). This also applies when the respective types are compared with the control groups at the different regeneration periods ($\chi 2$ test, $P = 0{,}6568$). Based on this similarity of HRP marking in control and graft tests, ratios and type affinity of the motoneurons can be compared between both test groups.

In the control series, the consolidated types IA and IB, IC and ID and IE were significantly distinguishable from one another, whereby and IE were significantly distinguishable from one another, whereby a size sequence was present in the diameter.

Figure 3.50 *Left:* Frequency of cell types following HRP muscle injection on the graft side, differentiated according to their localization in (*HRP2*) or outside of (*HRP2/F*) the TA area. *Right*: Diameter of cell types (*HRP2*) following various regeneration times.

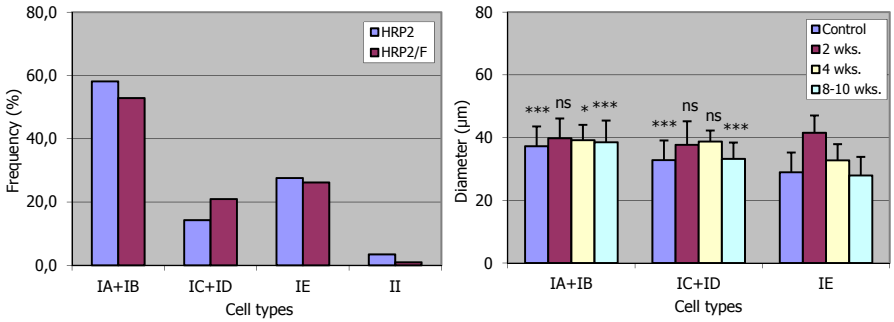

After a regeneration period of 2 weeks, no significant differences in diameter could be established between the types anymore. The mean diameter of type IE has the highest value in this period. Significant differences in diameter are present between type IA, IB and IE after 4 weeks (ANOVA, Turkey-Kramer posttest, P = 0.028). After 8-10 weeks, the distribution pattern of diameter is reestablished in comparison to the control side, and the differences are highly significant (ANOVA, Turkey-Kramer posttest, P<0.001). Like on the control side, the HRP labeling of the motoneurons is most intense in cells with a large diameter, while small motoneurons held less TMB dye product.

3.5.7.2. Postoperative classification of motoneurons by diameter

In contrast to the control experiments from HRP2 and HRP5, a classification of motoneurons into size classes by diameter and area histograms can only partially performed. The reason for this lies in the still low motoneuron count following a regeneration period of 2 to 4 weeks, which is depicted in the histograms by a rarefied beam pattern without evident structuring. Consequently, a bi- or trimodality of the diameter distribution could not be deduced from the histogram profile in 50% of the experiments. Classification into gamma, alpha 1 and alpha 2 motoneurons was alternatively performed according to the criteria defined in 3.4.4.6.2. A limiting diameter of 28.5 µm was taken as a basis for differentiating gamma from alpha neurons, and 37.5 µm for differentiation alpha 1 from alpha 2 neurons. Classification of motoneurons according to the histograms was possible for R827 to R822 at the later regeneration points. As the mean for the bimodal limiting diameter was 28.0 ± 0.9 µm calculated (span 27.0 µm to 28.5 µm), while the mean diameter for differentiating alpha 1 and alpha 2 motoneurons lay at 37.9 ± 1.9 µm (span 36.0 µm to 40.5 µm). The size classes in the diameter histograms are indicated in Figure 3.51.

Using these classification criteria, for the 3 cell types of the TA nucleus column in the control tests following HRP muscle injection (n = 10), 39% was calculated for alpha 1 and alpha 2 motoneurons respectively, and 22% for gamma motoneurons.

Table 3.15 Cell types of type I motoneurons of the TA cell column (*HRP2G*, *HRP2*) during regeneration.

	Alpha MN		Gamma MN		
	Cell count	Diameter (µm)	Cell count	Diameter (µm)	Gamma/ Alpha+Gamma
Control	77.5 ± 16.0	37.3 ± 5.5	21.6 ± 4.2	24.8 ± 2.9	0.22 ± 0.06
Graft					
2 wks post-op.	4.7 ± 4.0	41.0 ± 5.1	0.3 ± 0.6	26.5	0.03 ± 0.06
4 wks post-op.	10.5 ± 10.6	37.5 ± 4.3	0.5 ± 0.7	20.5	0.03 ± 0.04
8, 10 wks post-op.	43.0 ± 18.2	38.1 ± 5.8	12.3 ± 1.5	24.0 ± 2.8	0.24 ± 0.10

In the context of reinnervation following autologous nerve graft, it comes to a considerable change in the number of motor units and a change in size composition of the motoneuron pool of the TA nucleus columns. After a regeneration period of 2 weeks, the percentage of gamma motoneurons is reduced to 3%, a value that also remains unchanged after 4 weeks. Complementarily, the percentage of alpha neurons reaches 97% with a fractionation into 82% alpha 1 motoneurons and 15% alpha 2 motoneurons after 2 weeks.

Table 3.16 Division of alpha motoneurons (*HRP2G*, *HRP2*) during regeneration.

	Alpha 1 MN		Alpha 1/ Alpha+Gamma	Alpha 2 MN		Alpha 2/ Alpha+Gamma
	Cell count	Diameter (µm)		Cell count	Diameter (µm)	
Control	38.3 ± 11.0	41.4 ± 4.1	0.39 ± 0.10	39.2 ± 13.5	33.3 ± 3.1	0.39 ± 0.11
Graft						
2 wks post-op.	3.7 ± 3.1	42.5 ± 4.7	0.82 ± 0.16	1.0 ± 1.0	35.5 ± 2.3	0.15 ± 0.13
4 wks post-op.	6.5 ± 7.8	40.2 ± 3.2	0.48 ± 0.21	4.0 ± 2.8	33.2 ± 1.1	0.49 ± 0.25
8, 10 wks post-op.	19.3 ± 14.0	43.5 ± 3.7	0.33 ± 0.18	23.7 ± 10.8	33.7 ± 2.8	0.43 ± 0.12

The percentage of alpha 2 motoneurons increases after 4 weeks to 49%, while in contrast the percentage of alpha 1 motoneurons decreases to 48%. 8 weeks after autograft the percentage of gamma motoneurons is at 19%, alpha 2 motoneurons at 41% and alpha 1 motoneurons at 40%. After a regeneration period of 8-10 weeks for the population of gamma motoneurons, a percentage comparable to the control series values after 10 weeks is reached at 24%. The ratio of alpha 1 to alpha 2 motoneurons is 1:1.3 and in comparison to the control tests with a ration of 1:1, is offset to the detriment of the large alpha 1 motoneurons.

Figure 3.51 Histograms of areas and diameters of the TA nucleus column on the graft side over time. A classification of cells into gamma, alpha 1 and alpha 2 motoneurons was performed corresponding to the histogram profile of the diameter or the limiting diameters of 28.5 µm and 38.5 µm respectively.

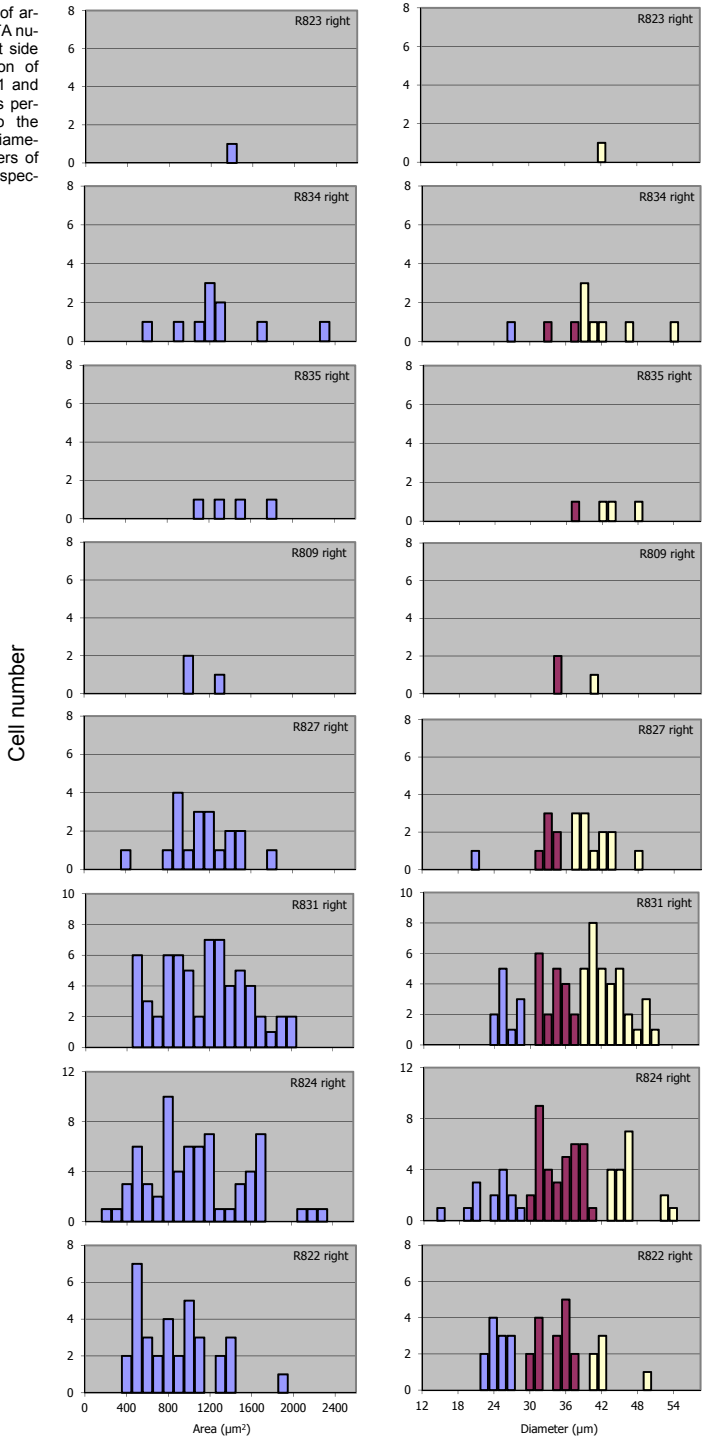

3.5.8. Postoperative distribution of cell types along the tibialis anterior nucleus column

The distribution of alpha 1, alpha 2 and gamma motoneurons on the graft side is shown separately and after various regeneration periods in Figure 3.52 for the individual tests. As in Figure 3.37 for the control series, the frequencies of the individual cell types are calculated for the 4 equidistant sections of the nucleus column. However, in the initial regeneration phase, motoneurons could not be consistently assigned to the three cell classes due to a still low cell count, so the bar graphs are partially incomplete.

Figure 3.52 Distribution of the alpha 1, alpha 2 and gamma motoneurons in the *HRP2G* graft series. The *left* half of the image depicts the distribution of motoneurons over the overall cell column, and the *right* side shows after allocation of the nucleus column into 4 segments from cranial to caudal. The distribution is consolidated for the regenerations period of 2, 4, 8 and 10 weeks.

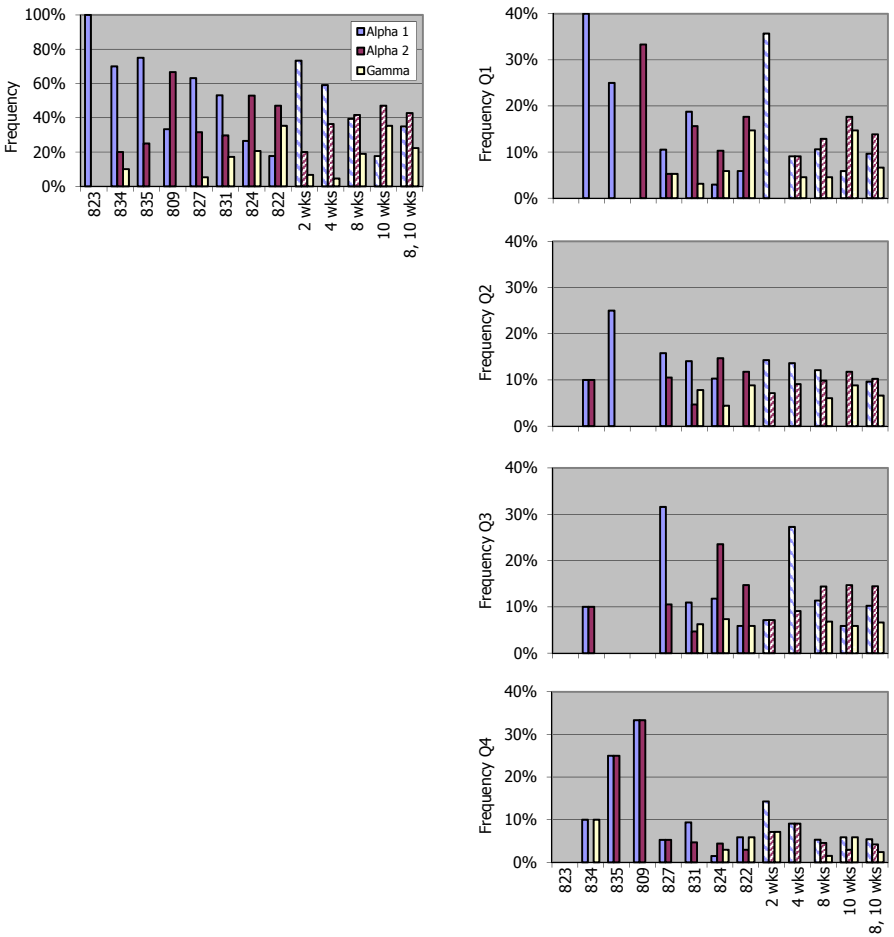

The individual cell types show a characteristic course of time with a continuous decline in frequency of the alpha 1 motoneurons, and a steady increase in alpha 2 and gamma motoneurons in the assessment period of 2 to 10 weeks. However, this pattern can only be established for the entire cell column and the two rostral segment quarters. The reduction of the initial cell count is less distinct for the alpha 2 cell population than for the gamma neurons.

Calculations of the alpha-gamma quotients in the control experiments following HRP muscle injection resulted in a value of 3.6 for the overall TA nucleus column. On the graft side, the quotient decreases from an initial 14.0 over 21.0 (4 weeks) and 4.1 (8 weeks) to 1.8 after 10 weeks. If the values for the time periods 8 and 10 weeks after autograft are consolidated, an alpha-gamma quotient of 3.6 is calculated for the overall cell column which only slightly differentiates from the control series. The highest value is reached here in the fourth quarter of the cell column with a quotient of 4.0. In contrast to the control tests with the highest cell count in the second quarter of the nucleus column, the motoneurons in the upper third quarters of the nucleus column are distributed almost evenly without a local maximum. The cell count of the fourth quarter is reduced to 48.6% on average.

For the consolidated data following a regeneration period of 8 and 10 weeks, the frequency of all cell types in the upper nucleus halves is larger corresponding to the outcome of the control series. Among the cell types, the percentage of alpha 2 motoneurons is highest is both nucleus halves. Based on the distribution of cell types in the four respective sections, and in contrast to the control series, a local maximum for alpha 1 motoneurons is present in the fourth segment quarter (control: first quarter), for the gamma motoneurons in the second segment quarter (control: fourth quarter). The alpha 2 neurons have a local frequency maximum in the upper and lower nucleus halves in both the graft and control series.

3.5.9. 2D reconstructions of motor nucleus columns following autograft over time

With knowledge of the relative x, y and z coordinates of all motoneurons of the HRP2G test series, reconstruction of multiple cell column in projection onto a mutual frontal, sagittal and transversal sectional plane is possible. On the basis of these measurements, quantitative parameters of the cell columns (Tables 3.8 and 3.12) and topographical relationships of the nucleus columns among one another are indicated. Figures 3.53-3.55 represents an overview of the nucleus columns on the control and graft sides at the assessed regeneration periods. The characteristics of the tibialis anterior muscle on the control side have been discussed under 3.4.4 with the cell columns of the other test series.

In Figures 3.53-3.53, the TA nucleus columns on the control side (with exception of R835) have a compact appearance with predominantly clear nucleus boundaries. The satellites and cell traits are repeatedly present medially, dorsomedially and dorsolaterally, and, together with the cell profile of R835, can only point to a partial marking of the motoneuron pool. For reasons of clarity, the representation of mismarked cells primarily located medially and caudally and that constitute a percentage of 15.2% was forgone (compare Figures 3.18 and 3.19). The position of these mismarked motoneurons

on the control side (HRP2G and HRP2C) corresponds to the 2-dimensional section images of the position of the motoneuron pool denoted as mismarked on the graft side. The average percentage of mismarked motoneurons on the graft side is 50.8%, but continuously decreases from 86.5% after 2 weeks to 2.9% after 10 weeks. When consolidating the data following 8 and 10 weeks, the percentage amounts to 26.2%.

Figure 3.53 2D reconstructions of the TA cell column on the control side (***a***, left half of image, ***b*** and ***d***) and the graft side (***a***, right half of image, ***c*** and ***e***) 2 weeks after an autologous radial nerve-common peroneal nerve autograft.

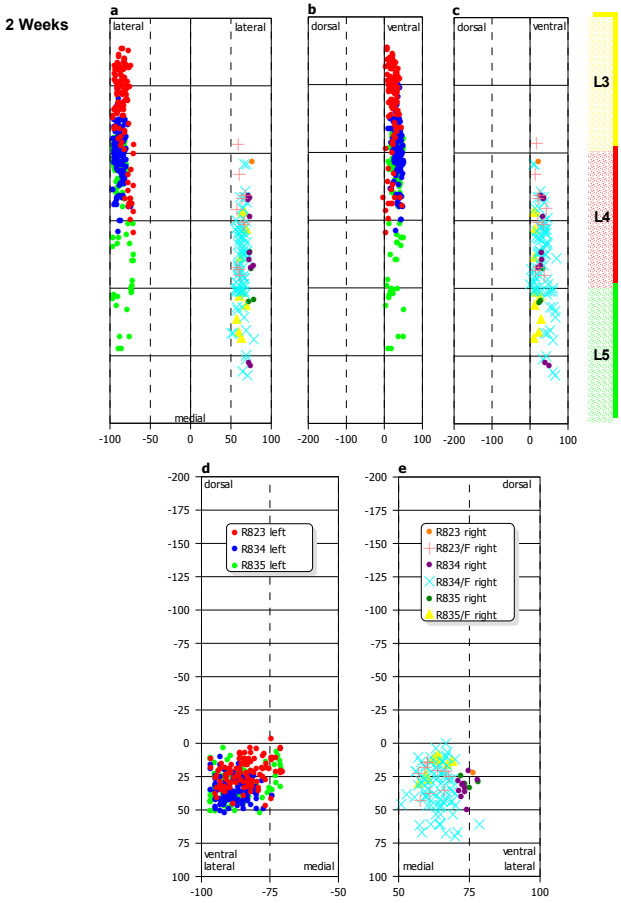

Figure 3.54 2D reconstructions of the TA cell column on the control side (***a***, left half of image, ***b*** and ***d***) and the graft side (***a***, right half of image, ***c*** and ***e***) 4 weeks after an autologous radial nerve-common peroneal nerve autograft.

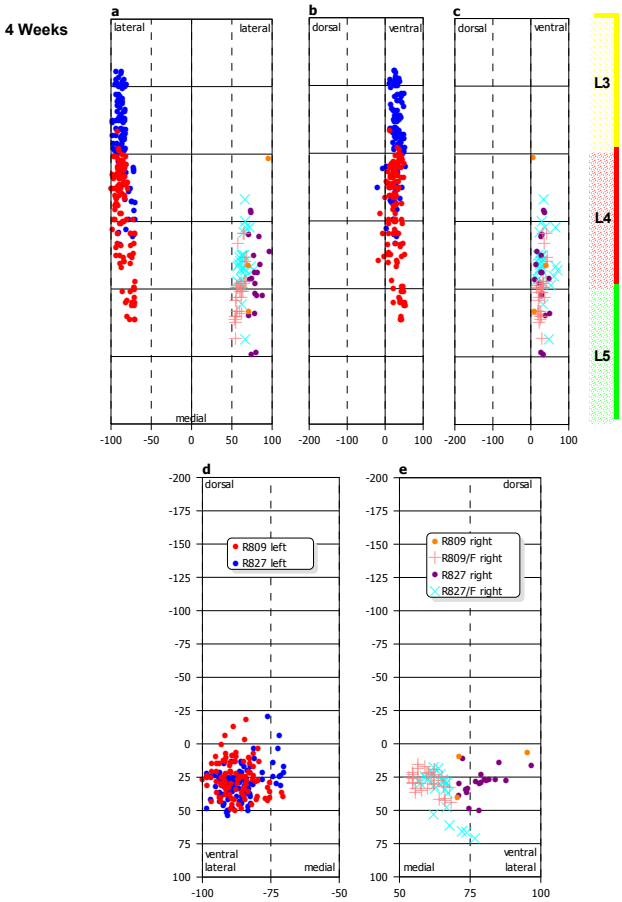

After a regeneration time of 2 weeks, only 1 to 15 motor units can be verified following HRP muscle injection, which corresponds to a regeneration quota of 0.9% to 8.5%. The motoneurons are located medially on horizontal reconstructions and are distributed singularly in a craniocaudal direction. After 4 weeks, the mean cell count increases, and the span of the reinnervation rate is 2.5% to 18.3%. The cell density becomes partly more compact, and motoneurons are now also present dorsolaterally on the spinal cord cross-section.

Figure 3.55 2D reconstructions of the TA cell column on the control side (***a***, left half of image, ***b*** and ***d***) and the graft side (***a***, right half of image, ***c*** and ***e***) 8-10 weeks after an autologous radial nerve-common peroneal nerve autograft.

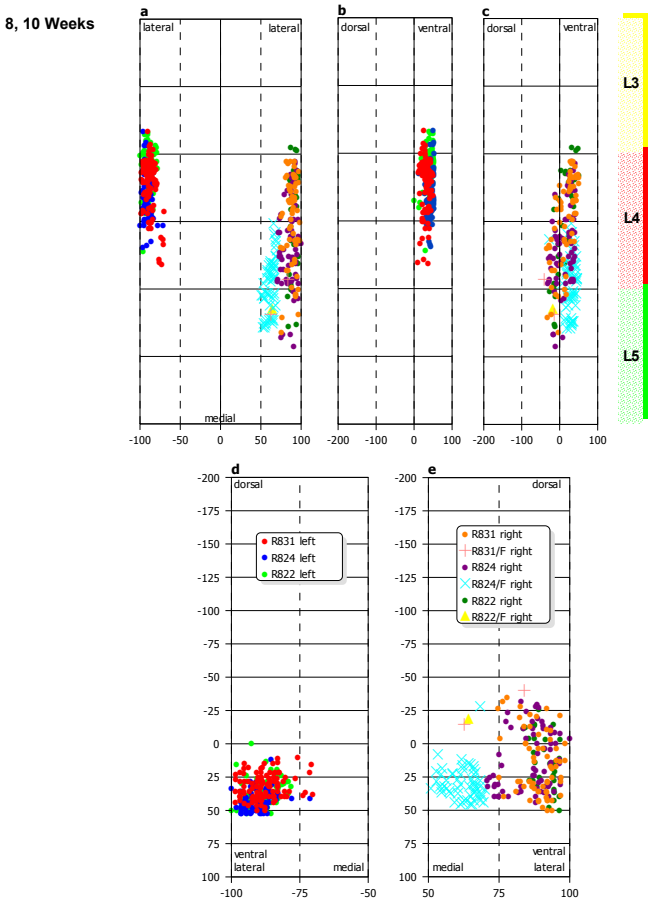

In the interval between 4 and 8 weeks, the number of motor units increases the most markedly and reinnervation rates of 59.8% to 73.1% are achieved. The morphology of the nucleus column corresponds strikingly to the cell columns of the HRP5 test series through the presence of motoneurons dorsal to the zero line.

4. Discussion

4.1. Topographical-anatomical requirements for the use of retrograde labeling techniques

4.1.1. Anatomy of the peroneal nerve innervation area

Knowledge of the progression of the common peroneal nerve, the distribution pattern and position of the muscle nerve branches, neighboring relationships and the spatial expansion of the innervated muscles is crucial for the peripheral application of retrograde transported marker substances. This applies, regardless of substance class, for the use of the tracer on severed muscle nerve branches or for muscle injection. In the case of retrograde marking of spinal cell columns by means of a nerve bath, the small spatial dimensions of the rat must be taken into account when planning. In the case of the muscle nerve branches of the tibialis anterior muscle, these dimensions allow the insertion of the catheter up to a maximum length of 3mm (see 2.1.4.2). The method of HRP muscle injection is prone to a diffusion of the enzyme into adjacent muscle and nerve compartments (Richmond et al., 1978; Yu, 1980; Janjua and Leong, 1981; Haase and Hrycyshyn, 1985, 1986; Swett et al., 1986; Haase, 1990) and requires knowledge of topographical-anatomical positional relationships in order to determine the diffusion routes and avoid a retrograde transport and the mismarking of spinal motoneurons through a transection of relevant nerve branches.

The monography by Greene (Greene, 1955) is considered as an anatomical reference for preparations in the rat. Some differences persist along the nerve and in muscular innervation between the Wistar-based rat strain used by Greene (Mus norvegicus albinus) and the Sprague-Dawley rates in these experiments. According to Greene, the common peroneal nerve enters the peroneal compartment between the peroneus longus and peroneus quartus muscles and there branches into the deep and superficial peroneal nerves. Only the peroneus longus and brevis muscles are innervated by the superficial peroneal nerve; all other muscles are supplied by the deep peroneal nerve (tibialis anterior, extensor digitorum longus, peroneus IV and V, extensor hallucis proprius, and extensor digitorum brevis II and III muscles).

First-hand preparations show a cutaneous branch not described by Greene which exits the sciatic nerve prior to its branching into the common peroneal nerve and tibial nerve in the middle of the upper leg, and arborizes subcutaneously after passing through the biceps anterior and posterior muscles (Figure 3.12). The common peroneal nerve is

grounded with its mesoneurium at the fascia of the lateral gastrocnemius muscle and enters into the peroneal compartment between the peroneus longus and peroneus V muscles. The nerve splits up into its terminal branches in the entry point area (Figure 3.15). Contrary to Greene, the deep peroneal nerve innervates, over a partially variable number of muscle nerve branches (in parentheses), the following muscles in order of exits: peroneus longus muscle (1), tibialis anterior muscle (1-3), extensor digitorum longus muscle (2), extensor hallucis proprius muscle (1), extensor digitorum brevis II (1) and III (1) muscles. Innervated by the superficial peroneal nerve: peroneus brevis muscle (2), peroneus IV muscle (1) and peroneus V muscle (1-2).

Detailed bibliographical references on number, diameter, and distribution pattern of muscle nerve branches in the rat are infrequent and incomplete. For the tibialis anterior muscle, which is used more frequently in the experiments, Peyronnard and Charron report 2 to 3 innervating nerve branches (Peyronnard and Charron, 1983a) which the number of 1 to 3 muscle nerve branches in the first-hand test series almost correspond to (Figure 3.16).

4.1.2. Morphometry of the lumbar spinal cord

On one hand, morphometric measurements of the lumbar spinal cord and spinal cord segments served quality assurance and, in conjunction with qualitative criteria, led to the exclusion of experiments exceeding a border quotient to describe the symmetrical properties (see 2.4.2.2.2). It should thereby be ensured that the accuracy of the localization data of spinal structures are increased, and the margin of error can be assessed. In HRP enzyme histochemistry in particular, with necessarily low concentrations of the fixing solution, the removal of frozen sections from the cryostat blade to the preheated slide is prone to forming cracks and compression of sections, and the indication of procedural standards is preferable. However, despite further dissemination of the HRP method for retrograde marking of spinal neurons, quality assurance criteria are not consistently performed (Burke et al., 1977; Landmesser, 1978b; Baulac and Meininger, 1981; Nicolopoulos-Stournaras and Iles, 1983; Peyronnard and Charron, 1983a; Smith and Hollyday, 1983; Ruigrok and Crowe, 1984).

Length and transverse diameter were measured for the lumbar spinal cord segments externally on the specimen following perfusion and internally on the histological section, so that the comparison of data allows an assessment of the histological reconditioning (freezing, sectioning, enzyme histochemistry) on these morphometric parameters. Allowing for all experiments, neither of the two measurement methods can determine a statistical difference for the segment length L2 to L6 (t test, $P = 0.4255$). However, if only the tests in which external as well as internal measurements were present are compared, a statistical difference with higher values is apparent in external measurement ($n = 9$, Wilcoxen test for paired differences, $P = 0.004$). On one hand, draining during reprocessing of the tissue and the external measurement method itself can be responsible for this difference in measurements. As the segment distances were tapped with a pair of dividers on the exterior of the minutien pins, a measurement of slightly larger values is conceivable. The difference between the measurement values of both measurements is indeed low, and led to a reduction of the externally measured segment length by 5.4%, and by basis of all test results by 2.2%. These values are in the

scale given by Burke et al. (Burke et al., 1977) of the 4-6% shrinkage of tissue following production of frozen sections and implementation of HRP enzyme histochemistry. Statistical differences in the transverse diameter of segments L3 and L4 were not verifiable between external and internal measurement. The calculated highly significant difference for L5 (Mann-Whitney rank sum test, $P<0.001$) originates from the fact that the spinal cord tapers sharply in this area, can only be vaguely determined in external measurement of the center between neighboring minutien pins, and the internal measurement is based on the mean transverse diameter. However, identical values can only be expected in the case of a linear decline of the transverse diameter and comparable measuring points between external and internal measurement.

Waibl (Waibl, 1973) presents detailed macroscopic-anatomical measurement results on morphometric parameters of the spinal column and spinal cord in the male albino rat (Rattus norvegicus). From a total of 22 tests animals (weight 355-465 g), complete preparations are reached in 6 animals. According to Waibl, the rat's lumbar column has a length of 40 mm, whereby the lumbar spinal cord ends at the first lumbar vertebral body. In first-hand test series ($n = 29$), segment 6 only projects itself onto vertebral body L1 in 3 animals (10.3%); in all other cases the lumbar spinal cord ends at the level of vertebral body L2 (Figure 3.9). The lumbar column is marked longer at 45.8 mm on average. In contrast, despite comparable measurement methodology and similar test animal weight (365.9 g on average), first-hand measurement values of the segment length and width are 0.5 mm smaller on average (span 0.2-0.8 mm). According to Waibl, the transverse diameter is larger than the length of all other lumbar segments, with the exception of L2. In the first-hand test series, this is only applicable to segments L3-L5.

Alternatively, the quantitative measurement of the spinal cord after positioning the coordinate system in section images (2.4.2.2) allows the specification of absolute x, y and z coordinates of motoneurons. Relative coordinates were calculated concerning the boundary of the gray matter, which in contrast to the white matter is less prone to damage in the reconditioning process. The clear localization of a cell in 3D space supplies an additional means for avoiding a double count of motoneurons in neighboring sections by the comparison of cell coordinates, when other cell parameters (cell contours, nuclei, nucleoli) do not allow it. The method enables the simultaneous 2D or 3D representation of multiple nucleus columns in the absence of technical-mechanical equipment for double or multiple marking, and the exclusion of mismarked motoneurons on cell coordinates. Interspecies differences in topography and structure of reconstructed nucleus columns are also graphically representable, and the results of different authors are comparable.

Previous representations of motor nucleus columns were based on the method by Elliott (Elliott, 1942) to prepare outline drawings of projected and enlarged histological sections or camera lucida drawings, to map motoneurons marked by chromatolysis or use of retrograde tracers and to transfer them on the respectively following section image (Romanes, 1951; Kaizawa and Takahashi, 1970; Cruce, 1974; McHanwell and Biscoe, 1981a; Nicolopoulos-Stournaras and Iles, 1983; Janjua and Leong, 1984). Stauffer et al. (Stauffer and Watt, 1976) used conventional neurophysiological techniques, but by interpreting the amplitude of antidromically or orthodromically evoked field potentials of selected motoneuron nuclei, were only able to approximately indicate the position of alpha motoneurons.

The determination of motoneuron localization in the first-hand experiments followed a procedure given by Hardman and Brown (Hardman and Brown, 1985, 1987) to standardize the absolute cell coordinates on the lateral and ventral boundaries of the gray matter in relation to the central canal. Hardman and Brown's goal was the mutual representation of all experiments in a 2D diagram in order to substantiate the dorsoventral organization of the motoneuron pool of the intercostal musculature of the rat, dependent of the proximodistal position of muscle fibers. This method was rendered more precisely by standards for adjusting a screened coordinate system to the section images and supplemented by a segmental standardization for defining the craniocaudal position of the motoneurons, whereby 2D reconstructions of the nucleus columns in horizontal and sagittal projections as well as 3D reconstructions could be calculated.

4.2. Reliability of the application of retrograde tracers

4.2.1. Horseradish peroxidase

Two different techniques for the application of HRP were chosen for marking motoneurons in the lumbar spinal cord. In the first variant, an HRP solution was injected into a single muscle to show the corresponding motoneuron pool. Since the evidence of a retrograde transport of exogenous protein in the peripheral (Kristensson, 1970; Kristensson and Olsson, 1971) and central nervous system (LaVail and LaVail, 1972), this method was repeatedly introduced to map spinal cell columns (Kristensson et al., 1971; Burke et al., 1977; Pellegrini et al., 1977; Richmond et al., 1978; Landmesser, 1978a; McHanwell and Biscoe, 1981a) and, following peripheral nerve lesion, for assessing the success of regeneration (Brushart and Mesulam, 1980; Brushart et al., 1983; Hardman and Brown, 1987). The two fundamental sources of error associated with the injection of HRP into the muscle, which have decisive influence on the results and their interpretation, consist in the diffusion of HRP into adjacent muscle and nerve compartments and in the incomplete labeling of the spinal motoneuron pool. The diffusion of protein, with the consequence of a possible mislabeling of spinal neurons, had already been prematurely perceived a technical-methodical problem of muscle injection (Burke et al., 1977; Richmond et al., 1978; Landmesser, 1978b; Hollyday, 1980; McHanwell and Biscoe, 1981a), since the absorption at the axonal terminals in the muscle by pinocytosis (Zacks and Saito, 1969) and also in the periaxonal (Hirano et al., 1969) and axonal space (Krishnan and Singer, 1973; Aldskogius et al., 1983) of intact extramuscular axons could be demonstrated. The attempt to achieve a homogenous infiltration of the target muscle and a complete representation of the motoneuron nucleus through high injection volumes of HRP was alleviated in particular by diffusion onto muscle endings with smaller diameters (Burke et al., 1970; Richmond et al., 1978).

In addition to this direct extension per continuitatem, the absorption into muscular vessels, a redistribution of HRP over the vascular route and a distribution over lymphogenous transport routes were likewise not excluded (Broadwell and Brightman, 1976; Fox and Powley, 1989). The venous injection led, in the case of mature mice, to the retrograde marking of motor, sensory, and autonomous neurons of the central as well as peripheral nervous system (Broadwell and Brightman, 1976; Dow et al., 1980).

A mismarking of spinal motoneurons following muscle injection was indirectly implied, due to the localization of neurons outside of the motoneuron nucleus. Selection regularly followed subjective criteria (Burke et al., 1977; Ha et al., 1980; McHanwell and Biscoe, 1981a; Nicolopoulos-Stournaras and Iles, 1983). Quantitative data on the localization of motoneurons and cell columns, like those in the experiments performed here (Tables 3.7, 3.8, 3.12 and 3.13), are only present in individual cases for the tibial nerve and common peroneal nerve of the rat following HRP nerve bath, but not for the nucleus columns of individual muscles (Swett et al., 1986). Extensive analyses with the goal of clarifying the cause of mismarked motoneurons are rare, and forgo stating the cell counts and selection criteria (Janjua and Leong, 1981; Haase and Hrycyshyn, 1986; Haase, 1990).

In the first-hand test series, the localization of mismarked motoneurons following injection of HRP into the tibialis anterior muscle was restricted to segments L3-L5, in which the TA nucleus columns of the rat are found under normal conditions (Figures 3.18, 3.20 and 3.26). HRP labeled thoracic and cervical neurons, like those described by Janjua and Leong (Janjua and Leong, 1981) following injection into the gastrocnemius muscle or extensor digitorum longus muscle of the rat, could not be verified for the tibialis anterior muscle.

To minimize the risk of a retrograde mismarking of spinal neurons through diffusion or contamination after muscle injection, the quantity of HRP was reduced and the injection technique was optimized (test series HRP2P1). A wrongly administered injection was avoided by control of the penetration depth and work angle. The placement of the Hamilton cannula during the minute-long inject was ensured by the use of a mechanical telescopic arm. Following injection, the perforation site on the muscle fascia was sealed with fibrin glue (Klueber and Ontell, 1984) and skin closure performed after a time delay, as a compression effect on the volume-increased muscle can lead to an amplified contamination of the adjacent tissue with peroxidase. The addition of Fast Green (Conn, 1969) to the HRP solution for the purpose of checking the quality of the injection (Hardman and Brown, 1987) counter-intuitively led to a markedly higher mismarking of motoneurons outside of the target nucleus column, in direct comparison to the internal control side (Table 3.4, Figures 3.19 and 3.20). The acidic dye, originally designated as a food colorant, found a use in staining cytoplasm and cellulose in plant histology and cytology. In electrophysiological experiments, Fast Green was applied via glass micropipettes to label motoneurons and Renshaw cells. The quality of the intracellular recordings should not be affected by the addition of the dye (Thomas and Wilson, 1965, 1966); however, the presynaptic release of neurotransmitters at hippocampal interneurons of the rat was inhibited (Van Hooft, 2002). Although toxic effects (Hansen et al., 1966) of Fast Green have been described, there is a lack of direct proof of an increase in the permeability of HRP at connective tissue barriers.

Through these control measures, a reduction of the percentage of 14.3% (HRP1P) of mismarked motoneurons after HRP injection into the tibialis anterior muscle to an average of 8.4% (n = 24) could be achieved. According to McHanwell and Biscoe (McHanwell and Biscoe, 1981a), a mismarking also cannot be avoided in careful, technical-methodical muscle injection or reduction of volumes or concentrations of the HRP solution, up to a limit in which a normal cell count is obtainable.

For these reasons, the muscle injection technique was modified and alternative types of application for retrograde tracers were sought out:

(1) The nerve branches of neighboring muscle or from relevant nerve trunks were severed prior to the muscle injection in order to prevent retrograde transport after diffusion of HRP into adjacent compartments (Burke et al., 1977; Brushart and Mesulam, 1980; McHanwell and Biscoe, 1981a; Brushart et al., 1983). Burke et al. (Burke et al., 1977) were able to hereby examine a mismarking of neurons outside of the target nucleus column following injection of HRP into the medial gastrocnemius and soleus muscles of the cat. According to McHanwell and Biscoe (McHanwell and Biscoe, 1981a), a diffusion of HRP from the injection site into the periphery can only be effectively prevented by the transection of adjacent nerve branches. First-hand tests with the injection of peroxidase into the tibialis anterior muscle following transection of the ipsilateral common peroneal nerve (HRP2P2, compare 3.4.3.1 and Table 3.4) showed a dorsolateral recess of HRP marking on the spinal cord cross-section, an area in which the TA motoneuron nucleus is normally found. The percentage of mismarked neurons in this area was low, at less than 1%. The medial, and less ventrolateral percentage of mismarked cells reached 32.2% for test R948, based on the mean cell count of 111.7 motoneurons in all HRP experiments (n = 26, with cell columns not marked with the addition of FG).

Particular problems appear in small animals like the rat and mouse if the nerve branches of neighboring muscles are to be severed to avoid a mismarking (Richmond et al., 1978; McHanwell and Biscoe, 1981a). In the HRP1G test series, based on the small dimensions, a preparation and transection of the nerve branches supplying the extensor digitorum longus and peroneus longus muscles and the sealing of the proximal nerve stumps by catheter without damaging the deep peroneal nerve or the muscle nerve branches supplying the tibialis anterior muscle, with a consequently insufficient retrograde transport of HRP, was not possible (compare Figures 2.1, 3.13-3.15). In the context of lesion experiments and injection of retrograde marker substances into atrophied muscle, with the risk of an alleviated diffusion into adjacent compartments, a check of the diffusion as a source of error for assessing regeneration success is, however, indispensable.

Potential mismarking in muscle injection has prompted Swett et al. (Swett et al., 1986) to advise against injections into the muscle for mapping motoneuron columns. On the other hand, there is no alternative to muscle injection if the overall motor unit, from the spinal motoneuron to the end organ muscle, is to be assessed in the context of regeneration experiments following peripheral nerve lesion and repair.

(2) The nerve branches supplying the target muscle were severed, and the proximal end of the nerve stump is immersed in an HRP solution (Richmond et al., 1978; Baulac and Meininger, 1979; Takahashi et al., 1980; Nicolopoulos-Stournaras and Iles, 1983; Peyronnard and Charron, 1983b; Brushart and Seiler, 1987). Alternatively, crystalline HRP (McHanwell and Biscoe, 1981a; Nicolopoulos-Stournaras and Iles, 1983; Janjua and Leong, 1984) or a piece of gel foam soaked in HRP solution was placed on the nerve stump after transection (Richmond et al., 1978). In addition to a combination of procedures (Swett et al., 1986; Crockett et al., 1987), the HRP solution was also intraneurally injected after severing the nerves, ligature of the proximal nerve endings and contusion

by means of glass micropipettes (Hashizume et al., 1988) or cannulae (Thangam et al., 1989).

Just as with the denervation of relevant nerve branches in the context of HRP muscle injection, the preparation of the just millimeter-thick, often multiple muscle nerve branches and the execution of the HRP nerve bath can be technically demanding in small animals. Special precautions must be adhered to in order to prevent the HRP solution from leaking or the nerves from breaking in the catheter. According to Swett et al. (Swett et al., 1986), a hemorrhage from nerval vessels should occur in 10-15% of preparations and is associated with a significantly lower cell count.

The risk of a mislabeling of neurons through contamination of the surrounding tissue is also present with this method, but a direct check is possible by sight due to the manipulations. This alone was deemed valid for the nerve bath method; a nerve injection was rejected due to insufficient monitoring possibilities (Takahashi et al., 1980; Swett et al., 1986).

4.2.2. Fluorescent dyes Diamidino Yellow and Fast Blue

The experiments with fluorescent dyes serves as external controls for the HRP tests in terms of the localization and number of retrograde labeled neurons. As opposed to HRP, Diamidino Yellow and Fast Blue have the advantage that they remain as suspensions at the injection site and the risk of a retrograde mismarking through diffusion is less present. Miyata and Kawai (Miyata and Kawai, 1991) measured a diffusion over 1.5 mm from the injection site after injection of 2µl of a 5% FB suspension into the extensor digitorum longus muscle of the rat. Like Capra and Wax (Capra and Wax, 1989) after injection of FB into the masseter muscle of the cat, they justified the low cell counts with the inadequate distribution in the muscle. Both Condé (Conde, 1987), following injection of FB or DY into the cerebral interposed nucleus of the cat, and Miyata and Kawai (Miyata and Kawai, 1991) deemed these fluorescent dyes unsuitable for quantitative studies. On the other hand, Illert et al. (Illert et al., 1982) and Hoover and Durkovic (Hoover and Durkovic, 1991) adhered to a strict denervation protocol in light of the peripheral diffusion they observed.

Following injection of DY and FB into the tibialis anterior muscle, transversal sections of the muscle were prepared after perfusion of individual test animals to monitor the distribution of the tracer in the area of the injection site. Although a quantitative measurement did not take place, the fluorescent dyes were located as a compact conglomeration at the end of the visible puncture channel, in a small area with an abrupt decline in concentration towards the periphery. The fluorescent dyes split up subfascially up to the epimysium; evidence for a transfascial diffusion into other muscle compartments did not emerge. A denervation of other muscles was also therefore not performed, as fluorescently marked motoneurons were not verifiable outside of the anticipated target spinal nucleus column. Compared with the cell count following HRP injection into the tibialis anterior muscle, 89.4% (n = 5) of the motoneuron pool was able to be marked with Fast Blue and 94.8% (n = 2) with DY (Table 3.6 and Figure 3.25).

Novikova et al. (Novikova et al., 1997) compared the fluorescent dyes Fast Blue and Fluoro-Gold with dextran conjugates in the long-term test to 12 months. All fluorescing substances were rated as nontoxic; Fast Blue recommended for long-term marking due to the constant cell count over the entire time span. However, the FB and DY labeled TA motoneurons of the R808 long-term test (F1P2; Figure 3.17, q) already showed torqued axons and dendrites after 56 days, as described by Bowe et al. (Bowe et al., 1992) after axonal regeneration. Toxic effects of the fluorescent dyes as a cause of the effects should not be excluded (Puigdellivol-Sanchez et al., 2002). Also, the number of motoneurons was reduced to 31% of the control values for FB, 17% for DY, so quantitative analyses are unreliable due to incomplete labeling of the motoneuron pool.

Admittedly, the simultaneous use of HRP and fluorescent dyes for double and multiple labeling of motoneurons showed a compatibility of both methods for DAPI (Yezierski and Bowker, 1981), Nuclear Yellow, Diamidino Yellow, Fast Blue (Katan et al., 1982; Conde, 1987; Klueber, 1987; Warton et al., 1988; Capra and Wax, 1989) and Fluoro-Gold (Schmued and Fallon, 1986; Swett et al., 1986); however, a quantitative analysis of morphometric parameters did not normally take place. The combination of HRP and Diamidino Yellow indicated a wash-out effect of the fluorescent dye through the HRP enzyme histochemistry, with the result of a markedly decreased cell count (Conde, 1987). A central diffusion (compare 3.4.1 and Figure 3.17, t-v) of Diamidino Yellow occurred in the first-hand HRPF2 test series only in a double labeling with HRP, corresponding to the observations by Yezierski and Bowker (Yezierski and Bowker, 1981) for DAPI. A quantitative evaluation was not possible due the false positive fluorescent labeling of the neurons.

4.3. Topography and organization of spinal motoneuron nuclei

For the understanding of the functional organization of cell columns in the spinal cord and of the segmental motor control under physiological and pathophysiological conditions, the concepts of the motor unit, the muscular unit and the motoneuron pool are essential (Burke, 1981; Henneman and Mendell, 1981). The concept of the motor unit was introduced by Sherrington in order to describe the close functional connection between the motor anterior horn cells and the muscle fibers they innervate, the muscular unit.

Anatomically, a skeletal muscle consists of a different number of parallel arranged muscle units where the individual muscle fibers of a motor unit do not spatially form a cohesive group, but are rather distributed over a limited territory in the muscle (Edstrom and Kugelberg, 1968; Brandstater and Lambert, 1973; Burke and Tsairis, 1973). However, a grouping of histochemically similar muscle fibers appears in the reinnervated muscle following a nerve lesion (Karpati and Engel, 1968; Kugelberg, 1973), which was related to a collateral sprouting of intact neurites of neighboring muscle fibers (Edds, 1950). Although the functionally vital difference between slow, 'red' and rapid, 'white' muscle have already been touched on by Ranvier (Ranvier, 1874), histochemical and electrophysiological techniques were the first to make the further classification into muscle types and the assignment to structural, mechanical and biochemical features possible. There is a variety of equivalent terms for the applicable three- or four-part classification plan (Brooke and Kaiser (Brooke and Kaiser, 1970): type I, IA, IB, IC; Peter et al. (Peter et al., 1972): SO (slow twitch-oxidative), FOG (fast twitch-oxidative-glycolytic), FG (fast twitch-glycolytic), ?; Burke et al. (Burke et al., 1973): S (slow twitch, fatigue-resistant), FR (fast twitch, fatigue-resistant), FF (fast twitch, fast-fatiguing), FI (fast twitch with intermediate fatigue resistance)).

The population of motoneurons which innervates a particular skeletal muscle is called a motoneuron pool (Henneman and Mendell, 1981), and is located as longitudinal, fusiform cell column in the lateral anterior horn of the gray matter in lamina IX, according to Romanes (Romanes, 1951; Rexed, 1952, 1964). The gray spinal cord matter in the cat was distinguished by Rexed using Nissl stains in 10 laminae. Cytoarchitectonic division proved itself for describing topographical relationships in anatomical and physiological studies on spinal connectivity. Its validity for all higher mammals was postulated and once again confirmed for the rat (Molander et al., 1984; Brichta and Grant, 1985). The cell columns occupy a similar position on cross-sections of the spinal cord regardless of species, which was established more by ontogenetic aspects than functional ones (Romanes, 1951; Landmesser, 1978b; Ruigrok and Crowe, 1984). The largest anterior horn cells of the spinal cord are located in the lamina IX (Rexed, 1964; Janzen et al., 1974), which consists of a medial and a lateral nucleus group and stretches over the entire length of the spinal cord. In the cervical and lumbar enlargements, further cell clusters are laterally distinguishable. It was assumed that the efferences of the individual clusters innervate different muscles or muscle groups. Based on the heterogeneous profile of the cells with large and small neurons, lamina IX can be differentiated from the adjacent laminae VII and VIII. Alpha motoneurons should correspond to the

large anterior horn cells in lamina IX, and gamma motoneurons to the smaller cells (Brichta and Grant, 1985).

There were already tests to clarify the inner structure of the spinal cord two centuries ago. Due to a lack of methodical requirements, however, they remained limited to the evidence of cell columns and their general morphological description, without which a functional assignment could be given (Clarke, 1850, 1858; Jakobsohn, 1908; Elliott, 1942, 1943, 1944).

Only with the development of retrograde marking techniques was it possible to produce an assignment between the peripheral effector (muscle, muscle group, nerve) and the affinity of the innervating motoneurons to a nucleus group in the spinal cord. Statements on the functional meaning and organization of the spinal motoneuron columns were thereby put on an anatomical basis. Initially, the modifications of motoneurons in the context of chromatolysis (Nissl, 1892) after a peripheral lesion served experimentally and under clinical pathological conditions as a topographical marker (Goering, 1928; Romanes, 1946; Sprague, 1948; Romanes, 1951; Sprague, 1951; Balthasar, 1952; Sharrard, 1955; Sterling and Kuypers, 1967; Kaizawa and Takahashi, 1970; Cruce, 1974).

Due to species differences in the manifestation of the degenerative reaction (Cammermeyer, 1968) and the associated problems identifying chromatolytic cells, contradictory findings on number, position and function of the cell columns were the result (Romanes, 1946; Kaizawa and Takahashi, 1970). Quantification was not reliable due to the often unverifiable chromatolysis in rats (Romanes, 1964; Kaizawa and Takahashi, 1970). The number of neurons was also underestimated due to the fact that the retrograde reaction is more distinct in larger cells than in small cells (Romanes, 1951).

Based on his studies on the localization of lumbar nucleus columns, Romanes consolidated the spinal organization principles (Romanes, 1951):

- A somatotopic relationship exists between the position of the effector and the localization of the spinal neurons in the craniocaudal and anterodorsal direction. Proximal muscles are innervated by motoneurons in the cranial segments of the anterior frontal horn area. In contrast, distal muscles are supplied by motoneurons in caudally located segments, which are more dorsally located in lamina IX.

- For the dorsal and ventral layer of the lumbosacral plexus of the cat, the assignment of motoneurons to 7 adjacent nucleus columns takes place, depending on which joint of the respective muscle becomes active.

The evidence of axonal transport (Weiss and Hiscoe, 1948) and the observation that exogenous protein is retrograde transported in the peripheral and central nervous system (Kristensson, 1970; Kristensson and Olsson, 1971; LaVail and LaVail, 1972) was the origin of a variety of experimental studies to map neurons and their innervation area under physiological and pathophysiological conditions. Since the introduction of horseradish peroxidase (HRP) to evidence of neuronal connections in the peripheral

(Kristensson and Olsson, 1971) and central (LaVail and LaVail, 1972) nervous system, studies detailed with this method have been performed for the organization of motor cell columns in monkeys (Janjua and Leong, 1984), cats (Burke et al., 1977; Horcholle-Bossavit et al., 1988), rats (Nicolopoulos-Stournaras and Iles, 1983; Peyronnard and Charron, 1983a), mice (McHanwell and Biscoe, 1981a) and in birds (Landmesser, 1978b; Hollyday, 1983; Smith and Hollyday, 1983), fish (Fritzsch et al., 1990) and amphibians (Ruigrok and Crowe, 1984).

After application of HRP to the peripheral muscle or nerve and a suitable latency period for the transport, the enzyme histochemically implemented dye product was able to be proven in the corresponding neurons. The concept positioned with chromatolysis by Romanes as cell markers (Romanes, 1951) of longitudinally oriented and definable cell columns as representation units of individual muscles was confirmed (Burke et al., 1977; Landmesser, 1978b; Hollyday, 1980; McHanwell and Biscoe, 1981a; Nicolopoulos-Stournaras and Iles, 1983). With the HRP method, a somatotopy was also verifiable between the rostrocaudal position of a motoneuron in the cell column and the muscle compartments supplied by individual muscle nerve branches (Kernell et al., 1985; Weeks and English, 1987; Balice-Gordon and Thompson, 1988). An organization of the cell pool according to the type of motor unit was not ascertainable (Weeks and English, 1987), as electrophysiological studies had already previously shown (Burke and Tsairis, 1973).

With the synthetization of retrograde transported fluorescent dyes of different colors and affinity to the cell components, a double and multiple marking of the interesting nucleus columns was possible (Kuypers and Huisman, 1984; Fritz et al., 1986b; Fritz et al., 1986a; Hoover and Durkovic, 1991). A topographical organization of the motoneurons corresponding to the peripheral innervation pattern could be confirmed with the combined application of fluorescent dyes for some muscles (Laskowski and Sanes, 1987; Horner and Kummel, 1993) but not for others (Choi and Hoover, 1996; Saad et al., 1997).

Despite methodical improvements and conjugation with wheat germ agglutinin (Mesulam, 1982), HRP is unsuitable in long-term tests due to the rapid proteolytic depletion (Divac and Mogensen, 1990), and a double labeling of individual cells or different marking of neighboring cell columns is impossible. This is achieved through the use of retrograde transported fluorescent dyes, which are generally used to obtain evidence of collateral projections in the central nervous system. Since the original description by Kristensson (Kristensson, 1970), further connections with partially diverse features have been synthesized in recent years (Keizer et al., 1983; Kuypers and Huisman, 1984; Schmued and Fallon, 1986; Honig and Hume, 1989; Katz and Iarovici, 1990). Through the targeted selection of different fluorescent markers, eventually in combination with HRP, the individual characteristics of the substances can then be exploited to answer more complex somatotopic issues.

Depending on the respectively used methods, different findings were made regarding the topographical and functional relationship of nucleus columns. With the chromatolysis method as a cell marker, according to Romanes (Romanes, 1951), cell groups in the cat are made up of motoneurons that admittedly innervate distinct muscles, but then affect the joints which become activated for a specific movement. Although the cell columns of individual muscles have a discreet structure, an almost complete overlapping

exists within the cell group between the muscles. The experiments by Burke (Burke et al., 1977) using horseradish peroxidase as a retrograde tracer have confirmed this concept for the medial gastrocnemius and soleus muscles. That functionally applied motor pools overlap was proven for several muscles in different species (Sprague, 1948; Cruce, 1974; Richmond et al., 1978; Nicolopoulos-Stournaras and Iles, 1983), and assumes that closely neighboring cells maintain a similar synaptic input (Wyman, 1973). On the other hand, a separate localization with only minimal overlap was verified in muscles in which an overlapping of cell columns was anticipated based on synergistic function (Fritz et al., 1986b; Fritz et al., 1986a; Horcholle-Bossavit et al., 1988; Hoover and Durkovic, 1991).

Fritz et al. (Fritz et al., 1986b; Fritz et al., 1986a) have determined that the cell density of nucleus columns in various muscles is different, and a correlation exists to its overlapping. This correlation had already previously been related to the individual phases of the gait cycle (Hollyday, 1980; Jacobson and Hollyday, 1982). Muscles that are active during the stance phase have a lower cell density and overlap more heavily than muscles that are innervated during the swing phase.

4.4. Topography of the tibialis anterior nucleus column

According to Rexed (Rexed, 1952), 2D and 3D reconstructions (Figures 3.21-3.23 and 3.29) show a localization in the anterior horn of the spinal cord, dorsolateral in lamina IX for the normal nucleus column of the tibialis anterior muscle of the rat. In the cat, the compact, fusiform nucleus column stretches from L3-L5, in projection onto the spinal column of T13 to L1. The area on the spinal cord cross-section corresponds with the ‘Column 2’ by Romanes (Romanes, 1951) and with the localization statement by Hoover and Durkovic (Hoover and Durkovic, 1991). A dorsolateral position of the tibialis anterior nucleus column in the rat is described by Peyronnard and Charron (Peyronnard and Charron, 1983a) and by Nicolopoulos-Stournaras and Iles (Nicolopoulos-Stournaras and Iles, 1983), and by McHanwell and Biscoe (McHanwell and Biscoe, 1981a) in the mouse. Standardized coordinates of the nucleus column of the tibialis anterior muscle were not given, so a comparison with the quantitative statements of this study is not possible. The segmental localization of the cell column is given with L3 and L4 by Nicolopoulos-Stournaras and Iles (Nicolopoulos-Stournaras and Iles, 1983), and with L4 and L5 by other authors (Ha et al., 1980; Peyronnard and Charron, 1983a). In connection with the appearance of two local frequency maximums of the cranial and caudal nucleus pole in this experimental study (Figure 3.26), the differences are possibly a manifestation of the pre- and post-fixation of the lumbar plexus described by Sherrington (Sherrington, 1892).

Over the course of the reinnervation phase following an autologous radial nerve-common peroneal nerve graft, the nucleus columns labeled with HRP are shifted in the caudal direction in comparison to the control side (Figure 4.1). According to Nicolopoulos-Stournaras and Iles (Nicolopoulos-Stournaras and Iles, 1983), the muscles inner-

vated by the superficial peroneal nerve are located in deeper segments than the cell columns of the tibialis anterior muscle, so a misinnervation through motoneurons of the peroneal compartment in the context of reinnervation is achieved.

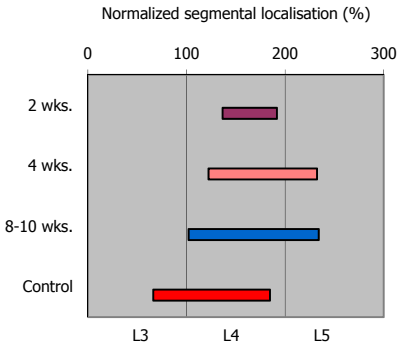

Figure 4.1 Segmental localization of the tibialis anterior nucleus column on the control and graft side.

4.5. Cell count of the tibialis anterior nucleus column in control experiments and following autograft

Before retrograde transported substances like HRP or fluorescent dyes for verification of neuronal connections in the peripheral (Kristensson and Olsson, 1971) or central (LaVail and LaVail, 1972) nervous system were introduced, the number and localization of the motoneurons of an innervated muscle could only be established with the retrograde degeneration method (Nissl, 1892). The motoneurons in the spinal cord were hereby identified and mapped following a peripheral lesion of their axons based on chromatolytic modifications (Goering, 1928; Romanes, 1946; Sprague, 1948; Romanes, 1951; Sprague, 1951; Balthasar, 1952; Kaizawa and Takahashi, 1970; Cruce, 1974). If the number of motor units alone was the object of scientific interest, the spinal ganglion was resected and the number of deafferented, myelinated nerve fibers was determined (Eccles and Sherrington, 1930).

The number of motoneurons determined by chromatolysis as a cell marker was nevertheless underestimated. Once, the histological modifications were less distinct, so only cells with a clear indication of the chromatolysis were included in the evaluation. Moreover, large motoneurons with normal cell physiognomy continued to be found, even in more extensive lesions. Finally, the later comparison of the cell count with the number of motor fibers of a muscle after extirpation of the corresponding posterior root ganglia confirmed the too-low values. Romanes (Romanes, 1951) ascribed this to the

fact that the smaller gamma motoneurons are not or only slightly subject to chromatolysis and therefore are somewhat overlooked. Kaizawa and Takahashi (Kaizawa and Takahashi, 1970) observed the same phenomenon in the rat.

However, the cell counts of a motoneuron pool are underestimated while using HRP, just as before with chromatolysis. Burke et al. (Burke et al., 1977) compared their results with the fiber counts by Boyd and Davey (Boyd and Davey, 1966) and determined that, for the gastrocnemius and soleus muscle of the cat, the number of alpha motoneurons is 10-15% lower, but the number of gamma motoneurons is 50% lower. McHanwell and Biscoe (McHanwell and Biscoe, 1981a) found 78% of Nissl-stained cells in the lateral anterior horn area were marked with HRP. Nicolopoulos-Stournaras and Iles (Nicolopoulos-Stournaras and Iles, 1983) report that the number of HRP labeled cells is only 70% of the motor fibers which are detected using acetylcholinesterase staining.

There are a number of reasons for this misunderstanding: (1) A consistent distribution of the HRP solution may possibly not be reached in the muscle after injection, where absorption to the alpha fibers is lower than to the gamma fibers (Biscoe and McHanwell, 1979). The results from the test series with the addition of Fast Green to the HRP solution contradicts this. Here, the entire muscle was stained green immediately after muscle injection. (2) Encapsulated organs, such as muscle spindles, impair access by HRP to the efferences (Richmond et al., 1978; McHanwell and Biscoe, 1981b). (3) In a subclass of gamma motoneurons, HRP is not transported (McHanwell and Biscoe, 1981b). (4) The number of gamma nerve fibers is overestimated (McHanwell and Biscoe, 1981b; Peyronnard and Charron, 1983a). (5) The sensitivity of the color reaction for representing HRP labeled motoneurons influences their cell count. Burke et al. (Burke et al., 1977) used the method by Graham and Karnovsky, McHanwell and Biscoe (McHanwell and Biscoe, 1981a) the method by Hanker et al. (Hanker et al., 1977). Both procedures are inferior in their method sensitivity with tetramethylbenzidine as a dye (Mesulam and Rosene, 1979). McHanwell and Biscoe were nevertheless unable to determine any diverging cell counts with TMB in preliminary trials concerning the quadriceps femoris muscle. (6) The exposure time of the HRP solution on the severed nerve stump likewise influences the cell count. In the tests by Nicolopoulos-Stournaras and Iles (Nicolopoulos-Stournaras and Iles, 1983), the nerve endings had only 15 minutes of contact with the HRP solution, which is ostensibly responsible for the low cell count (Crockett et al., 1987). (7) Strict criteria for the selection of cells can lead to a low cell count. On the other hand, Peyronnard and Charron (Peyronnard and Charron, 1983a) were able to show an almost absolute conformity between the number of myelinated fibers after resection of the posterior root ganglia and the HRP cell count for the TA of the rat. The motoneuron pool of TA consists of 154 cells (127-175), and the number of myelinated fibers is stated at 152 (128-180).

The large span stated in the literature of the cell numbers of nerval and muscular motoneuron pools after application of retrograde tracers (Table 4.1) cannot be conclusively accounted for by reference to biological variability alone. The consolidation of cell counts of the common peroneal nerve cell pool of the rat lets it be assumed that, for the span of 177 to 1760 cells, methodical differences are of critical importance and the knowledge of which is a requirement for an interpretation, especially in regeneration experiments. Nicolopoulos-Stournaras and Iles (Nicolopoulos-Stournaras and Iles,

1983) denote 104 cells for the foot musculature of the rat (20% HRP solution, contact time of the severed nerves 15 minutes), while in contrast Crockett et al. (Crockett et al., 1987) denote 560 cells (HRP crystals and 20-30% HRP gel in 2% DMSO, contact time at the proximal nerve stump 1-4 hours).

Crucial influence factors on the cell count are, besides the type of HRP application, the contact time of the tracer on the nerve (low cell count with Nicolopoulos-Stournaras and Iles (Nicolopoulos-Stournaras and Iles, 1983)), the survival time of the test animals (Neuhuber and Niederle, 1980), differences in sensitivity of the applied enzyme histochemical method for representing the peroxidase (low cell count with McHanwell and Biscoe (Mesulam and Rosene, 1979; McHanwell and Biscoe, 1981a)) and the choice of microscopic procedure. In first-hand test animals, it was shown that the number of labeled motoneurons is underestimated in the dark field and can be reduced in the first evaluation up to 52.6% of the cell count in the light field. The fundamental reason for this difference is in the weak staining of the type IE labeled somata, which can be overlooked in the dark field.

Regardless of the application of HRP, Nicolopoulos-Stournaras and Iles (Nicolopoulos-Stournaras and Iles, 1983) reported an adequate transport in only 70% of their tests. In the first-hand test series with HRP depicted here, an insufficient marking with a consequently lowered cell count is observed in 19% (muscle injection: 13%, HRP nerve bath: 45%).

The section thickness and the exclusion of cell fragments in neighboring sections also influence the results of cell counting. The delineation of a cell count or a diameter also takes place without an exclusion of the double-counting of neurons, however (Ha et al., 1980; Smith and Hollyday, 1983; Janjua and Leong, 1984), or there is a lack of detailed methodical indications of a selection process, especially when the nucleus or nucleolus are not depicted. Double counting can be reduced by a large section thickness or by consideration of corrective factors (Abercrombie, 1946). Using first-hand criteria (see 2.4.2.3.2), the percentage of doubled TA cells amounts to $13.9 \pm 4.7\%$ ($n = 26$, span 5.0-22.9%) with a section thickness of 40 µm. Fritz et al. (Fritz et al., 1986b) estimate the number of doubled motoneurons to be at 20-30%, after retrograde HRP marking of distal muscles of the anterior extremity of the cat.

4.6. Cell diameter and cell types of the tibialis anterior nucleus column on the control and graft side

Through the introduction of HRP as a retrograde transported, exogenous protein, not only could the localization and number of neurons be reliably determined, but their diameter as well. The as yet open question of whether the bimodal distribution of the fiber diameter of myelinated efferences (Eccles and Sherrington, 1930) corresponds to the same in the cell diameter was also able to be resolved for the posterior extremity muscles of the cat (Burke et al., 1977) and mouse (McHanwell and Biscoe, 1981b). With the exception of the plantar foot musculature of the mouse, a bimodal distribution pattern of the cell size was described by these authors. The relationships in the rat are still unclear (Brushart and Mesulam, 1980; Peyronnard and Charron, 1983a; Swett et al., 1986).

Peyronnard and Charron (Peyronnard and Charron, 1983a) observed two definable size classes in rats in 3 of 5 experiments. The limiting diameter was at 40 μm. In these experimental studies, a bimodal distribution of diameter was determined in 75% of the tests, and a trimodal distribution in 50%. The border area was determined to be 28.4 ± 1.2 μm for the gamma/alpha 1 transition and 36.6 ± 2.3 μm for the alpha 1/alpha 2 transition. The diameter of the somata labeled motoneurons in a cell column often show, depending on the species and muscle, a bimodal distribution. Following deafferentation, a similar distribution can be verified in the diameter spectrum of the myelinated fibers of the corresponding muscle nerves (Peyronnard and Charron, 1983b).

Although Eccles and Sherrington (Eccles and Sherrington, 1930) had already observed two populations of nerve fibers of different diameters in the fiber spectrum of different muscle nerves in the cat following excision of the posterior root ganglia, and had also determined that the small fibers did not contribute to muscle contraction, only Leksell (Leksell, 1945) found the correct explanation. He was able to show that these are conducive to the innervation of the muscle spindles. Because their axons exhibit a lower line velocity and stronger threshold excitation than alpha motor axons, a smaller cell diameter was concluded.

Anatomically, Nyberg-Hansen (Nyberg-Hansen, 1965) and van Buren and Frank (Van Buren and Frank, 1965) identified spinal cell nuclei with the retrograde degeneration method and classified the smaller cells as gamma motoneurons. According to electrophysiological typing of the anterior horn cells and subsequent intracellular labeling with HRP, a significant correlation between cell size, axon diameter and line velocity emerged for α and γ motoneurons. In addition to the line velocity beneath a critical value, the absence of a monosynaptic input of group Ia fibers and the lack of innervation of extrafusal muscle fibers were used as further criteria for identifying γ motoneurons (Cullheim and Kellerth, 1976; Cullheim and Ulfhake, 1979; Westbury, 1982; Moschovakis et al., 1991). Alpha and gamma motoneurons are homogenously distributed within the cell column (Eccles et al., 1960; Bryan et al., 1972; Burke et al., 1977) and are not arranged in separate cell nuclei (Sprague, 1951).

Based on physiological data, the α motoneurons were divided further into tonic anterior horn cells with small, slowly conducting axons which innervate slow motor units and exhibit a smaller cell diameter than phasic neurons, whose axons conduct more quickly and control the rapid motor units (Granit et al., 1956; Henneman and Olson, 1965; Henneman et al., 1965a).

Table 4.1 Cell counts for various muscles and nerves after the application of HRP or fluorescent dyes.

Author	Tracer	Application	Motoneuron pool	Test animal	CC	Survival time (hours)[1]	Cell count		Span
							M	s	
Nicolopoulos-Stournaras and Iles (1983)	HRP	Nerve bath, crystals	SN	Rat	1	48-72	627 [2]		
Janjua and Leong (1984)	HRP	Crystals	SN	Rat	20	48	2335.4	667.1	1060-3992
Own Experiments	HRP	Nerve bath	SN	Rat	2	65	1535.5	194.5	1398-1673
Brushart et al. (1980)	HRP	Muscle injection	TN	Rat	1	48	866		
Swett et al. (1986)	HRP	Nerve bath	TN	Rat	3	42-95	982.3	36.1	963-1024
Janjua and Leong (1984)	HRP	Crystals	TN	Rat	17	48	1651	410.6	849-2428
Brushart et al. (1980)	HRP	Muscle injection	CPN	Rat	6	48	395.3	27.3	368-434
Swett et al. (1986)	HRP	Nerve bath	CPN	Rat	10	42-95	632	27.3	587-660
McHanwell and Biscoe (1981)	HRP	Muscle injection, nerve bath	CPN	Mouse	2	24	184		177-191
McHanwell and Biscoe (1981)	HRP	Muscle injection, nerve bath	CPN	Mouse	5	48	188		185-195
Janjua and Leong (1984)	HRP	Crystals	CPN	Rat	18	48	926.4	412.3	440-1760
Brushart et al. (1983)	HRP	Muscle injection	CPN	Rat	5	48	396.8	30.2	368-434
Neuhuber and Niederle (1980)	HRP	Crystals	CPN	Rat	3	39	212.3		
		Crystals	CPN	Rat	4	72	322.3		
		Crystals	CPN	Rat	4	96	147.0		
Own Experiments	HRP	Nerve bath	CPN	Rat	1	68	382		
Nicolopoulos-Stournaras and Iles (1983)	HRP	Nerve bath, crystals	TA	Rat	1	48-72	130 [1]		
Peyronnard and Charron (1983)	HRP	Nerve bath	TA	Rat	8	60	159.3	19.5	134-184
	HRP	Nerve bath	TA	Rat	5	60	154.2	17.4	127-175
Peyronnard and Charron (1982)	HRP	Nerve bath	TA	Rat	8	48	154.6	35.9	100-192
Own Experiments	HRP	Nerve bath	TA	Rat	2	61-71	148.5	37.5	122-175
	HRP	Muscle injection	TA	Rat	24	46-56	108.7	15.3	80-132
	FB	Muscle injection	TA	Rat	5	4-9 d	97.2	12.6	82-113
	DY	Muscle injection	TA	Rat	2	4-6 d	103	2.8	101-105
Nicolopoulos-Stournaras and Iles (1983)	HRP	Nerve bath, crystals	LG	Rat	1	48-72	48 [3]		
Brunner et al. (1980)	Evans Blue	Muscle injection	LG	Rat	1	2-3d	35		
Own Experiments	DY	Muscle injection	LG	Rat	2	9 d	68.0	4.2	65-71

Abbreviations:
SN: Sciatic nerve, TN: Tibial nerve, CPN: Common peroneal nerve, TA: Tibialis anterior muscle, LG: Lateral gastrocnemius muscle; CC: Number of cell columns.
FB: Fast Blue, DY: Diamidino Yellow, HRP: Horseradish peroxidase.
M: Mean, s: Standard deviation.
[1] Recorded in hours, days: d.
[2] Highest cell count, totalized data from the individual tests.
[3] Highest cell count.

They likewise differentiate in their metabolic profile ((Campa and Engel, 1971; Sickles and Oblak, 1983; Ishihara et al., 1988; Edgerton et al., 1990), though compare (Mjaatvedt and Wong-Riley, 1986; Miyata and Kawai, 1991)), in their synthesis rate for protein (Petersen, 1966) and other physiological characteristics, like that of afterhyperpolarization, membrane resistance and rheobase current (Kernell, 1966; Fleshman et al., 1981). The differences in diameter distribution, originally only derived indirectly, were morphologically confirmed (Burke et al., 1977; Pellegrini et al., 1977; Ulfhake and Kellerth, 1982). Outside of α and γ motoneurons, a third type of neuron was proven, the β motoneuron, which is functionally considered as a part of a positive feed-back system. Its axons innervate extra- and intrafusal muscle fibers. Although its importance for motor control is emphasized, functional connections are not sufficiently clarified (Laporte et al., 1981).

4.7. Functional consequences

The peripheral nerves of the rat were often used as a model to study the effects of nerve lesions: Femoral nerve (Brushart, 1988), intercostal nerve (Hardman and Brown, 1987), sural nerve (Peyronnard et al., 1988b), tibial and peroneal nerves (Brushart and Mesulam, 1980; Brushart et al., 1983; Politis, 1985). Most notably, the readily accessible sciatic nerve is selected for biochemical (Peyronnard et al., 1988a), electrophysiological and functional tests to study the altered axon count (Jenq and Coggeshall, 1984), neurotropism (Lundborg et al., 1986), or alternatively for assessing various suture techniques for repairing peripheral nerves (Brushart and Mesulam, 1980; Brushart et al., 1981; Brushart et al., 1983).

Regarding the importance of neurotropic factors that decisively influence the growth of axon sprouts, the outcome of the R835 graft experiment is noteworthy. During the macroscopic preparation of the graft site after perfusion, it was apparent that the distal end of the graft was dislocated, but a continuity was produced through the regenerating fibers between the proximal graft and the distal nerve stump (Figure 3.39).

The experiments by Weiss and Taylor (Weiss and Tayler, 1943), which originally did not lead to proof of a neurotropism, have later been repeated and have by contrast shown that not only does a neurotropism exist, but also a high degree of specificity in the choice of target tissue (Lundborg et al., 1982a; Anderson and Turmaine, 1986; Mackinnon et al., 1986). This effect was able to be conveyed by a soluble factor from the distal nerve stump (Politis et al., 1982). The specificity of reinnervation was proven at several levels. Regenerating axons distinguish in tissue specificity between nerve and tendon, muscle or granulation tissue (Lundborg et al., 1986; Mackinnon et al., 1986). A specificity at the spinal root level was determined in the sympathetic (Wigston and Sanes, 1982) and motor (Farel and Wray, 1989) nervous system. Rostrocaudal gradients of position indicating molecules in the sympathetic ganglia and in the nerves supplying the intercostal muscles could be responsible for this (Suzue et al., 1990). In the area of the peripheral nerves, there is a selective regeneration of the nerve trunks and the fascicles (Sunderland, 1953; Politis, 1985; Seckel et al., 1986). The growing motor axons are thereby in the position to differentiate between motor and sensory fascicles (Brushart and Seiler, 1987; Brushart, 1988). The specificity is incomplete at the end organ level. Motor axons form endplates in the muscle, but sensory axons do not (Gutmann, 1945). There does not generally seem to be a selective reinnervation of muscle fiber types (Miledi and Stefani, 1969), except for in newborn rats (Soileau et al., 1987) and amphibians (Brown and Everett, 1991). The neuromuscular topography is reconstructed after the nerves are severed, so that rostral and caudal portions become innervated by the corresponding rostral and caudal halves of the motoneuron pool in the spinal cord (Laskowski and Sanes, 1988; Laskowski et al., 1991). In comparison, there doesn't seem to be a central, topographical specificity of the sensory projection field and spinal motor cell columns. Parallel to the regeneration of denervated sensory axons, the afferent projection area expands in the posterior horn of the spinal cord (Brushart et al., 1981) and in the brain stem (Renehan et al., 1989). In addition to this peripheral mechanism, central reasons for the afferent changes at the spinal cord level were discussed. An axonal sprouting of the central processes of the spinal ganglia would likewise explain the expansion of the innervation area and the shift of the receptive fields and be evidence of a

morphological reorganization (Brushart et al., 1981). Axon terminals of intact ganglion cells can also occupy via sprouting the synaptic seats freed-up after deafferentation of posterior horn cells. Alternatively, the reorganization of the receptive fields was established with unmasking mechanisms, which activate previously inhibited synaptic connections (Liu and Chambers, 1958; Devor and Wall, 1978). The original topography of the motor cell pool is not restored in mature animals (Brushart and Mesulam, 1980), in contrast to young ones (Hardman and Brown, 1985, 1987). These central changes are, in terms of the efferent lower leg of the peripheral nervous system, an expression of the misdistribution of regenerating axons at the lesion site and have a crucial influence on the structure and function of the motor units.

Aside from the peripheral misinnervation, which furthermore blocks a sprouting of axons in their original endoneurial sheaths, the non-restored spinal somatotopy and the decay of motoneurons (Torvik and Skjörten, 1971; Liebermann, 1974; Aldskogius et al., 1980; Scheib and Höke, 2013) and spinal ganglia (Ranson, 1909; Arvidsson, 1986; Himes and Tessler, 1989), a distinct sensitivity of cells towards damage was postulated for the functional deficits (Liebermann, 1974; Kuno et al., 1974b; Brushart and Mesulam, 1980; Risling et al., 1983a). This reaction is more pronounce following severing and contusion in the ganglion cells than in the motor posterior horn cells (Risling et al., 1980; Risling et al., 1983a) and seems to be dependent on the diameter of the cells ((Himes and Tessler, 1989; Rich et al., 1989), though compare (Risling et al., 1983b)). The magnitude and intensity of the transneural degeneration in the spinal posterior horn cells of the substantia gelatinosa are likewise dependent on size (Knyihar-Csillik et al., 1989).

Small neurons react the most strongly of all cells to a lesion; among them cell loss is highest and the regeneration process delayed and decelerated. Which types of the heterogeneous cell population of a motor nucleus column count among them was only inadequately clarified, and with partially contradictory results, through techniques of retrograde cell marking, electrophysiological methods of intracellular stimulation and derivation, and electroneurographical studies and enzyme histochemical staining processes (Thulin, 1960; Homma, 1969; Kuno et al., 1974b; Takano, 1976; Brushart and Mesulam, 1980). There seems to be a correlation between the restitution of a useful motor function and the recurrent gamma control of intrafusal muscle fibers, according to Thulin (Thulin, 1960). In comparison, Takano (Takano, 1976) was able to prove a virtually normal gait pattern in cats, even without regeneration of the gamma fibers. It was reported by Kuno (Kuno et al., 1974b) that the functionally distinct types of the alpha motoneurons react differently to an axotomy, relative to certain electrophysiological parameters. If the axons were allowed to sprout, the original electrophysiological characteristics were also restored (Kuno et al., 1974a).

The motoneuron pool's task exists in the controlled assignment of the innervated muscle, that of the motor unit in the graduated activation of muscular units. According to the 'task group' concept proposed by Loeb (Loeb, 1984; Loeb, 1990), subpopulations of motoneurons are recruited for a certain kinematic task. By definition, a correlation does not necessarily have to exist in the anatomy of certain cell nuclei, nerves or muscles. If the muscle is called upon for another kinematic task and ballistic or reflex move-

ments require another organization of motor units, other subpopulations become activated, possibly with the involvement of individual units of the first 'task group.' All elements which serve sensomotor control (α and γ motoneurons, muscle fibers and proprioceptive afferences) are thereby included in the term 'task group.'

In addition to this functional organization of motor units, an anatomical organization into neuromuscular compartments was proven for several muscles where a somatotopic relationship exists between the position of the motoneuron in the cell column, also less strongly correlated between cell size and the innervated muscular unit (Swett et al., 1970; Burke et al., 1977; English and Letbetter, 1982a, b; Weeks and English, 1987; Balice-Gordon and Thompson, 1988). As individual compartments can also be activated independently of one another (Russell et al., 1982), they were also considered the anatomical correlate of the task group (Weeks and English, 1985). Within a task group, the motor units are recruited reverse proportionally to cell size (Henneman and Mendell, 1981) or according to type (Fleshman et al., 1981; Sypert and Munson, 1981) so that, depending on the activity, first small, slow type S, then larger type FR and lastly large, rapid type FF units are applied. The 'size principle' could also be confirmed in humans (Milner-Brown et al., 1973; Desmedt and Godeaux, 1977; Riek and Bawa, 1992). After completely severing the nerve and an end-to-end suture, the size principle of recruiting motor units can be restored if the regenerating axon reinnervates its original muscles or synergists and the characteristics of the muscle fibers have respecified, so that their power and contraction velocity once again correlate with the cell size (Stein, 1988). This is possible following a lesion of the median nerve at the wrist (Thomas et al., 1987), but not above the elbow (Milner-Brown et al., 1974), because motor units of other motoneuron pools would be recruited with different functions due to misinnervation.

Aside from retrograde chromatolysis and transneural degeneration (Cowan, 1970), a variety of centrally morphological modifications were described following the lesion of peripheral nerves at the spinal cord level (Zochodne, 2008; Brushart, 2011). In addition to a deafferentation of motoneurons through synaptic stripping (Blinzinger and Kreutzberg, 1968), the retraction of the dendritic tree (Sumner and Sutherland, 1973) and the elimination of intramedullary axon collaterals from α motoneurons (Havton and Kellerth, 1990), surface changes were observed on the dorsal motor vagus nucleus of the rabbit, which were interpreted as dendritic and perikaryal sprouting (Engel and Kreutzberg, 1988). A growth of axon sprouts from the posterior root ganglion into the anterior root was established (Nam et al., 1989; Oh et al., 1989), as well as regeneration by excess axons (Havton and Kellerth, 1987) and the formation of dendraxons (Linda et al., 1985). The functional importance of this morphological reorganization is still unknown. A clarification of this cohesion is of great significance, because the functional consequences following a misinnervation of motor axons are determined by the quality of the sensory reinnervation and the ability of the central nervous system to compensate. It was established that mechanisms of central adaptation are present, after crossing peripheral nerves to antagonistic muscles, in non-human primates and humans (Sperry, 1945, 1947; Brinkman et al., 1983), but not in rats (Sperry, 1941) or cats (Gordon et al., 1986a, 1986b). At the spinal level, Eccles (Eccles et al., 1962) and Mendell and Scott (Mendell and Scott, 1975) only found sparse evidence of a synaptic reorganization. McMahon and Wall (McMahon and Wall, 1989) were nevertheless able to verify a reversal of the length of time facilitating the withdrawal reflex after crossing cutaneous

and muscle nerves in the adult rat. However, if the spinal capacity for adaptation is low, it could be deduced that the cortical centers have a fundamentally larger meaning for reorganization. This can be presumed from the massive cortical changes in the motor representation (Sanes et al., 1988; Fuhr et al., 1992) and the reorganization of the receptive fields (Merzenich et al., 1983; Pons et al., 1991).

5. Conclusion

Autologous nerve grafts are steadily regarded as the method of choice for bridging the nerve gaps resulting after peripheral nerve lesions with substance defects. Microsurgical techniques and the perineurial suture of corresponding fascicles have improved the functional results following peripheral nerve graft. However, regeneration success is often disappointing, despite the most thorough technique and expertise. The loss of spinal motoneurons associated with a nerve lesion and the growth of axon sprouts in inadequate endoneurial sheaths were held responsible as the reason for the lowered muscular strength, limited movement coordination and fine motor skills, poor differentiation and localization of sensory stimuli and for the lack of tactile gnosis.

In this experimental study, it is assumed that the central effects at the level of the spinal motoneuron nuclei show an image of the peripheral misinnervation in topographical-morphological terms, and can supply an explanatory model for the functional motor deficits after peripheral nerve graft. On the other hand, the plastic changes of a motor cell column in the reinnervation process influence the structural-functional relationships of the motor units in a variety of clinically relevant ways.

The experiments were performed on 45 mature male Sprague-Dawley rats (200-550g). Retrograde labeling techniques with horseradish peroxidase (HRP) and the fluorescent dyes Diamidino Yellow (DY) and Fast Blue (FB) as substances served to depict the spinal nucleus columns of different muscles and nerves. With the muscle injection technique and HRP as a retrograde tracer, a total of 46 motoneuron pools of the tibialis anterior muscle in 23 rats were labeled, with the alternative technique of an HRP nerve bath after severing the respective nerves in 6 rats marking the nucleus columns of the tibialis anterior muscle (n = 5), extensor digitorum longus muscle (n = 1), peroneus longus muscle (n = 1), extensor digitorum brevis II and III muscles (n = 1), extensor hallucis proprius muscle (n = 1) and the sciatic nerve (n = 2). The fluorescent dyes DY and FB were used for external control of localization and cell count of the motoneuron column after HRP labeling.

Additionally, in individual experiments the stability of these fluorescent dyes in the cell and the quantitative applicability of the data obtained in long-term tests, as well as the compatibility with HRP enzyme histochemistry in terms of a double labeling,

were reviewed. The nucleus columns of the tibialis anterior muscle (n = 8) and the lateral gastrocnemius muscle (n = 2) were retrogradely labeled with fluorescent markers after muscle injection. In combination with HRP, DY was injected into the tibialis anterior muscle or applied onto the severed muscle nerve branches in 2 rats, and the common peroneal nerve was immersed in an HRP solution.

While using HRP as a retrograde marker, the animals were transcardially perfused 45-72 hours after muscle injection or HRP nerve bath and the obtained spinal cord block L2-L6 was morphometrically measured. The 40 µm thick transversal spinal cord sections were enzyme histochemically stained with tetramethylbenzidine as a dye, according to a protocol by Mesulam et al. (Mesulam, 1978; Mesulam et al., 1980) in a modified format. Part of the sections were histologically counter-stained with thionine or neutral red. In the experiments with fluorescent labeling, perfusion took place after 4-9 days, and the likewise 40 µm thick transversal sections were evaluated after fluorescent excitation at 340-380 nm in incident light.

In the center of these experimental studies stand the central changes of the tibialis anterior muscle motoneuron nuclei after microsurgical, autologous nerve graft of a 1 cm long radial nerve segment in the severed, ipsilateral common peroneal nerve in 8 Sprague-Dawley rats. In pentobarbital narcosis, the right common peroneal nerve was severed 5 mm before its entry into the muscle, and the obtained radial nerve segment was epineurially end-to-end coapted with 10-0 Ethilon® suture material under the surgical microscope. After 2, 4, 8 and 10 weeks, HRP was injected into both sides of the tibialis anterior muscle, the animals transcardially perfused 46-61 hours later, and the sections enzyme histochemically stained and evaluated in the light and dark fields.

To reconstruct the cell columns, the spinal cord sections were delineated after HRP enzyme histochemistry via a drawing tube, a two-dimensionally screened coordinate system aligned on the section images with the origin in the central canal and the position of a motoneuron standardized on the lateral and ventral outline of the gray matter. As the segmental localization of the spinal cord block measurement was known after perfusion, the craniocaudal position of a motoneuron could also be given within the spinal cord segment in absolute and relative coordinates. Through this process it was possible to absolutely and relatively give the x, y and z coordinates of the motoneurons and the localization of the nucleus columns, and to reconstruct the nucleus columns from multiple experiments in one mutual representation.

Parameters for evaluation were the cell count of the motoneuron column, cell diameter, diameter distribution in the segment, cell density and morphometric data based on 2D and 3D reconstructions of the nucleus column. Quantitative data was able to be compiled from 48 nucleus columns of the tibialis anterior muscle, including 8 cell columns following radial nerve-common peroneal nerve autograft, the sciatic nerve (n = 2), the common peroneal nerve (n =1), the extensor digitorum brevis II and III muscle (n = 1) and the lateral gastrocnemius muscle (n = 1). Based on strict requirements for section quality, 26 cell columns of the tibialis anterior muscle and 1 cell column of the extensor digitorum brevis II and III muscle were reconstructed in 2D and 3D.

The nucleus column of the tibialis anterior muscle of the rat is localized in the anterior horn of the spinal horn, dorsolateral in lamina IX according to Rexed (Rexed, 1952) from L3 to L5, in projection onto the vertebral column from T13-L1. This area corresponds with column 2 in the cat by Romanes (Romanes, 1951). The cell column has a compact, fusiform appearance and is oriented in a craniocaudal direction in horizontal reconstructions, primarily parallel to the gray matter/white matter border, while it is ventrodorsal in sagittal reconstructions. The cell column has a mean length of 3.13 ± 0.44 mm, while the mean diameter is 0.34 ± 0.06 mm in horizontal reconstructions and 0.37 ± 0.11 mm in sagittal reconstructions. On the spinal cord cross-section, retrograde labeled motoneurons in a mediolateral direction are found in an area of 0.92 ± 0.06 mm to 1.28 ± 0.08 mm (relative: 72.5 ± 2.8% to 98.1 ± 1.2%) and in a dorsoventral direction from 0.05 ± 0.11 mm to –0.34 ± 0.05 mm (relative -7.0 ± 17.4% to 51.6 ± 2.7%).

The average cell count of the nucleus column of the tibialis anterior muscle after HRP application totals 111.7 ± 19.7 (n = 26). Clear differences in the cell count show a dependence on the type of application. After HRP nerve bath, the mean cell count is considerably higher at 148.5 (n = 2) compared to 108.7 ± 15.3 (n =24) after muscle injection. As the percentage of smaller motoneurons, presumably of gamma motoneurons, is higher after HRP nerve bath, an impeded access of the peroxidase into the muscle spindles after muscle injection was deduced (Richmond et al., 1978; McHanwell and Biscoe, 1981b). The motoneuron count after fluorescent labeling is even higher compared to HRP muscle injection at 98.9 ± 10.8 (n = 7). The highest cell density along the cell column lies in the upper third and gradually decreases caudally. All given cell counts are corrected for double counting, and their percentage is at 13.9 ± 4.7%.

Histograms of diameter show a bimodal distribution in 75%, and a trimodal distribution in 50%. Beginning with these distributions, it was assumed that the three size classes are corresponded with different populations of alpha and gamma motoneurons. Smaller alpha motoneurons should innervate slow type S (slow) muscle fibers and larger motoneurons should innervate faster type FF (fatigue resistant) and type FR (fast-fatigable) muscle fibers (Henneman and Olson, 1965; Burke et al., 1973). The limiting diameter of the three size classes was calculated to be 28.4 ± 1.2 µm for the gamma/alpha 1 transition and 36.6 ± 2.3 µm for the alpha 1/alpha 2 transition. Through the impeded entry into the interior of the muscle spindles after HRP muscle injection, the percentage of gamma motoneurons is 22%, but 46% after HRP nerve bath. The percentage of gamma motoneurons of 46% corresponds well with the values given by Peyronnard and Charron (Peyronnard and Charron, 1983a) for the cell count and number of small myelinated nerve fibers after deafferentation of the tibialis anterior muscle. A local clustering of certain size classes of motoneurons along the craniocaudal axis of the cell column was not verifiable. Contrary to the results by Strick et al. (Strick et al., 1976) and Burke et al. (Burke et al., 1977), a higher intensity of HRP labeling for gamma motoneurons versus alpha motoneurons could not be confirmed. If anything, the intracellular density of the HRP dye product was, assessed by a semi-quantitative typing, higher for larger motoneurons.

Two weeks after autologous transplantation of a radial nerve segment into the common peroneal nerve, the cell column of the tibialis anterior muscle consists of individual motoneurons or spatially separated cell clusters. The labeled motoneurons are, in comparison to the internal control side, localized in the medial periphery of the area normally occupied by the cell column. After 4 weeks, the number of reinnervated motor units more than doubled from an average of 4,5% (2 weeks) to 9.7%, and reaches 57.8% of the cell count of the opposite side after 8 and 10 weeks. After 8 weeks, partially after 4 weeks, the nucleus columns once again have a fusiform appearance with a lower cell density in comparison to the control side, and reach to the lateral border of the gray matter. Diameter and maximum expansion of the nucleus columns increase depending on the time, and correspond to the values of the control side after 8 weeks. 3D reconstructions let it be recognized that all nucleus columns of the graft side are caudally offset in comparison to the control side and, with the exception of the test after 10 weeks, are limited to segments L4 and L5. After 10 weeks, the cell column reaches the caudal area of L3 and as the sole nucleus column, extends over 3 segments. The initially high percentage of the medially and caudally localized motoneurons lets a regressive misinnervation by motoneurons, which originally innervated other muscles or muscle groups, be presumed over the course of reinnervation. The analysis of cell density distribution in the regeneration process shows a restitution of the density maximum in the rostral area of the cell column after 8 and 10 weeks, nevertheless without reaching the homogenous distribution of the control side.

A fundamental result of this experimental study lies in the fact that the reinnervation procedures after autologous nerve graft are connected, depending on the time, with a change in the number of motor units and the diameter spectrum of motoneurons. Considering the limiting diameter defined for the three size classes of the alpha 1, alpha 2, and gamma motoneurons for the control side, there appears a considerable reduction of the percentage of gamma motoneurons from a normal 22% to 3% after 2 and 4 weeks. Complementarily, the percentage of alpha neurons is at 97%, with an alpha 2 percentage of 15% after 2 weeks and 49% after 4 weeks. After a regeneration period of 8 and 10 weeks, the gamma motoneurons achieve the values of the control side with a percentage of 24%.

The central effects of a peripheral radial nerve-common peroneal nerve autograft were studied using retrograde labeling techniques, using the example of the tibialis anterior motoneuron pool of the rat. Depending on the point in time and the status of the reinnervation, a reduced number of motoneurons is recruited for a certain kinematic task. Through misinnervation and modification in the diameter spectrum, the cell pool differentiates itself in its structural and functional organization from the original muscle innervating nucleus column. If the task of the motoneuron pool in the controlled application of the innervated muscle consists of the motor unit in the graduated activation of muscular units (Loeb, 1984; Loeb, 1990), and the recruitment of motor units takes place reversely proportional to cell size (Henneman and Mendell, 1981) or according to type (Fleshman et al., 1981; Sypert and Munson, 1981), the failure of a size population leads to disruptions in the recruiting process and to neurological deficits. A connection between the restitution of a useful motor function after peripheral nerve lesion and the

recurring gamma control of intrafusal muscle fibers was conjectured by Thulin (Thulin, 1960).

The model shown here, for evaluation of the success of regeneration following a peripheral nerve lesion using parameters for retrograde labeled cell columns, can also be used to review therapeutic strategies, where for example, there is a need to prove the efficacy of neurotrophic or neurotropic substances on regeneration.

Appendix

Table A.1 Perfusion diagram for test series HRP2 according to Mesulam (1982) in a modified format.

1.	**Washing solution 1:** 200 to 300 ml 0.9% NaCl and 0.4% sodium nitrite in a 0.1 M phosphate buffer pH 7.4 Perfusion time: 2 to 3 minutes
2.	**Fixing solution:** 1000 ml 1.25% glutaraldehyde solution and 1% paraformaldehyde solution in a 0.1 M phosphate buffer pH 7.4 Perfusion time 30 minutes
3.	**Washing solution 2:** 1000 ml 10% saccharose in a 0.1 M phosphate buffer pH 7.4 Perfusion time: 30 minutes
4.	**Sugar solution for preparation of the spinal cord:** 200 ml, composition as per 3
5.	**Buffer interim solution for storage until freezing:** 200 ml 0.1 M phosphate buffer pH 7.4

Table A.2 HRP enzyme histochemistry for the HRP2 test series according to Mesulam (1982) in a modified format.

1.	6 shifts in distilled water (15 s)
2.	Preincubation in solution A: 180 mg sodium nitroprusside (Sigma®, S-0501) in 10 ml 0.2 M acetic acid and 185 ml distilled water and solution B: 10 mg Tetramethylbenzidin (Sigma®, T-2885) in 5 ml absolute alcohol at 19-23° C in the dark
3.	Start of reaction through addition of 5 ml 0.3% H_2O_2, in the first tests from 2-10 ml 0.3% H_2O_2 Further incubation at 19-23° C in the dark
4.	6 shifts in 0.01 M acetate buffer pH 3.3 chilled at 0-4° C with dry ice (30 seconds)
5.	Air-drying sections 4 hours to 15 days
6.	Distilled water (10 s)
7.	Ethanol 70%, 95%, 2 X 100% (10 s respectively)
8.	Xylol, 2 X (2 minutes respectively)

Table A.3 Neutral red counterstaining (Burck, 1982; Mesulam, 1982)

1.	1% neutral red (Merck®) in a 0.1 M acetate buffer pH 4.8	2.5-3.0 minutes
2.	Dist. water	10 seconds
3.	Ethanol 70%	10 seconds
4.	Ethanol 95 %	10 seconds
5.	Ethanol 100%, 2 X	10 seconds
6.	Xylol, 2 X	2.0 minutes

Table A.4 Thionine counterstain (Adams, 1980)

1.	Methyl salicylate	3.0 minutes
2.	Ethanol 100%	10 seconds
3.	Ethanol 95%	10 seconds
4.	Ethanol 70%	10 seconds
5.	0.1 M acetate buffer pH 3.7	1.0 minute
6.	0.1% thionine (Sigma®) in a 0.1 M acetate buffer pH 3.7	30 seconds
7.	0.1 M acetate buffer pH 3.7	1.0 minute
8.	Ethanol 70%	30 seconds
9.	Ethanol 95 %	30 seconds
10.	Ethanol 100%, 2 X	30 seconds
11.	Methyl salicylate	30 seconds
12.	Xylol	2.0 minutes

Table A.5 Adjustment of color intensity of the H.E. counterstain (Romeis, 1968). The aim is a dull nucleus-plasma staining which allows a morphometric analysis in the light field without covering the fluorescent marking.

Test	**1**	**2**	**3**	**4**	**5**	**6**
Slide	**1;2**	**3**	**4**	**5**	**6**	**7**
Coating	**-**	**+**	**+**	**+**	**+**	**+**
Temperature (°C)	**7**	**7**	**7**	**7**	**7**	**7**
1. Hemalaun according to Mayer 0.1% (min)	1	1	1	1	1.5	1.75
2. Dist. water (min)	1	2	2	2	2	2
3. Dist. water (min)	1	4	4	4	2	2
4. Dist. water (min)	1	4	4	-	-	-
5. Eosin 0.1% (min)	2	5	2	1	1	1
6. Dist. water (min)	1	1	1	1	1	1
7. Alcohol 80% (min)	1	3	3	3	3	3
8. Alcohol abs. (min)	2	3	3	3	-	3
9. Xylol (min)	1.5	3	3	3	3	3
Evaluation:	Overstained; section loss	Eosin too strong	Eosin still too strong	Hemalaun too weak	White matter too dark	Still too much eosin; best staining

Table A.6 Combination of fluorescent labeling (DY and FB) and histological counterstaining using hemalaun according to Mayer (Burck, 1982).

Test	**1**	**2**	**3**
Slide	**2**	**3**	**4;16**
Coating	**+**	**+**	**+**
Temperature (°C)	**6**	**-3**	**-3**
1. Hemalaun according to Mayer 0.1% (min)	1.75	2	2
2. Dist. water (min)	2	-	30 seconds
3. Alcohol abs. (min)	-	1	1
4. Xylol (min)	-	1	1
Evaluation:	Background yellow-greenish; fluorescence overlaid	Background yellow-greenish; fluorescence overlaid	Background yellow-greenish; fluorescence overlaid. Cell borders unclear

Table A.7 Adjustment of the color intensity of the Nissl stain in sections 1 to 9 by variation of the incubation parameters (Romeis, 1968). Sections 10 to 12: The aim is an equivalent representation of the nucleus-plasma staining in the light field and of the fluorescence marking in fluorescent microscopy. Sections from fluorescence test R711 with FB marking of the nucleus column of the tibialis anterior muscle and DY marking of the nucleus column of the lateral gastrocnemius muscle were used. Sketches were initially prepared of the fluorescing cells in lamina IX without covering. After Nissl staining, the fluorescent marked motoneurons were attempted to be located once again by means of the sketches. The residual intensity of the fluorescence was evaluated, as well as the depiction of the cell boundaries, the autofluorescence of the background through the histological counterstaining and diffusion of the fluorescent dye into other, previously unmarked neurons.

Test	**1**	**2**	**3**	**4**	**5**	**6**	**7**	**8**	**9**	**10**	**11**	**12**
Slide	**8**	**9**	**10**	**11**	**12**	**13**	**14**	**15**	**16**	**15**	**1**	**13**
Coating	**+**	**+**	**+**	**+**	**+**	**+**	**+**	**+**	**+**	**+**	**+**	**+**
Temperature (°C)	**8**	**8**	**8**	**8**	**8**	**8**	**8**	**8**	**8**	**10**	**4**	**0**
1a. Cresyl violet 1% (min)	1	30 seconds	30 seconds	15 seconds	30 seconds	13	-	-	-	-	-	-
1b. Cresyl violet 0.5% (min)	-	-	-	-	-	-	10	5	15	15	13	13
2. Dist. water (min)	-	2	4	5.5	3	3	3	3	3	3	2	3
3. Alcohol 70% (min)	-	-	2	-	-	-	-	-	-	-	-	-
4a. Alcohol 96% (min)	1	1	2	3	3	3	3	3	-	-	-	-
4b. Alcohol 96% and 4 drops glacial acetic acid (min)	-	-	-	-	-	-	-	-	3	3	2	3
4c. Alcohol 96% (min)	-	-	-	-	-	-	-	-	3	3	2	3
4d. Isopropyl alcohol 100% (min)	-	-	-	-	-	-	-	-	2	2	1	2
5. Xylol (min)	-	-	-	-	-	2	3	3	2	2	1	2
Evaluation:	Section loss; overstaining	Section loss; overstaining	Overstaining	Section loss	Section loss	Overstaining	Overstaining	Section loss; unstained areas	FB, especially DY, overlaid, cell borders unclear, background lightly red		Not as well stained as 1	Background light red; not DY, FB more discernible, areas without Nissl staining

Table A.8 Combination of fluorescence labeling (DY and FB) and counterstaining using Cresyl violet (Burck, 1982).

Test	**1**	**2**
Slide	**5**	**7**
Coating	**+**	**+**
Temperature (°C)	**3**	**3**
1. Cresyl violet 0.5% (min)	12	12
2a. Dist. water (min)	3	1
2b. Dist. water (min)	-	1
3. Alcohol 96% and 4 drops glacial acetic acid (min)	3	3
4. Alcohol 96% (min)	3	3
5. Xylol (min)	2	2
Evaluation:	Weak cell staining; intense light red background. Fluorescence overlaid	Cell staining even weaker; intense light red background. Fluorescence overlaid

Table A.9 Combination of fluorescence labeling (DY and FB) with rapid Nissl counterstaining (Burck, 1982).

Test	**1**	**2**	**3**
Slide	**33**	**6**	**8**
Coating	**+**	**+**	**+**
Temperature (°C)	**8**	**8**	**8**
1. Cresyl violet 0.5% in a 0.1 M Ac buffer pH 3.9 (min)	10	10	10
2. Ac buffer pH 3.9 (min)	1	2	2
3. Alcohol 100% (min)	2	3	3
4. Xylol (s)	10 seconds	20 seconds	20 seconds
Evaluation:	Weak cell staining; light red background. Fluorescence overlaid	DY and FB; weak cell staining	Best stain; light red background still overlays

Table A.10 Length of the vertebral bodies (mm).

Rat	Test	Weight (g)	T11	T12	T13	L1	L2	L3	L4	L5	L6
R764	HRP2P	220		5.4	5.0	5.3	6.6	7.0	7.1	7.1	
R765	HRP2P	206			5.5	5.6	6.1	6.6	6.6	6.8	
R766	HRP2P	215			5.3	5.6	6.7	6.7	6.7	6.7	6.7
R807	HRP2P	250		4.5	4.8	5.9	6.3	6.9	7.1	6.9	6.1
R817	HRP2P	260			4.9	6.0	6.0	6.8	7.2	6.6	6.8
R948	HRP2C1	300		3.7	6.5	6.9	6.6	7.1	7.4	7.4	7.4
R963	HRP2C1	275			5.1	5.8	6.6	6.9	7.0	7.1	6.8
R1078	HRP2C2	400		4.2	6.2	6.7	8.0	8.0	8.3	8.4	8.3
R1079	HRP2C2	361			5.2	6.5	7.3	7.8	7.8	7.8	7.8
R823	HRP2G	220			5.4	6.2	6.7	7.4	7.2	6.7	6.5
R834	HRP2G	360			5.9	6.3	7.4	7.8	7.4	7.8	7.8
R835	HRP2G	350			5.5	6.4	6.9	7.8	7.8	7.8	7.8
R809	HRP2G	420			5.7	6.7	7.7	8.3	8.4	7.8	7.9
R827	HRP2G	370			6.0	7.0	7.5	8.1	7.9	7.9	7.3
R832	HRP2G	390			5.7	6.7	7.2	7.9	8.1	7.7	7.8
R824	HRP2G	480		4.4	5.8	6.8	8.0	8.6	8.5	8.5	8.5
R831	HRP2G	450		4.0	6.3	6.9	8.5	8.9	8.8	8.9	8.5
R822	HRP2G	470		4.2	5.7	6.7	7.4	8.2	8.2	8.1	8.2
R818	HRP3P	290		3.4	4.9	6.1	6.8	7.0	7.2	7.7	6.8
R1080	HRP4P	235		3.6	4.9	6.1	6.9	7.2	7.2	7.6	7.6
R1095	HRP5C	477			6.3	7.2	8.1	8.1	8.7	8.9	7.8
R1106	HRP5C	480		4.3	6.8	7.3	8.3	8.9	8.7	8.9	8.9
R1107	HRP5C	438		6.0	6.8	7.5	8.4	8.8	8.8	8.5	8.7
R1115	HRP5C	456	4.7	5.7	6.3	7.2	8.4	8.5	9.2	9.2	8.7
R1149	HRP5C	553		5.3	6.3	7.5	8.5	8.9	8.9	9.0	9.0
R711	F1P1	340	4.9	4.9	5.4	6.4	6.9	6.9	6.9	6.9	6.9
R808	F1P2	390		5.3	6.4	7.5	8.1	8.5	8.3	8.6	7.2
R1113	HRPF1P	476		4.3	6.4	7.2	8.2	8.8	8.8	9.1	8.6
R1156	HRPF2P	478		5.1	6.3	7.0	8.3	8.9	8.9	9.2	8.6
n			2	17	29	29	29	29	29	29	27
M			4.8	4.6	5.8	6.6	7.4	7.8	7.9	7.9	7.7
s			0.1	0.8	0.6	0.6	0.8	0.8	0.8	0.8	0.8

Table A.11 Segment length: external measurements (mm).

Rat	Test	Weight (g)	L1		L2		L3		L4		L5		L6	
			left	right	left	right	left	right	left	right	left	right	left	right
R743	HRP1P	350				2.9		2.4		1.9		1.4		1.9
R731	HRP1G	380		2.9		3.9		2.4		2.9		2.4		2.4
R732	HRP1G	420		3.3		3.9		2.6		2.5		3.1		3.2
R733	HRP1G	380				3.4		2.7		2.8		2.4		1.2
R764	HRP2P	220		3.1		2.5		2.8		2.4		2.6		1.8
R765	HRP2P	206		3.1		3.6		2.8		2.2		2.2		1.2
R766	HRP2P	215		2.3		3.4		2.4		2.5		2.5		1.9
R807	HRP2P	250				2.3		2.8		2.2		3.0		2.2
R817	HRP2P	260				3.7		3.4		2.4		2.3		2.9
R948	HRP2C1	300		3.4		3.2		3.4		2.0		2.1		2.7
R963	HRP2C1	275		3.3		2.9		3.1		2.2		2.1		1.8
R1074	HRP2C2	294	2.2	2.2	2.4	3.0	2.9	2.3	2.5	2.9	2.0	2.2	2.4	2.2
R1075	HRP2C2	312	3.3	3.4	3.6	3.7	3.2	3.2	2.7	2.8	2.7	3.0	2.5	2.2
R1078	HRP2C2	400	3.9	3.8	4.1	4.0	2.9	3.3	2.9	3.3	2.0	2.2	2.6	2.3
R1079	HRP2C2	361			3.6	3.1	3.2	3.1	2.3	2.3	2.7	2.6	2.3	2.4
R823	HRP2G	220		3.2		3.2		2.8		1.9		2.5		2.4
R834	HRP2G	360		3.1		3.3		2.4		2.8		1.7		2.3
R835	HRP2G	350		2.2		3.7		3.2		2.0		2.7		2.3
R809	HRP2G	420		4.7		3.6		2.8		3.0		2.2		2.4
R827	HRP2G	370				3.7		2.8		2.8		2.3		2.7
R832	HRP2G	390		2.9		3.3		3.1		2.9		2.0		2.0
R824	HRP2G	480		4.0		3.4		2.6		3.2		2.5		2.2
R831	HRP2G	450		3.1		3.3		2.3		3.5		2.0		2.1
R822	HRP2G	470		4.7		2.6		3.0		2.9		2.9		2.0
R818	HRP3P	290		3.3		3.7		3.6		2.8		1.6		2.6
R1080	HRP4P	235	3.4	3.4	3.2	3.3	2.9	3.1	2.9	2.9	2.6	2.2	2.6	2.9
R1095	HRP5C	477	4.5	4.4	4.0	3.9	3.8	3.9	3.2	3.2	3.3	3.6	2.2	1.9
R1106	HRP5C	480			3.8	3.8	2.8	3.1	3.0	3.0	2.3	2.4	2.6	2.8
R1107	HRP5C	438	3.7	3.8	3.3	2.9	3.0	3.0	2.9	3.0	2.6	2.8	2.0	2.2
R1115	HRP5C	456	3.6	3.9	4.4	3.8	3.2	3.3	1.9	2.9	2.3	2.2	2.7	2.7
R1149	HRP5C	553	4.3	4.4	3.5	3.4	2.5	2.5	3.0	3.4	3.1	3.1	1.9	2.7
R711	F1P1	340		4.4		3.4		2.9		2.9		2.4		1.9
R808	F1P2	390				2.7		2.9		3.5		2.2		1.9
R1113	HRPF1P	476	3.8	3.7	3.5	3.4	3.3	3.5	2.5	2.9	3.2	2.5	2.0	2.7
R1156	HRPF2P	478	3.3	4.1	4.1	4.1	3.0	2.2	3.2	2.9	2.8	2.9	2.6	2.6
n			10	27	12	35	12	35	12	35	12	35	12	35
M			3.6	3.5	3.6	3.4	3.1	2.9	2.8	2.7	2.6	2.4	2.4	2.3
s			0.6	0.7	0.5	0.4	0.3	0.4	0.4	0.4	0.4	0.5	0.3	0.4

Table A.12 Segment length: internal measurements (mm).

Rat	Test	Weight (g)	L2		L3		L4		L5		L6	
			left	right	left	right	left	right	left	right	left	right
R743	HRP1P	350				1.96		1.68				
R731	HRP1G	380		3.80		2.96		2.32				
R732	HRP1G	420		3.00		2.40		2.88				
R733	HRP1G	380		3.40		2.80		2.52				
R765	HRP2P	206		3.40		2.72		1.84		1.96		
R766	HRP2P	215		3.24		2.20		2.68		2.16		
R817	HRP2P	260		3.28		3.16		2.48		2.28		
R948	HRP2C1	300		3.16		3.24		1.56		1.80		3.04
R1074	HRP2C2	294	2.24	2.80	2.72	2.24	2.32	2.80	1.96	1.84	1.80	1.92
R1075	HRP2C2	312	3.12	3.32	3.08	2.96	2.52	2.56	2.36	2.40		
R1078	HRP2C2	400	3.92	3.72	2.76	3.12	2.76	3.20	1.88	1.88	2.32	2.20
R1079	HRP2C2	361	3.48	3.48	2.92	2.88	2.24	2.36	2.48	2.40	2.00	2.08
R823	HRP2G	220		2.88		2.84		2.04		2.44		2.50
R834	HRP2G	360		3.32		2.24		2.84		1.68		2.30
R835	HRP2G	350		3.20		3.12		1.92		2.80		
R809	HRP2G	420		3.52		2.60		2.72		1.96		
R827	HRP2G	370		3.72		2.88		2.88		2.48		2.10
R824	HRP2G	480				2.40		2.96		2.36		
R831	HRP2G	450				2.12		3.48		2.12		2.24
R822	HRP2G	470				3.28		3.00		2.88		2.12
R818	HRP3P	290		3.68		3.56		2.68		1.56		2.40
R1080	HRP4P	235	2.96	2.96	2.84	2.88	2.72	2.68	2.48	2.04		2.70
R1095	HRP5C	477	3.68	3.48	2.52	2.60	2.72	2.84	2.72	2.88	1.68	1.72
R1106	HRP5C	480	3.60	3.60	2.68	3.16	2.96	2.80	2.16	2.28	2.20	2.88
R1107	HRP5C	438			2.80	2.76	2.76	2.96	2.32	2.32	2.04	2.00
R1115	HRP5C	456	4.36	3.64	2.96	3.04	2.08	2.80	2.20	2.20		
R1149	HRP5C	553	3.44	3.28	2.56	2.48	3.00	3.52	3.12	2.96	2.40	2.48
R808	F1P2	390				3.04		3.40				
R1113	HRPF1P	476	3.04	3.04	3.24	3.24	2.32	2.80	3.20	2.48	1.88	2.32
R1156	HRPF2P	478	3.96	4.04	2.76	2.36	3.00	2.84	2.68	2.60	2.20	2.20
n			11	24	12	30	12	30	12	25	9	16
M			3.44	3.37	2.82	2.77	2.62	2.67	2.46	2.27	2.06	2.28
s			0.58	0.31	0.21	0.40	0.31	0.49	0.41	0.38	0.24	0.33

Table A.13 Cross-sectional diameter of the segments: external measurements (mm).

Rat	Test	Weight (g)	T12	T13	L1	L2	L3	L4	L5	L6
R731	HRP1G	380			2.9	3.3	3.3	3.1	2.4	
R732	HRP1G	420			2.8	3.1	3.4	2.9	2.4	
R733	HRP1G	380			2.7	2.9	3	2.9	2.2	
R764	HRP2P	220			3.2	3.5	3.3	3.5	2.8	2.3
R765	HRP2P	206			3.1	3.2	3.2	3	2.5	
R766	HRP2P	215			3.2	3.3	3.6	3.5	2.7	2.3
R807	HRP2P	250			3.2	3.5	3.7	3.7	3	2.4
R817	HRP2P	260			2.8	3.1	3.4	3.1	2.7	1.8
R948	HRP2C1	300			2.9	2.9	3.2	3.1	2.3	1.9
R963	HRP2C1	275			3	3.2	3.4	3	2.6	3.2
R1074	HRP2C2	294			3.3	3.3	3.6	3.4	2.5	2.4
R1075	HRP2C2	312			3.1	3.1	3.5	3.4	2.8	2.3
R1078	HRP2C2	400			3.4	3.7	3.7	3.5	2.8	2.4
R1079	HRP2C2	361			3.2	3.4	3.4	3.7	3	2.4
R823	HRP2G	220		2.8	2.7	3.3	3.2	2.8	1.9	1.7
R834	HRP2G	360		3	3.2	3.4	3.4	2.9	2.5	2.1
R835	HRP2G	350		3.1	3.2	3.5	3.6	3.6	2.8	2.1
R809	HRP2G	420		3.2	3.4	3.8	3.8	3.4	2.9	2.4
R827	HRP2G	370			3.2	3.7	3.6	3.2	2.2	1.9
R832	HRP2G	390		3.1	3.3	3.4	3.6	3.5	2.8	2.4
R824	HRP2G	480		2.9	2.8	3.1	3.3	3.2	2.7	2.1
R831	HRP2G	450		3.2	3.1	3.6	3.8	3.4	2.8	2.3
R822	HRP2G	470		3	3.3	3.3	3.3	3.1	2.5	1.9
R818	HRP3P	290		2.7	2.8	3.3	3.6	3.1	2.5	2
R1080	HRP4P	235		2.8	3.3	3.3	3.2	3.4	2.6	2.1
R1095	HRP5C	477		3.2	3.3	3.5	3.7	3.5	2.6	2.4
R1106	HRP5C	480			3.2	3.8	3.6	3.5	2.9	2.5
R1107	HRP5C	438		3.1	3.4	3.8	3.7	3.5	2.8	2.3
R1115	HRP5C	456	2.7	2.7	3.1	3.3	3.7	3.5	2.9	2.3
R711	F1P1	340				2.9	3.4	3.4	2.9	2.4
R808	F1P2	390			3.4	3.6	3.6	2.9	2.5	2.2
R1113	HRPF1P	476		3	3.1	3.5	3.4	3.4	2.7	2.2
R1156	HRPF2P	478	3.2	3.3	3.5	3.9	3.9	3.7	3.1	2.4
n			2	15	32	33	33	33	33	29
M			3.0	3.0	3.1	3.4	3.5	3.3	2.6	2.2
s			0.4	0.2	0.2	0.3	0.2	0.3	0.3	0.3

Table A.14 Length of the anterior roots from entry in the spinal cord as far as the spinal ganglia.

Rat	Test	Weight (g)	L1		L2		L3		L4		L5		L6	
			left	right	left	right	left	right	left	right	left	right	left	right
R1095	HRP5	477			18	18	22	22	26	26	30	31	35	36
R1106	HRP5	480	10	9	19	17	26	24	30	29	34	33	39	40
R1107	HRP5	438	17	19	25	21	29	27	35	32	38	38	44	44
R1115	HRP5	456			19	19	23	21	25	27	31	32	36	36
R1149	HRP5	552	13	14	18	18	24	24	29	28	34	33	39	39
R1113	HRPF1	485	14	13	18	17	23	25	30	27	36	35	41	42
n			4	4	6	6	6	6	6	6	6	6	6	6
M			13.5	13.8	19.5	18.3	24.5	23.8	29.2	28.2	33.8	33.7	39.0	39.5
s			2.9	4.1	2.7	1.5	2.6	2.1	3.5	2.1	3.0	2.5	3.3	3.2

Table A.15 Cross-sectional diameter of the segments: internal measurements (mm).

Rat	Test	Weight (g)	White matter			Gray matter		
			L3	L4	L5	L3	L4	L5
R766	HRP2P	215	3.52	3.32	3.08	2.58	2.66	2.48
R1074	HRP2C2	294	3.00	2.90		2.28	2.29	
R823	HRP2G	220	3.22	3.13	2.90	2.47	2.47	2.29
R834	HRP2G	360	3.31	3.21	2.62	2.50	2.51	2.11
R835	HRP2G	350	3.43	3.45	3.32	2.66	2.75	2.65
R809	HRP2G	420	3.60	3.41	3.23	2.65	2.62	2.63
R827	HRP2G	370	3.48	3.28	2.78	2.77	2.68	2.32
R824	HRP2G	480	3.21	3.19	2.94	2.33	2.45	2.27
R831	HRP2G	450	3.56	3.56	3.21	2.65	2.71	2.48
R822	HRP2G	470	3.24	3.17	2.99	2.28	2.36	2.21
R1095	HRP5C	477		3.50	3.39		2.66	2.60
R1107	HRP5C	438	3.50	3.27		2.71	2.67	
R808	F1P2	390	3.40	3.19		2.54	2.61	
n			12	13	9	12	13	9
M			3.37	3.28	3.05	2.53	2.57	2.40
s			0.18	0.18	0.24	0.17	0.14	0.19

Table A.16 Longitudinal diameter of the segments: internal measurements (mm).

Rat	Test	Weight (g)	White matter			Gray matter		
			L3	L4	L5	L3	L4	L5
R766	HRP2P	215	2.37	2.22	2.14	1.64	1.67	1.61
R1074	HRP2C2	294	2.10	2.05		1.58	1.56	
R823	HRP2G	220	2.36	2.52	2.49	1.76	1.84	1.82
R834	HRP2G	360	2.30	2.30	1.92	1.68	1.73	1.43
R835	HRP2G	350	2.28	2.40	2.42	1.72	1.80	1.85
R809	HRP2G	420	2.54	2.53	2.43	1.84	1.86	1.82
R827	HRP2G	370	2.24	2.23	2.01	1.66	1.66	1.52
R824	HRP2G	480	2.09	2.15	2.04	1.47	1.49	1.41
R831	HRP2G	450	2.22	2.26	2.21	1.61	1.66	1.69
R822	HRP2G	470	2.21	2.29	2.18	1.55	1.59	1.56
R1095	HRP5C	477		2.48	2.47		1.78	1.78
R1107	HRP5C	438	2.52	2.28		1.69	1.70	
R808	F1P2	390	2.29	2.25		1.61	1.61	
n			12	13	10	12	13	10
M			2.29	2.30	2.23	1.65	1.69	1.65
s			0.14	0.14	0.21	0.10	0.11	0.17

References

Abercrombie M (1946) Estimation of nuclear population from microtome sections. Anat Rec 94:239-247.

Adams JC (1977) Technical considerations on the use of horseradish peroxidase as a neuronal marker. Neuroscience 2:141-145.

Adams JC (1980) Stabilizing and rapid thionin staining of TMB-based HRP reaction product. Neurosci Lett 17:7-9.

Aebischer P, Guenard V, Brace S (1989) Peripheral nerve regeneration through blind-ended semipermeable guidance channels: effect of the molecular weight cutoff. J Neurosci 9:3590-3595.

Aebischer P, Valentini RF, Winn SR, Galletti PM (1988) The use of a semi-permeable tube as a guidance channel for a transected rabbit optic nerve. Prog Brain Res 78:599-603.

Aguayo AJ, Bunge RP, Duncan PD, Wood PM, Bray GM (1979) Rat Schwann cells cultured in vitro can ensheath axons regenerating in mouse nerves. Neurology 29:589.

Albert E (1885) Einige Operationen am Nerven. Wien Med Presse 26:1285-1288.

Aldskogius H, Barron KD, Regal R (1980) Axon reaction in dorsal motor vagal and hypoglossal neurons of the adult rat. Light microscopy and RNA-cytochemistry. J Comp Neurol 193:165-177.

Aldskogius H, Arvidsson J, Kinnman E (1983) Movement of horseradish peroxidase after its entry into intact and damaged peripheral nerve axons. Exp Neurol 79:862-866.

Anderson PN, Turmaine M (1986) Peripheral nerve regeneration through grafts of living and freeze-dried CNS tissue. Neuropathol Appl Neurobiol 12:389-399.

Anderson PN, Nadim W, Turmaine M (1991) Schwann cell migration through freeze-killed peripheral nerve grafts without accompanying axons. Acta Neuropathol (Berl) 82:193-199.

Ansselin AD, Pollard JD (1990) Immunopathological factors in peripheral nerve allograft rejection: quantification of lymphocyte invasion and major histocompatibility complex expression. J Neurol Sci 96:75-88.

Archibald SJ, Krarup C, Shefner J, Li ST, Madison RD (1991) A collagen-based nerve guide conduit for peripheral nerve repair: an electrophysiological study of nerve regeneration in rodents and nonhuman primates. J Comp Neurol 306:685-696.

Arvidsson J (1986) Transganglionic degeneration in vibrissae innervating primary sensory neurons of the rat: a light and electron microscopic study. J Comp Neurol 249:392-403.

Balice-Gordon RJ, Thompson WJ (1988) The organization and development of compartmentalized innervation in rat extensor digitorum longus muscle. The Journal of physiology 398:211-231.

Ballance C, Duel AB (1932) The operative treatment of facial palsy. Arch Otolaryngol 15:1-70.

Ballin RH, Thomas PK (1969) Changes at the nodes of ranvier during wallerian degeneration: an electron microscope study. Acta Neuropathol (Berl) 14:237-249.

Balthasar K (1952) [Morphology of the spinal tibialis-and peroneus nuclei in the cat: topography, architecture, course of axons and dendrites of the motoric neurons and the intermediate neurons in the segments L6-S2.]. Arch Psychiatr Nervenkr Z Gesamte Neurol Psychiatr 188:345-378.

Barnes R, Bacsich P, Wyburn GM, Kerr AS (1946) A study of the fate of nerve homografts in man. Br J Surg 34:34-41.
Bassett CA, Campbell JB, Husby J (1959) Peripheral nerve and spinal cord regenertion: factors leading to success of a tubulation technique employing millipore. Exp Neurol 1:386-406.
Baulac M, Meininger V (1979) [Motoneural organisation of the anterior horn with respect to the peripheral nerves in the rat (as studied by the method of retrograde transport of horseradish peroxidase)(author's transl)]. Rev Neurol (Paris) 135:789-802.
Baulac M, Meininger V (1981) [Organization of pectoral muscle motor neurons in the rat. Contribution to the study of the axillary arch (Achselbogen)]. Acta Anat (Basel) 109:209-217.
Bentivoglio M, Kuypers HG, Catsman-Berrevoets CE (1980) Retrograde neuronal labeling by means of Bisbenzimide and Nuclear Yellow (Hoechst S 769121). Measures to prevent diffusion of the tracers out of retrogradely labeled neurons. Neurosci Lett 18:19-24.
Beuche W, Friede RL (1984) The role of non-resident cells in Wallerian degeneration. J Neurocytol 13:767-796.
Bielschowsky M, Unger E (1917) Die Überbrückung großer Nervenlücken. J Psych Neurol 22:267-318.
Biscoe TJ, McHanwell S (1979) Localization of motoneurones supplying hind limb muscles in the mouse [proceedings]. The Journal of physiology 296:37P.
Blinzinger K, Kreutzberg G (1968) Displacement of synaptic terminals from regenerating motoneurons by microglial cells. Z Zellforsch Mikrosk Anat 85:145-157.
Böhler J (1962) Nervennaht und homoioplastische Nerventransplantation mit Millipore-Umscheidung. Langenbecks Arch Chir 301:900-905.
Bora FW, Jr. (1967) Peripheral nerve repair in cats. The fascicular stitch. J Bone Joint Surg Am 49:659-666.
Bowe CM, Evans NH, Vlacha V (1992) Progressive morphological abnormalities observed in rat spinal motor neurons at extended intervals after axonal regeneration. J Comp Neurol 321:576-590.
Boyd I, Davey M (1966) The composition of peripheral nerves. In: Control and innervation of skeletal muscle (Andrew B, ed), pp 35-47. Edinburgh: Churchill Livingstone.
Brandstater ME, Lambert EH (1973) Motor unit anatomy. Type and spatial arrangement of muscle fibers. In: New Developments in Electromyography and Clinical Neurophysiology (Desmedt JE, ed), pp 14-22. Basel: Karger.
Bratton BR, Kline DG, Coleman W, Hudson AR (1979) Experimental interfascicular nerve grafting. J Neurosurg 51:323-332.
Braun RM (1966) Comparative studies of neurorrhaphy and sutureless peripheral nerve repair. Surg Gynecol Obstet 122:15-18.
Brichta AM, Grant G (1985) Cytoarchitectural organization of the spinal cord. In: Hindlimb and spinal cord. (Paxinos G, ed), pp 293-301. Orlando: Academic Press.
Brinkman C, Porter R, Norman J (1983) Plasticity of motor behavior in monkeys with crossed forelimb nerves. Science 220:438-440.
Broadwell RD, Brightman MW (1976) Entry of peroxidase into neurons of the central and peripheral nervous systems from extracerebral and cerebral blood. J Comp Neurol 166:257-283.
Brooke MH, Kaiser KK (1970) Muscle fiber types: how many and what kind? Arch Neurol 23:369-379.
Brooks D (1955) The place of nerve-grafting in orthopaedic surgery. The Journal of bone and joint surgery 37-A:299-305; passim.
Brown DR, Everett AW (1990) Compartmental and topographical specificity of reinnervation of the glutaeus muscle in the adult toad (Bufo marinus). J Comp Neurol 292:363-372.
Brown DR, Everett AW (1991) Position- and fibre type-dependent selectivity by regenerating motor axons in reformation of the topographical projection to the glutaeus muscle in the adult toad (Bufo marinus). J Comp Neurol 309:495-506.
Brown MC, Perry VH, Lunn ER, Gordon S, Heumann R (1991) Macrophage dependence of peripheral sensory nerve regeneration: possible involvement of nerve growth factor. Neuron 6:359-370.
Brushart TM (1988) Preferential reinnervation of motor nerves by regenerating motor axons. J Neurosci 8:1026-1031.
Brushart TM (1989) Preferential motor reinnervation: Pathway regulation. Soc Neurosc Abstr 15:333.
Brushart TM (1991) Central course of digital axons within the median nerve of Macaca mulatta. J Comp Neurol 311:197-209.

Brushart TM (2011) Nerve Repair: Oxford University Press, Inc.
Brushart TM, Mesulam MM (1980) Alteration in connections between muscle and anterior horn motoneurons after peripheral nerve repair. Science 208:603-605.
Brushart TM, Seiler WA (1987) Selective reinnervation of distal motor stumps by peripheral motor axons. Exp Neurol 97:289-300.
Brushart TM, Henry EW, Mesulam MM (1981) Reorganization of muscle afferent projections accompanies peripheral nerve regeneration. Neuroscience 6:2053-2061.
Brushart TM, Tarlov EC, Mesulam MM (1983) Specificity of muscle reinnervation after epineurial and individual fascicular suture of the rat sciatic nerve. J Hand Surg [Am] 8:248-253.
Bryan RN, Trevino DL, Willis WD (1972) Evidence for a common location of alpha and gamma motoneurons. Brain Res 38:193-196.
Bryan RN, Trevino DL, Coulter JD, Willis WD (1973) Location and somatotopic organization of the cells of origin of the spino-cervical tract. Exp Brain Res 17:177-189.
Bunge MB, Bunge RP, Carey DJ, Cornbrooks CJ, Eldrige CF, Williams AK, Wood PM (1983) Axonal and non-axonal influences on Schwann cell development. In: Developing and regenerating nervous system (Coates PW, Markwald RR, Kenny AD, eds). New York.
Bunnell S (1927) Surgery of the nerves of the hand. Surg Gynecol Obstet 44:145-152.
Burck H-C (1982) Histologische Technik. Stuttgart, New York: Georg Thieme Verlag.
Burke RE (1981) Individual system control. Hospital Engineering 35:18-32.
Burke RE, Tsairis P (1973) Anatomy and innervation ratios in motor units of cat gastrocnemius. J Physiol 234:749-765.
Burke RE, Rymer WZ (1976) Relative strength of synaptic input from short-latency pathways to motor units of defined type in cat medial gastrocnemius. J Neurophysiol 39:447-458.
Burke RE, Rudomin P, Zajac FE, 3rd (1970) Catch property in single mammalian motor units. Science 168:122-124.
Burke RE, Levine DN, Tsairis P, Zajac FE, 3rd (1973) Physiological types and histochemical profiles in motor units of the cat gastrocnemius. J Physiol 234:723-748.
Burke RE, Levine DN, Salcman M, Tsairis P (1974) Motor units in cat soleus muscle: physiological, histochemical and morphological characteristics. J Physiol 238:503-514.
Burke RE, Strick PL, Kanda K, Kim CC, Walmsley B (1977) Anatomy of medial gastrocnemius and soleus motor nuclei in cat spinal cord. J Neurophysiol 40:667-680.
Cairns H, Young JZ (1940) Surgical and mechanical treatment of peripheral nerves. Lancet 236:123-125.
Cajal SR (1928) Degeneration and regeneration of the nervous system. Oxford: Oxford University Press.
Cammermeyer J (1968) Species differences in the initial retrograde reaction of motor neurons. J Neuropathol Exp Neurol 27:114-115.
Campa JF, Engel WK (1971) Histochemical and functional correlations in anterior horn neurons of the cat spinal cord. Science 171:198-199.
Capra NF, Wax TD (1989) Distribution and central projections of primary afferent neurons that innervate the masseter muscle and mandibular periodontium: a double-label study. J Comp Neurol 279:341-352.
Causey G, Stratmann CJ (1953) The spread of failure of conduction in degenerating mammalian nerve. J Physiol 121:215-223.
Choi JY, Hoover JE (1996) The organization of acromiodeltoid and spinodeltoid motor nuclei in rat spinal cord. Brain Res 738:146-149.
Clarke JL (1850) Researches into the structure of the spinal cord. Philos Trans R Soc Lond B Biol Sci 141:607-621.
Clarke JL (1858) Further researches on the grey substance of the spinal cord. Philos Trans R Soc Lond B Biol Sci 149:437-467.
Conde F (1987) Further studies on the use of the fluorescent tracers fast blue and diamidino yellow: effective uptake area and cellular storage sites. J Neurosci Methods 21:31-43.
Conn HJ (1969) H.J. Conn´s Biological Stains. Baltimore: Williams & Wilkings Comp.
Council MR (1920) The diagnosis and treatment of peripheral nerve injuries. In. London: Her Majesty's Stationery Office.

Cowan WM (1970) Anterograde and retrograde transneuronal degeneration in the central and peripheral nervous system. In: Contemporary research methods in neuroanatomy (Nauta W, Ebbeson S, eds), p 217. New York: Springer.
Crockett DP, Harris SL, Egger MD (1987) Plantar motoneuron columns in the rat. J Comp Neurol 265:109-118.
Cruce WL (1974) The anatomical organization of hindlimb motoneurons in the lumbar spinal cord of the frog, Rana catesbiana. J Comp Neurol 153:59-76.
Cullheim S, Kellerth JO (1976) Combined light and electron microscopic tracing of neurons, including axons and synaptic terminals, after intracellular injection of Horseradish Peroxidase. Neurosci Lett 2:307-313.
Cullheim S, Ulfhake B (1979) Observations on the morphology of intracellularly stained gamma-motoneurons in relation to their axon conduction velocity. Neurosci Lett 13:47-50.
Dahlin LB, Danielsen N, Ochi M, Lundborg G (1988) Axonal growth in mesothelial chambers: effects of a proximal preconditioning lesion and/or predegeneration of the distal nerve stump. Exp Neurol 99:655-663.
Danielsen N, Williams LR, Dahlin LB, Varon S, Lundborg G (1988) Peripheral nerve regeneration in Gore-tex chambers. Scand J Plast Reconstr Surg Hand Surg 22:207-210.
Daniloff JK, Levi G, Grumet M, Rieger F, Edelman GM (1986) Altered expression of neuronal cell adhesion molecules induced by nerve injury and repair. J Cell Biol 103:929-945.
Das Gupta TK (1967) Mechanism of rejection of peripheral nerve allografts. Surg Gynecol Obstet 125:1058-1068.
Davis L, Cleveland DA (1934) Experimental studies in nerve transplants. Ann Surg 99:271-283.
De Vito JL, Clausing KW, Smith OA (1974) Uptake and transport of horseradish peroxidase by cut end of the vagus nerve. Brain Res 82:269-271.
Dellon AL (1981) Evaluation of sensibilty and re-education of sensation in the hand. Baltimore: Williams & Wilkins.
Desmedt JE, Godeaux E (1977) Ballistic contractions in man: characteristic recruitment pattern of single motor units of the tibialis anterior muscle. J Physiol (Lond) 264:673-693.
Devor M, Wall PD (1978) Reorganization of spinal cord sensory map after peripheral nerve injury. Nature 276:75-76.
Divac I, Mogensen J (1990) Long-term retrograde labelling of neurons. Brain Res 524:339-341.
Dow PR, Shinn SL, Ovalle WK (1980) Ultrastructural study of a blood-muscle spindle barrier after systematic administration of Horseradish Peroxidase. Am J Anat 157:375-388.
Ducker TB, Hayes GJ (1970) Peripheral nerve grafts: experimental studies in the dog and chimpanzee to define homograft limitations. J Neurosurg 32:236-243.
Duel AB (1933) History of develoment of the surgical treatment of facial palsy. Surg Gynecol Obstet 56:382-390.
Duel AB (1934) Operative treatment of facial palsy. Br Med J 2:1027-1031.
Eccles JC, Sherrington CS (1930) Numbers and contraction-values of individual motor-units examined in some muscles of the limb. Proceedings of the Royal Society of London Series B: Biological Sciences 106:326-357.
Eccles JC, Eccles RM, Iggo A, Lundberg A (1960) Electrophysiological studies on gamma motoneurones. Acta Physiol Scand 50:32-40.
Eccles JC, Eccles RM, Shealy CN, Willis WD (1962) Experiments utilizing monosynaptic excitatory action on motoneurons for testing hypotheses relating to specificity of neuronal connections. J Neurophysiol 25:559-580.
Edds MV (1950) Collateral regeneration of residual motor axons in partially denervated muscles. J Exp Zool 113:517-551.
Edgerton VR, Roy RR, Chalmers GR (1990) Does the size principle give insight into the energy requirements of motoneurons? In: The segmental motor system (Binder MD, Mendell LM, eds), p 150. Oxford: Oxford University Press.
Edshage S (1964) Peripheral nerve suture. Acta Chirurgica Scandinavia 331 (suppl):1-104.
Edstrom L, Kugelberg E (1968) Properties of motor units in the rat anterior tibial muscle. Acta Physiol Scand 73:543-544.

Elliott HC (1942) Studies on the motor cells of the spinal cord I Distribution in the normal human cord. Am J Anat 70:95-117.
Elliott HC (1943) Studies on the motor cells of the spinal cord II Distribution in the normal human fetal cord. Am J Anat 72:29-38.
Elliott HC (1944) Studies on the motor cells of the spinal cord IV Distribution in experimental animals. J Comp Neurol 81:97-103.
Emonet-Denand F, Jami L, Laporte Y (1975) Skeleto-fusimotor axons in the hind-limb muscles of the cat. J Physiol 249:153-166.
Engel AK, Kreutzberg GW (1988) Neuronal surface changes in the dorsal vagal motor nucleus of the guinea pig in response to axotomy. J Comp Neurol 275:181-200.
English AW, Letbetter WD (1982a) Anatomy and innervation patterns of cat lateral gastrocnemius and plantaris muscles. Am J Anat 164:67-77.
English AW, Letbetter WD (1982b) A histochemical analysis of identified compartments of cat lateral gastrocnemius muscle. Anat Rec 204:123-130.
Evans PJ, Bain JR, Mackinnon SE, Makino AP, Hunter DA (1991) Selective reinnervation: a comparison of recovery following microsuture and conduit nerve repair. Brain Res 559:315-321.
Farel PB, Wray SE (1989) Regenerative specificity of motor axons when reinnervation is partially suppressed. J Neurobiol 20:69-80.
Fawcett JW, Keynes RJ (1986) Muscle basal lamina: a new graft material for peripheral nerve repair. Journal of Neurosurgery 65:354-363.
Fawcett JW, Keynes RJ (1990) Peripheral nerve regeneration. Annu Rev Neurosci 13:43-60.
Fleshman JW, Munson JB, Sypert GW, Friedman WA (1981) Rheobase, input resistance, and motor-unit type in medial gastrocnemius motoneurons in the cat. J Neurophysiol 46:1326-1338.
Foerster O (1916) Schussverletzungen der peripheren Nerven und ihre Behandlung. Muenchener Medizinische Wochenschrift 8:283.
Forssman J (1898) Über die Ursachen, welche die Wachstumsrichtung der peripheren Nervenfasern bei der Regeneration bestimmen. Beiträge zur Pathologischen Anatomie 24:56-100.
Fox EA, Powley TL (1989) False-positive artifacts of tracer strategies distort autonomic connectivity maps. Brain Res Brain Res Rev 14:53-77.
Fritz N, Illert M, Saggau P (1986a) Location of motoneurones projecting to the cat distal forelimb. I. Deep radial motornuclei. J Comp Neurol 244:286-301.
Fritz N, Illert M, Reeh P (1986b) Location of motoneurones projecting to the cat distal forelimb. II. Median and ulnar motornuclei. J Comp Neurol 244:302-312.
Fritzsch B, Sonntag R, Dubuc R, Ohta Y, Grillner S (1990) Organization of the six motor nuclei innervating the ocular muscles in lamprey. J Comp Neurol 294:491-506.
Fuhr P, Cohen LG, Dang N, Findley TW, Haghighi S, Oro J, Hallett M (1992) Physiological analysis of motor reorganization following lower limb amputation. Electroencephalogr Clin Neurophysiol 85:53-60.
Gattuso JM, Glasby MA, Gschmeissner SE, Norris RW (1989) A comparison of immediate and delayed repair of peripheral nerves using freeze-thawed autologous skeletal muscle grafts--in the rat. British Journal of Plastic Surgery 42:306-313.
Geldmacher J (1975) [Proceedings: Sutures and transplantation of nerves]. MMW Munch Med Wochenschr 117:363-364.
Glasby MA, Gilmour JA, Gschmeissner SE, Hems TE, Myles LM (1990) The repair of large peripheral nerves using skeletal muscle autografts: a comparison with cable grafts in the sheep femoral nerve. British Journal of Plastic Surgery 43:169-178.
Gluck T (1880) Ueber Neuroplastik auf dem Wege der Transplantation. Archiv für klinische Chirurgie 25:606-616.
Goering JH (1928) An experimental analysis of the motor-cell columns in the cervical enlargement of the spinal cord in the albino rat. J Comp Neurol 46:125-151.
Gordon T, Stein RB, Thomas CK (1986a) Innervation and function of hind-limb muscles in the cat after cross-union of the tibial and peroneal nerves. J Physiol 374:429-441.
Gordon T, Stein RB, Thomas CK (1986b) Organization of motor units following cross-reinnervation of antagonistic muscles in the cat hind limb. J Physiol 374:443-456.

Grabb WC, Bement SL, Koepke GH, Green RA (1970) Comparison of methods of peripheral nerve suturing in monkeys. Plast Reconstr Surg 46:31-38.
Granit R, Henatsch H-D, Steg G (1956) Tonic and phasic ventral horn cells differentiated by post-tetanic potentiation in cat extensors. Acta Physiol Scand 37:114-126.
Greene EC (1955) Anatomy of the rat. New York: Hafner Publishing Co.
Gruber H (1976) Identification of motor and sensory funiculi in cut nerves and their selective reunion. Br J Plast Surg 29:70-73.
Guenard V, Kleitman N, Morrissey TK, Bunge RP, Aebischer P (1992) Syngeneic Schwann cells derived from adult nerves seeded in semipermeable guidance channels enhance peripheral nerve regeneration. The Journal of Neuroscience : the Official Journal of the Society For Neuroscience 12:3310-3320.
Gulati AK (1988) Evaluation of acellular and cellular nerve grafts in repair of rat peripheral nerve. J Neurosurg 68:117-123.
Gulati AK (1998) Immune response and neurotrophic factor interactions in peripheral nerve transplants. Acta Haematol 99:171-174.
Gulati AK, Cole GP (1990) Nerve graft immunogenicity as a factor determining axonal regeneration in the rat. J Neurosurg 72:114-122.
Gutmann E (1945) The reinnervation of muscle by sensory nerve fibers. J Anat 79:1-8.
Gutmann E, Sanders FK (1942) Functional recovery following nerve grafts and other types of nerve bridge. Brain Res 65:373-408.
Gutmann E, Young J (1944) The reinnervation of muscle after various periods of atrophy. J Anat 78:15-43.
Guttmann RD (1981) Developing ways of reducing allograft immunogenicity. Can Med Assoc J 124:143-145.
Ha H, Kao T, Tan EC (1980) Muscle sensory neurons in the spinal ganglia in the rat determined by the retrograde transport of horseradish peroxidase. Exp Neurol 70:438-445.
Haase P (1990) Explanation for the labeling of cervical motoneurons in young rats following the introduction of horseradish peroxidase into the calf. J Comp Neurol 297:471-478.
Haase P, Hrycyshyn AW (1985) Labeling of motoneurons supplying the cutaneous maximus muscle in the rat, following injection of the triceps brachii muscle with horseradish peroxidase. Neurosci Lett 60:313-318.
Haase P, Hrycyshyn AW (1986) On the diffusion of horseradish peroxidase into muscles and the "spurious" labeling of motoneurons. Exp Neurol 91:399-403.
Hakstian RW (1968) Funicular orientation by direct stimulation. An aid to peripheral nerve repair. J Bone Joint Surg Am 50:1178-1186.
Hallin RG (1990) Microneurography in relation to intraneural topography: somatotopic organisation of median nerve fascicles in humans. J Neurol Neurosurg Psychiatry 53:736-744.
Hanker JS, Yates PE, Metz CB, Rustioni A (1977) A new specific, sensitive and non-carcinogenic reagent for the demonstration of horseradish peroxidase. Histochem J 9:789-792.
Hansen WH, Long EL, Davis KJ, Nelson AA, Fitzhugh OG (1966) Chronic toxicity of three food colourings: Guinea Green B, Light Green SF Yellowish and Fast Green FCF in rats, dogs and mice. Food Cosmet Toxicol 4:389-410.
Hantaz-Ambroise D, Vigny M, Koenig J (1987) Heparan sulfate proteoglycan and laminin mediate two different types of neurite outgrowth. J Neurosci 7:2293-2304.
Hardman VJ, Brown MC (1985) Spatial organization within rat motoneuron pools. Neurosci Lett 60:325-329.
Hardman VJ, Brown MC (1987) Accuracy of reinnervation of rat internal intercostal muscles by their own segmental nerves. J Neurosci 7:1031-1036.
Hashizume K, Kanda K, Burke RE (1988) Medial gastrocnemius motor nucleus in the rat: age-related changes in the number and size of motoneurons. J Comp Neurol 269:425-430.
Havton L, Kellerth JO (1987) Regeneration by supernumerary axons with synaptic terminals in spinal motoneurons of cats. Nature 325:711-714.
Havton L, Kellerth JO (1990) Elimination of intramedullary axon collaterals of cat spinal alpha-motoneurons following peripheral nerve injury. Exp Brain Res 79:65-74.

Henneman E, Olson CB (1965) Relations between Structure and Function in the Design of Skeletal Muscles. J Neurophysiol 28:581-598.
Henneman E, Mendell LM (1981) Functional organization of motoneuron pool and its inputs. In: Handbook of Physiology: The Nervous System (Brooks VB, ed), pp 423-507. Bethesda, Maryland: American Physiological Society.
Henneman E, Somjen G, Carpenter DO (1965a) Functional Significance of Cell Size in Spinal Motoneurons. J Neurophysiol 28:560-580.
Heumann R, Lindholm D, Bandtlow C, Meyer M, Radeke MJ, Misko TP, Shooter E, Thoenen H (1987) Differential regulation of mRNA encoding nerve growth factor and its receptor in rat sciatic nerve during development, degeneration, and regeneration: role of macrophages. Proc Natl Acad Sci U S A 84:8735-8739.
Highet WB, Sanders FK (1943) The effects of stretching nerves after suture. Br J Surg 30:355-369.
Highet WB, Holmes W (1943) Traction injuries to the lateral popliteal nerve and traction injuries to peripheral nerves after suture. Br J Surg 30:212-233.
Hiller F (1951) Nerve regeneration in grafts. J Neuropath Clin Neurol 1:5-14.
Himes BT, Tessler A (1989) Death of some dorsal root ganglion neurons and plasticity of others following sciatic nerve section in adult and neonatal rats. J Comp Neurol 284:215-230.
Hirano A, Becker NH, Zimmerman HM (1969) Isolation of the periaxonal space of the central myelinated nerve fiber with regard to the diffusion of peroxidase. J Histochem Cytochem 17:512-516.
Hollowell JP, Villadiego A, Rich KM (1990) Sciatic nerve regeneration across gaps within silicone chambers: long-term effects of NGF and consideration of axonal branching. Exp Neurol 110:45-51.
Hollyday M (1980) Organization of motor pools in the chick lumbar lateral motor column. J Comp Neurol 194:143-170.
Hollyday M (1983) Development of motor innervation of chick limbs. Prog Clin Biol Res 110 Pt A:183-193.
Holmes W (1947) Histological observations on the repair of nerves by autografts. Br J Surg 35:167-173.
Holmes W, Young JZ (1942) Nerve regeneration after immediate and delayed suture. J Anat 77:63-95.
Homma S (1969) Peripheral nerve regeneration and muscle receptor reconstruction. Electroencephalogr Clin Neurophysiol 27:720.
Honig MG, Hume RI (1989) Dil and diO: versatile fluorescent dyes for neuronal labelling and pathway tracing. Trends Neurosci 12:333-335, 340-331.
Hoover JE, Durkovic RG (1991) Morphological relationships among extensor digitorum longus, tibialis anterior, and semitendinosus motor nuclei of the cat: an investigation employing the retrograde transport of multiple fluorescent tracers. J Comp Neurol 303:255-266.
Horcholle-Bossavit G, Jami L, Thiesson D, Zytnicki D (1988) Motor nuclei of peroneal muscles in the cat spinal cord. J Comp Neurol 277:430-440.
Horner M, Kummel H (1993) Topographical representation of shoulder motor nuclei in the cat spinal cord as revealed by retrograde fluorochrome tracers. J Comp Neurol 335:309-319.
Horowitz SH (1989) Therapeutic strategies in promoting peripheral nerve regeneration. Muscle Nerve 12:314-322.
Hubbard JH (1972) The quality of nerve regeneration Factors independent of the most skillful repair. The Surgical Clinics of North America 52:1099-1108.
Hudson AR, Hunter D, Kline DG, Bratton BR (1979) Histological studies of experimental interfascicular graft repairs. J Neurosurg 51:333-340.
Hurtado H, Knoops B, Van den Bosch De Aguilar P (1987) Rat sciatic nerve regeneration in semipermeable artificial tubes. Exp Neurol 97:751-757.
Ide C (1983) Nerve regeneration and Schwann cell basal lamina: observations of the long-term regeneration. Arch Histol Jpn 46:243-257.
Ide C, Osawa T, Tohyama K (1990) Nerve regeneration through allogeneic nerve grafts, with special reference to the role of the Schwann cell basal lamina. Prog Neurobiol 34:1-38.
Ikeda K (1966) Succesful peripheral nerve homotransplantation by use of high voltage electron irradiation. Arch Jpn Chir 35:679-705.

Illert M, Fritz N, Aschoff A, Hollander H (1982) Fluorescent compounds as retrograde tracers compared with horseradish peroxidase (HRP). II. A parametric study in the peripheral motor system of the cat. J Neurosci Methods 6:199-218.

Ishihara A, Naitoh H, Araki H, Nishihira Y (1988) Soma size and oxidative enzyme activity of motoneurones supplying the fast twitch and slow twitch muscles in the rat. Brain Res 446:195-198.

Ito T, Ishikawa F (1964) Experimental study on funicular suture of the peripheral nerve injuries. Orthop Surg (Tokyo) 15:821-826.

Ito T, Hirotani H, Yamamoto K (1976) Peripheral nerve repairs by the funicular suture technique. Acta Orthop Scand 47:283-289.

Jabaley ME, Wallace WH, Heckler FR (1980) Internal topography of major nerves of the forearm and hand: a current view. J Hand Surg [Am] 5:1-18.

Jacobson RD, Hollyday M (1982) A behavioral and electromyographic study of walking in the chick. J Neurophysiol 48:238-256.

Jacoby W (1972) [Evaluation and treatment of traumatic nerve lesions]. Klin Wochenschr 50:757-767.

Jacoby W, Fahlbusch R, Mackert B, Braun B, Rolle J, Schnell J (1970) [Bridging of peripheral nerve defects with lyophilised and disantigenised homologous grafts]. Munch Med Wochenschr 112:586-589.

Jakobsohn L (1908) Über die Kerne des Rückenmarkes. Neurologisches Zentralblatt 27:617-626.

Janjua MZ, Leong SK (1981) Labelling of cervical and thoracic spinal neurones following injection of horseradish peroxidase in the leg muscles of rats. Brain Res 223:386-390.

Janjua MZ, Leong SK (1984) Organization of neurons forming the femoral, sciatic, common peroneal and tibial nerves in rats and monkeys. Brain Res 310:311-323.

Janzen RW, Speckmann EJ, Caspers H (1974) Distribution of large ventral horn cells in the lumbar cord of the rat. Cell Tissue Res 151:159-170.

Jenq CB, Coggeshall RE (1984) Regeneration of axons in tributary nerves. Brain Res 310:107-121.

Jenq CB, Coggeshall RE (1987) Permeable tubes increase the length of the gap that regenerating axons can span. Brain Res 408:239-242.

Johnson EM, Jr., Taniuchi M, DiStefano PS (1988) Expression and possible function of nerve growth factor receptors on Schwann cells. Trends Neurosci 11:299-304.

Johnson IP (1986) A quantitative ultrastructural comparison of alpha and gamma motoneurons in the thoracic region of the spinal cord of the adult cat. J Anat 147:55-72.

Johnson IP, Sears TA (1988) Ultrastructure of interneurons within motor nuclei of the thoracic region of the spinal cord of the adult cat. J Anat 161:171-185.

Kaizawa J, Takahashi I (1970) Motor cell columns in rat lumbar spinal cord. Tohoku J Exp Med 101:25-33.

Karpati G, Engel WK (1968) "Type grouping" in skeletal muscles after experimental reinnervation. Neurology 18:447-455.

Katan S, Gottschall J, Neuhuber W (1982) Simultaneous visualization of horseradish peroxidase and Nuclear Yellow in tissue sections for neuronal double labeling. Neurosci Lett 28:121-126.

Katz LC, Iarovici DM (1990) Green fluorescent latex microspheres: a new retrograde tracer. Neuroscience 34:511-520.

Keizer K, Kuypers HG (1989) Distribution of corticospinal neurons with collaterals to the lower brain stem reticular formation in monkey (Macaca fascicularis). Exp Brain Res 74:311-318.

Keizer K, Kuypers HG, Huisman AM, Dann O (1983) Diamidino yellow dihydrochloride (DY . 2HCl); a new fluorescent retrograde neuronal tracer, which migrates only very slowly out of the cell. Exp Brain Res 51:179-191.

Kernell D (1966) Input resistance, electrical excitability, and size of ventral horn cells in cat spinal cord. Science 152:1637-1640.

Kernell D, Verhey BA, Eerbeek O (1985) Neuronal and muscle unit properties at different rostro-caudal levels of cat's motoneurone pool. Brain Res 335:71-79.

Kerns JM, Lucchinetti C (1992) Electrical field effects on crushed nerve regeneration. Exp Neurol 117:71-80.

Kevetter GA, Willis WD (1982) Spinothalamic cells in the rat lumbar cord with collaterals to the medullary reticular formation. Brain Res 238:181-185.

Keynes RJ (1987) Schwann cells during development and regeneration: leaders or followers? Trends Neurosci 10:137-139.
Kirklin JW, Murphey F, Berkson J (1949) Suture of peripheral nerves; factors affecting prognosis. Surg Gynecol Obstet 88:719-730.
Kline DG (1990) Caution in the evaluation of results of peripheral nerve surgery. In: Peripheral nerve lesions (Samii M, ed). Berlin: Springer Verlag.
Klueber KM (1987) Role of muscle neurotization in the reinnervation of murine muscle grafts. Anat Rec 219:370-373, 429-333.
Klueber KM, Ontell M (1984) A new approach to intramuscular placement of horseradish peroxidase. Muscle Nerve 7:127-129.
Knyihar-Csillik E, Rakic P, Csillik B (1989) Transneuronal degeneration in the Rolando substance of the primate spinal cord evoked by axotomy-induced transganglionic degenerative atrophy of central primary sensory terminals. Cell Tissue Res 258:515-525.
Kosaka M (1990) Enhancement of rat peripheral nerve regeneration through artery-including silicone tubing. Exp Neurol 107:69-77.
Krishnan N, Singer M (1973) Penetration of peroxidase into peripheral nerve fibers. Am J Anat 136:1-14.
Kristensson K (1970) Transport of fluorescent protein tracer in peripheral nerves. Acta Neuropathol (Berl) 16:293-300.
Kristensson K, Olsson Y (1971) Retrograde axonal transport of protein. Brain Res 29:363-365.
Kristensson K, Olsson Y, Sjostrand J (1971) Axonal uptake and retrograde transport of exogenous proteins in the hypoglossal nerve. Brain Res 32:399-406.
Kugelberg E (1973) Histochemical composition, contraction speed and fatiguability of rat soleus motor units. J Neurol Sci 20:177-198.
Kuhlendahl H, Mumenthaler M, Penzholz H, Rottgen P, Schliack H, Struppler A (1972) [Treatment of peripheral nerve lesions by homologous nerve-implants]. Z Neurol 202:251-256.
Kuno M, Miyata Y, Munoz-Martinez EJ (1974a) Properties of fast and slow alpha motoneurones following motor reinnervation. J Physiol 242:273-288.
Kuno M, Miyata Y, Munoz-Martinez EJ (1974b) Differential reaction of fast and slow alpha-motoneurones to axotomy. J Physiol 240:725-739.
Kuypers HG, Huisman AM (1984) Fluorescent neuronal tracers. In: Advances in cellular neurobiology (Fedoroff S, ed), pp 307-340. Orlando, Florida: Academic Press, Inc.
Landmesser L (1978a) The development of motor projection patterns in the chick hind limb. J Physiol 284:391-414.
Landmesser L (1978b) The distribution of motoneurones supplying chick hind limb muscles. J Physiol 284:371-389.
Langley JN, Hashimoto M (1917) On the suture of separate nerve bundles in a nerve trunk and on internal nerve plexuses. J Physiol (Lond) 51:318-346.
Laporte Y, Emonet-Denand F, Jami L (1981) The skeletofusimotor or ß-innervation of mammalian muscle spindles. Trends Neurosci 4:97-99.
Laskowski MB, Sanes JR (1987) Topographic mapping of motor pools onto skeletal muscles. J Neurosci 7:252-260.
Laskowski MB, Sanes JR (1988) Topographically selective reinnervation of adult mammalian skeletal muscles. J Neurosci 8:3094-3099.
Laskowski MB, Norton AS, Berger PK (1991) Branching patterns of the rat phrenic nerve during development and reinnervation. Exp Neurol 113:212-220.
LaVail JH, LaVail MM (1972) Retrograde axonal transport in the central nervous system. Science 176:1416-1417.
Le-Beau JM, LaCorbiere M, Powell HC, Ellisman MH, Schubert D (1988) Extracellular fluid conditioned during peripheral nerve regeneration stimulates Schwann cell adhesion, migration and proliferation. Brain Research 459:93-104.
Leksell L (1945) The action potential and excitatory effects of the small ventral root fibres to skeletal muscle. Acta Physiol Scand 10:1-84.
Leong SK, Tan CK (1987) Central projection of rat sciatic nerve fibres as revealed by Ricinus communis agglutinin and horseradish peroxidase tracers. J Anat 154:15-26.

Levinthal R, Brown WJ, Rand RW (1978a) Fascicular nerve allograft evaluation. Part 2: comparison with whole-nerve allograft by light microscopy. J Neurosurg 48:428-433.
Levinthal R, Brown WJ, Rand RW (1978b) Fascicular nerve allograft evaluation. Part 1: comparison with autografts by light microscopy. J Neurosurg 48:423-427.
Lewis HP, McLaurin RL (1966) Application of tissue transplant technique to nerve grafting. Surg Forum 17:432-433.
Liebermann AR (1974) Some factors affecting retrograde neuronal responses to axonal lesions. In: Essays on the Nervous System (Bellairs R, Gray EG, eds), pp 71-124. Oxford: Clarendon Press.
Linda H, Risling M, Cullheim S (1985) 'Dendraxons' in regenerating motoneurons in the cat: do dendrites generate new axons after central axotomy? Brain Res 358:329-333.
Lindholm D, Heumann R, Meyer M, Thoenen H (1987) Interleukin-1 regulates synthesis of nerve growth factor in non-neuronal cells of rat sciatic nerve. Nature 330:658-659.
Liu CN, Chambers WW (1958) Intraspinal sprouting of dorsal root axons; development of new collaterals and preterminals following partial denervation of the spinal cord in the cat. AMA Arch Neurol Psychiatry 79:46-61.
Loeb GE (1984) The control and responses of mammalian muscle spindles during normally executed motor tasks. Exerc Sport Sci Rev 12:157-204.
Loeb GE (1990) The functional organization of muscles, motor units, and tasks. In: The segmental motor system (Binder MD, Mendell LM, eds). Oxford: Oxford University Press.
Longo FM, Manthorpe M, Skaper SD, Lundborg G, Varon S (1983) Neuronotrophic activities accumulate in vivo within silicone nerve regeneration chambers. Brain Res 261:109-116.
Lubinska L (1977) Early course of Wallerian degeneration in myelinated fibres of the rat phrenic nerve. Brain Res 130:47-63.
Lundborg G, Longo FM, Varon S (1982a) Nerve regeneration model and trophic factors in vivo. Brain Res 232:157-161.
Lundborg G, Dahlin LB, Danielsen N, Nachemson AK (1986) Tissue specificity in nerve regeneration. Scand J Plast Reconstr Surg 20:279-283.
Lundborg G, Dahlin LB, Danielsen N, Gelberman RH, Longo FM, Powell HC, Varon S (1982b) Nerve regeneration in silicone chambers: influence of gap length and of distal stump components. Exp Neurol 76:361-375.
Lundborg G, Dahlin LB, Danielsen N, Hansson HA, Johannesson A, Longo FM, Varon S (1982c) Nerve regeneration across an extended gap: a neurobiological view of nerve repair and the possible involvement of neuronotrophic factors. J Hand Surg [Am] 7:580-587.
Lunn ER, Brown MC, Perry VH (1990) The pattern of axonal degeneration in the peripheral nervous system varies with different types of lesion. Neuroscience 35:157-165.
Mackinnon SE, Dellon AL (1988) Surgery of the peripheral nerve. Stuttgart, New York: Georg Thieme Verlag.
Mackinnon SE, Dellon AL (1990a) Clinical nerve reconstruction with a bioabsorbable polyglycolic acid tube. Plastic and Reconstructive Surgery 85:419-424.
Mackinnon SE, Dellon AL (1990b) Clinical nerve reconstruction with a bioabsorbable polyglycolic acid tube. Plast Reconstr Surg 85:419-424.
Mackinnon SE, Hudson AR, Hunter DA (1985) Histologic assessment of nerve regeneration in the rat. Plast Reconstr Surg 75:384-388.
Mackinnon SE, Hudson AR, Falk RE, Kline D, Hunter D (1984) Peripheral nerve allograft: an assessment of regeneration across pretreated nerve allografts. Neurosurgery 15:690-693.
Mackinnon SE, Dellon AL, Lundborg G, Hudson AR, Hunter DA (1986) A study of neurotrophism in a primate model. J Hand Surg [Am] 11:888-894.
Mackinnon SE, Hudson AR, Bain JR, Falk RE, Hunter DA (1987a) The peripheral nerve allograft: an assessment of regeneration in the immunosuppressed host. Plast Reconstr Surg 79:436-446.
Mackinnon SE, Hudson AR, Bain JR, Falc RE, Hunter D (1987b) The peripheral nerve allograft: An assessment of regeneration in the immunosuppressed host. Plastic and Reconstructive Surgery 79:436.
Madison R, da Silva CF, Dikkes P, Chiu TH, Sidman RL (1985) Increased rate of peripheral nerve regeneration using bioresorbable nerve guides and a laminin-containing gel. Exp Neurol 88:767-772.

Marmor L (1963) Regeneration of peripheral nerve defects by irradiated homograft. Lancet 281:1191-1192.
Marmor L (1972) Nerve grafting in peripheral nerve. Surg Clin North Am 52:1177-1187.
Martini R, Schachner M, Faissner A (1990) Enhanced expression of the extracellular matrix molecule J1/tenascin in the regenerating adult mouse sciatic nerve. J Neurocytol 19:601-616.
McHanwell S, Biscoe TJ (1981a) The localization of motoneurons supplying the hindlimb muscles of the mouse. Philos Trans R Soc Lond B Biol Sci 293:477-508.
McHanwell S, Biscoe TJ (1981b) The sizes of motoneurons supplying hindlimb muscles in the mouse. Proc R Soc Lond B Biol Sci 213:201-216.
McMahon SB, Wall PD (1989) Changes in spinal cord reflexes after cross-anastomosis of cutaneous and muscle nerves in the adult rat. Nature 342:272-274.
Medawar PB (1944) The behaviour and fate of skin autografts and skin homografts in rabbits. J Anat 78:176-199.
Mendell LM, Scott JG (1975) The effect of peripheral nerve cross-union on connections of single Ia fibers to motoneurons. Exp Brain Res 22:221-234.
Merzenich MM, Kaas JH, Wall J, Nelson RJ, Sur M, Felleman D (1983) Topographic reorganization of somatosensory cortical areas 3b and 1 in adult monkeys following restricted deafferentation. Neuroscience 8:33-55.
Mesulam MM (1978) Tetramethyl benzidine for horseradish peroxidase neurohistochemistry: a non-carcinogenic blue reaction product with superior sensitivity for visualizing neural afferents and efferents. J Histochem Cytochem 26:106-117.
Mesulam MM (1982) Principles of Horseradish Peroxidase neurohistochemistry and their applications for tracing neural pathways - axonal transport, enzyme histochemistry and light microscopic analysis. In: Tracing neural connections with Horseradish Peroxidase (Mesulam M, ed). New York: John Wiley & Sons.
Mesulam MM, Rosene DL (1979) Sensitivity in horseradish peroxidase neurohistochemistry: a comparative and quantitative study of nine methods. J Histochem Cytochem 27:763-773.
Mesulam MM, Hegarty E, Barbas H, Carson KA, Gower EC, Knapp AG, Moss MB, Mufson EJ (1980) Additional factors influencing sensitivity in the tetramethyl benzidine method for horseradish peroxidase neurohistochemistry. J Histochem Cytochem 28:1255-1259.
Michon J, Masse P (1964) Le moment optimum de la suture nerveuse dans les plaies du membre superieur. Rev Chir Orthop 50:205-212.
Michon J, Amend P, Merle M (1990) Microsurgical repair of peripheral nerve lesions: a study of 150 injuries of the median and ulnar nerves. In: Peripheral nerve lesions. (Samii M, ed). Berlin: Springer Verlag.
Miledi R, Stefani E (1969) Non-selective re-innervation of slow and fast muscle fibres in the rat. Nature 222:569-571.
Millesi H (1967) [Nerve transplantation for reconstruction of peripheral nerves injured by the use of the microsurgical technic]. Minerva Chir 22:950-951.
Millesi H (1968) [On the problem of overbridging defects of the peripheral nerves]. Wien Med Wochenschr 118:182-187.
Millesi H (1969a) [Reconstruction of transsected peripheral nerves and nerve transplantation]. Munch Med Wochenschr 111:2669-2674.
Millesi H (1969b) Mikrochirurgische Wiederherstellung peripherer Nerven. Handchirurgie 2:74-81.
Millesi H (1984) Nerve grafting. Clin Plast Surg 11:105-113.
Millesi H, Meissl G, Berger A (1972) The interfascicular nerve-grafting of the median and ulnar nerves. J Bone Joint Surg Am 54:727-750.
Millesi H, Meissl G, Berger A (1976) Further experience with interfascicular grafting of the median, ulnar, and radial nerves. The Journal of Bone and Joint Surgery American Volume 58:209-218.
Milner-Brown HS, Stein RB, Yemm R (1973) The orderly recruitment of human motor units during voluntary isometric contractions. J Physiol 230:359-370.
Milner-Brown HS, Stein RB, Lee RG (1974) Pattern of recruiting human motor units in neuropathies and motor neurone disease. J Neurol Neurosurg Psychiatry 37:665-669.
Mirsky R, Jessen KR, Schachner M, Goridis C (1986) Distribution of the adhesion molecules N-CAM and L1 on peripheral neurons and glia in adult rats. J Neurocytol 15:799-815.

Miyata H, Kawai Y (1991) Soma diameter and oxidative enzyme activity of identified a-motoneurons: application of a retrograde fluorescent neuronal tracer. Brain Res 544:141-144.
Mjaatvedt AE, Wong-Riley MTT (1986) Double-labeling of rat a-motoneurons for cytochrome oxidase and retrogradely transported [^{3}H]WGA. Brain Res 368:178-182.
Molander C, Xu Q, Grant G (1984) The cytoarchitectonic organization of the spinal cord in the rat. I. The lower thoracic and lumbosacral cord. J Comp Neurol 230:133-141.
Morris JH, Hudson AR, Weddell G (1972) A study of degeneration and regeneration in the divided rat sciatic nerve based on electron microscopy. IV. Changes in fascicular microtopography, perineurium and endoneurial fibroblasts. Z Zellforsch Mikrosk Anat 124:165-203.
Moschovakis AK, Burke RE, Fyffe RE (1991) The size and dendritic structure of HRP-labeled gamma motoneurons in the cat spinal cord. J Comp Neurol 311:531-545.
Motulsky H (1995) Intuitive Biostatistics. New York: Oxford University Press.
Müller H (1990) Biochemical manipulation of the microenviroment in experimental nerve regeneration chambers. In: Peripheral nerve lesions (Samii M, ed). Berlin: Springer Verlag.
Müller H, Williams LR, Varon S (1987) Nerve regeneration chamber: evaluation of exogenous agents applied by multiple injections. Brain Res 413:320-326.
Nam SC, Kim KJ, Leem JW, Chung K, Chung JM (1989) Fiber counts at multiple sites along the rat ventral root after neonatal peripheral neurectomy or dorsal rhizotomy. J Comp Neurol 290:336-342.
Neuberger TJ, Cornbrooks CJ (1989) Transient modulation of Schwann cell antigens after peripheral nerve transection and subsequent regeneration. J Neurocytol 18:695-710.
Neuhuber W, Niederle B (1980) Differential labeling by horseradish peroxidase of small and large spinal neurons of rats. Neurosci Lett 20:131-134.
Nicholson OR, Seddon HJ (1957) Nerve repair in civil practice. Results of treatment of median and ulnar nerve lesions. Br Med J 2:1065-1071.
Nicolopoulos-Stournaras S, Iles JF (1983) Motor neuron columns in the lumbar spinal cord of the rat. J Comp Neurol 217:75-85.
Nissl F (1892) Über die Veränderungen der Ganglienzellen am Facialiskern des Kaninchens nach Ausreissung der Nerven. All Z Psychiat 48:197-198.
Norris RW, Glasby MA, Gattuso JM, Bowden RE (1988) Peripheral nerve repair in humans using muscle autografts A new technique. The Journal of Bone and Joint Surgery British Volume 70:530-533.
Novikova L, Novikov L, Kellerth JO (1997) Persistent neuronal labeling by retrograde fluorescent tracers: a comparison between Fast Blue, Fluoro-Gold and various dextran conjugates. J Neurosci Methods 74:9-15.
Nyberg-Hansen R (1965) Anatomical demonstration of gamma motoneurons in the cat`s spinal cord. Exp Neurol 13:71-81.
Oh UT, Kim KJ, Baik-Han EJ, Chung JM (1989) Electrophysiological evidence for an increase in the number of ventral root afferent fibers after neonatal peripheral neurectomy in the rat. Brain Res 501:90-99.
Oppenheim RW, Haverkamp LJ, Prevette D, McManaman JL, Appel SH (1988) Reduction of naturally occurring motoneuron death in vivo by a target-derived neurotrophic factor. Science 240:919-922.
Osawa T, Tohyama K, Ide C (1990) Allogeneic nerve grafts in the rat, with special reference to the role of Schwann cell basal laminae in nerve regeneration. J Neurocytol 19:833-849.
Pappas PW (1971) The use of a chrome alum-gelatin (subbing) solution as a general adhesive for paraffin sections. Stain Technol 46:121-124.
Pellegrini M, Pompeiano O, Corvaja N (1977) Identification of different size motoneurons labeled by the retrograde axonal transport of horseradish peroxidase. Pflugers Arch 368:161-163.
Perry VH, Brown MC, Gordon S (1987) The macrophage response to central and peripheral nerve injury. A possible role for macrophages in regeneration. J Exp Med 165:1218-1223.
Peter JB, Barnard RJ, Edgerton VR, Gillespie CA, Stempel KE (1972) Metabolic profiles of three fiber types of skeletal muscle in guinea pigs and rabbits. Biochemistry (Mosc) 11:2627-2633.
Petersen RP (1966) Cell size and rate of protein synthesis in ventral horn neurones. Science 153:1413-1414.

Peyronnard JM, Charron L (1980) Muscle reorganization after partial denervation and reinnervation. Muscle Nerve 3:509-518.
Peyronnard JM, Charron L (1983a) Motoneuronal and motor axonal innervation in the rat hindlimb: a comparative study using horseradish peroxidase. Exp Brain Res 50:125-132.
Peyronnard JM, Charron L (1983b) Decreased horseradish peroxidase labeling in deafferented spinal motoneurons of the rat. Brain Res 275:203-214.
Peyronnard JM, Charron LF, Messier JP, Lavoie J (1988a) Differential effects of distal and proximal nerve lesions on carbonic anhydrase activity in rat primary sensory neurons, ventral and dorsal root axons. Exp Brain Res 70:550-560.
Peyronnard JM, Charron L, Lavoie J, Messier JP, Bergouignan FX (1988b) A comparative study of the effects of chronic axotomy, crush lesion and re-anastomosis of the rat sural nerve on horseradish peroxidase labelling of primary sensory neurons. Brain Res 443:295-309.
Philipeaux J-M, Vulpian A (1870) Note sur des essais de greffe d'un troncon du nerf lingual entre les deux bouts du nerf hypoglosse, apres excision d'un segment de ce dernier nerf. Arch Physiol Norm Path 3:618-620.
Platt H (1919) On the results of bridging gaps in injured nerve trunks by autogenous fascial tubulization and autogenous nerve grafts. Br J Surg 7:384-389.
Politis MJ (1985) Specificity in mammalian peripheral nerve regeneration at the level of the nerve trunk. Brain Res 328:271-276.
Politis MJ, Ederle K, Spencer PS (1982) Tropism in nerve regeneration in vivo. Attraction of regenerating axons by diffusible factors derived from cells in distal nerve stumps of transected peripheral nerves. Brain Res 253:1-12.
Pollard JD, Fitzpatrick L (1973a) A comparison of the effects of irradiation and immunosuppressive agents on regeneration through peripheral nerve allografts: an ultrastructural study. Acta Neuropathol (Berl) 23:166-180.
Pollard JD, Fitzpatrick L (1973b) An ultrastructural comparison of peripheral nerve allografts and autografts. Acta Neuropathol (Berl) 23:152-165.
Pons TP, Garraghty PE, Ommaya AK, Kaas JH, Taub E, Mishkin M (1991) Massive cortical reorganization after sensory deafferentation in adult macaques. Science 252:1857.
Puigdellivol-Sanchez A, Prats-Galino A, Ruano-Gil D, Molander C (1998) Sciatic and femoral nerve sensory neurones occupy different regions of the L4 dorsal root ganglion in the adult rat. Neurosci Lett 251:169-172.
Puigdellivol-Sanchez A, Valero-Cabre A, Prats-Galino A, Navarro X, Molander C (2002) On the use of fast blue, fluoro-gold and diamidino yellow for retrograde tracing after peripheral nerve injury: uptake, fading, dye interactions, and toxicity. J Neurosci Methods 115:115-127.
Raivich G, Hellweg R, Kreutzberg GW (1991) NGF receptor-mediated reduction in axonal NGF uptake and retrograde transport following sciatic nerve injury and during regeneration. Neuron 7:151-164.
Ranson SW (1909) Alterations in the spinal ganglion cells following neurotomy. J Comp Neurol 19:125-153.
Ranvier L (1874) De quelques faits relatifs a l`histologie et á la physiologie des muscles striés. Arch Physiol Norm Pathol 6:1-15.
Reinoso BS, Castro AJ (1989) A study of corticospinal remodelling using retrograde fluorescent tracers in rats. Exp Brain Res 74:387-394.
Renehan WE, Rhoades RW, Jacquin MF (1989) Structure-function relationships in rat brainstem subnucleus interpolaris: VII. Primary afferent central terminal arbors in adults subjected to infraorbital nerve section at birth. J Comp Neurol 289:493-508.
Rexed B (1952) The cytoarchitectonic organization of the spinal cord in the cat. J Comp Neurol 96:414-495.
Rexed B (1964) Some Aspects of the Cytoarchitectonics and Synaptology of the Spinal Cord. Prog Brain Res 11:58-92.
Rich KM, Alexander TD, Pryor JC, Hollowell JP (1989) Nerve growth factor enhances regeneration through silicone chambers. Exp Neurol 105:162-170.
Richardson PM, Ebendal T (1982) Nerve growth activities in rat peripheral nerve. Brain Res 246:57-64.

Richmond FJ, Scott DA, Abrahams VC (1978) Distribution of motoneurones to the neck muscles, biventer cervicis, splenius and complexus in the cat. J Comp Neurol 181:451-463.
Riek S, Bawa P (1992) Recruitment of motor units in human forearm extensors. J Neurophysiol 68:100-108.
Riley DA, Sanger JR, Matloub HS, Yousif NJ, Bain JL, Moore GH (1988) Identifying motor and sensory myelinated axons in rabbit peripheral nerves by histochemical staining for carbonic anhydrase and cholinesterase activities. Brain Res 453:79-88.
Risling M, Cullheim S, Hildebrand C (1983a) Reinnervation of the ventral root L7 from ventral horn neurons following intramedullary axotomy in adult cats. Brain Res 280:15-23.
Risling M, Aldskogius H, Hildebrand C (1983b) Effects of sciatic nerve crush on the L7 spinal roots and dorsal root ganglia in kittens. Exp Neurol 79:176-187.
Risling M, Remahl S, Hildebrand C, Aldskogius H (1980) Structural changes in kittens' ventral and dorsal root L7 after early postnatal sciatic nerve transection. Exp Neurol 67:265-279.
Romanes GJ (1946) Motor localization and the effects of nerve injury on the ventral horn cells of the spinal cord. J Anat 80:117-131.
Romanes GJ (1951) The motor cell columns of the lumbo-sacral spinal cord of the cat. J Comp Neurol 94:313-363.
Romanes GJ (1964) The Motor Pools of the Spinal Cord. Prog Brain Res 11:93-119.
Romeis B (1968) Mikroskopische Technik. Oldenburg, München.
Rosene DL, Mesulam MM (1978) Fixation variables in horseradish peroxidase neurohistochemistry. I. The effect of fixation time and perfusion procedures upon enzyme activity. J Histochem Cytochem 26:28-39.
Ruigrok TJ, Crowe A (1984) The organization of motoneurones in the turtle lumbar spinal cord. J Comp Neurol 228:24-37.
Russell CJ, Dunbar DC, Rushmer DS, Macpherson JM, Phillips JO (1982) Differential activity of innervation subcompartments of cat lateral gastrocnemius during natural movements. Society for Neuroscience Abstracts 8:948.
Saad M, Dubuc R, Widmer CG, Westberg KG, Lund JP (1997) Anatomical organization of efferent neurons innervating various regions of the rabbit masseter muscle. J Comp Neurol 383:428-438.
Sakellarides H (1962) A follow-up study of 172 peripheral nerve injuries in the upper extremity in civilians. J Bone Jt Surg 44-A:140-148.
Samii M (1981) Discussion about the critical distance beyond a nerve graft should be used. In: Posttraumatic peripheral nerve regeneration. Experimental basis and clinical implications. (Gorio A, Millesi H, Mingrino S, eds), p 357. New York: Raven Press.
Samii M, Wallenborn R (1972) [Experimental studies on the effect of tension on the results of regeneration following nerve sutures]. Acta Neurochir (Wien) 27:87-110.
Samii M, Scheinpflug W (1974) [Clinical, electromyographic and quantitative histological investigations following nerve transplants--an experimental study (author's transl)]. Acta Neurochir (Wien) 30:1-29.
Sanders FK (1942) The repair of large gaps in the peripheral nerves. Brain 65:281-337.
Sanders FK, Young JZ (1942) The degeneration and reinnervation of grafted nerves. J Anat 76:143-164.
Sanes JN, Suner S, Lando JF, Donoghue JP (1988) Rapid reorganization of adult rat motor cortex somatic representation patterns after motor nerve injury. Proc Natl Acad Sci U S A 85:2003-2007.
Scheib J, Höke A (2013) Advances in peripheral nerve regeneration. Nature reviews Neurology 9:668-676.
Schlaepfer WW (1974) Calcium-induced degeneration of axoplasm in isolated of rats peripheral nerve. Brain Res 69:203-215.
Schmued LC, Fallon JH (1986) Fluoro-Gold: a new fluorescent retrograde axonal tracer with numerous unique properties. Brain Res 377:147-154.
Schröder JM, Seiffert KE (1970) Die Feinstruktur der neuromatösen Neurotisation von Nerventransplantaten. Virchows Archiv Abt B Zellpathologie 5:219-235.
Seckel BR, Ryan SE, Gagne RG, Chiu TH, Watkins E (1986) Target-specific nerve regeneration through a nerve guide in the rat. Plast Reconstr Surg 78:793-800.

Seddon HJ (1947) The use of autogenous grafts for the repair of large gaps in peripheral nerves. Brit J Surg 35:151-167.
Seddon HJ (1963) Nerve grafting. J Bone Jt Surg 45-B:447-461.
Seddon HJ, Holmes W (1944) The late condition of nerve homografts in man. Surg Gyn Obst 79:342-351.
Seddon HJ, Young JZ, Holmes W (1942) The histological condition of a nerve autograft in man. Brit J Surg 29:378-384.
Seiffert KE, Maxison H, Schindler P, Schröder JM (1972) Experimental and clinical studies on homologous nerve transplantation. Zbl Neurochir 33:119-130.
Sendtner M, Kreutzberg GW, Thoenen H (1990) Ciliary neurotrophic factor prevents the degeneration of motor neurons after axotomy. Nature 345:440-441.
Sharrard WJ (1955) The distribution of the permanent paralysis in the lower limb in poliomyelitis. A clinical and pathological study. J Bone Jt Surg 37B:540-458.
Sherrington CS (1892) Notes on the arrangment of some motor fibres in the lumbo-sacral plexus. J Physiol (Lond) 13:621-772.
Sickles DW, Oblak TG (1983) A horseradish peroxidase labeling technique for correlation of motoneuron metabolic activity with muscle fiber types. J Neurosci Methods 7:195-201.
Simpson SA, Young JZ (1945) Regeneration of fibre diameter after cross-union of visceral and somatic nerves. J Anat 79:48-65.
Singh R (1976) Experience with allografts in the surgery of peripheral nerves (experimental study). Acta Neurochir (Wien) 34:195-201.
Skagerberg G, Bjorklund A, Lindvall O (1985) Further studies on the use of the fluorescent retrograde tracer True Blue in combination with monoamine histochemistry. J Neurosci Methods 14:25-40.
Sketelj J, Bresjanac M, Popovic M (1989) Rapid growth of regenerating axons across the segments of sciatic nerve devoid of Schwann cells. J Neurosci Res 24:153-162.
Smith CL, Hollyday M (1983) The development and postnatal organization of motor nuclei in the rat thoracic spinal cord. J Comp Neurol 220:16-28.
Smith JW (1964) Microsurgery of Peripheral Nerves. Plast Reconstr Surg 33:317-329.
Smith RG, Appel SH (1983) Extracts of skeletal muscle increase neurite outgrowth and cholinergic activity of fetal rat spinalmotor neurons. Science 219:1079-1081.
Soileau LC, Silberstein L, Blau HM, Thompson WJ (1987) Reinnervation of muscle fiber types in the newborn rat soleus. J Neurosci 7:4176-4194.
Sperry RW (1941) The effect of crossing nerves to antagonistic muscles in the hind limb of the rat. J Comp Neurol 75:1-19.
Sperry RW (1945) The problem of central nervous reorganization after nerve regeneration and muscle transposition. Q Rev Biol 20:311-369.
Sperry RW (1947) Effect of crossing nerves to antagonistic limb muscles in the monkey. Arch Neurol Psychiat 58:452-473.
Sprague JM (1948) A study of motor cell localization in the spinal cord of the rhesus monkey. Am J Anat 82:1-26.
Sprague JM (1951) Motor and propriospinal cells in the thoracic and lumbar ventral horn of the rhesus monkey. J Comp Neurol 95:103-124.
Spurling RG, Lyons WR, Whitcomb BB, Woodhall B (1945) The failure of whole fresh homogenous nerve grafts in man. J Neurosurg 2:79-101.
Stauffer EK, Watt DG (1976) Referencing procedure for location of lumbosacral alpha-motoneurons. Pflugers Arch 366:269-271.
Stein RB (1988) Reorganization of motor unit properties after surgical repair and reinnervation of human nerves. In: The current status of peripheral nerve regeneration. (Gordon T, Stein RB, Smith PA, eds), p 135. New York: Alan R. Liss.
Sterling P, Kuypers HG (1967) Anatomical organization of the brachial spinal cord of the cat. II. The motoneuron plexus. Brain Res 4:16-32.
Stockli KA, Lottspeich F, Sendtner M, Masiakowski P, Caroll P, Gotz R, Lindholm D, Thoenen H (1989) Molecular cloning, expression and regional distribution of rat ciliary neurotrophic factor. Nature 342:920-923.

Stookey B (1922) Surgical and mechanical treatment of peripheral nerves. Philadelphia.
Strick PL, Burke RE, Kanda K, Kim CC, Walmsley B (1976) Differences between alpha and gamma motoneurons labeled with horseradish peroxidase by retrograde transport. Brain Res 113:582-588.
Sumner BE, Sutherland FI (1973) Quantitative electron microscopy on the injured hypoglossal nucleus in the rat. J Neurocytol 2:315-328.
Sunderland S (1953) Funicular suture and funicular exclusion in the repair of severed nerves. Br J Surg 40:580-587.
Sunderland S (1978) Nerves and Nerve Injuries. New York: Churchill Livingston.
Suzue T, Kaprielian Z, Patterson PH (1990) A monoclonal antibody that defines rostrocaudal gradients in the mammalian nervous system. Neuron 5:421-431.
Swett JE, Eldred E, Buchwald JS (1970) Somatotopic cord-to-muscle relations in efferent innervation of cat gastrocnemius. Am J Physiol 219:762-766.
Swett JE, Wikholm RP, Blanks RH, Swett AL, Conley LC (1986) Motoneurons of the rat sciatic nerve. Exp Neurol 93:227-252.
Sypert GW, Munson JB (1981) Basis of segmental motor control: motoneuron size or motor unit type? Neurosurgery 8:608-621.
Takahashi K, Satomi H, Ise H, Yamamoto T (1980) A method of HRP bathing of transected peripheral nerves using a rubber bag.--Its technique and advantage. Anat Anz 147:251-254.
Takano K (1976) Absence of the gamma-spindle loop in the reinnervated hind leg muscles of the cat: "alpha-muscle". Exp Brain Res 26:343-354.
Thangam S, Indirani K, Devanandan MS (1989) Differentiation of alpha and gamma motoneurons by the retrograde uptake of horseradish peroxidase. J Anat 166:35-42.
Thomas CK, Stein RB, Gordon T, Lee RG, Elleker MG (1987) Patterns of reinnervation and motor unit recruitment in human hand muscles after complete ulnar and median nerve section and resuture. J Neurol Neurosurg Psychiatry 50:259-268.
Thomas RC, Wilson VJ (1965) Precise localization of Renshaw cells with a new marking technique. Nature 206:211-213.
Thomas RC, Wilson VJ (1966) Marking single neurons by staining with intracellular recording microelectrodes. Science 151:1538-1539.
Thulin CA (1960) Electrophysiological studies of peripheral nerve regeneration with special reference to the small diameter (Gamma) fibers. Exp Neurol 2:598-612.
Torvik A, Skjörten F (1971) Electron microscopic observations on nerve cell regeneration and degeneration after axon lesions. I. Changes in the nerve cell cytoplasm. Acta Neuropathol 17:248-264.
Ulfhake B, Cullheim S (1981) A quantitative light microscopic study of the dendrites of cat spinal gamma -motoneurons after intracellular staining with horseradish peroxidase. J Comp Neurol 202:585-596.
Ulfhake B, Kellerth JO (1982) Does a-motoneuron size correlate with motor unit type in cat triceps surae? Brain Res 251:201-209.
Usbeck W (1976) Nerve suture without tension, a method for repairing transected peripheral nerves. Acta Neurochir (Wien) 34:215-216.
Van Buren JM, Frank K (1965) Correlation between the morphology and potential field of a spinal motor nucleus in the cat. Electroenceph Clin Neurophysiol 19:112-126.
Van Hooft JA (2002) Fast Green FCF (Food Green 3) inhibits synaptic activity in rat hippocampal interneurons. Neurosci Lett 318:163-165.
Verburgh CA, Voogd J, Kuypers HG, Stevens HP (1990) Propriospinal neurons with ascending collaterals to the dorsal medulla, the thalamus and the tectum: a retrograde fluorescent double-labeling study of the cervical cord of the rat. Exp Brain Res 80:577-590.
Waibl H (1973) Zur Topographie der Medulla spinalis der Albinoratte (Rattus norvegicus). Adv Anat Embryol Cell Biol 47:7-42.
Waller AV (1850) Experiments on the section of glosssopharyngeal and hypoglossal nerves of the frog, and observations on the alterations produced thereby in the structure of their primitive fibres. Phil Trans R Soc Lond B 140:423-429.

Walton RL, Brown RE, Matory WE, Borah GL, Dolph JL (1989) Autogenous vein graft repair of digital nerve defects in the finger: a retrospective clinical study. Plast Reconstr Surg 84:944-949.
Wang GY, Hirai KI, Shimada H, Taji S, Zhong SZ (1992) Behavior of axons, schwann cells and perineurial cells in nerve regeneration within transplanted nerve grafts: effects of anti-laminin and anti-fibroectin antisera. Brain Res 583:216-226.
Warton SS, Dyson SE, Harvey AR (1988) Visual thalamocortical projections in normal and enucleated rats: HRP and fluorescent dye studies. Exp Neurol 100:23-39.
Waynforth HB (1980) Experimental and Surgical Technique in the Rat. London: Academic Press.
Weeks OI, English AW (1985) Compartmentalization of the cat lateral gastrocnemius motor nucleus. J Comp Neurol 235:255-267.
Weeks OI, English AW (1987) Cat triceps surae motor nuclei are organized topologically. Exp Neurol 96:163-177.
Weiss P, Tayler AC (1943) Repair of peripheral nerves by grafts of frozen-dried nerve. Proc Soc Exp Biol Med 52:326-328.
Weiss P, Tayler AC (1944) Further experimental evidence against `neurotropism' in nerve regeneration. J Exp Zool 95:233-257.
Weiss P, Hiscoe HB (1948) Experiments of the mechanism of nerve growth. Exp Neurol 107:315-395.
Wekerle H, Schwab M, Linington C, Meyermann R (1986) Antigen presentation in the peripheral nervous system: Schwann cells present endogenous myelin autogantigens to lymphocytes. Eur J Immunol 16:1551-1557.
Westbury DR (1982) A comparison of the structures of alpha and gamma-spinal motoneurones of the cat. J Physiol 325:79-91.
Wigston DJ, Sanes JR (1982) Selective reinnervation of adult mammalian muscle by axons from different segmental levels. Nature 299:464-467.
Williams LR, Danielsen N, Müller H, Varon S (1988) Influence of the acellular fibrin matrix on nerve regeneration success within the silicone chamber model. In: The current status of peripheral nerve regeneration (Gordon T, Stein RB, Smith PA, eds), p 111. New York: Alan R. Liss.
Williams LR, Longo FM, Powell HC, Lundborg G, Varon S (1983) Spatio-temporal progress of peripheral nerve regeneration within a silicone chamber: parameters for a bioassay. J Comp Neurol 218:460-470.
Wyman RJ (1973) Somatotopic connectivity or species connectivity? In: Control of posture and locomotion, Plenum (Stein RB, Pearson KG, Smith RS, Redford JB, eds). New York: Plenum.
Yezierski RP, Bowker RM (1981) A retrograde double label tracing technique using horseradish peroxidase and the fluorescent dye 4'-,6-diamidino-2-phenylindole 2HC1 (DAPI). J Neurosci Methods 4:53-62.
Young JZ, Holmes W (1940) Nerve regeneration. Importance of the peripheral stump and the value of nerve grafts. Lancet 2:128-129.
Young JZ, Medawar PB (1940) Fibrin suture of peripheral nerves. Lancet 2:126-128.
Young L, Wray RC, Weeks PM (1981) A randomized prospective comparison of fascicular and epineural digital nerve repairs. Plast Reconstr Surg 68:89-93.
Yu WH (1980) Uptake sites of horseradish peroxidase after injection into peritoneal structures: defining some pitfalls. J Neurosci Methods 2:123-133.
Zachary RB, Holmes W (1946) Primary suture of nerves. Surg Gynecol Obstet 82:632-651.
Zacks SI, Saito A (1969) Uptake of exogenous horseradish peroxidase by coated vesicles in mouse neuromuscular junctions. J Histochem Cytochem 17:161-170.
Zalewski AA, Silvers WK (1980) An evaluation of nerve repair with nerve allografts in normal and immunologically tolerant rats. J Neurosurg 52:557-563.
Zalewski AA, Gulati AK (1982) Evaluation of histocompatibility as a factor in the repair of nerve with a frozen nerve allograft. J Neurosurg 56:550-554.
Zalewski AA, Gulati AK (1984) Survival of nerve allografts in sensitized rats treated with cyclosporin A. J Neurosurg 60:828-834.
Zochodne DW (2008) Neurobiology of Peripheral Nerve Regeneration: Cambridge University Press.

List of Tables

TABLE 2.1 SUMMARY OF ALL TESTS SHOWING RETROGRADE TRACER AND APPLICATION METHODS EMPLOYED. 28

TABLE 2.2 TEST SERIES HRP2P1 WITH THE ADDITION OF FAST GREEN ON THE LEFT. 31

TABLE 2.3 EVALUATION OF SECTION QUALITY. 41

TABLE 2.4 CLASSIFICATION OF HRP LABELED MOTONEURONS. 42

TABLE 2.5 PROTOCOL FORMS FOR DOCUMENTATION OF THE TRIAL PARTS. 45

TABLE 3.1 ***A***. QUALITY ASSESSMENT OF THE SPINAL CORD SECTIONS USING BASIC PARAMETERS (PRESENCE OR LACK OF THE CENTRAL CANAL, NUMBER OF MISSING SECTIONS, EVALUATION OF SECTION QUALITY IN QUALITATIVE TERMS AND USING QUANTITATIVE MEASUREMENTS). 47

TABLE 3.1 ***B***. QUALITY ASSESSMENT OF THE SPINAL CORD SECTIONS IN GRAFT SERIES HRPG2. 48

TABLE 3.2 INTERSEGMENTAL LUMBAR PLEXUS. 56

TABLE 3.3 FREQUENCY OF INTERSEGMENTAL DORSAL ANASTOMOSES. 57

TABLE 3.4 MISLABELED MOTONEURONS FOLLOWING HRP APPLICATION. 68

TABLE 3.5 CELL COUNT FOLLOWING THE APPLICATION OF HRP TO VARIOUS NERVES AND MUSCLE NERVE BRANCHES. 70

TABLE 3.6 LABELING OF SPINAL CELL COLUMNS USING FLUORESCENT DYES. 73

TABLE 3.7 PARAMETERS OF THE CELL COLUMN OF THE TIBIALIS ANTERIOR AND EXTENSOR DIGITORUM BREVIS MUSCLES (*R1107*). 81

TABLE 3.8 PARAMETERS OF THE CELL COLUMN OF THE TIBIALIS ANTERIOR MUSCLE ON THE CONTROL SIDE IN GRAFT SERIES *HRP2G*. 83

TABLE 3.9 DIAMETER AND AREA OF THE MN FOLLOWING HRP MUSCLE INJECTION AND HRP NERVE BATH. 88

TABLE 3.10 MORPHOMETRIC PARAMETERS OF THE GAMMA, ALPHA 1 AND ALPHA 2 MOTONEURONS FOLLOWING CLASSIFICATION BASED ON THE HISTOGRAMS FROM TEST SERIES ***HRP2*** (TA MUSCLE INJECTION) AND ***HRP5*** (HRP NERVE BATH). COMPARE WITH **FIGURE 3.37**. 91

TABLE 3.11 EVALUATION AND MEASUREMENT OF THE GRAFT SITE. 98

TABLE 3.12 PARAMETERS OF THE TA CELL COLUMN FOLLOWING RADIAL NERVE-COMMON PERONEAL NERVE AUTOGRAFT ON THE RIGHT. 105

TABLE 3.13 PARAMETERS OF THE TA/F CELL COLUMN ON THE RIGHT FOLLOWING AUTOGRAFT. 106

TABLE 3.14 DIAMETER AND AREA OF THE TA MOTONEURON COLUMNS FOLLOWING AUTOGRAFT. 112
TABLE 3.15 CELL TYPES OF TYPE I MOTONEURONS OF THE TA CELL COLUMN (*HRP2G*, *HRP2*) DURING REGENERATION. 115
TABLE 3.16 DIVISION OF ALPHA MOTONEURONS (*HRP2G*, *HRP2*) DURING REGENERATION. 115

TABLE 4.1 CELL COUNTS FOR VARIOUS MUSCLES AND NERVES AFTER THE APPLICATION OF HRP OR FLUORESCENT DYES. 138

TABLE A.1 PERFUSION DIAGRAM FOR TEST SERIES HRP2 ACCORDING TO MESULAM (1982) IN A MODIFIED FORMAT. 148
TABLE A.2 HRP ENZYME HISTOCHEMISTRY FOR THE HRP2 TEST SERIES ACCORDING TO MESULAM (1982) IN A MODIFIED FORMAT. 148
TABLE A.3 NEUTRAL RED COUNTERSTAINING (BURCK, 1982; MESULAM, 1982) 148
TABLE A.4 THIONINE COUNTERSTAIN (ADAMS, 1980) 149
TABLE A.5 ADJUSTMENT OF COLOR INTENSITY OF THE H.E. COUNTERSTAIN (ROMEIS, 1968). THE AIM IS A DULL NUCLEUS-PLASMA STAINING WHICH ALLOWS A MORPHOMETRIC ANALYSIS IN THE LIGHT FIELD WITHOUT COVERING THE FLUORESCENT MARKING. 149
TABLE A.6 COMBINATION OF FLUORESCENT LABELING (DY AND FB) AND HISTOLOGICAL COUNTERSTAINING USING HEMALAUN ACCORDING TO MAYER (BURCK, 1982). 149
TABLE A.7 ADJUSTMENT OF THE COLOR INTENSITY OF THE NISSL STAIN IN SECTIONS 1 TO 9 BY VARIATION OF THE INCUBATION PARAMETERS (ROMEIS, 1968). SECTIONS 10 TO 12: THE AIM IS AN EQUIVALENT REPRESENTATION OF THE NUCLEUS-PLASMA STAINING IN THE LIGHT FIELD AND OF THE FLUORESCENCE MARKING IN FLUORESCENT MICROSCOPY. SECTIONS FROM FLUORESCENCE TEST R711 WITH FB MARKING OF THE NUCLEUS COLUMN OF THE TIBIALIS ANTERIOR MUSCLE AND DY MARKING OF THE NUCLEUS COLUMN OF THE LATERAL GASTROCNEMIUS MUSCLE WERE USED. SKETCHES WERE INITIALLY PREPARED OF THE FLUORESCING CELLS IN LAMINA IX WITHOUT COVERING. AFTER NISSL STAINING, THE FLUORESCENT MARKED MOTONEURONS WERE ATTEMPTED TO BE LOCATED ONCE AGAIN BY MEANS OF THE SKETCHES. THE RESIDUAL INTENSITY OF THE FLUORESCENCE WAS EVALUATED, AS WELL AS THE DEPICTION OF THE CELL BOUNDARIES, THE AUTOFLUORESCENCE OF THE BACKGROUND THROUGH THE HISTOLOGICAL COUNTERSTAINING AND DIFFUSION OF THE FLUORESCENT DYE INTO OTHER, PREVIOUSLY UNMARKED NEURONS. 150
TABLE A.8 COMBINATION OF FLUORESCENCE LABELING (DY AND FB) AND COUNTERSTAINING USING CRESYL VIOLET (BURCK, 1982). 150
TABLE A.9 COMBINATION OF FLUORESCENCE LABELING (DY AND FB) WITH RAPID NISSL COUNTERSTAINING (BURCK, 1982). 150
TABLE A.10 LENGTH OF THE VERTEBRAL BODIES (MM). 151
TABLE A.11 SEGMENT LENGTH: EXTERNAL MEASUREMENTS (MM). 152
TABLE A.12 SEGMENT LENGTH: INTERNAL MEASUREMENTS (MM) 153
TABLE A.13 CROSS-SECTIONAL DIAMETER OF THE SEGMENTS: EXTERNAL MEASUREMENTS (MM) 154
TABLE A.14 LENGTH OF THE ANTERIOR ROOTS FROM ENTRY IN THE SPINAL CORD AS FAR AS THE SPINAL GANGLIA. 154
TABLE A.15 CROSS-SECTIONAL DIAMETER OF THE SEGMENTS: INTERNAL MEASUREMENTS (MM). 155
TABLE A.16 LONGITUDINAL DIAMETER OF THE SEGMENTS: INTERNAL MEASUREMENTS (MM). 155

List of Figures

FIGURE 2.1 DISSECTION AND APPLICATION OF HRP TO SEVERED MUSCLE NERVE BRANCHES. ***A***, LABELING THE NERVE BRANCHES, ***B***, IMMERSION OF THE BRANCHES IN A DMSO SOLUTION, ***C***, APPLICATION OF HRP, ***D***, CLOSING THE CATHETER. 35

FIGURE 2.2 ***A***, SPINAL CORD SECTION WITH HRP LABELED CELLS. ***B***, OUTLINE DRAWING WITH APPLIED COORDINATES SYSTEM FOR LOCALIZATION OF THE MOTONEURONS..... 41

FIGURE 3.1 LENGTH OF THE VERTEBRAL BODIES (MEAN VALUES IN MM)..... 49

FIGURE 3.2 DEPENDENCY OF THE VERTEBRAL BODY LENGTH ON WEIGHT. 49

FIGURE 3.3 SEGMENT LENGTH WITH EXTERNAL (***A***) AND INTERNAL (***B***) MEASUREMENT (MEAN VALUES IN MM). *RIGHT* DIAGRAM SIDE: SEGMENT LENGTH WITH MEASUREMENT ON THE RIGHT SPINAL CORD SIDE, *LEFT* DIAGRAM SIDE: MEASUREMENTS ON THE LEFT..... 50

FIGURE 3.4 DEPENDENCY OF THE LENGTH OF THE LUMBAR SPINAL CORD ON WEIGHT FOR EXTERNAL (***A***) AND INTERNAL (***B***) MEASUREMENT. 50

FIGURE 3.5 CROSS-SECTIONAL DIAMETER OF THE SEGMENTS (MEAN VALUES IN MM). 51

FIGURE 3.6 CROSS-SECTIONAL DIAMETER OF THE SPINAL CORD SEGMENTS L3-L5 (INTERNAL MEASUREMENT IN MM)..... 52

FIGURE 3.7 LONGITUDINAL DIAMETER OF THE SPINAL CORD SEGMENTS L3-L5 (INTERNAL MEASUREMENT IN MM). 52

FIGURE 3.8 DIFFERENCE IN HEIGHT LOCALIZATION BETWEEN THE SPINAL CORD AND SPINAL COLUMN..... 53

FIGURE 3.9 SEGMENTS L1 TO L6 PROJECTED ONTO THE SPINAL COLUMN FOR EXTERNAL MEASUREMENT. VB: VERTEBRAL BODY, S: SPINAL SEGMENT. 54

FIGURE 3.10 MORPHOMETRY OF THE LUMBAR SPINAL CORD. *ABOVE:* PREPARATION OF THE LUMBAR SPINAL CORD WITH NERVE ROOTS. LENGTH OF THE ANTERIOR ROOTS: BLACK, SEGMENT LENGTH: RED, SEGMENT DIAMETER: BLUE. *BELOW:* LENGTH OF THE ANTERIOR ROOTS IN MM (ORDINATE AXIS). 55

FIGURE 3.11 DIFFICULTY OF A DETERMINATION USING THE INTERSEGMENTAL PLEXUS. 57

FIGURE 3.12 ANATOMY OF THE PERONEAL NERVE INNERVATION AREA (R1104). 58

FIGURE 3.13 THE INNERVATION AREA OF THE COMMON PERONEAL NERVE: SCHEMATIC DRAWINGS WITH LONGITUDINAL MEASUREMENT OF THE NERVE SEGMENTS (DISTANCES IN MILLIMETERS). 59

FIGURE 3.14 BRANCHES OF THE COMMON PERONEAL NERVE (R1103). 60

FIGURE 3.15 THE INNERVATION AREA OF THE DEEP PERONEAL NERVE. 61

FIGURE 3.16 BRANCHING MODEL OF THE MUSCLE NERVE BRANCHES SUPPLYING THE TIBIALIS ANTERIOR MUSCLE (1-3) AND THE EXTENSOR DIGITORUM LONGUS MUSCLE. 62

FIGURE 3.17 MORPHOLOGY OF THE MOTONEURONS LABELED WITH HRP (***A-H***) AND THE FLUORESCENT DYES FAST BLUE (***L-M***) AND DIAMIDINO YELLOW (***O-P***). MOTONEURONS FOLLOWING IMMERSION OF THE SCIATIC NERVE IN A HRP SOLUTION (**R818,** ***A, I-K***). SPINAL CORD CROSS-SECTION WITH INSERTION CHANNEL TRANSVERSE THROUGH THE POSTERIOR HORNS USING MINUTIEN PINS FOR SEGMENT MARKING (**R818,** ***A***). TIBIALIS ANTERIOR MOTONEURONS FOLLOWING APPLICATION OF HRP TO THE MUSCLE NERVE BRANCHES (**R1095,** ***B-D***) OR INJECTION INTO THE MUSCLE (**R766,** ***E-H***). RECONSTRUCTION OF THE ANTERIOR HORN CELLS WITH THEIR FIBER ORIENTATION IN 6 ADJACENT SECTION IMAGES (WITH DENDRAXON, ***D***). MOTONEURONS OF THE CELL COLUMN OF THE TIBIALIS ANTERIOR MUSCLE, 56 DAYS AFTER THE INJECTION OF FB INTO THE MUSCLE (**R808,** ***P-S***). COMBINATION OF HRP AND DY. INJECTION OF DY INTO THE TIBIALIS ANTERIOR MUSCLE 9 DAYS PRIOR TO IMMERSION OF THE PERONEAL NERVE IN A 40% HRP SOLUTION (**R1156,** ***T-V***). 63

FIGURE 3.18 *R327* (*HRP1P*), 3D RECONSTRUCTION OF THE NUCLEUS COLUMN OF THE TIBIALIS ANTERIOR MUSCLE FOLLOWING INJECTION OF A 5% HRP SOLUTION INTO THE MUSCLE. *RIGHT SIDE:* **YELLOW**, *LEFT SIDE:* **ROT**. MISMARKED MOTONEURONS OUTSIDE THE CELL COLUMN OF THE TIBIALIS ANTERIOR MUSCLE ARE CIRCLED IN RED. 66

FIGURE 3.19 *R766* (*HRP2P1*), THREE-DIMENSIONAL RECONSTRUCTION OF THE TIBIALIS ANTERIOR MUSCLE CELL COLUMN. *RIGHT SIDE:* **YELLOW**, *LEFT SIDE:* **ROT**. ADDITION OF 0.1% FAST GREEN ON THE LEFT. MISLABELED MOTONEURONS OUTSIDE THE CELL COLUMN OF THE TIBIALIS ANTERIOR MUSCLE ARE CIRCLED IN RED. 69

FIGURE 3.20 CELL COUNT OF THE MOTONEURON COLUMN OF THE TIBIALIS ANTERIOR MUSCLE FOLLOWING CORRECTION OF DUPLICATED AND MISLABELED NEURONS. 69

FIGURE 3.21 *R1095*, 3D RECONSTRUCTION OF THE NUCLEUS COLUMN OF THE TIBIALIS ANTERIOR MUSCLE. APPLICATION OF HRP TO THE MUSCLE NERVE BRANCHES. EXPANSION OF THE CELL COLUMN ON THE SPINAL CORD SECTION IN RELATIVE COORDINATES. 71

FIGURE 3.22 *R1149*, 3D RECONSTRUCTION OF THE NUCLEUS COLUMN OF THE TIBIALIS ANTERIOR MUSCLE. APPLICATION OF HRP TO THE MUSCLE NERVE BRANCHES. EXPANSION OF THE CELL COLUMN ON THE SPINAL CORD SECTION IN RELATIVE COORDINATES. 71

FIGURE 3.23 *R1107*, 3D RECONSTRUCTION OF THE NUCLEUS COLUMN OF THE EXTENSOR DIGITORUM BREVIS II AND III MUSCLE. APPLICATION OF HRP TO THE MUSCLE NERVE BRANCHES. EXPANSION OF THE CELL COLUMN ON THE SPINAL CORD SECTION IN RELATIVE COORDINATES. 71

FIGURE 3.24 COMBINATION OF SEVERAL MOTOR NUCLEUS COLUMNS. 74

FIGURE 3.25 CELL COUNTS OF DIFFERENT MUSCLES OR NERVES FOLLOWING RETROGRADE TRANSPORT OF HRP OR FLUORESCENT DYES. THE ERROR INDICATORS FOLLOWING THE HRP NERVE BATH SHOW THE MAXIMUM VALUES, AND THE STANDARD DEVIATION IN OTHER TESTS. 76

FIGURE 3.26 SEGMENTAL POSITION OF 31 CELL COLUMNS OF THE TIBIALIS ANTERIOR MUSCLE. THE RELATIVE POSITIONS OF THE CRANIAL AND CAUDAL POLES OF THE TA CELL COLUMNS AND OF THE AVERAGE ARE INDICATED IN PERCENTAGE VALUES FOLLOWING STANDARDIZATION OF THE SEGMENTS TO 100. THE DELINEATED HISTOGRAMS

illustrate the segmental frequency distribution. The percentage data of the right ordinate applies to the length of the nucleus columns. 77

Figure 3.27 Segmental localization of the motoneuron columns. 78

Figure 3.28 Segmental and vertebrogenic localization of the different motoneuron columns. VB: Vertebral body, S: Spinal segment. 78

Figure 3.29 2D reconstruction of nucleus columns of the tibialis anterior muscle following HRP muscle injection (*R327*, *R766* and *R1074*) or HRP application to the severed muscle nerve branches (*R1095* and *R1149*). ***A***, absolute cell position on the mediolateral, ***B***,***C*** on the dorsolateral axis. 82

Figure 3.30 Interpolated cell density figure from 16 TA cell columns on the control side in the ***A***,***B*** transversal, ***C***,***D*** horizontal and ***E***,***F*** sagittal sectional planes. The numerical data from the x and y axes correspond to relative coordinates, based on the boundary of the spinal cord. The z axis depicts the rostrocaudal expansion of the nucleus column which was divided into 8 sections. To represent all control tests, the relative cell coordinates were totalized in a grid with an edge length of 10% and 15% (***A***,***B***) or of 10% and 1/8 of the nucleus column in a craniocaudal direction (***C***-***F***). 85

Figure 3.31 Cell density of the TA cell column on the ***A***, transversal, ***B***,***C*** horizontal and ***C***,***E*** sagittal sectional planes. The ordinates and abscissa in ***A*** denote the relative coordinates based on the boundary of the gray spinal cord matter. For the display in ***B***-***E***, the cell columns were divided into 8 sections and the interpolated cell density distribution was calculated. Figures ***B*** and ***D*** represent the left, and ***C*** and ***E*** the right sides of the spinal cord. 86

Figure 3.32 Histograms of area and diameter for the motoneurons of 12 HRP labeled cell columns of the tibialis anterior muscle. 87

Figure 3.33 ***A***, Cumulated figure and ***B***, distribution of the cell diameter in test series HRP5 and HRP2..... 88

Figure 3.34 Diameter distribution of the motoneurons from 12 nucleus columns in the craniocaudal (z axis), mediolateral (x axis) and ventrodorsal (y axis) directions; light blue (10-20 µM), yellow (20-30 µM), blue (30-40 µM), green (40-50 µM) and red (50-60 µM). 89

Figure 3.35 *Left:* Frequency of cell types based on the HRP marking pattern in the experiments from test series ***HRP2*** (n = 10) and ***HRP5*** (n = 2). *Right*: Depiction of the average diameters and their standard deviation for cell types from the 2 test series. The cell types are consolidated into groups IA+B, IC+D, IE and II. 90

Figure 3.36 Histograms of areas and diameters in test series ***HRP5*** and ***HRP2***. The classification of diameter took place based on the distribution pattern in different size classes. With missing bi- or trimodal distribution of diameter, a limiting diameter of 28.5 µM was taken as a basis for differentiating alpha to gamma motoneurons, and a limiting diameter of 37.5 µM for differentiating type S and type FG motoneurons. 92

Figure 3.37 Distribution of the alpha 1, alpha 2 and gamma motoneurons in the HRP control tests. The *left* half of the image depicts the distribution of motoneurons over the overall cell column, and the *right* side shows after allocation of the nucleus column into 4 segments from cranial to caudal. 95

FIGURE 3.38 2D RECONSTRUCTIONS OF 10 CELL COLUMNS OF THE TIBIALIS ANTERIOR MUSCLE FOLLOWING HRP MUSCLE INJECTION (*R327*, *R766*, *R1074*), HRP NERVE BATH (*R1095*, *R1149*) AND FOLLOWING MUSCLE INJECTION OF THE FLUORESCENT DYES DY AND FB (*R808*). FIRST, THE NUCLEUS COLUMN OF THE EXTENSOR DIGITORUM BREVIS II AND III MUSCLES IS SHOWN ON THE RIGHT AFTER HRP NERVE BATH. THE NUCLEUS COLUMNS OF *R327* ARE ONLY SHOWN ON THE TRANSVERSAL RECONSTRUCTIONS DUE TO MISSING SEGMENTAL ATTRIBUTION. 97

FIGURE 3.39 THE PREPARATION DRAWINGS ON THE GRAFT SITE ON THE RIGHT ARE NOT TO SCALE, AND FOR REASONS OF CLARITY ARE SHOWN EXAGGERATEDLY. THE DISTANCES WERE MEASURED BETWEEN THE STILL VISIBLE SUTURE SITES, AND FROM THE DISTAL SUTURE SITE TO THE ENTRANCE OF THE COMMON PERONEAL NERVE INTO THE PERONEAL COMPARTMENT. THE PERCENTAGE OF SCAR FORMATION IN THE AREA OF THE AUTOLOGOUS RADIAL NERVE INTERPOSITION GRAFT WAS SEMI-QUANTITATIVELY EVALUATED. 99

FIGURE 3.40 SEGMENTAL LOCALIZATION OF THE MOTONEURON COLUMNS FOLLOWING LESION OR GRAFT. PC#: TRANSECTION OF THE COMMON PERONEAL NERVE. 100

FIGURE 3.41 2D RECONSTRUCTIONS OF THE TIBIALIS ANTERIOR NUCLEUS COLUMN 2 WEEKS AFTER RADIAL NERVE-PERONEAL NERVE AUTOGRAFT. *LEFT*: CONTROL SIDE, *RIGHT*: GRAFT SIDE WITH RECONSTRUCTION OF THE TA CELL COLUMN (BLUE) AND OF MOTONEURONS THAT WERE CLASSIFIED AS MISLABELED BASED ON RELATIVE COORDINATES (VIOLET). 102

FIGURE 3.42 2D RECONSTRUCTIONS OF THE TIBIALIS ANTERIOR NUCLEUS COLUMN 4 WEEKS AFTER RADIAL NERVE-PERONEAL NERVE AUTOGRAFT. *LEFT*: CONTROL SIDE, *RIGHT*: GRAFT SIDE WITH RECONSTRUCTION OF THE TA CELL COLUMN (BLUE), MISLABELED MOTONEURONS (VIOLET). 103

FIGURE 3.43 2D RECONSTRUCTIONS OF THE TIBIALIS ANTERIOR MUSCLE NUCLEUS COLUMN 8 WEEKS (*R831*, *R824*) AND 10 WEEKS (*R822*) AFTER RADIAL NERVE-PERONEAL NERVE AUTOGRAFT. *LEFT*: CONTROL SIDE, *RIGHT*: GRAFT SIDE WITH RECONSTRUCTION OF THE TA CELL COLUMN (BLUE), MISLABELED MOTONEURONS (VIOLET). 104

FIGURE 3.44 *R827*, 3D RECONSTRUCTION OF THE TA NUCLEUS COLUMN 4 WEEKS AFTER A RADIAL NERVE-COMMON PERONEAL NERVE AUTOGRAFT *RIGHT* (YELLOW), CONTROL SIDE *LEFT* (RED). THE SCALING OF THE COLOR SCALE IS IDENTICAL IN FIGURES 3.44-3.46. THE CELL COUNT OF THE GRAFT TO CONTROL SIDE IS 18.3%. 108

FIGURE 3.45 *R831*, 3D RECONSTRUCTION OF THE TA NUCLEUS COLUMN 8 WEEKS AFTER A RADIAL NERVE-COMMON PERONEAL NERVE AUTOGRAFT *RIGHT* (YELLOW), CONTROL SIDE *LEFT* (RED). THE CELL COUNT OF THE GRAFT TO CONTROL SIDE IS 59.8%. 108

FIGURE 3.46 *R822*, 3D RECONSTRUCTION OF THE TA NUCLEUS COLUMN 10 WEEKS AFTER A RADIAL NERVE-COMMON PERONEAL NERVE AUTOGRAFT *RIGHT* (YELLOW), CONTROL SIDE *LEFT* (RED). THE CELL COUNT OF THE GRAFT TO CONTROL SIDE IS 39.1%. 108

FIGURE 3.47 CELL COUNT OF THE TA MOTONEURONS ON THE CONTROL AND GRAFT SIDES FOLLOWING HRP MUSCLE INJECTION. 109

FIGURE 3.48 CELL DENSITY DISTRIBUTION OF THE TA CELL COLUMN ON THE CONTROL SIDE (***A***, LEFT HALF OF IMAGE, ***B*** AND ***D***) AND THE GRAFT SIDE (***A***, RIGHT HALF OF IMAGE, ***C*** AND ***E***). THE TESTS WITH IDENTICAL POSTOPERATIVE SURVIVAL TIMES ARE CONSOLIDATED. REPRESENTATION ON THE ***A***, TRANSVERSAL, ***B,C*** HORIZONTAL AND ***C,E*** SAGITTAL SECTIONAL PLANES. THE ORDINATES AND ABSCISSA IN ***A*** DENOTE THE RELATIVE COORDINATES BASED ON

THE BOUNDARY OF THE GRAY SPINAL CORD MATTER. FOR THE DISPLAY IN ***B-E***, THE CELL COLUMNS WERE DIVIDED INTO 8 SECTIONS AND THE INTERPOLATED CELL DENSITY DISTRIBUTION WAS CALCULATED. 111

FIGURE 3.49 CUMULATIVE REPRESENTATION OF DIAMETERS ON THE CONTROL SIDE AND GRAFT SIDE FOLLOWING DIFFERENT POSTOPERATIVE PERIODS..... 112

FIGURE 3.50 *LEFT:* FREQUENCY OF CELL TYPES FOLLOWING HRP MUSCLE INJECTION ON THE GRAFT SIDE, DIFFERENTIATED ACCORDING TO THEIR LOCALIZATION IN (*HRP2*) OR OUTSIDE OF (*HRP2/F*) THE TA AREA. *RIGHT*: DIAMETER OF CELL TYPES (*HRP2*) FOLLOWING VARIOUS REGENERATION TIMES. 114

FIGURE 3.51 HISTOGRAMS OF AREAS AND DIAMETERS OF THE TA NUCLEUS COLUMN ON THE GRAFT SIDE OVER TIME. A CLASSIFICATION OF CELLS INTO GAMMA, ALPHA 1 AND ALPHA 2 MOTONEURONS WAS PERFORMED CORRESPONDING TO THE HISTOGRAM PROFILE OF THE DIAMETER OR THE LIMITING DIAMETERS OF 28.5 µM AND 38.5 µM RESPECTIVELY. 116

FIGURE 3.52 DISTRIBUTION OF THE ALPHA 1, ALPHA 2 AND GAMMA MOTONEURONS IN THE *HRP2G* GRAFT SERIES. THE *LEFT* HALF OF THE IMAGE DEPICTS THE DISTRIBUTION OF MOTONEURONS OVER THE OVERALL CELL COLUMN, AND THE *RIGHT* SIDE SHOWS AFTER ALLOCATION OF THE NUCLEUS COLUMN INTO 4 SEGMENTS FROM CRANIAL TO CAUDAL. THE DISTRIBUTION IS CONSOLIDATED FOR THE REGENERATIONS PERIOD OF 2, 4, 8 AND 10 WEEKS. 117

FIGURE 3.53 2D RECONSTRUCTIONS OF THE TA CELL COLUMN ON THE CONTROL SIDE (***A***, LEFT HALF OF IMAGE, ***B*** AND ***D***) AND THE GRAFT SIDE (***A***, RIGHT HALF OF IMAGE, ***C*** AND ***E***) 2 WEEKS AFTER AN AUTOLOGOUS RADIAL NERVE-COMMON PERONEAL NERVE AUTOGRAFT..... 119

FIGURE 3.54 2D RECONSTRUCTIONS OF THE TA CELL COLUMN ON THE CONTROL SIDE (***A***, LEFT HALF OF IMAGE, ***B*** AND ***D***) AND THE GRAFT SIDE (***A***, RIGHT HALF OF IMAGE, ***C*** AND ***E***) 4 WEEKS AFTER AN AUTOLOGOUS RADIAL NERVE-COMMON PERONEAL NERVE AUTOGRAFT..... 120

FIGURE 3.55 2D RECONSTRUCTIONS OF THE TA CELL COLUMN ON THE CONTROL SIDE (***A***, LEFT HALF OF IMAGE, ***B*** AND ***D***) AND THE GRAFT SIDE (***A***, RIGHT HALF OF IMAGE, ***C*** AND ***E***) 8-10 WEEKS AFTER AN AUTOLOGOUS RADIAL NERVE-COMMON PERONEAL NERVE AUTOGRAFT..... 121

FIGURE 4.1 SEGMENTAL LOCALIZATION OF THE TIBIALIS ANTERIOR NUCLEUS COLUMN ON THE CONTROL AND GRAFT SIDE. 134

Index

A

Acetate buffer 148, 149
Acrylic 24
Allograft 19
Alpha motoneurons 92, 94, 96, 135
  Type FF (fatigue-resistant) 145
  Type FR (fast-fatiguable) 145
  Type S (slow) 145
Anastomosis 56
Artifacts 42, 89, 90
Autograft ..... XI, 32, 47, 58, 79, 98, 99, 109, 115, 118, 144, 146
Autotransplantation 20
Axon elongation 24
Axon sprouts 17, 20, 22, 139, 143

B

Basal lamina 19, 23
Beta motoneurons 94

C

C57BL/Ola mice 23
Cat 127, 128, 131, 132, 135, 136, 145
Cell adhesion 23
Cell count 34, 42, 43, 46, 72, 79, 84, 94, 107, 109, 120, 126, 134
Cell cultures 25
Cell density 34, 43, 68, 85, 110, 145
Central canal 40, 48, 51, 98, 101, 144
Chromalaun gelatin 38
Chromatolysis 124, 131, 132, 134, 141
Ciliary neurotrophic factor 22
Coaptation 20, 33
Collagen 18, 23, 24
Contact guidance 22
Control series 91, 107, 113, 117, 118
Cyanoacrylate adhesive 29

D

Degeneration 21, 23, 26, 134, 137, 140, 141
Dendrites 62, 65, 129
DePeX 30, 32
Depth sensibility XI
Diamidino Yellow 26, 27, 37, 38, 39, 44
Diffusion 32, 33, 66, 69, 101, 122, 125, 127, 128
DMSO 34, 37, 136
Double labeling 38, 39, 65, 80, 129, 132, 143
Double root 57

E

End plate 20, 139
Endoneurial sheath 18, 140, 143
End-to-end suture ..... XI, 17, 26
Entactin 23

Enzyme histochemistry 27, 32, 51, 62, 75, 123, 143
Epineurium 18

F

Fascicle 18, 25, 139
Fascicle suture 22
Fast Blue 26, 27, 37, 38, 44, 64, 72, 77, 128, 143
Fast Green 31, 67, 72, 79, 126, 135
Fiber count 24, 135
Fiber exchange 40
Fibrin glue 21, 33
Fibrin matrix 24
Fibronectin 23
Fixing 29, 37
Fluorescent dyes 37, 64, 75, 128, 132, 134
Fluoro-Gold 128
Formaldehyde 29
Frequency distribution 79, 96, 113

G

Gamma motoneurons 44, 92, 95, 114, 117, 135
Glial cells 23, 25, 64
Glucose 29
Glutaraldehyde 29, 76
Graft
  acellular 19, 23
  autologous 17, 24, 58, 107, 133, 146
  heterologous 18
Graft rejection 18
Gray matter 44, 49

H

Heparan sulfate proteoglycan 23
Homografts 19
Horseradish peroxidase 27, 125, 143
HRP nerve bath 70, 77, 80, 84, 90, 94, 97, 113, 126, 143
Hydrogen peroxide 30, 62
Hyperesthesia XI

K

Kinesthesia XI

L

L1 glycoprotein 23
Lamina IX 40, 64, 65, 72, 131, 133
Laminin 23, 24
Limiting diameter 88, 91, 114, 137, 145
Long-term experiment 37, 44, 64, 65, 73, 75, 128, 143

M

Macrophages 18, 21
Main histocompatibility complex 18
Matrix 23
Millipore 24
Misinnervation 25, 101, 134, 140
Mismarking 27, 70, 72, 101, 122, 125, 128
Motor axons 23, 25, 137
Motor units 120, 137, 141
Mouse 127, 136
Muscle compartments 33, 73, 128
Muscle extracts 25
Muscle grafts 25
Muscle injection 34
Muscle spindle 135, 145
Muscles
  biceps femoris muscle 30, 98
  extensor digitorum brevis 97
  extensor digitorum brevis muscle 35, 77, 143
  extensor digitorum brevis muscles 36
  extensor digitorum longus 79
  extensor digitorum longus muscle 35, 36, 61, 128
  extensor hallucis proprius muscle 36, 123, 143
  gastrocnemius muscle 30, 72, 126, 144

peroneus brevis muscle 58, 123
peroneus IV muscle 59, 123
peroneus longus muscle 35, 58, 127
peroneus V muscle 123
tibialis anterior muscle 27, 30, 35, 40, 43, 46, 56, 61, 70, 77, 109, 133

N

N–CAM 23
Nerve bath 36, 39, 70, 87, 122, 128
Nerve damage 17
Nerve graft 25, 107, 115, 133, 143
Nerve growth factor (NGF) 21
Nerve lesion ..... XI, 22, 125, 130, 139, 143
Nerve root 40, 55
Nerves
common peroneal nerve 32, 58, 65, 72
deep peroneal nerve 36, 58, 66, 72, 122, 127
radial nerve 30, 40, 58, 79, 98, 133, 144
sciatic nerve 33, 58, 72, 80, 143
superficial peroneal nerve 58, 122, 134
sural nerve 139
tibial nerve 33, 65, 70, 101, 122, 126
Neural graft 33
Neuroma 20, 24, 98
Neuromatous neurotization 26
Neurotrophic factors 24
Neurotropism 22, 139
n-hexane 29
Nidogen 23

P

Paraformaldehyde 37, 64, 148
Paresthesia XI
Pentobarbital 27, 30, 31, 37, 46, 144
Perfusion 31, 34, 35, 37, 46, 64, 76, 123, 144
Perfusion pressure 29
Phosphate buffer 37, 148
Plexus 40, 49, 55, 131, 133
Polyester 24
Polyglycolic acid 24
Predenervation 18, 24
Pruning 26
PVC hose 32, 34

Q

Quality assurance 123

R

Rabbit 19, 141
Rat .....XI, 18, 27, 46, 58, 122, 135, 139
Reconstruction 22, 30, 32, 64, 66, 82, 97, 107, 120, 144
Regeneration ..... XII, 18, 75, 98, 120, 125, 135, 141, 143
Regeneration chamber 25
Regeneration result 99
Reinnervation .....XI, 23, 99, 115, 121, 133, 139
Remak cells 23
Retrograde tracers 125
Rompun 31
Root entry zone 40

S

Saccharose 29, 148
Schwann cells 18, 24
Sciatic nerve 40
Segment length 29, 39, 45, 50, 51, 80, 123
Silicone 24
Size principle 141
Sodium nitrite 29
Sodium nitroferricyanide 30
Somatotopy 132, 140
Spinal column 29, 46, 49, 53, 79, 124, 133
Spinal cord 29, 37, 39, 49, 50, 79, 87, 123, 134

Stereognosis XI
Superior muscular artery 30, 32, 58
Survival time 29, 38, 75, 101, 136
Suture
epineurial 17, 20, 21, 22, 25
interfascicular 20, 22, 26
perineurial 22, 30, 33, 143
Suture material 144
Synaptic stripping 141

T

Tactile gnosis 143
Tension 17, 26
Tetramethylbenzidine 62, 135, 144, 148
Topography 25, 36, 58, 124, 140
Tracer 34, 61, 67, 70, 84, 96, 122
Transection 27, 32, 70, 101, 122, 127

V

Vertebral body length 45, 49
Vetranquil 31

W

Washing solution 29, 148
White matter 41
Wound healing 48

Y

Y-prosthesis 22

Reorganization of a Spinal Motoneuron Nucleus following Autologous Nerve Graft in the Rat

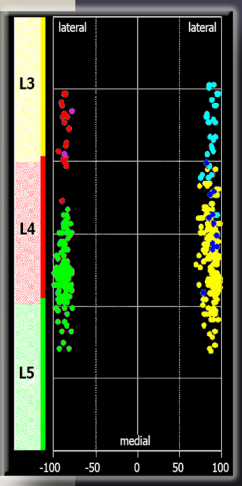

Autologous nerve grafts are steadily regarded as the method of choice for bridging the nerve gaps resulting after peripheral nerve lesions with substance defects. Microsurgical techniques and the perineurial suture of corresponding fascicles have improved the functional results following peripheral nerve graft.

However, regeneration success is often disappointing, despite the most thorough technique and expertise. The loss of spinal motoneurons associated with a nerve lesion and the growth of axon sprouts in inadequate endoneurial sheaths were held responsible as the reason for the lowered muscular strength, limited movement coordination and fine motor skills, poor differentiation and localization of sensory stimuli and for the lack of tactile gnosis.

In this experimental study, it is assumed that the central effects at the level of the spinal motoneuron nuclei show an image of the peripheral misinnervation in topographical-morphological terms, and can supply an explanatory model for the functional motor deficits after peripheral nerve graft.

On the other hand, the plastic changes of a motor cell column in the reinnervation process influence the structural-functional relationships.

ISBN 978-3-8391-6777-9

9 783839 167779

www.bod.de

BoD™
BOOKS on DEMAND